University of Salford MANCHESTER

MECHANISMS OF MEDULLOBLASTOMA VULNERABILITY AND NEW TARGETED THERAPIES

MARTA BUZZETTI

School of Science, Engineering and Environment
University of Salford, UK

Submitted in partial fulfilment of the requirements for the Degree of Doctor of Philosophy, 2020.

To Enrico,

Contents

List of figures

List of tables

Acknowledgements

Many people have contributed to the accomplishment of this challenging experience. Four years of joy and despair that are wrapped up into such a short title, named “PhD”. The list of thanks should be as long as the word “acknowledgement”, but I will try to be concise:

First and foremost, I would like to thank my mentor, Gianpiero Di Leva, for fulfilling my dream of doing research in a foreign land (or should I say lands), for always guiding me, for the time and energy spent, and for giving me the best resources for learning.
I would also like to express my gratitude to all the supervisory team Sarah Withers, Rhod Elder, and especially Caroline Topham for the helpful advices and support throughout my PhD journey.

I would like to thank Dr. Carlo Croce for giving me the invaluable opportunity to join his renowned team of experts at The Ohio State University (US). This experience allowed me to complete part of my project, boosted my research skills and it was an all-round self development step for me. During the time I spent there, I also met woderful people, which always made me feel at home and that I now call friends. To Douglas, thank you for the patience, for teaching me everything you know and for always being there for me outside the lab. To Marina, thank you for the laughter, thank you for the tears, and a special thanks for keeping me fit! I know with you I found a friend for life. Thank you to Paolo Fadda for the technical support for the Nanostring analyses in this project. Thank you also to Alessia, Valerio, Dario, Anna and Luigi for all the good moments together and for being my Italian family abroad.

I would like to express my gratitude to Michela Garofalo, for welcoming me in her laboratory at the Cancer Research UK institute, giving me the chance to complete experiments for my research and contribute to their own projects. To Tiziana, Manuela, Sakis, Peter, Lei and Lucy, thank you for making me feel part of the team and for your friendship.

I would like to express my appreciation to Mattia Chiesa for the huge contribution with the RNAseq analyses showed in this research; and to Yuri D’Alessandra, my first mentor, thank you for your constant guidance and for always believing in me.

Thank you to the Doctoral Training Alliance for providing financial support to conduct my PhD research and to the University of Salford.

I would like to extend my gratitude to my colleagues, but above all friends, at the University of Salford over the past 4 years: Alice, Arvind, Emyr, Chiara, Filippo, Marco, Camillo, Matteo, Fanni, Eleonora, Giuseppe and Claudia. A special thanks goes to my friend Dimitrios, who started this journey with me, who always supported me and prevented me to go insane over the long hours in the lab; without you none of this would have been the same. To my friend and sister from another mister, Sonia. I am grateful we happened to be in the same team, for all the ups and downs we went through together and for always being there for me; I'm sure thousands more adventures are in front of us.
From outside the laboratory, I would like to thank Giuliana and Mara. Thank you for the laughter, for making me go to the gym and for being great friends.

To Lorenzo: 4 years ago, when I moved to Manchester, you were the first person I met. Who knew you were also the most important throughout it all?! Words cannot express the love I feel for you, thank you for being the best friend I could ask for and for making me a better person. And Fabian, I will never forget our endless life conversations, you always understood me without the need of talking. I can't imagine my life without you both.

To all my long-time friends, thank you for your support and for staying close to me despite the distance. I could not ask for better friends.

Last, but not least, the biggest thank you goes to my family. To my mother Anna, for always encouraging me and for her unconditional love. To my grandparents, you are my North Star throughout life; I would be totally lost without you. A special thanks goes to my grandfather for the scientific discussions and from whom, I believe, I took the tendency of always dissecting things to their core.
To my "little" brother Enrico, I dedicate all of this. You are the wisest and most genuine person I know. Thank you for always lifting me up in the toughest times, none of this would have been possible without you.

Declaration

Presented work has been carried out in roughly three years for the Award of the degree of Doctor of Philosophy by the University of Salford. This research has been funded by the Applied Bioscience for Health program of the Doctoral Training Alliance (DTA) scheme.

No portion of this work referred to in this thesis has been submitted in support of an application for another degree or qualification in this or any other university or other institutes of learning.

Although the author performed the majority of the experiments, part of the showed data is the result of the collaboration with other peers. Specifically, bioinformatic analyses on the microRNA NanoString screening, shown in paragraph 5.2.8, has been carried out by Paolo Fadda (The Ohio State University, OH, US) and analyses of the RNAseq data, shown in paragraphs 4.2.5.2 and 5.2.4, have been performed by Mattia Chiesa (Centro Cardiologico Monzino, Milan, Italy).

Abbreviations

3’	three prime
5’	five prime
BAK	BCL2 Antagonist Killer 1
BAX	BCL-2 associated X protein
BCL-2	B-cell lymphoma 2
BCL-XL	B-cell Lymphoma-Extra Large
BH3	BCL-2 Homology 3
bp	base pair(s)
cDNA	complementary DNA
CDK	cyclin dependant kinase
CDKi	cyclin dependant kinase inhibitor
CGCP	cerebellar granule cell precursor
CRISPR	clustered regularly interspaced short palindromic repeats
DMSO	dimethyl sulfoxide
DNA	deoxyribonucleic acid
FC	fold change
FACS	fluorescence-activated cell sorter
G3	group 3
G4	group 4
GO	gene ontology
IgG	immunoglobulin
IC50	inhibitory concentration at 50% effect
Kb	kilo base
kDA	kilo Dalton
MB	medulloblastoma
MCL-1	myeloid cell leukemia 1
miRNA	microRNA
MIZ-1	Myc-Interacting Zinc Finger Protein 1
mRNA	messenger RNA
OD	optical density
p	phospho

PCR	polymerase chain reaction
q	quantitative
Rb	retinoblastoma protein
RNA	ribonucleic acid
RNAi	ribonucleic acid interference
RT	reverse transcription
SD	standard deviation
SDS-PAGE	sodium dodecyl sulfate polyacrylamide gel electrophoresis
SEM	standard error of measurement
SHH	Sonic hedgehog
siRNA	small interfering RNA
UTR	untranslated region
WNT	Wingless

Abstract

Medulloblastoma (MB) is the most common malignant paediatric brain tumour accounting for about 20% of all childhood brain cancers. Over the last decade, a consensus has been reached over the existence of 4 main molecular subtypes, known as WNT-activated MB, SHH-activated MB, group 3 MB and group 4 MB. Despite their extreme heterogeneity, medulloblastoma patients are still uniformly treated with a combination strategy that encompasses surgery, radiation therapy and chemotherapy. The standard of care has now reached a plateau failing to cure more than 50% of the diagnosed children resulting in debilitating long-term side effects; therefore, there is an urgent need for developing new targeted therapies.

The aim of this PhD research was focused on expanding the knowledge of MB biology and providing tailored therapeutic options to be used in the clinic:

Project 1. A well-defined feature of MB is the genetic alterations of the cell cycle machinery, which controls cell cycle progression and transcription. Therefore, pharmacologic intervention to inhibit the activity of specific cyclin-dependant kinases (CDK) is an attractive therapeutic approach to boost MB standard of care, reducing morbidities associated with specific treatments.

Herein, we identified the pan-CDKi, dinaciclib, as a promising and more effective alternative to palbociclib, a CDK4/6 inhibitor currently pursued in clinical studies. We present evidence supporting dinaciclib's ability to inhibit MB proliferation, impair cancer stemness and induce apoptosis at considerably lower doses than palbociclib. Furthermore, sequencing data confirmed that dinaciclib is a potent apoptotic inducer, possibly through transcriptional shifts mediated by MYC downregulation and RNA polymerase II phosphorylation reduction.

Finally, we observed the *in vitro* pharmacological synergy when using dinaciclib with clinically used chemotherapeutic drugs and BH3 mimetics, an approach that may boost therapeutic efficacy and reduce treatment-related morbidities.

Project 2. Group 3 MB patients have the worst overall survival rates, with MYC amplification/overexpression being the strongest adverse prognostic factor. Furthermore, the repressive transcriptional complex formed by MYC and MIZ1 is required for the maintenance of the group 3 MB identity.

Considering the failure of MYC-targeted therapies and the importance of MYC/MIZ1 interaction, we hypothesised that targeting MIZ1 might represent a valid therapeutic strategy tailored to MYC-driven group 3 MB patients.

Here we proved that the knockdown of MIZ1 specifically inhibits proliferation of group 3 MB cells by reducing MYC expression and MYC-regulated microRNA networks. From computational predictions that identified miR-124-3p as a miRNA targeting MIZ1, we confirmed through luciferase assay in vitro that miR-124-3p binds to the 3' untranslated region of MIZ1 and represses its protein levels. Over-expression of miR-124-3p impairs proliferation of group 3 cells, mimicking the effects obtained after MIZ1 silencing. Transcriptomic analysis identified essential genes and pathways controlled by miR-124-3p in group 3 MB, which predominantly clustered around different aspects of cell cycle and cell division regulation determining vulnerable pathways that could be therapeutically pursued and targeted in future studies.

Finally, we show that miR-124-3p synergises with currently used chemotherapeutic agents, further highlighting the potential of miR-124-3p for the treatment of group 3 patients.

Chapter 1:

Background

1.1 Introduction to cancer

Cancer is a broad term that includes a collection of heterogeneous diseases, benign and malignant, which can be generally characterised by one predominant feature: an uncontrolled cell growth. Invasion is an additional property of cancer and is what separates malignant tumours from benign tumours. It occurs when cancerous cells detach from their primary site and infiltrate into surrounding tissues to form secondary tumours or metastasis (Bashyam, 2002). When reviewing cancer biology, it is mandatory to refer to the invasive propensity of the tumour, as it is a major prognostic factor for most cancers.

Overall, tumours are made of cells that have gone awry and escaped the strict regulatory system that controls proliferation and ensures homeostatic signals and functions of the primary tissue (Donley & Thayer, 2013).

There can be a variety of causes, inherited or acquired, that favour this cell deviance but, ultimately, all causes impact upon gene expression, which is why cancer is defined as a genetic disease. Tracing back to the control centre of the cell, the human genome in the nucleus holds those strict instructions, in the form of proteins or RNA, that make cells behaving normally. Gene alterations are called mutations, and they are responsible for acquired capabilities of the cells that progressively initiate them to be tumorigenic and subsequently malignant (Hanahan & Weinberg, 2000). Furthermore, epigenetic modifications that do not affect the DNA sequence but determine changes in gene expression are equally crucial for cancer acquired functions. Ultimately, malignant transformation is determined by the interplay of genetic and epigenetic mechanisms.

1.1.1 The hallmarks of cancer

In 2000, Hanahan and Weinberg described six acquired characteristics or hallmarks that are essential for cancer pathogenesis and progression: sustained proliferative signalling, evasion from growth suppressors, invasion and metastasis activation, induction of replicative immortality, angiogenesis promotion and cell death escape. Since then, these features have been used as a general guideline to understanding cancer's complex underpinnings since they are widely applicable, despite the evident diversity of cancers (Hanahan & Weinberg, 2000, 2011).

A decade later, the authors updated the hallmark model adding two “emerging” cancer characteristics: reprogramming of the metabolic processes and evasion of the immune response.

The metabolic rewiring translates specifically in the glycolytic dependence of cancer cells, which preferentially rely on glucose consumption to supply energy for cell growth and division (Hanahan & Weinberg, 2011).

Secondly, the evasion of the immune system comes from the theory that the immune system would control and block the rise of tumorigenic cells (cancer immune surveillance). Nonetheless, there is increasing evidence that tumours develop regardless of the immune system status and, if anything, cancer cells are shaped with immune resistant properties thanks to the immune selective pressure, in a process referred to as “cancer immunoediting”) (Fouad & Aanei, 2017)

Lastly, the authors identified two “enabling characteristics” necessary to acquire the hallmarks mentioned above. The first requirement is that cancer cells must accumulate mutations over time, which bypass DNA damage checkpoints and become genomically unstable. As previously mentioned, only through mutation can cancer cells acquire new functions and out-compete normal cells (Hanahan & Weinberg, 2000).

In the updated version of their cancer hallmarks, Hanahan and Weinberg added a new enabling trait, which is tumour-promoting inflammation. Notably, this addition to the panel has been considered controversial since inflammatory cells are active components of the immune system, and they are known to be tumour suppressive and favour response to immunotherapy (Fouad & Aanei, 2017). Nonetheless, inflammation might enhance and enable tumour progression by different mechanisms such as secretion of pro-survival, pro-migration, and anti-detection molecules to the tumour microenvironment (Hanahan & Weinberg, 2011).

With the fast-growing progress in cancer research and the knowledge regarding the widely applicable hallmarks of cancer development and progression, and enabling features, novel targeted therapies are emerging. Therapeutic options have been classified according to their ability to target specific cancer hallmarks, as shown in Figure 1.

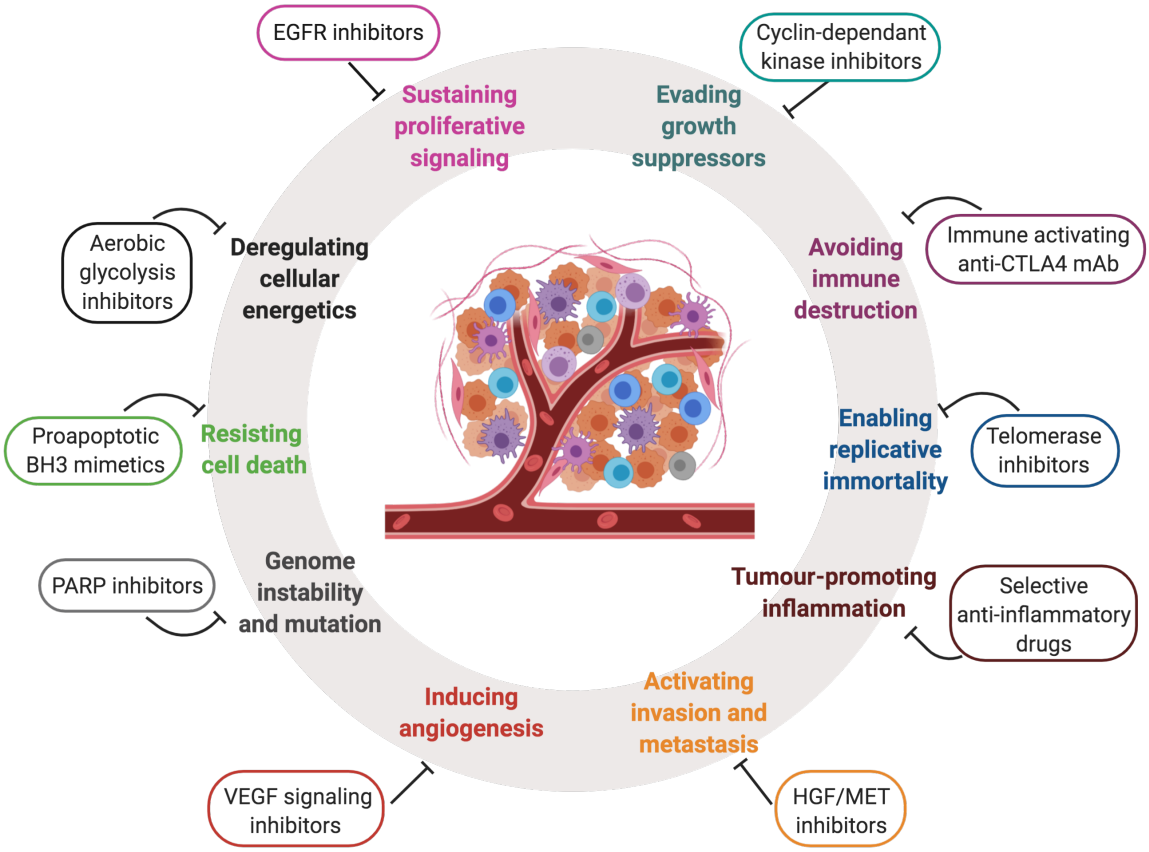

Figure 1 | The hallmarks of cancer and targeted therapies.

The figure, adapted from (Hanahan & Weinberg, 2011), illustrates the ten characteristics that shape cancer identity and respective targeting therapeutic strategies.

To date, more than 200 types of tumours have been described (CRUK 2017) and, even though they share common properties, diversification is still possible thanks to the varying degrees of dependency of different tumour types on the hallmarks and by the different mechanisms through which they can be acquired. For example, as previously mentioned, the most explicative feature of cancer cells is their autonomy in growth signals, which allows them to proliferate unconditionally. Cells can achieve that status by producing growth factor ligands themselves or stimulating adjacent stromal cells to produce proliferative growth factors, or they can increase the presence of receptors in the cell surface becoming more sensitive to growth factors.

Ultimately, this sustained heterogenous trend, extended to the other cancer features, is the cause of the current failure to pinpoint treatment and avoid resistance. Indeed, despite the

specificity of targeted treatments, cancer cells are still able to adapt from them to re-acquire functional tumorigenic features in a process known as cancer resistance, which is followed by relapse. The reasons why treatments fail and cancer cells become resistant can be different, there might be diverse parallel pathways to support core hallmarks so that a specific drug for one pathway is not sufficient to turn off completely the targeted functionality or cancer cells can modify their degree of dependence on a particular core feature and start relying more on other non-targeted features (Hanahan & Weinberg, 2011).

Therefore, despite an increased understanding of the determinants of cancer and improved lifestyle, cancer incidence in the developed world has continued to rise, with a lifetime risk of developing cancer in the UK of 50% for males and 45% for females, according to 2016 statistics, and this is projected to increase by 2% between 2014 and 2035 (CRUK,2020). Moreover, according to the latest cancer statistics of 2016, 363,615 people were diagnosed with cancer in the UK and, in 2017, 166,544 died because of it in the UK (CRUK, 2020).

These statistics highlight the urgent need to improve therapeutics and clinical outcomes.

1.1.2 Childhood cancer

According to Cancer Research UK statistics, childhood cancer, defined as cancer diagnosis in patients under 15 years of age, is quite rare representing only 1% of all new cancer cases in the UK, with cancer being predominantly a disease that affects the elderly (CRUK, 2020).

Central nervous system (CNS) tumours represent the second most common group of cancers under 14 years of age after leukaemia (Figure 2) and account for 34% of all cancer deaths in children (CRUK, 2020).

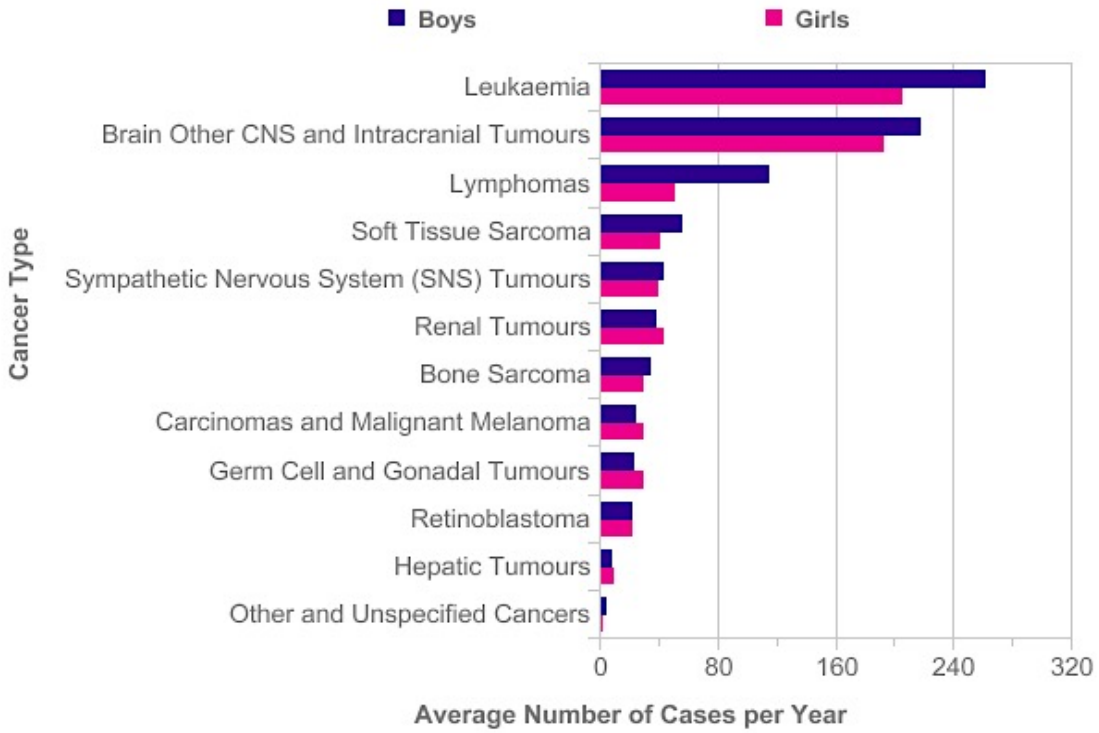

Figure 2 | Cancer incidence statistics for children (0-15 years old) in the UK (cruk.org/cancerstats).

Commonly, childhood cancers have an embryonic origin, in contrast to adult cancers, which primarily arise in regions derived from epithelial tissues.

The 2016 update of the WHO classification of embryonal tumours of CNS identifies four main variants: medulloblastoma, embryonal tumour with multilayered rosettes (ETMR), Atypical teratoid/rhabdoid tumours (AT/RT) and other CNS embryonal tumours, which includes medulloepithelioma, CNS neuroblastoma, CNS ganglioneuroblastoma, and CNS embryonal tumour not otherwise specified (Louis et al., 2016).

For the first time since 2007, this re-classification of embryonal tumours recognised the importance of the molecular advances to implement the existing histological features knowledge, in a new attempt to improve diagnosis and therapeutic approaches.

Medulloblastoma is by far the most common form, comprising 63% of intracranial embryonal neuroepithelial tumours (Ostrom et al., 2018).

1.2 Medulloblastoma: a disease with unique heterogeneity

Medulloblastoma (MB) is historically defined as an embryonic tumour, which arises from undeveloped precursor cells located in the cerebellum (Bailey & Cushing, 1925). It is the most common childhood malignancy of the brain and accounts for 20% of all brain tumours (Crawford et al., 2007). MB is predominantly diagnosed in children between 3 to 15 years old (70% of all diagnoses) although a 10-15% of cases are reported in young infants below 3 years of age (Crawford et al., 2007).

Medulloblastoma is the perfect example to highlight the striking heterogeneity of cancer, identifiable at every level of MB biology. In the last decade, multiple studies have tried to dissect MB heterogeneity, first at histopathological and then molecular levels, to identify diagnostic parameters that could provide the most effective patient stratification.

1.2.1 Histology of medulloblastoma

Firstly, according to the World Health Organization 2016 (WHO), MB is classified in five histological variants concerning pathological manifestation: classic, desmoplastic/nodular (D/N), medulloblastoma with extensive nodularity (MBEN), anaplastic and large cell medulloblastoma (Figure 3) (Louis et al., 2016).

Classic MB is the most frequent histological subtype, accounting for around 70% of all diagnoses (D. W. Ellison, 2010; Gilbertson & Ellison, 2008; Gulino et al., 2008; B. L. Pizer & Clifford, 2009). Phenotypically, is characterised by sheets of densely packed and undifferentiated cells, which are small, round and with a high nuclear/cytoplasm ratio. Nuclei are hyperchromatic and well visible after haematoxylin and eosin staining (D. Ellison, 2002). A small percentage of these tumours is also characterised by the presence of “rosettes”, which consist of nuclei arranged in a circular fashion around cytoplasmic processes (Gulino et al., 2008).

10-15% of MB patients are affected by Desmoplastic/Nodular medulloblastomas named after the presence of distinctive reticulin-free nodules of neurocytic cells in the tissue surrounded by more proliferative and desmoplastic cells in the reticulin-rich internodular space (D. W. Ellison, 2010; Gilbertson & Ellison, 2008; Gulino et al., 2008; B. L. Pizer & Clifford, 2009).

Medulloblastomas with Extensive Nodularity (MBEN) comprise 2% of all MB and are very similar to the D/N morphology having the same nodular and internodular regions, although in these tumours the first component is much more extensive than the second one. These tumours are often associated with a more favourable prognosis (D. Ellison, 2002; McManamy et al., 2007).

Anaplastic medulloblastomas are mainly characterised by regions of anaplasia, where nuclear pleomorphism, cell wrapping, high mitotic activity and apoptotic bodies are more diffused than other groups (Louis et al., 2007).

The Large Cell medulloblastoma variant shows cells with abundant cytoplasm, large nucleus and marked nucleoli (Giangaspero et al., 1992).

Often, MBEN and D/N medulloblastomas are further grouped as “desmoplastic” tumours, and Large Cell and anaplastic medulloblastomas are also combined (LCA) due to overlapping morphological and prognostic characteristics. Generally, MBENs and D/N medulloblastomas, which together account for 10-20% of cases, have been shown to have better outcomes than classic tumours, while LCA tumours, although present in 5-10% of patients are more aggressive with a mortality peak over 3 years of age (Eberhart et al., 2002; McManamy et al., 2007).

Overall, each subtype is ranked as grade IV cancer by the WHO 2016, underlying the undifferentiated appearance and the highly aggressive nature shared between subgroups.

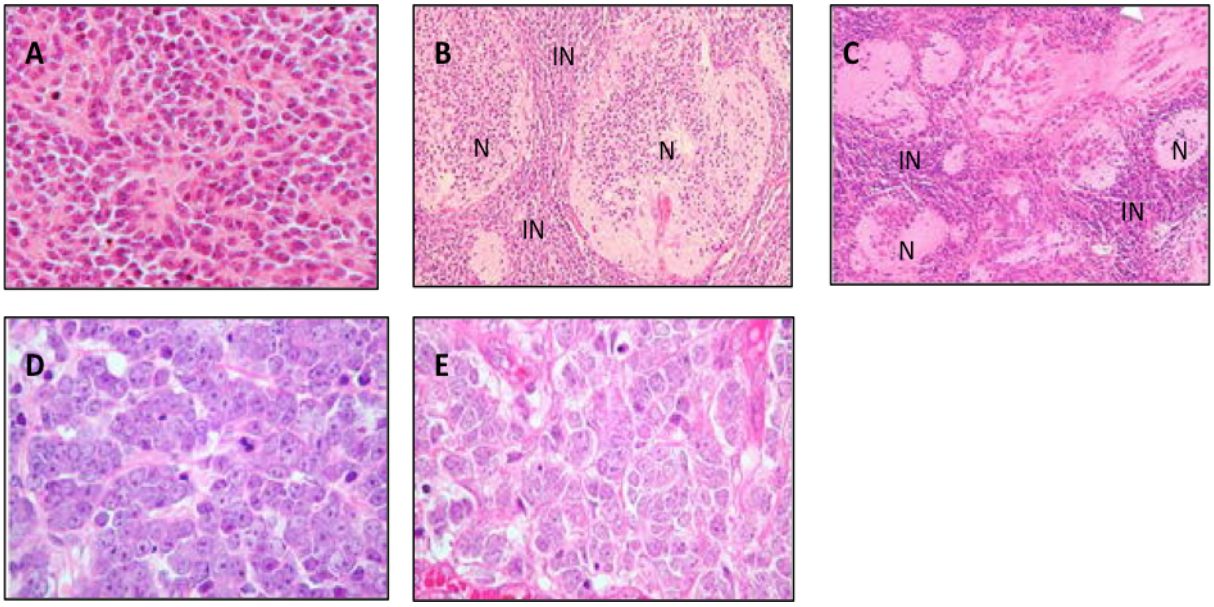

Figure 3 | Histopathological forms of medulloblastoma.

Microscopic sections of MB forms stained with haematoxylin and eosin:
A) Masses of small cells define classic MB. B) Desmoplastic/Nodular MB histology characterized by nodules (N) and internodules areas (IN) C) MBEN histology is very similar to desmoplastic/nodular MB histology with nodules (N) and internodules (IN). D) Anaplastic MB histological pattern displays an increased mitotic rate and a high number of apoptotic bodies. E) Large cell MB histology consists of enlarged nuclei and prominent nucleoli. Adapted from (D. W. Ellison, 2010).

1.2.2 Molecular classification of medulloblastoma

In the last decade, it became increasingly clear that a histology-based approach alone fails to acknowledge the striking intra-subgroup heterogeneity that most of the time is reflected in the differential outcomes for patients affected by the same variant. A considerable international effort to define the transcriptional identity of MB tumours (Kool et al., 2008; Northcott, Nakahara, et al., 2009; G. Robinson, Parker, Kranenburg, et al., 2012; Thompson et al., 2006) has come to a consensus over the existence of four main MB molecular subgroups: 1) Wingless (WNT) activated MB, 2) Sonic Hedgehog (SHH) activated MB, 3) Group 3 MB and 4) Group 4 MB (Northcott, Nakahara, et al., 2009; Taylor et al., 2012). WNT and SHH subgroups are better molecularly characterised and therefore are named after developmental pathways that are perturbed and are known to trigger initiation of those specific subgroups, while Group 3 and Group 4 are yet to be fully characterised. Table 1 presents a summary of the molecular and clinical features of each subgroup.

A distinctive gene background reflects differential outcomes for patients, other than explaining the cause. In the following paragraphs, a detailed outline of all MB sub-groups is presented.

1.2.2.1 Wnt-activated medulloblastoma

This variant comprises 10% of all medulloblastomas and is associated with the best prognosis for patients, with very rare metastatic diffusion and recurrence of the tumours (Juraschka & Taylor, 2019).

The characteristic molecular abnormalities of WNT MBs are mainly mutations in the β-catenin gene, *CTNNB1*. These mutations lead to constitutive activation of the WNT pathway fueling tumour proliferation (Clifford et al., 2006; Taylor et al., 2012).

The second most common aberrancy for WNT MBs lacking *CTNNB1* mutations is on the tumour suppressor APC gene (Waszak et al., 2018).

Other genes with common mutations are DDX3X (36%), SMARCA4 (19%), TP53 (14%, CSNK2B (14%), PIK3CA (11%) and EPHA7 (8%) (Jones, Jäger, et al., 2012; Northcott et al., 2017).

Only rare genomic aberrations have been described for this subgroup, with the deletion of one copy of chromosome 6 (monosomy 6) being the most frequent (79%) (Clifford et al., 2006; Shih et al., 2014; Taylor et al., 2012).

1.2.2.2 SHH-activated medulloblastoma

Patients are usually either infants (≤ 3 years old) or adolescents (> 16 years old) (Northcott et al., 2011), with a good 5-year survival rate of 75%. Infants and younger children have a better prognosis than adults (Schroeder & Gururangan, 2014). Metastatic forms are rare and associated with other poor prognostic factors such as LCA histology and older age at diagnosis (Roussel & Robinson, 2013).

In this context**,** the developmental control under SHH signalling pathway malfunctions at different levels resulting in constitutive activation of the pathway. Most commonly, the tumour suppressor gene PTCH1 is inactivated (43%) (Goodrich et al., 1997; Kool et al., 2014), which encodes for the Shh receptor, patched. In the absence of its ligand, the patched receptor binds to smoothened receptor (SMO) preventing signalling initiation within the cell. In MB, this brake is absent, leading to constitute activation of the SHH pathway.

Other common mutations that cooperate for the same signalling activation are deletion of SUFU (10%), which is another suppressor of SHH pathway, amplification of SMO (9%) and GLI2

(9%), which is a transcription factor normally activated by SMO, and MYCN (7%) (Jones, Jager, et al., 2012; G. Robinson, Parker, Kranenburg, et al., 2012).

TP53, KMT2D, TP53, BCOR, DDX3X, LDB1 are also found frequently mutated even if they are not strictly characteristic of SHH MBs (Jones, Jager, et al., 2012; G. Robinson, Parker, Kranenburg, et al., 2012; Zhukova et al., 2013).

Particularly, patients bearing TP53 mutations are currently considered a high-risk population (Ramaswamy et al., 2016).

1.2.2.3 Group 3 medulloblastoma

Group 3 is the most aggressive type of medulloblastoma, with a high frequency of metastasis at diagnosis and 5-year overall survival rate of 50% (Northcott, Shih, et al., 2012; Taylor et al., 2012). Few molecular features have been demonstrated to be responsible for the tumorigenesis of this subgroup. One of the most crucial genomic aberrations is the amplification of the oncogene c-Myc (15% of diagnosis), which is also associated with a worse prognosis. MYCN amplification is also accounted as driver factor in this subgroup, although it is less frequent than MYC aberrations (5%). Group 3 also harbours an OTX2 amplification, which is considered a master transcription factor for cerebellar development, and usually in a mutually exclusive fashion with MYC amplification, suggesting the existence of two different driving pathways for Group 3 tumourigenesis (Y. Lu et al., 2017). Less common mutations are found in chromatin remodelling proteins encoded by SMARCA4 (9%), KMT2D (5%), CTDNEP1 (5%) and multiple possible mutations in the lysine-specific demethylase (*KDM*) gene family (Northcott et al., 2011). Structural variations in enhancers position are responsible for the overexpression of the oncogenes GFI1 or GFI1B in these tumours (Northcott et al., 2014). Mostly, Group 3 tumours present widespread distinctive genome instability disclosed as a gain of chromosome 1q and 7, isochromosome 17q (predictive of outcome), and loss of 10q and 16q chromosomes (Northcott, Shih, et al., 2012).

1.2.2.4 Group 4 medulloblastoma

Group 4 tumours have a considerably higher incidence in males (3:1) (Taylor et al., 2012) and generally occur in children but may be found in adults (Roussel and Robinson, 2013).

Survival rates for this subgroup are intermediate, even though metastasis occurrence is frequent (Ramaswamy et al., 2016).

The most common drivers of group 4 tumours are the amplification of *MYCN* and CDK6 (6%), overexpression of PRDM6 (17%) and duplication of SNCAIP (Northcott et al., 2017). Isochromosome 17q is also observed and associated with high-risk patients (Schwalbe et al., 2017).

Additionally, mutations in chromatin-remodelling genes are described in this group, such as KDM6A, ZYMYM3, and CHD7 (6-9%) (Northcott et al., 2017).

Table 1 | Clinical and genomic features of medulloblastoma subgroups.
(Cavalli et al., 2017)

	Subgroup	WNT	SHH	Group 3	Group 4
Clinical Characteristics	% of Cases	10	30	25	35
	Age at Diagnosis				
	Gender Ratio (M:F)	1:1	1:1	2:1	3:1
	Anatomic Location				
	Histology	Classic, Rarely LCA	Desmoplastic, Classic, LCA	Classic, LCA	Classic, LCA
	Metastasis at Diagnosis (%)	5-10	15-20	40-45	35-40
	Recurrence Pattern	Rare; Local or metastatic	Local	Metastatic	Metastatic
	Prognosis	Very good	Infants good, others intermediate	Poor	Intermediate
Molecular Characteristics	Proposed Cell of Origin	Progenitor cells in the lower rhombic lip	Granule precursors of the external granule layer	Neural stem cells	Unipolar brush cells
	Recurrent Gene Amplifications	-	*MYCN* *GLI1* or *GLI2*	*MYC* *MYCN* *OTX2*	*SNCAIP* *MYCN* *OTX2* *CDK6*
	Recurrent SNVs	*CTNNB1* *DDX3X* *SMARCA4* *TP53*	*PTCH1* *TERT* *SUFU* *SMO* *TP53*	*SMARCA4* *KBTBD4* *CTDNEP1* *KMT2D*	*KDM6A* *ZMYM3* *KTM2C* *KBTBD4*
	Cytogenetic Events ■ Gain ■ Loss	6	3q, 9p 9q, 10q, 17p	1q, 7, 18 8, 10q, 11, 16q i17q	7, 18q 8, 11p, X i17q
	Other Recurrent Genetic Events	-	-	*GFI1* and *GFI1B* enhancer hijacking	*PRDM6*, *GFI1*, and *GFI1B* enhancer hijacking

Age: Infant Child Adult

1.2.3 The origin of medulloblastoma subgroups

Another factor that should be considered to understand MB complexity is that different MB subgroups trace back to the different anatomic site of origin in the embryonic cerebellum and to location-specific mutations, which account for differential cell fates (Gibson et al., 2010). From a histological point of view, desmoplastic subtypes seem to originate from precursors located in the fourth ventricle (Gilbertson & Ellison, 2008; Thompson et al., 2006) while classic variants seem to differentiate from precursors located in the rhombic lip, which forms after the closure of the neural tube during development (Gibson et al., 2010; Marino, 2000).

Furthermore, the generation of mouse models for the different MB subgroups shed light on the possible embryonic origin of the tumours. WNT MB arises from progenitor cells located in the embryonic dorsal brainstem (Gibson et al., 2010; Kawauchi et al., 2012; Taylor et al., 2012). SHH tumours arise from cerebellar granule cell precursors (CGCPs), which persist in the external granular layer (EGL), do not differentiate and do not migrate in the internal granular layer (IGL) of the developing cerebellum (G. H. Huang et al., 2016; Vladoiu et al., 2019). Group 3 and group 4 origin is still not well characterised, particularly group 4's where preclinical models recapitulating tumour development are lacking. Nonetheless, both subgroups might originate in similar locations from neural stem cells in the hindbrain or the brainstem (Figure 4).

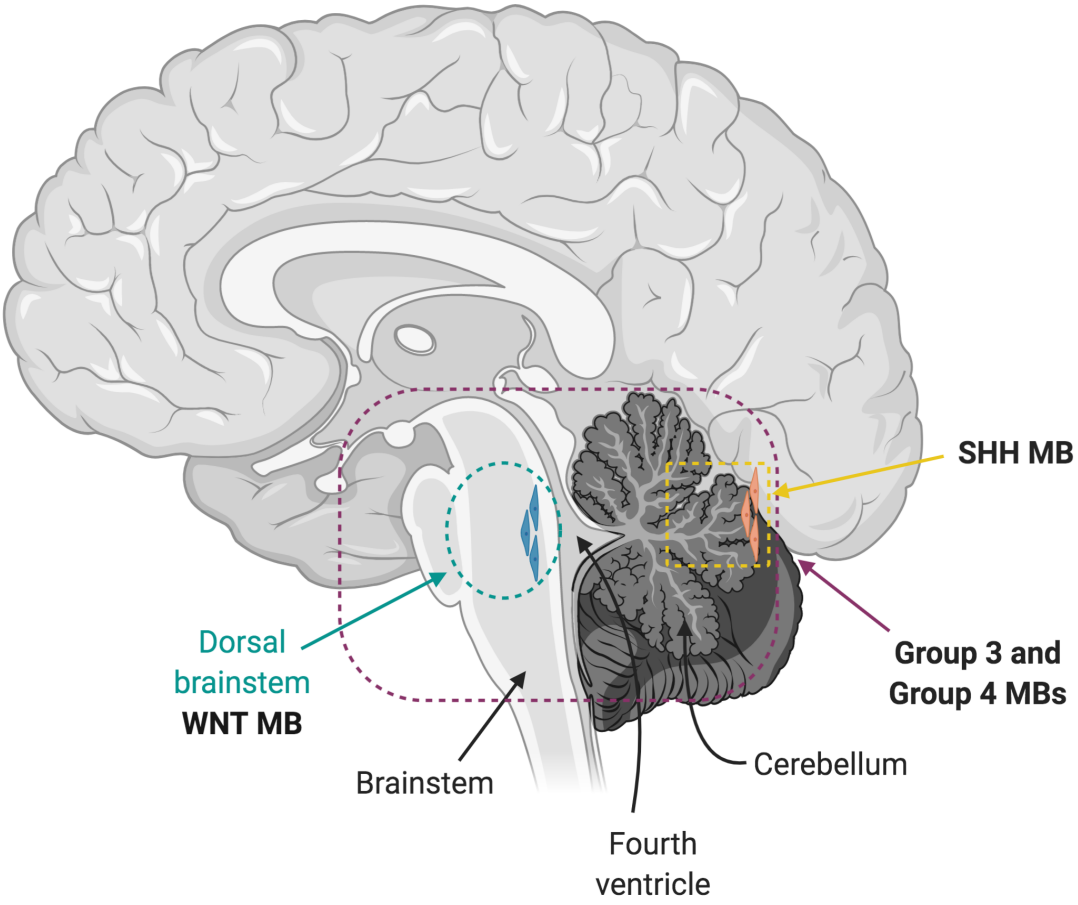

Figure 4 | Different origins of medulloblastoma subgroups.

The figure outlines the different anatomical sites of origin of medulloblastoma. MB subgroups originate from dysregulation of normal cerebellum developmental processes. It all starts from a few neural progenitors, differentially located, that undergo specific pathway and driver gene alterations.

To date, it is well established that there is a fine line between embryogenesis and tumorigenesis, as they share the same pathways involved in proliferation, differentiation, programmed cell death and angiogenesis to name a few which, if inappropriately activated, turn healthy tissues into tumours (Gilbertson & Ellison, 2008; Kelleher et al., 2006; Silvia Marino, 2005b). Cerebellar developmental stages are finely orchestrated by those pathways that are found deregulated at different gene levels in the cerebellar progenitor cells.

These oncogenic driver pathways and common mutations define MB subgroup identity, as they were explored in detail in the previous paragraph.

1.2.4 Risk stratification of medulloblastoma

Risk stratification is required to design appropriate treatment regimens for patients. For the past few decades, clinicians during patients evaluation took into account age at diagnosis, the extent of surgical resection, metastatic stage and histological variant (Pei et al., 2016). Broadly in this system, patients older than 3 years of age are deemed "standard risk" if they do not present metastasis at diagnosis (namely M0 according to Chang staging classification (Laurent et al., 1985)), having total or near-total surgical resection (less than 1.5cm^2) and with classic histology tumours. All the other patients were classified as "high risk" if presenting metastatic tumours (ranging from M1 to M4 stage) at diagnosis, residual tumour greater than 1.5cm^2 and other histological variants (Dhall, 2009; B. Pizer & Clifford, 2008; B. L. Pizer & Clifford, 2009).

In 2016, molecular features were integrated with the traditional phenotype-based classification of medulloblastoma from 2007, accounting for better prediction of prognosis (S. L. Pomeroy et al., 2002). In the new WHO classification, the main revision for medulloblastomas concerns SHH MB subgroup, which has been further sub-classified SHH-TP53 wild type, SHH-TP53 mutant (Table 2) (Louis et al., 2016).

Table 2 | Summary of the 2016 WHO Classification of medulloblastoma and clinical correlations. (Archer, 2017)

WHO classification subgroup	Histology subtype	**Prognosis and demographic notes**
Medulloblastoma, WNT-activated	Classic	Low risk
	Large cell/anaplastic (very rare)	Uncertain clinicopathological significance
Medulloblastoma, SHH-activated, TP53 mutant	Classic (rare)	High risk
	Large cell/anaplastic	High risk; prevalent in children aged 7–17 y
	Desmoplastic/nodular (very rare)	Uncertain clinicopathological significance
Medulloblastoma, SHH-activated, TP53 wild type	Classic	Standard risk
	Large cell/anaplastic	Uncertain clinicopathological significance
	Desmoplastic/nodular	Low risk in infants; prevalent in infants and adults
	Extensive nodularity	Low risk in infants
Medulloblastoma, non-WNT/non-SHH, group 3	Classic	Standard risk
	Large cell/anaplastic	High risk
Medulloblastoma, non-WNT/non-SHH, group 4	Classic	Standard risk
	Large cell/anaplastic (rare)	Uncertain clinicopathological significance

WNT = wingless; SHH = Sonic hedgehog

More recently, risk stratification criteria have also been updated and tailored on MB subgroups and specific molecular aberrations, such as MYC and MYCN amplification, defining a consensus on four new risk categories: low risk (>90 % survival), standard risk (75–90 % survival), high risk (50–75 % survival) and very high risk (<50 % survival) (Table 3) (Ramaswamy et al., 2016).

Table 3 | Risk stratification for medulloblastoma patients ages 3-17 years old.
(Juraschka and Taylor 2019)

<table>
<tr><th>Risk Category</th><th>Low Risk</th><th>Standard Risk</th><th>High Risk</th><th>Very High Risk</th></tr>
<tr><td>Survival (%)</td><td>>90</td><td>75-90</td><td>50-75</td><td><50</td></tr>
<tr><td rowspan="3">Subgroup, clinical and molecular characteristics</td><td>Non-metastatic</td><td>Non-metastatic, TP53 WT and no MYCN amplification</td><td rowspan="2">One or both:
• Metastatic
• MYCN amplification</td><td rowspan="2">TP53 Mutation</td></tr>
<tr><td rowspan="2">Non-metastatic and Chromosome 11 loss</td><td>Non-metastatic and no MYC amplification</td></tr>
<tr><td>Non-metastatic and no chromosome 11 loss</td><td>Metastatic</td><td>Metastatic</td></tr>
</table>

MB classification is in continuous evolution, revealing the struggle of confining MB heterogeneity into strict parameters. While acknowledging the importance of genome-based criteria is the first step towards more individualised targeted therapy, a lot still needs to be done to improve the cross-talk between the bench and the clinic.

1.2.5 Current treatment and future perspectives

Appropriate therapeutic choice directly follows patient risk stratification, the criteria of which have been updated and improved as discussed in the previous paragraph.

To date, the standard of care for medulloblastoma is a combination of surgery, craniospinal irradiation and chemotherapy (Kool et al., 2008; Northcott, Shih, et al., 2012). Overall, this therapeutic strategy achieves long term event-free survival rates of 60% for patients with metastatic tumours and 80% for patients with non-metastatic medulloblastoma (Packer et al., 2006). Nonetheless, almost all of the survivors face debilitating late complications that each of the therapeutic options might cause (Moxon-Emre et al., 2014).

As mentioned, surgery is usually the first option, in applicable cases, after diagnosis. It is mainly performed to alleviate symptoms caused by tumour mass, such as increased intracranial pressure (headache) and ataxia. One of the major drawbacks that have been reported in 25% of cases after surgery is the occurrence of the cerebellar mutism syndrome that leads to detrimental effects on speech ability (Wibroe et al., 2017), in addition to the risk of other neurocognitive deficits that might occur from performing surgery in such critical regions of the brain, even more so in children (Northcott et al., 2017; Rutkowski et al., 2005).
Adjuvant therapy is started within a month from surgery with radiation therapy to the brain and spinal cord, which positively kills medulloblastoma radiosensitive cells. However, the price for improved survival is the occurrence of secondary cancers, hearing loss, cardiovascular dysfunctions, hormone deficits, growth and cognitive impairments (Bansal et al., 2015; Gurney et al., 2003; Packer, 2008). Efforts to reduce these adverse effects, especially in younger children have taken place. Currently, proton beam technology is being examined in place of photon-based therapy to lower doses and for more targeted delivery of radiation, sparing exposure to adjacent tissues, although evaluations on this matter are still in early stages (Giantsoudi et al., 2016; Yock et al., 2016).
After 6 weeks from radiotherapy, multi-drug chemotherapy is adopted. The most common chemotherapeutic agents used are vincristine, cisplatin, cyclophosphamide and lomustine. Cycles of a different combination of these agents have been implemented as they have different ability to stop vital tumour functions, interfering for example with mitosis and cytostructures (vincristine) or with DNA replication and transcription (alkylating agents), and therefore potential different combinatory effects. Chemotherapy as well can result in delayed effects among which secondary tumours (i.e. leukaemia after alkylating agents), ototoxicity and infertility are the most frequently documented (Packer et al., 1999, 2006).
Due to the detrimental cognitive effect that radiotherapy has proven to have on infants, the current standard of care for these patients is surgery and chemotherapy only, even at high dosage (Duffner, 2004; Fouladi et al., 2008; Merchant et al., 2008; Mulhern et al., 2017).
Taken together, these observations highlighted the urgency of developing more risk-adapted and targeted therapies to reduce side-effects and improve survival. For instance, this led current clinical trials (NCT01878617, NCT02066220, NCT02724579, NCT02212574) for the low-risk WNT-activated MB subgroup investigating the possibility of reducing conventional therapy to improve patient's quality of life and reduce long-term sequelae.

The understanding of the molecular underpinnings of medulloblastoma and the improved prognostication have brought new targeted strategies to be tested in clinical trials, holding the great promise to change MB care once and for all.

Different drugs have been recently studied for SHH-activated MB treatment, which can be easily explained by the fact that molecular mechanisms underlying SHH tumourigenesis are mostly defined. Recently, SMO antagonists have been studied to contrast the unrestrained SHH signalling activation. A specific SMO inhibitor, called vismodegib, proved to be effective in phase II on a small cohort of SHH MB patients harbouring PTCH1 or SMO mutations, although its effect seems to be temporary and valid only for this sub-population (80% of SHH patients) (Buonamici et al., 2010; Ransohoff et al., 2015; G. W. Robinson et al., 2015; Zhukova et al., 2013). Another recent study showed how the multikinase inhibitor foretinib hampers, *in vitro* and in preclinical murine models, SHH MB tumour growth and invasion by targeting c-Met, which is directly responsible for metastatic variants of this subgroup, suggesting the potential for clinical evaluation (Faria et al., 2015). Another clinical trial (https://clinicaltrials.gov/ct2/show/NCT03434262) is evaluating the effects of the treatment with the CDK4/6 inhibitor ribociclib and trametinib, gemcitabine or sonidegib on resistant SHH MB.

Experimental studies on Group 3 MB have flourished in the past few years, drawn by its particularly dismal prognosis, trying to decode an underlying molecular order for this subgroup. Particularly, given that MYC amplification is a critical marker for poor outcome, efforts have been directed towards MYC inhibition. Currently, two promising agents effective against MYC-overexpressing tumours (Morfouace et al., 2014), pemetrexed and gemcitabine, have been included in an ongoing trial (SJMB12), which is testing new possible drug combination for high-risk Group 3 and 4 with c-MYC/MYCN amplification (S. Pomeroy et al., 2017).

In another attempt to target MYC, inhibitors of BET bromodomain proteins, which cooperate for the functions of MYC, have been studied (Delmore et al., 2011). Specifically, JQ1 a BRD4 inhibitor proved to be effective suppressing MYC transcription and because of that inhibiting cell viability and promoting senescence *in vitro* and in xenograft models of MYC-amplified MB (Bandopadhayay et al., 2014; Venkataraman et al., 2014). JQ1 has a short half-life, which does not allow clinical practice but a phase I clinical trial is ongoing to test other BET inhibitors (CPI-

0610, MK-8628) in adults (Archer et al., 2017). So far, no direct MYC targeting strategy has been successful, and mainly this is since MYC has no characterised ligand-binding domain.

A clinical trial testing the efficacy of palbociclib, a CDK 4/6 inhibitor, in paediatric brain tumours is ongoing (NCT02255461). This directly followed the promising results of a preclinical study, where MYC-amplified Group 3 mice improved survival rates after palbociclib treatment (Cook Sangar et al., 2017).

Epigenetic targeting molecules, which have been shown to have predominantly cytostatic effects, are also studied in combination with cytotoxic drugs to boost antitumourigenic effects. The HDAC inhibitor vorinostat proved to be effective when in combination with temozolomide or bortezomib in two completed phase I clinical trials (NCT01076530, NCT00994500) for paediatric patients with recurrent CNS tumours (Gopalakrishnan et al., 2015; Hummel et al., 2013; Muscal et al., 2013). Currently, vorinostat is being tested in combination with isotretinoin and chemotherapy in young patients with embryonal CNS tumours (NCT00867178) (Gopalakrishnan et al., 2015).

Finally, Group 4 MB, despite being the most common medulloblastoma, is also the most heterogeneous and least understood variant. The lack of clearly characterised driving oncogenes represents a major drawback for the development of targeted therapies for this variant.

1.3 Cell cycle

Cell cycle is a controlled process through which cells can proliferate, dividing and duplicating genetic information. Proliferation occurs with the progression of the four distinct phases of the cell cycle: G1, S, G2 and M and advancement through these phases is strictly regulated by positive and negative signals (Otto & Sicinski, 2017). Specifically, there are mitogenic proteins such as cyclins and cyclin-dependent kinases (CDKs), which form complexes that favour cell cycle progression and their negative regulators (CDK inhibitors) represented by proteins belonging to the INK4 family ($p16^{INK4A}$, $p15^{INK4B}$, $p18^{INK4C}$, $p19^{INK4D}$) and the CIP/KIP family ($p21^{CIP1}$, $p27^{KIP1}$, $p57^{KIP2}$) (Malumbres & Barbacid, 2001) (Figure 5).

CDKs are a family of serine-threonine kinases, which are always present in the inactive form. Different CDKs are activated by specific cyclins produced at a specific time of the cell cycle, forming heterodimer complexes with partner CDKs, in which cyclins constitute the regulatory subunits and CDKs the catalytic subunits.

The role of CDKs is not limited to cell cycle progression. Only CDK2, CDK4 and CDK6 are involved in interphase and CDK1 in mitosis (M). Another essential subgroup of CDKs such as CDK7, CDK8, CDK9, CDK11 and CDK20, are involved in regulating transcription (Malumbres, 2014). CDK9, for example, is the catalytic subunit of the positive transcription elongation factor b (P-TEFb) multiproteic complex, which in association with Cyclin-T1, phosphorylates the carboxyl-terminal domain (CTD) of the RNA polymerase II at Ser2 allowing the RNA transcription elongation (Garriga & Graña, 2004)(Rickert et al., 1996). Similarly, CDK7 is a component of the TFIIH complex, which, bound to cyclin H, also phosphorylates the CTD domain of the RNA polymerase II but at Ser5 and Ser7 regulating transcription initiation (Malumbres, 2014).

Furthermore, despite CDK5 being classified as a cell cycle kinase, it is considered an atypical CDK since its activation is primarily dependent on non-cyclin proteins (P35 and P39), which are mainly expressed in neurons, and for its broad influence on gene expression, differentiation and senescence among other mechanisms (Arif, 2012; Cheung, Zelda H Ip, 2012).

The two overarching stages of the cell cycle are the interphase, where most of the cell growth occurs, and mitosis. Most of the cells do not advance in the cell cycle towards cell division, but they are rather arrested in the so-called G0 stage. Mitotic signals can be responsible for

stimulating those cells to re-enter the cell cycle, but some will permanently remain in G0 as differentiated or senescent cells (Otto & Sicinski, 2017).

The first and longest phase of the cell cycle is G1, where cyclin D is produced under mitogenic stimulations to activate CDK 4/6. Cyclin D/CDK4/6 complex is responsible for the phosphorylation of the retinoblastoma tumour suppressor protein (Rb) and for switching cells from G1 to S phase. Hyperphosphorylation of Rb abolishes its suppressive influence on the transactivation domain of the E2F transcription factors leading to the activation of genes involved in cell cycle progression, including cyclin E and A and other genes involved in DNA replication among other processes (Dimova & Dyson, 2005; Soucek et al., 1997). Importantly, cyclin E/CDK2 complex further phosphorylates Rb protein, creating a positive feedback loop and fuelling even more G1/S transition. Cyclin D/CDK4/6 are in turn accountable for maintaining the activation of CDK2 by sequestering $p21^{CIP1}$ and $p27^{KIP1}$ which would otherwise inhibit CDK2 activation (Bornstein et al., 2003; Harbour et al., 1999; Lundberg & Weinberg, 1998; Montagnoli et al., 1999). Cyclin A is required in the S phase where it is specifically produced becoming more abundant than cyclin E to favour complexing with CDK2 and inducing DNA synthesis. In the G2 phase, cyclin A-CDK1 complex is formed and eventually, upon degradation of cyclin A, cyclin B is solely present in the G2 phase to bind CDK1 favouring the mitotic entry (Schafer, 1998).

As previously mentioned, inhibitory signals are exerted by the upregulation of INK4 and CIP/KIP families, where INK4 proteins inhibit CDK4 and CDK6, while CIP/KIPs mostly block the activity of CDK2 and CDK1. On top of these negative regulators, ubiquitylation of specific cyclins is a key mechanism for the cell to move out of one phase and into the next, further controlling the timing of activity of each specific cyclin/CDK complex. This process allows the targeting of the cyclin by proteasome and irreversible degradation (Hershko, 1997; Weissman, 2001).

Finally, cell cycle checkpoints are pivotal to detect DNA damage (i.e. single or double-strand breaks), arrest the cell cycle and allow repair before normal cell growth and division can occur. At the end of G1 phase, DNA damage is sensed by checkpoint kinase 2 (CHK2), which activates P53 tumour suppressor and in turn P21. P21 inhibits CDK/cyclins complexes and leads to cell cycle arrest and DNA repair (El-Deiry et al., 1993). Conversely, activated CHK1 mediates cell cycle arrest in S and G2 phases (O'Connell et al., 1997; Sanchez et al., 1997).

As previously discussed, cell cycle dysregulation is one of the ten hallmarks of cancer cells. Cells that progress unchecked throughout cell cycle phases will gain genomic instability and acquire oncogenic functions growing uncontrollably, forming malignant masses and eventually spreading in the body.

Among all cancers, many cell cycle abnormalities have been associated with medulloblastoma. In the past decades, studies have supported the idea that aberrant cell growth from CGCPs, which mainly give rise to SHH MBs, is mediated by lesions of pRB pathway, which is responsible for cell genomic instability and MB development (Marino 2005; Bhatia 2010). Focal amplification and overexpression of CDK 4/6 and CCND1/2 genes were found to be triggers of pRB inactivation and oncogenic phenotype in childhood medulloblastoma (Cook Sangar et al., 2017). Despite CDK2 having been shown to be dispensable in several tumour types, it is required in MYC-overexpressing malignancies to inhibit senescence mediated by the Ras pathway (Campaner et al., 2010; Gillam et al., 2015; Hydbring & Larsson, 2010; Macias et al., 2007; Martín et al., 2005; Padmakumar et al., 2009). CDK2 together with CDK1 phosphorylation is indeed critical for MYC protein stability (Hydbring & Larsson, 2010; Sjostrom et al., 2005). At the same time, overexpression of MYC activates CDK2 and increases cyclin A/E gene expression, pushing cell cycle progression (Amati et al., 1998; Jansen-Durr et al., 1993).

Uziel et al. reported that loss of the cyclin D-dependent kinases inhibitor, $p18^{Ink4c}$, contributes to enhancing proliferative properties of MB cells in mice pointing once more towards the importance of an aberrant Rb pathway background for MB tumorigenesis (Uziel et al., 2006). Interestingly, CDK5 has been recently shown to be correlated with cell cycle due to its ability to phosphorylate Rb and pathways such as DNA repair and apoptosis through the activation of CK1 (Ianes et al., 2016; Pozo et al., 2013).

Finally, overexpression or amplification of CDKs has been reported in medulloblastoma accounting for an adverse prognosis for patients (Song et al., 2019; Whiteway et al., 2013).

Overall, uncontrolled cell proliferation has been the focus of study for cancer research and the regulatory molecules of this cell cycle machinery have been considered potential targets for therapeutic approaches (Otto & Sicinski, 2017). More importantly, CDKs have proven to be highly responsive to drugs, becoming attractive targets for cancer therapy (Shapiro, 2006).

In the past few years, many effective CDKis have been developed, as will be discussed further in the next section.

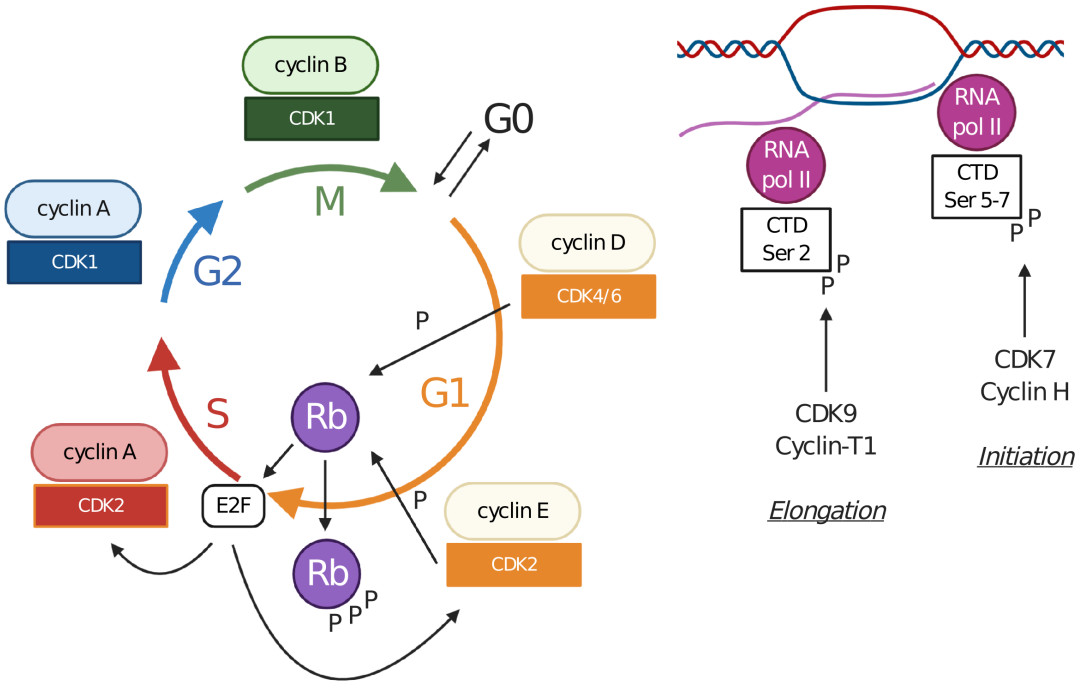

Figure 5 | CDKs regulation of cell cycle and transcription.

The cell cycle is divided into 4 phases: G1, S, G2 and M. G0 is a quiescent phase. The initiation of the cell cycle in G1 is regulated by cyclin D-CDK4/6 complexes, which start Rb phosphorylation that is continued by cyclin E-CDK2 complexes. Rb becomes hyperphosphorylated and releases the E2F transcription factors, which in turn induce the transcription of genes that allow cell cycle progression. Cyclin A-CDK2 control the S-phase and DNA synthesis and, lastly, cyclin A-CDK1 and cyclin B-CDK1 complexes regulate the G2-M phase. Transcription is controlled by the phosphorylation of the CTD domain of the RNA pol II by CDK7 and CDK9. CDK7 activity starts the elongation step of transcription, whereas CDK) activity controls the elongation of the RNA.

1.3.1 CDK inhibitors

Over the years, many strategies have been considered when attempting to inhibit CDK activity, and to date over 50 compounds have been described (Fischer, 2001). Despite their chemical differences, all CDK inhibitors are low molecular weight compounds that inhibit the activation of CDK catalytic activity, binding to ATP-binding site (Knockaert et al., 2002).

The first compounds ever-created exhibited poor specificity towards individual CDKs, and they are known as "pan-CDK inhibitors". Flavopiridol (Tolero Pharmaceuticals) represents the most significant first-generation compound being the first to be tested in clinical trials in 1997 and pursued until phase II (Otto & Sicinski, 2017). Although promising results from preclinical studies, flavopiridol is considered not effective to be used in single-agent therapy due to high toxicities at therapeutic concentrations, especially in solid tumours (Aklilu et al., 2003; Burdette-Radoux et al., 2004; G. Liu et al., 2004).

More selective and potent drugs were then created, given the failure of the first generation of CDKi. Dinaciclib (Merck & Co.), AT7519 (Astex Therapeutics) and milciclib (Tiziana Life Sciences) are referred to as second-generation CDKis.

Among these, dinaciclib has been the most extensively studied in the clinic. Dinaciclib inhibits CDK 1, CDK 2, CDK 5 and CDK 9 activity at IC_{50} values in the 1-4 nM range *in vitro*. It is more than 100 times more effective in RB phosphorylation inhibition and has a therapeutic index more than 10 times higher than flavopiridol (Parry et al., 2010). Unfortunately, preclinical studies and early clinical trials demonstrated little activity and cytotoxicity of dinaciclib in a variety of tumours such as non-small cell lung cancer, acute leukaemias (AML and ALL), triple-negative breast cancer (Flynn et al., 2015; Gojo et al., 2013; Mita et al., 2014; Stephenson et al., 2014). However, studies from phase I/II show partial responses in patients with relapsed multiple myeloma (Kumar et al., 2015). Besides, last year a phase III clinical trial was just terminated due to "program prioritization and reasons unrelated to safety or efficacy issues occurred", nonetheless showing that dinaciclib treatment could result in a better progression-free survival and overall survival than ofatumumab for patients with relapsed/refractory chronic lymphocytic leukaemia (CLL) (Ghia et al., 2017).

Interestingly, MYC-dependant tumours proved to be uniquely sensitive to dinaciclib. Dinaciclib displayed high efficacy in preclinical mouse models of MYC-overexpressing triple-negative breast cancer and MYC-driven B cell lymphomas were induced tumour regression and improved survival (Gregory et al., 2015; Horiuchi et al., 2012). Moreover, dinaciclib

significantly reduced growth in several patient-derived T-cell acute lymphoblastic leukaemia (T-ALL) cell lines and a T-ALL cell xenograft model (Moharram et al., 2017).

Currently, a phase I study is investigating the use of dinaciclib in combination with pembrolizumab in patients with advanced breast cancer, with interest in the relationship between MYC-status and clinical response (NCT01676753).

In brain tumour settings, such as in neuroblastoma, dinaciclib has been proven to be very effective *in vitro* and *in vivo* in MYCN transgenic mouse model. In MYC-driven MB, combination therapy targeting CDK2 and BET bromodomains to impair MYC stabilisation efficiently reduced group 3 MB tumour growth *in vivo* and promoted apoptosis (Bolin et al., 2018). Finally, dinaciclib was also shown to enhance cell sensitivity to chemotherapy (X. X. Chen et al., 2015), further suggesting the potential benefit of using this drug in combination therapies.

In the past decade, three specific CDKis against CDK4/6 demonstrated to be clinically successful: palbociclib (Pfizer), ribociclib also known as LEE01 (Novartis) and abemaciclib (Eli Lilly) (Sherr et al., 2016).

Palbociclib and ribociclib are approved by the Food and Drug Administration (FDA) for the treatment of advanced breast cancer (Finn et al., 2016; Hortobagyi et al., 2016). Palbociclib has been frequently studied for medulloblastoma treatment. Palbociclib treatments resulted in increased radiosensitivity in medulloblastoma while its antineoplastic properties were reduced when combined with chemotherapy (McClendon et al., 2012; Whiteway et al., 2013). Palbociclib blocks tumour growth in Patient-Derived Xenograft (PDX) mouse models of SHH and Group 3 medulloblastoma (Cook Sangar et al., 2017). Although palbociclib studies seem promising for its use in the treatment of Group 3 and SHH medulloblastomas, the persistence of tumour cells is still a concern.

Overall, despite CDKis proved to have quite successful effects on cell cycle, still a lot has to be done regarding pharmacokinetic and pharmacologic profiles of these compounds. One of the main difficulties that has been encountered in the clinic is defining an appropriate administration and sequence schedule maintaining reasonable toxicity ranges. Combination treatments of CDKis and cytotoxic drugs are often referred to as necessary to eradicate tumours (Diaz-Padilla et al., 2009; Malumbres et al., 2008).

1.4 MYC in medulloblastoma

c-MYC is part of the MYC protein family, together with MYCN and MYCL (Roussel & Robinson, 2013). These proteins are basic Helix-loop-Helix (bHLH) transcription factors the activity of which strictly depends on the interaction with other bHLH co-factors, namely MAX and MIZ-1. MYC/MAX heterodimer works as a transcriptional activator binding to Enhancer-box (E-box) sites, while MYC/MIZ-1 interaction results in the transcriptional repression of target genes (Wiese et al., 2013).

Lack of MYC proteins is embryonic lethal in mice since they are crucial for normal development (Davis et al., 1993; Stanton et al., 1992). Moreover, MYC proteins regulate numerous cellular processes such as proliferation, differentiation, cell cycle progression, metabolism and apoptosis, mainly controlling transcription of associated genes through different regulatory mechanisms (Eilers & Eisenman, 2008; Tansey & P., 2014). For example, MYC promotes cell cycle progression by inducing the expression of cyclin D2, CDK4 and E2F members, which play a crucial role for G1/S transition, and alternatively inhibiting the expression of p21 and p27 when bound to MIZ1 (Bretones et al., 2015; Nasi et al., 2001). In the same way, MYC triggers apoptosis by controlling the balance between pro-apoptotic and anti-apoptotic genes. MYC reduces the expression of the anti-apoptotic BCL-2 and BCL-XL proteins and, at the same time, induces pro-apoptotic proteins such as BIM and BAX (Eischen et al., 2001; Mitchell et al., 2000; Muthalagu et al., 2014).

As a consequence of their crucial role in key cellular functions, when MYC members activity is upregulated, they switch into potent oncogenes that have been associated with more than half of human cancers, especially c-Myc (Dang, 2012).

Amplification or overexpression of MYC family members (c-Myc and MycN) is found in the most aggressive forms of medulloblastoma tumours (Roussel & Robinson, 2013). As already mentioned, MycN amplification accounts for a more invasive and drug-resistant variant of SHH MB (D. W. Ellison et al., 2011; Kessler et al., 2009) and c-Myc amplification is a defining feature in Group 3 pathogenesis, associated with worst prognosis among all MB subgroups (Northcott, Jones, et al., 2012). A peculiar feature of MB is that MYC family members expression is subgroup-specific and context-specific for the different MB cerebellar progenitors. While SHH and group 4 MBs are associated with MYCN expression, group 3 and WNT subgroups express predominately MYC (G. Robinson, Parker, & Kranenburg, 2012). In 2012 Kawauchi et al. demonstrated that overexpressing MYC in murine GCNPs resulted in

group 3 MB tumour-like formation, whereas the same degree of overexpression of MYCN in the same precursors originated SHH MB (Kawauchi et al., 2012).

The biological reasons behind these differential fates are still not completely understood.

MYC tumorigenic functions are more significantly linked with group 3 MB than other subgroups, where its expression is mostly a marker of SHH or WNT pathway activity (Roussel & Robinson, 2013). Additionally, Vo et al. recently showed that group 3 development is enabled by the interaction between MYC and MIZ-1, which represses important genes for neuronal differentiation and fosters tumour progression (Vo et al., 2016). Interestingly, the same group showed that MYC and MYCN have a different binding affinity with MIZ-1, although MYC proteins have always been considered to be functionally redundant, and that this would be a determinant of MB subgroup. MYCN has a lower binding affinity for MIZ1, leading to a weaker gene expression reduction and to a typical genetic background for SHH MB. Alternatively, MYC has a higher affinity for MIZ-1 and strongly represses genes involved in neuronal differentiation allowing group 3 MB to retain a stem-like state (Figure 6) (Vo et al., 2016).

MIZ1 expression is found widespread in the developing cerebellum, and it can act as a positive or negative regulator of transcription depending on binding partners (Wanzel et al., 2003).

To date, MYC targeting strategies still have not met the clinical need. As mentioned before, this is mainly due to the lack of MYC druggable binding sites and to MYC tangled transcriptional regulations. Therefore, the targeting of MYC down-stream pathways or interactors is currently the most favourable way to hamper MYC-driven tumours.

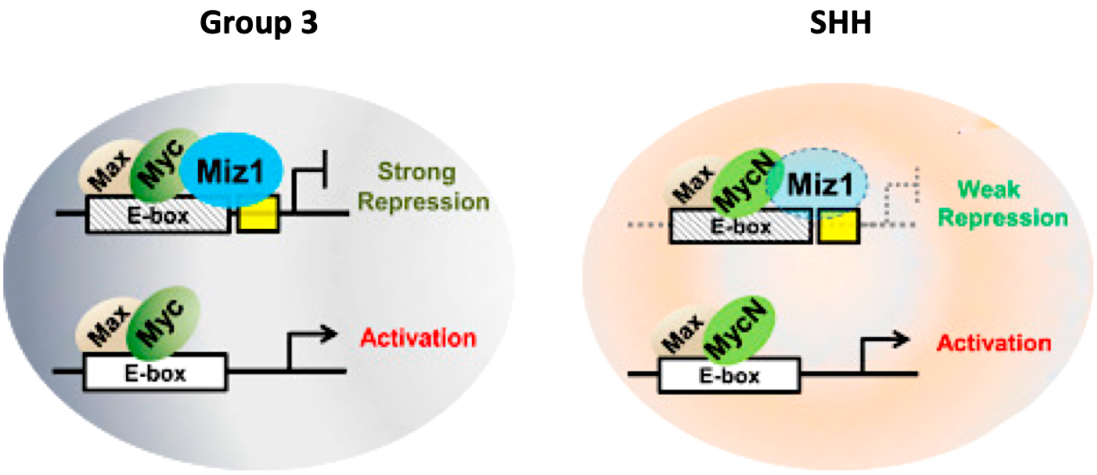

Figure 6 | MB subgroup-specific binding affinity of MYC/MIZ1 complex.

The different binding affinity of MYC and MYCN with MIZ1, but not MAX, elicits different transcriptional effects in MB: MYC/MIZ1 interaction induces strong repression of genes involved in neuronal differentiation, survival and ciliogenesis in group 3 MB compared to SHH MB. Adapted from (Mathsyaraja & Eisenman, 2016b).

1.5 microRNAs

MicroRNAs (miRNAs) are a family of small, endogenous non-coding RNAs (of about 22 nucleotides) that regulate gene expression in a sequence-specific manner (Lau et al., 2001).

The first evidence of the existence of miRNAs dates back to the '90s. Lin-4 and, later on, let-7 were the first small non-coding RNAs to be discovered to have a role in developmental transitions in the nematode C. elegans (R. C. Lee et al., 1993; Reinhart et al., 2000). To date, thousands of miRNAs have been identified in flies, worms and mammals. They are evolutionarily conserved across different species and, in many cases, ubiquitously expressed (M. Lagos-Quintana et al., 2001).

miRNA biogenesis starts with transcription in the nucleus: each miRNA is transcribed, as part of a much larger primary transcript (pri-miRNA), by the RNA polymerase II (Pol II) (Y. Lee et al., 2004). The pri-miRNAs can be quite long (over 1kb) and fold into at least one hairpin structure containing imperfectly base-paired stems and a terminal loop. Either one or more than one mature miRNA sequences can be present on each pri-miRNA.

While in the nucleus, pri-miRNAs are recognized and processed into smaller secondary miRNA precursors (or pre-miRNAs) by a RNase III family nuclease, Drosha (Denli et al., 2004). In particular, Drosha is part of the so-called “microprocessor complex” in which it interacts with

DiGeorge syndrome critical region gene 8 (DGCR8), also known as Pasha in *D. melanogaster* and *C. elegans*, a double-stranded RNA binding protein required for the proper processing (Han et al., 2006), that mainly consists in cropping the stem of the pri-miRNAs leaving a 3' overhang of 2 nucleotides (Y. Lee et al., 2003).

The precursor molecules generated by the microprocessor complex are single-stranded, hairpin-shaped RNAs of about 70-100nt which then exit the nucleus with the help of Exportin-5 (Exp5) and the binding of Exp5 with its cofactor, Ran guanosine triphosphate (RAN-GTP) (Yi et al., 2003).

Once in the cytoplasm, the pre-miRNAs require further processing. They are cleaved by Dicer, another RNase III endonuclease, with a function similar to Drosha (Bernstein et al., 2001). This enzyme lops off the double-stranded loop of the pre-miRNA leaving, as a product of its cleaving reaction, imperfect miRNA duplexes. Each duplex comprises two antiparallel and not fully complementary strands (both of about 22nt) with 5' phosphates and 3' overhangs of two nucleotides. Most of the time, only one of these two strands is going to become the mature miRNA. The reason behind this should perhaps be ascribed to minor thermodynamic stability at 5' end of one of the two strands, which regulate the entry into the RISC complex (Schwarz et al., 2003). The less stable strand can either be accumulated at a lower level than its partner strand, but still be used to generate a mature miRNA (Chiang et al., 2010), be processed as much as the mature miRNA from the other strand (Krichevsky, 2003; Mariana Lagos-Quintana et al., 2002) or be degraded (Ambros et al., 2003).

Once the miRNA-duplex has been created, it is bound by AGO2, in humans a protein of the Argonaute family, composed of four members (AGO1-4). AGO2 is dedicated to microRNA mediated silencing reactions (Hammond et al., 2001); it binds to Argonaute-cofactor GW182 and other proteins to generate the "miRISC complex" (microRNA Induced Silencing Complex) (Filipowicz et al., 2008). Upon loading, the mature miRNA act as a guide strand because of its complementary to the target mRNA (Figure 7).

The importance of miRNAs relies on their function in regulating gene expression and on the consequent physiological implication that this regulation may have. miRNAs have been shown to regulate important physiological processes such as metabolism, development (Kloosterman & Plasterk, 2006), cell proliferation (Gangaraju & Lin, 2009), differentiation and apoptosis (Bushati & Cohen, 2007).

miRNA regulation occurs at a post-transcriptional level, and the imperfect (in metazoans) complementarity of microRNAs with 3' UTR (untranslated region) of target mRNAs provokes the repression of mRNA translation (Doench & Sharp, 2004).

The key component for this miRNA-mRNA pairing is the so-called the "seed sequence", which generally encompasses nucleotide positions 2 to 8 in the mature microRNA (Bartel, 2009), and is considered the most conserved portion of miRNAs (Lewis et al., 2003).

It has been shown that miRNA regulation on gene expression is a complex and strictly regulated event since each miRNA can recognize many targets (Lim et al., 2005) and each mRNA can be targeted by several different miRNAs at the same time (Wu et al., 2010).

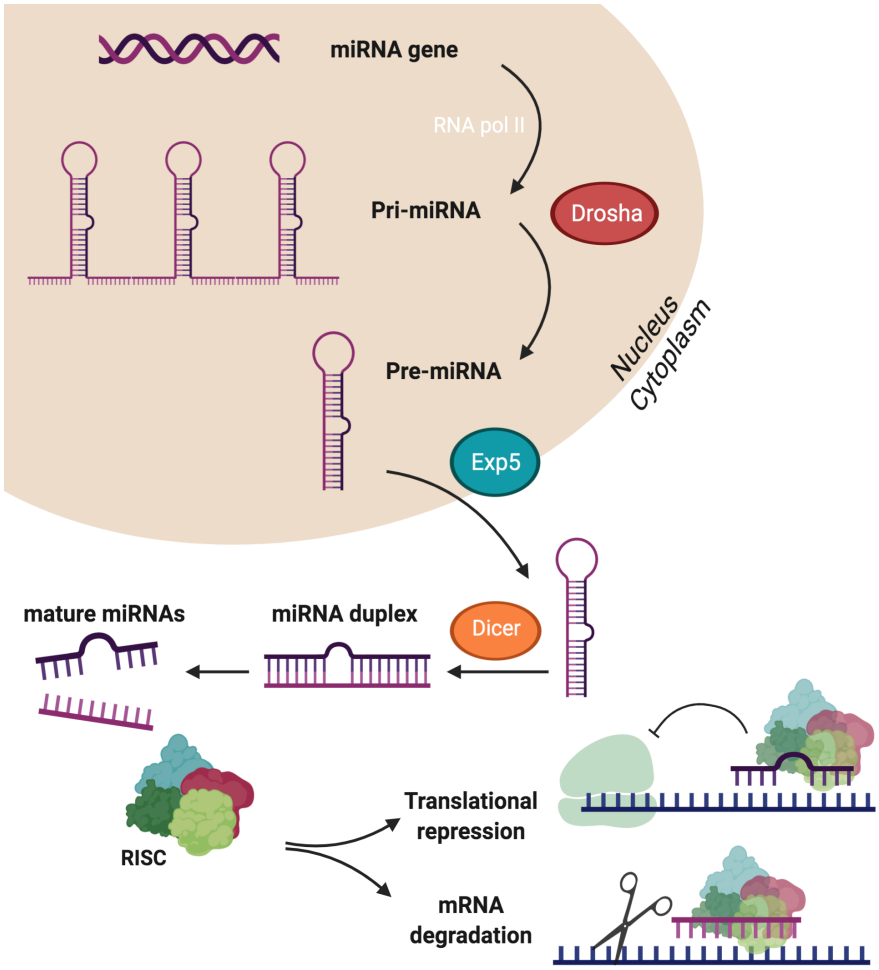

Figure 7 | The current model for the biogenesis of microRNAs.

In the nucleus, pri-microRNAs are transcribed by the RNA polymerase II (RNA pol II) and processed by Drosha to form hairpin looped pre-miRNAs. Then, pre-miRNAs exit into the cytoplasm through Exportin 5 (Exp5) and are further processed by Dicer to form mature miRNAs. Mature miRNAs post-transcriptionally modulate target genes by binding to specific sequences in their 3'UTR. According to complementarity strength with the target mRNA, miRNAs can either repress translation or induce transcript degradation.

1.5.1 miRNAs biological role

miRNAs have been demonstrated to exhibit high evolutionary conservation over a wide range of species (Lim et al., 2003). Over 2000 mature miRNA sequences have been reported in humans (according to miRBase, Release 21). This high number of miRNAs, combined with the fact that each miRNA can target multiple mRNAs, has led to the estimate that more than 30% of the human genome is regulated by miRNAs (Lewis et al., 2005).

miRNAs have been shown to play a part in varying aspects of physiologic processes, such as development (Kloosterman & Plasterk, 2006), cell proliferation (Gangaraju & Lin, 2009), differentiation and apoptosis (Bushati & Cohen, 2007). In particular, their expression profiles differ greatly in various cell types and tissues, some miRNAs have been proposed as specifically expressed at particular developmental stages and as being species-specific. For example, miRNAs regulate development of hematopoietic system (C.-Z. Chen et al., 2004), morphogenesis of epithelial tissues (Yi et al., 2006), they are involved in many metabolic processes (Esau et al., 2006) and orchestrate numerous aspects of central nervous system development (Small & Olson, 2011).

Conversely, their deregulation or altered expression has been associated with the pathological development of many maladies among all neurological disorders, cardiovascular disease and particularly they modulate all the hallmarks of cancer (Lu et al. 2005; van Rooij et al. 2007; Di Leva et al. 2014).

Because of that, miRNAs have various potential applications and have been proposed as novel biomarkers and therapeutic targets.

1.5.2 miRNAs in medulloblastoma

As discussed, medulloblastoma pathogenesis and the acquisition of tumorigenic functions are driven by mutations and gene expression alterations. miRNAs, as post-transcriptional regulators, can influence the expression of oncogenes and tumour suppressor genes in different cancers.

One of the first pieces of evidence of miRNA having a cancer-causing role was in 2006 when Cimmino *et al*. showed that miR-15a and miR-16-1 negatively regulated the anti-apoptotic B cell lymphoma 2 (BCL2) protein in chronic lymphocytic leukaemia (Cimmino et al., 2005).

miRNAs are also referred to as oncogenes or tumour suppressors, and they are up-regulated or down-regulated in cancer compared to normal tissues respectively (Di Leva et al., 2014). Notably, MYC plays a prominent role in controlling transcription of both oncogenic and tumour suppressive miRNAs. On the one hand, MYC up-regulates the expression of the oncogenic 17-92 cluster, which have been shown to drive cell proliferation, induce angiogenesis and stop apoptosis in different cancer types including brain cancers (Mendell, 2008; Ventura et al., 2008). On the other, MYC represses let-7 family members expression leading to increased proliferation in cancer (Lujambio & Lowe, 2012).

A great deal of research has been recently focused on microRNAs involvement in cancer; nonetheless, the study of the role of microRNAs in medulloblastoma is still in its infancy.

Few miRNAs are found altered and have been documented to have tumour-suppressing or tumour-promoting activity in *in vitro* and/or *in vivo* models (Cavalli et al., 2017; Garg et al., 2015). *Ferretti et al.* were one of the first to unravel miRNA regulation patterns in MB, reporting an overall miRNAs downregulation compared to controls and proving miR-9 and miR-125 as tumour growth inhibitors (Ferretti et al., 2009).

Moreover, the same group was one of the first to correlate miRNA profile with specific molecular features of MB and not with MB as individual clinical entity, showing interestingly that MB tumours with a higher expression of c-Myc exhibited a signature of miRNAs (miR-181b, miR-128a, miR-128b) that was differentially expressed compared to other subgroups without c-Myc overexpression (Ferretti et al., 2009).

Once again, the 17-92 cluster deserves a special mention among frequently up-regulated miRNAs in medulloblastoma (6% of MBs). Its upregulation has been linked more frequently to MB tumours relying on the activation of SHH signalling (Uziel et al., 2009). The proliferative effects of the cluster have been confirmed both in cell and mouse models for SHH MB (Murphy et al., 2013; Northcott, Fernandez-L, et al., 2009).

1.5.2.1 miR-124

miR-124 is highly expressed in all brain regions except for the pituitary gland (Baroukh & Van Obberghen, 2009), and its role is essential for the maintenance of neuronal identity (Conaco et al., 2006). Given its abundance in the brain, it's not surprising that alterations in miR-124 expression lead to neurodegenerative diseases, such as Alzheimer's and Parkinson, strokes or brain tumours (Sun et al., 2015).

miR-124 is specifically highly expressed in differentiating and mature neurons and external granule cells of the normal cerebellum, which are believed to be cells of origin of MB (Li et al., 2009). Accordingly, miR-124 is also one of the most frequently down-regulated miRNAs in MB (Pierson et al., 2008). In this context, it acts as tumour-suppressor inhibiting cell proliferation and MB progression *in vitro* and *in vivo* via direct targeting of CDK6, a master regulator for G0/G1 progression (Silber et al., 2013). miR-124 has also been shown to down-regulate SLC16A1 in medulloblastoma. SLC16A1 is responsible for the efflux of lactic acid during aerobic glycolysis, and its knockdown leads to cell death in MB (K. K. W. Li et al., 2009).

One of the key prognostic factors for medulloblastoma is the presence of metastasis at diagnosis. miR-124 has been shown to target the SOX9 gene, which is frequently overexpressed in WNT and SHH MB, recently associated with MB malignancy and metastasis (Suryo Rahmanto et al., 2016; Swartling et al., 2012).

Altogether, miR-124 holds great potential for malignant MB treatment.

Chapter 2:

Materials & Methods

2.1 Cell culture

The following medulloblastoma cell lines have been used in this study: DAOY, ONS76 and UW228 (SHH subgroup), HD-MB03 (group 3 subgroup), CHLA-01-MED and CHLA-01R-MED (group 4 subgroup). DAOY, CHLA-01-MED were purchased from American Type Culture Collection (ATCC) and HD-MB03, ONS76, UW228 were kindly provided by Dr. Chris Jones. DAOY, ONS76, UW228 and HD-MB03 cells were grown in a monolayer in Roswell Park Memorial Institute (RPMI) 1640 medium supplemented with 10% (vol/vol) FBS and 1% (vol/vol) Penicillin-Streptomycin antibiotics (Invitrogen). CHLA-01-MED and CHLA-01R-MED suspension cells were cultivated in DMEM:F12 medium with 20 ng/mL human recombinant EGF, 20 ng/mL human recombinant basic FGF, and B-27 Supplement (Invitrogen) to a final concentration of 2% (vol/vol).

All cell lines were incubated at 37°C and 5% CO_2 and passaged every three days upon confluency.

2.2 3D spheroid culture

3D spheroids of HD-MB03 cells were generated with a forced floating strategy, seeding 500 cells/well in the Nunclon Sphera 96-well microplate with super low cell attachment surface (ThermoFisher). The plate was then centrifuged at 200 g for 2 minutes, to gather all cells at the bottom of each well. Cells were incubated at 37°C and 5% CO_2 for 3 days to allow spheroid formation. Spheroid formation was assessed through phase-contrast microscopy at BioTek Cytation 3 Image reader (BioTek).

Spheroid volume was measured using the following formula $\frac{Lenght\ x\ Width^2}{2}$ (Jensen et al., 2008).

2.3 Drugs

All CDK inhibitors used and respective CDK selectivity are listed below in Figure 8 and Table 4. All compounds were purchased from MedChemExpress and stock solution were stored at -20°C for short term storage and -80°C for long term storage. CDKis were used with a 0-10 µM concentration range.

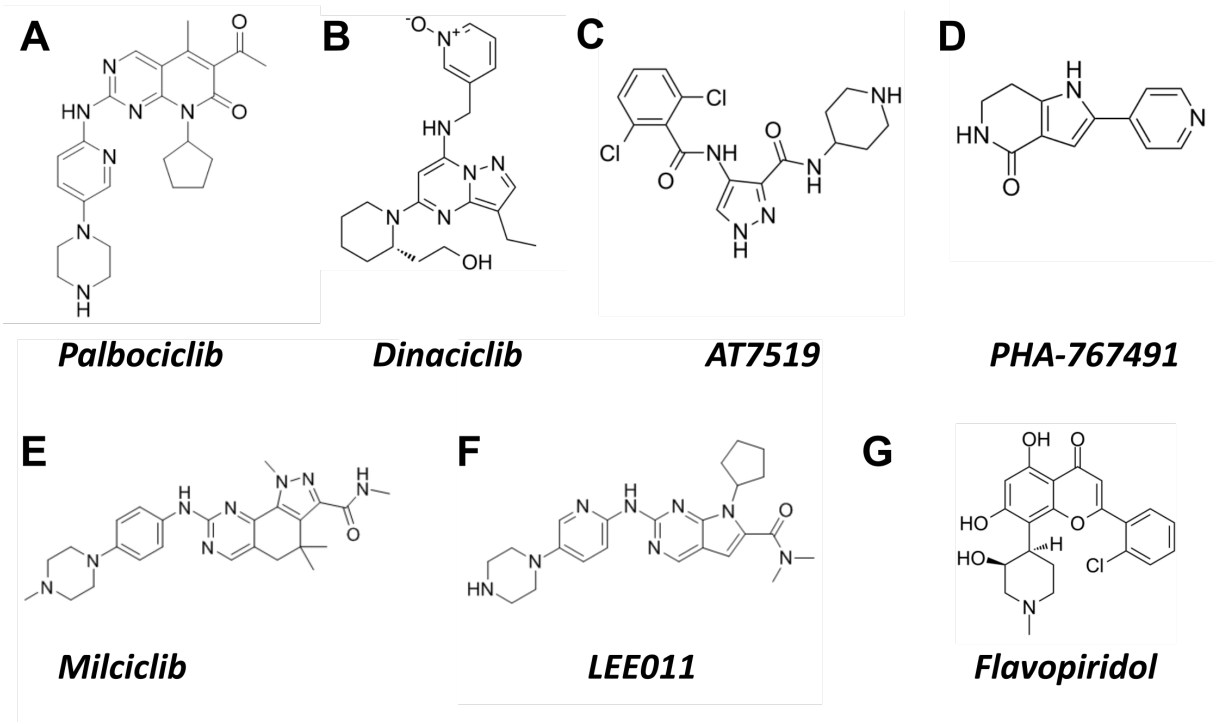

Figure 8 | Chemical structures of CDKis used in the study.

Table 4 | Selectivity of CDK inhibitors used in the study.

The "+" show which CDKs are targeted by each compound as they are indicated by the manufacturer.

CDK Inhibitor	CDK1	CDK2	CDK4	CDK5	CDK6	CDK7	CDK9
Palbociclib			++++		+++		
Dinaciclib	++++	++++		++++			++++
AT7519	++	++	++	+++	++	+	+++
PHA-767491	+	++		+			+++
Milciclib	+	++	++	+		++	
LEE011			+++		+++		
Flavopiridol	+++	+++	+++				

Vincristine and cisplatin were employed in this study as chemotherapeutic agents (MedChemExpress). These compounds were used at 0-10 μM and 0-100 μM concentration ranges respectively.

BH3 mimetic compounds were purchased from APExBIO and they all target with high specificity anti-apoptotic Bcl-2 proteins. Specifically, we used Navitoclax, an inhibitor of BCL-XL, BCL-2 and BCL-w, Maritoclax, a selective MCL-1 inhibitor, and WEHI 539, a selective BCL-XL inhibitor. All BH3 mimics were tested at 0-100μM concentrations.

The calculation of the IC_{50} of the compounds and graphs were performed using Graphpad Prism 5.0 software in short-term proliferation assays (72h treatments), as described.

2.4 Generation of chemo-resistant cells

Group 3 MB vincristine- and cisplatin-resistant cells were derived from parental HD-MB03 cells by continuous exposure to the primary inhibitors. Initially, IC_{50} values for each drug were obtained from dose-response results over 72h treatment of the sensitive HD-MB03 cells using MTT assay. Each resistant cell line was treated starting with a low concentration of the drugs (100-fold less than IC_{50}) until full recovery of the cells. The cells were passaged every two days and treated with the drugs the following day. Drug concentration was slowly increased until at least 2-fold IC_{50} was reached. This development period was carried out for approximately 6 months, after which time IC_{50} concentrations were re-assessed in each chemo-resistant cell line and compared to parental cells. After that, cells were maintained continuously in the presence of the respective inhibitor.

2.5 Transfection

Transfections were performed using Lipofectamine 2000 or Lipofectamine RNAiMax (Invitrogen) as suggested by the manufacturer's instructions. HD-MB03 cells were cultured to 50–60% confluence in 6-well plates at 200,000 cells/well, in antibiotics-free RPMI medium, and then transfected with 50-100 nM of specific siRNA or pre-miRNA for 72 h. Specifically, only single siRNAs for MCL-1 were transfected at 50nM final concentration. siRNAs pools (SMARTpool) used from Dharmacon consists of a mixture of 4 different siRNAs targeting the

gene of interest, accounting for a better knockdown. A list of all transfected siRNAs and pre-miRNAs can be found in Table 5.

The day after transfection, cell culture medium was changed to avoid lipofectamine toxicity effects on cells.

Table 5 | List of RNA molecules used in this study.

RNA molecule name	Supplier
siGENOME Non-Targeting siRNA Pool #1	Dharmacon (#D-001206-13-05)
siRNA Non-Targeting Control	Dharmacon (#D-001810-10-05)
SMARTpool siRNAs ZBTB17 (MIZ1)	Dharmacon (#L-012659-00-0005)
SMARTpool siRNAs MYC	Dharmacon (#L-003282-02-0005)
SMARTpool siRNAs CDK1	Dharmacon (#L-003224-00-0005)
SMARTpool siRNAs CDK2	Dharmacon (#L-003236-00-0005)
SMARTpool siRNA CDK9	Dharmacon (#L-003243-00-0005)
siRNA MCL1 #1	Qiagen (#SI03069003)
siRNA MCL1 #2	Qiagen (#SI00131768)
Pre-miR miRNA Precursor Negative Control #1	ThermoFisher scientific (#AM17110)
Pre-miR miRNA Precursor hsa-miR-124-3p	ThermoFisher scientific (#PM10691)

2.6 CRISPR/Cas9 genome editing

To establish MYC and MIZ1 knockouts, we used the CRISPR-Cas9 system following the workflow represented in Figure 9.

Briefly, 100 nmol of crMYC (Edit-R Human MYC, Dharmacon) and crMIZ1 (Edit-R Human ZBTB17 crRNA, Dharmacon), Table 6, were transfected in HD-MB03 cells together with an equimolar amount of trans-activating crRNA (Edit-R CRISPR-Cas9 Synthetic tracrRNA, Dharmacon) and 1 µg of hCMV-PuroR-Cas9 expression plasmid (Dharmacon).

Table 6 | crMYC and crMIZ1 target region.

crRNA name	Target sequence
crMYC	GGTGTGACCGCAACGTAGGA
crMIZ1	CTGGTGCACGGTCTTCACGT

Positively transfected cells were selected using 750 ng/ml puromycin, starting from the 48 h after transfection. Selected cells were grown as a single cell in 96-well plates and then expanded for DNA extraction of isogenic cell lines and long-term storage. Transfections were performed with Lipofectamine 2000 (Invitrogen) as previously stated.

2.6.1 DNA extraction

Genomic DNA was extracted from crMYC, crMIZ1 and Cas9 HD-MB03 cells right after puromycin selection and from the different crMYC and crMIZ1 isogenic cell lines.
Briefly, collected cells were incubated overnight at 60°C with 700 µl Lysis Buffer (50 mM Tris-HCl, pH 8.0, 100 mM EDTA, 100 mM NaCl, 1% SDS) and 35 µl 10 mg/ml Proteinase K. The following day, 20 µl 10 mg/ml RNase A (DNase-free) were added to the samples and then incubated at 37°C for 2 h. 500 µl Phenol:Chloroform:Isoamyl Alcohol (PCI, 25:24:1) was added to the samples, mixed and then centrifuged at 12,000 x g for 5 min. The aqueous layer was collected, and a chloroform extraction was performed in 500 µl chloroform. The aqueous phase was transferred in a new tube containing 100% isopropanol to allow DNA precipitation upon centrifugation. White DNA pellets were washed twice with 70% ethanol and then left to dry and resuspended in nuclease-free water.
DNA was quantified using Nanodrop-2000c spectrophotometer (Thermo Scientific).

2.6.2 CRISPR efficiency

The Alt-R Genome Editing Detection Kit (IDT), based on T7EI nuclease assay, was used to screen for and characterize any insertions/deletions (Indels) present in each HD-MB03 MYC and MIZ1 mutagenised pools. Specifically, 40 ng of gDNA was PCR-amplified using the primer

set (Table 7) specific for the crRNA-targeted regions with My Taq Red Mix (Bioline) following the manufacturer's instructions.

Table 7 | Primers used for crMYC and crMIZ1 targeted regions.
All primers were ordered from Eurofins.

Gene name	Primer sequence
MYC Forward	5'-CCCGCGACGATGCCCCTCAACG-3'
MYC Reverse	5'-GGCCTGGGCGGGCTTCGCTTAC-3'
MIZ1 Forward	5'-CCCCAGAGCACCTCCTGCTG-3'
MIZ1 Reverse	5'-CACTGCAGCTCCCACCGGC-3'

All of the primers were validated for optimal annealing temperature. To visualize the T7EI digestion products, a 2% agarose gel in 1xTBE buffer (National Diagnostics) was prepared and stained with SYBR Safe DNA Gel Stain (Invitrogen). DNA bands were visualized using the GBox system (Syngene) and taking as a reference the molecular weight marker Quick-Load 1 kb DNA Ladder (NEB).

2.6.3 Sequencing

100 ng of single clone's DNA was amplified using My Taq Red Mix (Bioline), following manufacturer's recommendations. PCR products were purified using FavorPrep PCR Clean-UP Kit (Favorgen) and sent for Sanger sequencing at Source BioScience laboratory (UK).

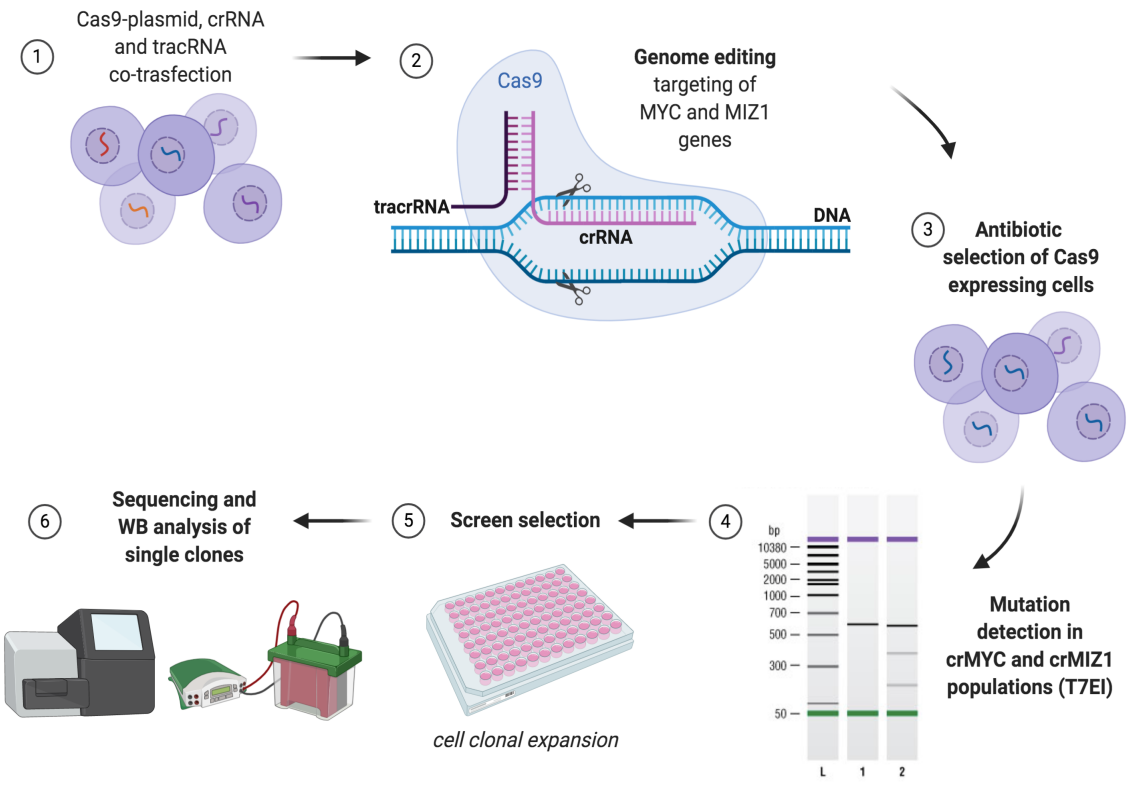

Figure 9 | CRISPR/CAS9 gene knockout workflow.

1-2) HD-MB03 cells were co-transfected with Cas9 expressing plasmid, tracRNA and crRNAs targeting MYC and MIZ1 respectively. Genome editing will occur only in the cells receiving all 3 molecules. 3) After 48h from transfection, CRISPR pools were selected for Cas9 plasmid with puromycin antibiotic. 4) Following selection, cell populations were screened to detect mutation in MYC and MIZ1 genes by T7EI digestion. Mismatches will form fragments with different sizes when resolved in agarose gel. 5-6) After assessing the efficacy of the editing, cells were clonally expanded to collect DNA and proteins for sequencing and western blot analyses.

2.7 RNA extraction

Total RNA was extracted from cell pellets with 1 ml of TRI Reagent (Sigma-Aldrich) each time, following the manufacturer's protocol. RNA was dissolved in 30-50 µl of RNase-free water and then measured using Nanodrop-2000c spectrophotometer (Thermo Scientific). Specifically, samples selected for further microRNA expression screening were purified using RNA Clean-up and Concentration Kit (Norgen) as per instructions to obtain high-quality RNA.

2.8 RNA profiling

2.8.1 miRNA high-throughput screening

Medulloblastoma samples selected for miRNA expression profiling were sent at The Ohio State University genomic facility, and the detection was performed on the NanoString nCounter Human microRNA expression assay (Figure 10) (NanoString Technologies). Specifically, 180 ng of high-quality total RNA was used as input material, and each selected sample was submitted in triplicate.

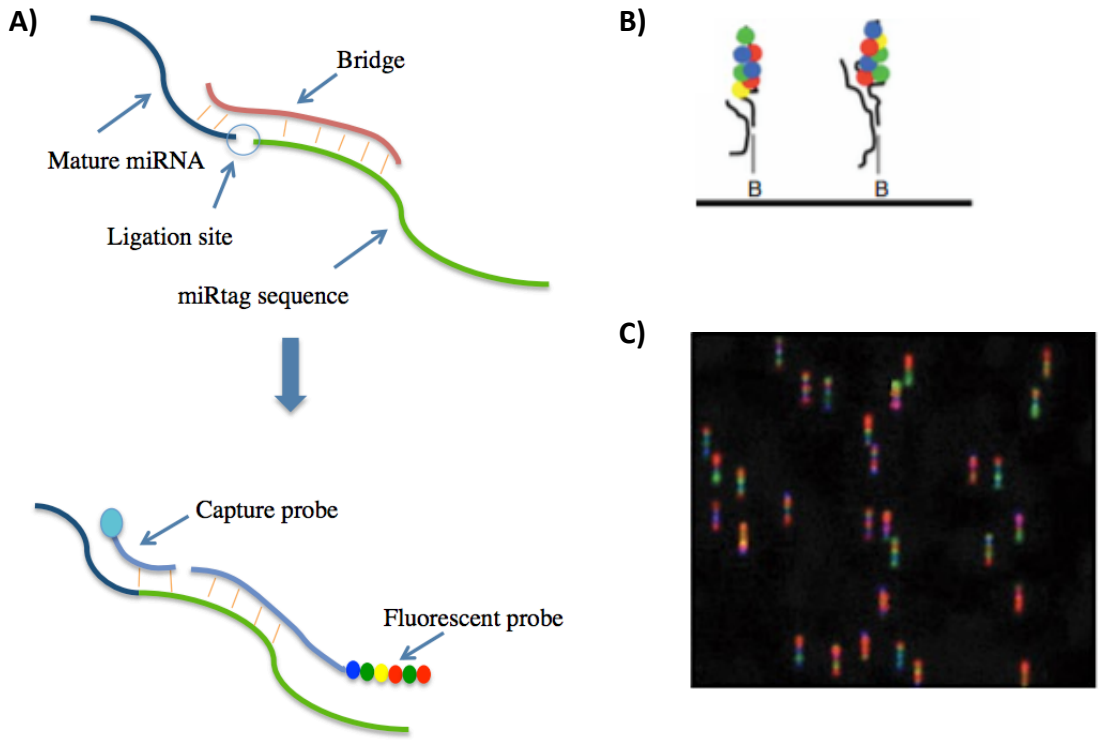

Figure 10 | Overview of NanoString miRNA assay.

Briefly, A) this detection method consists of a first step where every mature miRNA present in the sample is paired with a miRNA-specific bridge oligonucleotide, which in turn is required for the correct ligation of the miRNA-tag at its 3'. The tagged microRNAs are hybridized with probes specific for each tag sequence, which are made of a biotin label, that allows subsequent miRNA capture, and a reporter portion that consists in a fluorescent barcode. B) Each tagged-miRNA:probe complex is then immobilised on a streptavidin-coated cartridge, C) fluorescent barcodes are counted by the nCounter Digital Analyzer and values assigned to the corresponding miRNA identity. Overall, these highly miRNA-specific steps confer the system of a great sensibility and specificity, allowing a quantitative readout of 800 human microRNAs. Adapted from (Geiss et al., 2008).

A panel of microRNAs was analysed in HD-MB03 transfected with siRNA negative CTRL vs HD-MB03 transfected with siRNA MIZ1 comparison groups.
After miRNA screening, data normalization and analyses, including heat map generation, were performed using the nSolver software by Paolo Fadda from The Ohio State University genomic facility.

2.8.2 RNA-sequencing

Sequencing libraries for pre-miR-CTRL vs pre-miR-124 transfected HD-MB03 cells and DMSO vs Dinaciclib treated HD-MB03 cells, each submitted in triplicate at the Sequencing facility of the Cancer Research UK – Manchester Institute, were prepared by using the QuantSeq kit (Lexogen) and run on an Illumina NextSeq sequencer for 76bp. RNA-seq analyses were performed by Mattia Chiesa from the Immunology and Functional Genomics Unit, Centro Cardiologico Monzino (Italy). Briefly, reads were quality checked and aligned to a human reference genome. Differential expression was evaluated using the R DaMiRseq package (Chiesa et al., 2017).

2.9 Computational analysis

Gene ontology analysis (GO) (http://geneontology.org) for differentially expressed genes, from both RNA-seq datasets or publicly available datasets from the R2: Genomics Analysis and Visualization Platform (https://hgserver1.amc.nl/cgi-bin/r2/main.cgi), was performed by ranking the selected genesets. The cut-off for the final list of genes was *p-value* < 0.05.

2.10 miRNA and mRNA RT-qPCR: expression analyses and RNA profiling validation

For quantitative PCR studies of microRNAs, RNA samples were diluted in RNAse-free water at the concentration of 50 ng/µl in order to use 50 ng of the RNA solution in each RT assay for technical consistency. Total RNA was reverse transcribed to cDNA using specific miRNA primers and the reagents of TaqMan MicroRNA Reverse Transcription kit (ThermoFisher). Specifically, TaqMan RT probes are stem-looped with a miRNA-specific single-stranded region

and a double-stranded universal fragment (universal primer-specific), this structure avoids annealing of the primer to pre- and pri-miRNAs and allows only mature miRNA reverse transcription, thereby conferring high specificity of the assay. Therefore, total RNA has been reverse transcribed in a reaction volume scaled down to 7.5 µl. This was comprised of 0.075 µl of 100 mM dNTPs, 0.75 µl of RT buffer (10X), 0.094 µl of RNase Inhibitor (20 units/µl), 0.5 µl Multiscribe RT enzyme (50 units/µl), 3.581 µl of nuclease-free water and 1.5 µl of miRNA-specific stem looped primer (5X). Lastly, 1 µl (50 ng) of RNA was added to each reaction volume. Samples were vortexed and incubated in a GeneAmp PCR System 9700 Fast Thermal Cycler (Applied Biosystems) according to manufacturer's instructions.

Then, 1 µl of diluted RT product was amplified in 10 µl PCR reactions including 5 µl of 2X TaqMan Fast Advanced Master Mix (Applied Biosystems), 3.5 µl of nuclease-free water, 0.5 µl of miRNA-specific primer (20X). All reactions were run in triplicate on a 7900HT Sequence Detection System (Applied Biosystems) as per manufacturer's protocol.

For quantitative PCR studies of mRNA, complementary DNA (cDNA) was synthesized from 500 ng of RNA as input with Superscript III First-Strand Synthesis kit (Thermo Fisher) according to manufacturer's instructions. Then, 1 µl of diluted cDNA (50 ng/µl) from each reaction was amplified with the FS Universal SYBR Green Master Rox master mix (Roche) as per manufacturer's protocol. All reactions were run on a Lightcycler 96 instrument (Roche).

Results were expressed as Ct (cycle threshold) levels, defined as the fractional cycle number at which the fluorescence passes the fixed threshold. The threshold is a numerical value, which is set as a significant point above the background signal (baseline fluorescence) and allows accurate measurement of only the fluorescence deriving from target presence in a well.

Relative expression was calculated using the comparative Ct method (2-ΔΔCt) (Schmittgen & Livak, 2008). Each Ct value was normalized (ΔCt) to the corresponding Ct value of the housekeeping microRNA or gene to allow comparison between different samples. Specifically, U6 or RNU44 were used as housekeeping microRNAs, and 18s or Actin were used as housekeeping genes. Next, relative expression was calculated with the formula $2^{-\Delta Ct}$ and an average of the three technical replicates was taken. Final results are expressed as fold changes $\left(\frac{2^{-\Delta Ct}\ treated}{2^{-\Delta Ct}\ control}\right)$ of different miRNAs or mRNAs (average of three biological triplicates) ± SD.

2.11 SDS-polyacrylamide gel electrophoresis (PAGE) and Western Blot

Cells were cultured in 10-cm dishes, collected adding ice-cold PBS and scraping the dishes. Pellets were obtained by centrifugation and proteins extracted in Triple lysis buffer composed of 50 mM Tris-HCl (pH=7.5), 150 mM NaCl, 0.1% SDS, 1% NP-40 and 0.5% sodium deoxycholate. Protease inhibitor cocktail set III (EMD Millipore), and phosphatase inhibitor cocktail set II (EMD Millipore) were always added to the buffer before lysis. Samples were then vortexed for 30 min at 4 °C, and cell lysates were cleared by centrifugation at 13,000 rpm for 10 min at 4 °C. Briefly, equal amounts of protein lysates (50 µg each time) and molecular weight marker (Precision Plus Protein Kaleidoscope, Bio-Rad Laboratories) were separated by 4-20% SDS-polyacrylamide gel electrophoresis (Bio-Rad), transferred to 0.45 µm nitrocellulose membranes (Bio-Rad) and blocked in 5% (w/vol) skim milk in PBS-T (PBS, 0.1% (w/vol) Tween 20) for 1h at room temperature. Immunoblots were carried out with specific primary antibody incubation overnight at 4 °C, three washes with PBS-T, followed by species-specific horseradish peroxidase-conjugated antibodies incubation for 1h at room temperature (GE Healthcare). Chemiluminescence was induced with SuperSignal West Pico Chemiluminescent Substrate and SuperSignal West Dura Chemiluminescent Substrate (Thermo Fisher). Finally, signal detection was possible through X-ray film exposure (Phenix).

A complete list of all primary and secondary antibodies used can be found in Table 8. GAPDH, Vinculin, Actin and Tubulin were used as loading controls.

Table 8 | List of all antibodies used in the study.

Primary Antibody	Supplier
MIZ-1 (1:500)	Cell Signaling (#14300)
PARP (1:500)	Cell Signaling (#9532)
Cleaved PARP (1:500)	Cell Signaling (#D64E10)
MYC (1:1000)	Abcam (#Ab32072)
GAPDH (1:10.000)	EMD Millipore (#Ab2302)
CDK1 (1:500)	Cell Signaling (#9116)
CDK2 (1:500)	Cell Signaling (#2546)
CDK5 (1:500)	Cell Signaling (#12134)
CDK9 (1:500)	Cell Signaling (#2316)
MCL-1 (1:200)	Santa Cruz (sc-12756)
Actin (1:10.000)	Santa Cruz (sc-47778)
Rb (1:500)	Cell Signaling (#9313)
p-Rb (1:500)	Cell Signaling (#8516)
RNA polymerase II (1:1000)	Abcam (#ab140509)
p-RNA polymerase II (Ser 2) (1:1000)	Abcam (#ab193468)
Vinculin (1:5000)	Cell Signaling (#13901)
Tubulin (1:5000)	Cell Signaling (#2125)
BCL2 (1:500)	Santa Cruz (#sc-7382)
BCLXL (1:500)	Cell Signaling (#2764)
BAX (1:500)	Cell Signaling (#5023)

Secondary Antibody	Supplier
anti-Mouse IgG, HRP-linked whole Ab (from sheep) (1:2000)	GE Healthcare (#NA931)
anti-Rabbit IgG, HRP-linked whole Ab (from donkey) (1:5000)	GE Healthcare (#NA934)

2.11.1 Densitometric analysis

A semiquantitative analysis of western blot data was possible through measurement of each band optical intensity. This was possible using the Image J software (http://imagej.nih.gov/ij/). Each target value was normalised to the respective value of the loading control protein (GAPDH, actin, vinculin or tubulin). Data were expressed as a percentage relative to the control and bar charts were created using the GraphPad Prism 5 software.

2.12 Short-term proliferation assay

Cells were seeded in 96-well plates at a density of 1000 cells/well DAOY, 2000 cell/well HD-MB03, 2500 cell/well UW228, 1200 cell/well ONS76 and 5000 cells/well CHLA-01-MED for short-term viability assays (72h).

Short-term viability of adherent cells after different treatment conditions was determined in quadruplicates and examined by Thiazolyl Blue tetrazolium bromide (MTT) (Alfa Aesar) assay or Sulforhodamine B sodium salt (SRB) (Sigma-Aldrich) assay whereas suspension cells viability was measured by Alamar blue (Alfa Aesar) resazurin assay. For MTT assays, metabolically active cells were detected adding 50 µl of Thiazolyl Blue Tetrazolium Bromide 3mg/ml (Alfa Aesar) to the medium of each well. After 3h of incubation, the medium was removed and 200 µl of DMSO was added to each well to solubilise the cells and dissolve the formazan crystals. Finally, the optical density of the formazan solution in each well was analysed using the FLUOstar Omega microplate reader (BMG Labtech) at 540 nm. For SRB assays, cells were washed with PBS and then fixed for 1 hour with 100 µl of 10% trichloroacetic acid (TCA). Cells were washed and left to dry overnight. The next day 100 µl of SRB was added to each well. Protein-bound SRB was first washed with 1% acetic acid and then solubilised with Tris base solution 10 mM pH 10.5. Absorbance was measured at 540 nM using FLUOstar Omega reader (BMG Labtech).

For resazurin assay, 40 µl of the reagent (0.15 mg/ml) was added to each well and, after 24h incubation, colour changes were measured through FLUOstar Omega reader (BMG Labtech).

Drugs were always tested using a 0-10 µM concentration range at 1:10 fold dilution except for cisplatin, which was tested using 0-100 µM at 1:2.5 fold dilution.

All results were normalized to untreated controls and reported as the average +/- SD. IC50 values and statistical analyses were performed using GraphPad Prism 5 software.

2.13 Long-term proliferation assay

For long-term viability assay (9 days), HD-MB03 were plated at 200 cells/well. All cells were maintained at 37 °C in a 5% CO_2 incubator. After 24h from seeding, cells were treated in quadruplicates every three days, following the same concentration ranges and fold dilution ratios used for the short-term viability assay.

Long-term viability was assessed by crystal violet staining (0.5% w/v, Sigma-Aldrich) for 20 minutes on a bench rocker at room temperature, rinsed with water and air-dried overnight. Crystal violet staining was dissolved by adding 200 µl of methanol to each well. The optical density of crystal violet solution was measured using FLUOstar Omega reader (BMG Labtech) at 570 nm wavelength.

The statistical analysis was performed with GraphPad Prism 5 software.

2.14 Washout Assay

Cells were seeded in 6-well plates at 200,000 cells/well and treated the next day with increasing concentrations of the selected drugs for further 24h. Then, cells were counted again and seeded for long term analyses at 200 cells/well in 6-well plates. Cells were monitored over 2 additional weeks, with media replacement every two days. At the endpoint, survivor strains were stained with crystal violet solution (0.5% w/v, Sigma-Aldrich).

2.15 Apoptotic Assay

Caspase 3/7 activity assays after siRNAs transfections were performed using the Caspase-Glo 3/7 Assay system (Promega) under manufacturer's instructions. Briefly, MB cells were plated for 24h in 96-well plates (2000 cells/well) and transfected with the selected siRNAs. Caspase-Glo reagent was added to culture media after 72h from transfection. Luminescence was measured using the Varioskan microplate reader (Thermo Scientific). All results were normalized to non-targeting control siRNA values.

Caspase 3/7 activity assessment after dinaciclib and palbociclib treatment was performed using CellEvent Caspase-3/7 Green Detection Reagent (ThermoFisher) in 2D and 3D MB cell cultures. Briefly, for 2D treatments, HD-MB03 cells were plated at 3500 cells/well in 96-well

plate, and for 3D experiments, spheroids were generated as previously described (2.1.1). In both culture settings, cells were treated with 100nM of the CDKis tested for 24h. Then, Caspase-3/7 reagent was added to culture media at 3μM final concentration and incubated for 30 min before imaging. BioTek Cytation 3 Image reader (BioTek) was used to identify the fluorescence of caspase active cells.

2.16 Time-lapse microscopy

Cells were seeded in a 96-well plate (Starstedt) at a density of 2500 cells/well and incubated for 24h. Next day, cells were treated with different drugs being studied or transfected as specified in the relevant method's section. Each treatment condition was performed in technical quadruplicates. The plate was then maintained at 37°C and 5% CO_2 in the Cytation 3 system (Biotek). Phase-contrast images were recorded every 15 minutes for 72h at 100X magnification. Images were exported in mp4 format from the Gen5 software. Changes in cell morphology were assessed by visually analysing the fate of 30 cells per condition, across the 4 replicate wells.

At the beginning of each video, we identified a single cell in interphase, and we recorded its progress throughout the cell cycle interpreting frame to frame by eye.

Single cell fate interpretation was performed using the following criteria (Figure 11):

- Mitotic entry: cells round up
- Apoptosis: cells round up to shrinking and cytoplasm condensation (early apoptosis) and then cell fragmentation occurs (late apoptosis);
- Mitotic slippage: just one large tetraploid cell comes out of the mitotic phase. Cells flatten back again in interphase and do not undergo anaphase.

Finally, timing results and statistical analysis for each cell fate was presented using GraphPad Prism 5, following Taylor group analyses (Topham et al., 2015).

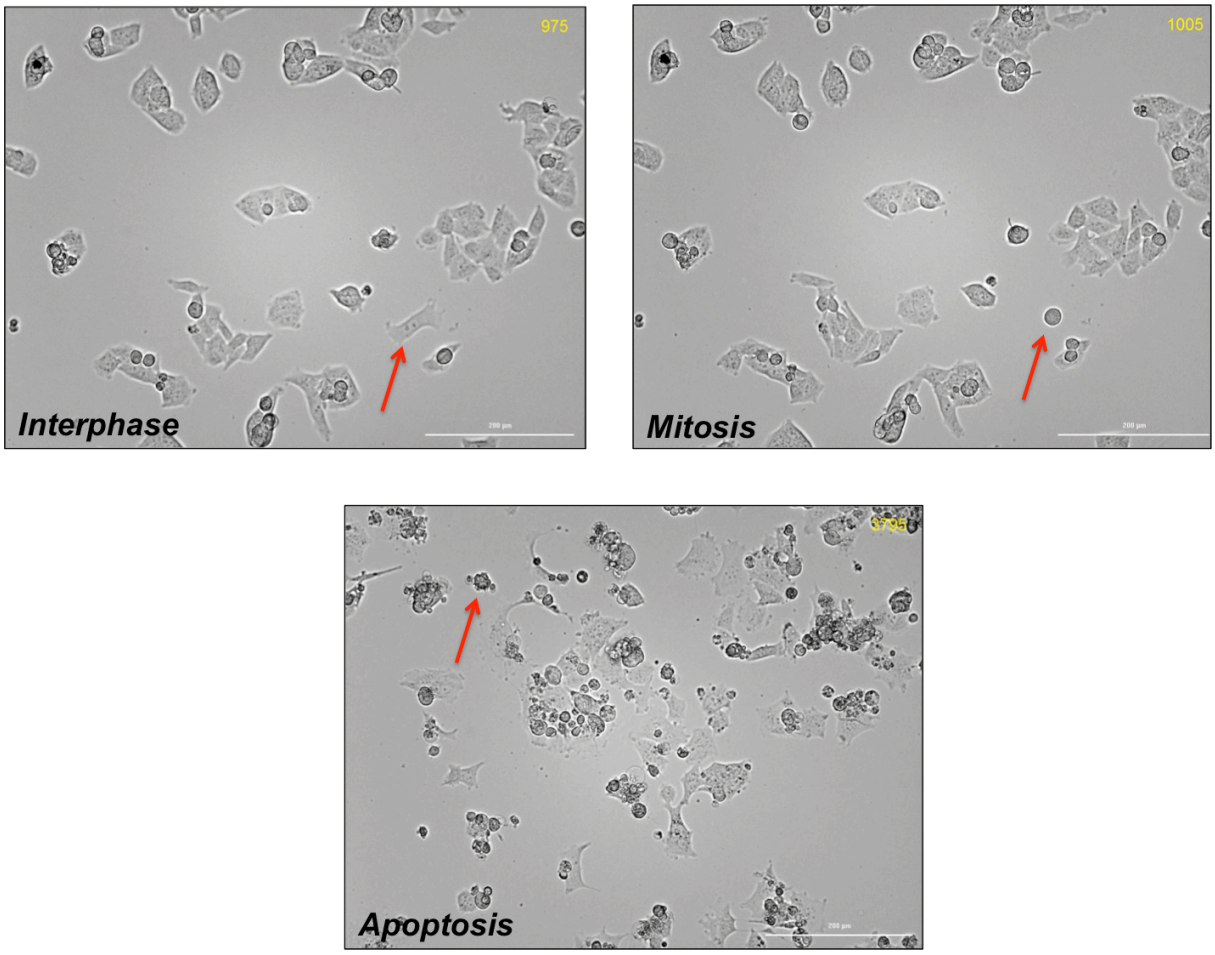

Figure 11 | Phase-contrast cell morphology assessment in time-lapse microscopy.

Red arrows indicate tracked cells: Flattened cells are considered in interphase as DNA is not condensed; the same cell round-up undergoing mitosis. A cell in apoptosis will be round-up but presenting fragmentation and apoptotic bodies. The yellow number at the top left corner of each frame represents the minutes passed from the start of the recording. Images are captured by Cytation 3 system at 100X magnification (Biotek).

2.17 Tumour Sphere Assay

Low adhesion 6-well plates were prepared by coating with 1.5 ml of 1.2% Poly 2-hydroxyethyl methacrylate (PolyHema, Sigma). HD-MB03 cells were first treated with scalar concentrations of dinaciclib and palbociclib (0.001 µM, 0.1 µM and 1 µM) for 72h. Cells were trypsinised and manually disaggregated using a 25-gauge needle. 5000 cells/well were plated in low adhesion 6-well plates and cultured in Neural Precursor Media: DMEM/F12 (ThermoFisher) containing 10 ml of B27 (50X), 20 ng/ml Epidermal Growth Factor (EGF), and 20 ng/ml basic fibroblast growth factor (bFGF) (ThermoFisher).

After 5 days, the spheres were visualized and counted using an inverted microscope (Zeiss Primovert). Spheres were counted only if presenting a diameter of at least 50 µm, using an eyepiece graticule at x40 magnification. Tumour sphere assay was always performed in three technical replicates and repeated three times independently.

2.18 Propidium iodide staining and cell cycle analysis

Cells were plated in 6-well plates at 250,000 cells/well and treated with CDKis the following day for 24h. On the day of collection, cells were trypsinised, washed with PBS, and fixed with cold 70% ethanol for 30 min while being vortexed. Cells were washed twice with cold PBS before flow-cytometric analysis. First, 50 µl of 100 µg/ml RNAse A was added to each sample cell pellet and incubated for 15 min at 37 ˚C, this to avoid RNA staining contamination. Then, cells were stained for 15 minutes at room temperature adding 200 µl of propidium iodide (PI) solution (50 µg/ml) (Sigma-Aldrich). Specifically, PI is a fluorescent molecule that stains DNA intercalating between bases. Therefore, fluorescence detected is directly proportional to the DNA content of the cell. Based on the DNA amount, it is possible to identify cell population fractions across the Sub-G1, G1, S and G2/M phases of the cell cycle by flow cytometry.
Samples were loaded onto the BD FACSVerse flow cytometer (BD Biosciences), and data analysed using the BD FACSuite software (BD Biosciences). Graphs were represented using GraphPad Prism 5.0 software as percentage of gated cells in each phase of the cell cycle.

2.19 Cloning and Luciferase reporter assay

2.19.1 Cloning of MIZ1 binding site into pGL3 vector

To confirm miR-124-3p binding to MIZ1 gene, we generated a luciferase reporter construct where the 3′ -UTR sequence of wild-type MIZ1 binding site was cloned downstream of the luciferase-coding sequence in a pGL3-control vector (Promega) at the *Xba*I restriction site. The oligonucleotides used for cloning are presented in the Table 9, and they were designed following Targetscan prediction for MIZ1/miR-124-3p binding sites (Xba-MIZ-3UTR forward and reverse). Briefly, the oligonucleotides were annealed at 95°C for 2 min and cooled down

to 25°C over 45 minutes. Then, 5 µg of pGL3-control vector and 20 µl of the annealed oligonucleotides (100µM) were digested separately with 20 units of *Xba*I restriction enzyme in 10x CutSmart buffer (New England Biolabs) in a 50 µl reaction volume for 1 h at 37°C. Restriction digest products of the pGL3 vector and the annealed primers were run on a 1% and 2% agarose gel electrophoresis, respectively. Digested products were each purified using the Favorprep Gel/PCR purification mini kit (Favorgen), following the manufacturer's instructions, and quantified using Nanodrop-2000c spectrophotometer (Thermo Scientific).

To avoid vector re-circularisation during the ligation step, 1 µg of the purified pGL3 vector was dephosphorylated in a reaction with Alkaline Phosphatase, Calf Intestinal (CIP) in 10x CutSmart buffer (New England Biolabs).

The ligation of the annealed oligonucleotides with the digested and dephosphorylated pGL3-control vector was done following the ligation step conditions described in the Rapid DNA Dephos & Ligation Kit (Roche). Ligation product was transformed into α-Select Competent Cells (Bioline) via heat-shock for selection and amplification of the construct. LB-Agar plates with ampicillin selection were inoculated with the transformation solution and incubated overnight at 37°C. We then performed single colony PCR screening using backbone-specific primers (pGL3 forward and reverse), designed to anneal sites that flank the insert site (Table). PCR reactions were performed using the MyTaq Red Mix (Bioline) according to the manufacturer's instructions. PCR products were analysed on a 2% agarose gel via electrophoresis and imaged using a G:box apparatus (SynGene) (Figure 12).

Among the 28 colonies screened, 5 were selected as putatively positive for the presence of the cloned insert, and further grown in 10 ml LB broth under ampicillin selection (50 µg/µl) overnight at 37°C and 220 rpm. Purified plasmid DNA was obtained using the QIAprep spin miniprep kit (Qiagen) following the manufacturer's instructions. Finally, the 5 purified DNA vectors were sent for Sanger sequencing further to confirm the presence and the orientation of the insert.

Among the 5 analysed constructs, we picked 4 for further testing: two, which we called "wild-type" constructs having one or 3 copies of the binding site sequence in the correct plasmid orientation (from 5' to 3'), and the other two, which we defined as "reverse" constructs having one or 3 copies of the binding site sequence in the opposite plasmid orientation (from 3' to 5').

Table 9 | List of oligonucleotides used for cloning.

For Xba-MIZ-3UTR oligos, in bold is presented the predicted binding site sequence for miR-124-3p, obtained from TargetScan program and sequences in italic are those recognised by *XbaI* restriction enzyme. pGL3 primers are designed in regions of the backbone plasmid flanking the insert.

Oligonucleotide	Sequence
Xba-MIZ-3UTR Forward	5'-*gcatgg*TCTAGATGGTTATATTCTGTATCAAAATTGGAA **GTGCCTT**CCTTCCACATTACCTAAGAACCAGTTTCTAGAaatgtc-3'
Xba-MIZ-3UTR Reverse	5'-*gacatt*TCTAGAAACTGGTTCTTAGGTAATGTGGAAGG AAGGCACTTCCAATTTTGATACAGAATATAACCATCTAGA*ccatgc*-3'
pGL3 Forward	5'-GCGGAGGAGTTGTGTTTGTGGACG-3'
pGL3 Reverse	5'-TATCATGTCTGCTCGAAGCGGCCG-3'

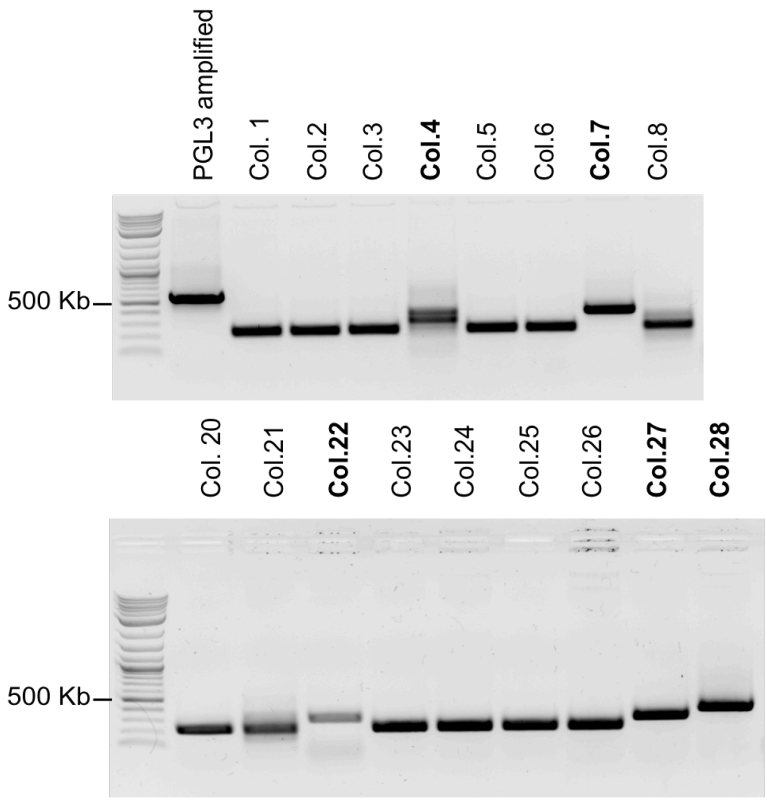

Figure 12 | MIZ1-3'UTR cloning efficiency.

Images show PCR product bands from 17 colonies of 28 screened for MIZ1-3'UTR insert. Samples were run on 2% agarose gel and images were taken at the G: box apparatus (SynGene). Quick-Load 100 bp DNA Ladder (NEB) was used in the first lane as reference. Samples in bold were selected for Sanger sequencing.

2.19.2 Dual-Luciferase reporter assay

The pGL3 vector containing the cloned 3' UTR sequence of wild-type or reverse MIZ1 (250ng) was co-transfected along with a pRL-Renilla control vector (50ng) (Promega) and with 100nM of the precursor miR-124-3p (pre-124-3p) or negative control (pre-CTRL) into Human embryonic kidney 293T cells (HEK293T) for 24 h. Cells were then lysed and treated according to the Dual-Luciferase System Protocol (Promega). Luminescence was recorded in the Varioskan microplate reader (ThermoFisher), and the values of Renilla luminescence were used to normalise firefly luciferase activity. The ratios of Firefly/Renilla values were used for result interpretation.

Chapter 3:

Hypotheses and Aims

Medulloblastoma is a deadly disease with survivors suffering from severe therapy-associated side effects. Current therapies fail to recognise medulloblastoma patient's heterogeneity. To date, generalised treatments have reached a plateau in survival, and leptomeningeal metastasis is always a fatal event. Therefore, there is a pressing need for innovative targeted approaches to improve survival for high-risk patients and reduce treatment-related sequelae. In this context, this research is divided into two projects with the same overarching goal: providing new therapeutic options for MB patients by focusing on 1) the identification of suitable CDK inhibitors for MB cells; 2) the role of MYC/MIZ1/miRNA regulation within G3 MB cells.

PROJECT1: Amplification or overexpression of CDKs act as a powerful trigger for medulloblastoma development. Therefore, CDKs inhibition may represent a valuable option for targeted therapeutic interventions implementing the current standard of care. Specifically, we assess the efficacy of pan-CDKs inhibitors versus the specific CDK4/6 inhibitors, currently evaluated in the clinical setting. The main aims of this project are:

AIM1.1: to identify a potent pan-CDKi candidate for medulloblastoma treatment to be used in a comparative study with CDK4/6 inhibitors.

Tasks:

- Determine the anti-proliferative efficacy of CDKis with different selectivity and specificity in medulloblastoma cell lines;
- Characterise cytotoxic or cytostatic effects of selected CDKi in MB cells (cell cycle distribution and apoptotic response);
- Evaluate the effect of CDKis on tumour stemness;

AIM1.2: to characterise the molecular mechanisms underlying medulloblastoma sensitivity to the proposed CDKi.

Tasks:

- Define the transcriptomic profiles of CDKi treated MB cells (RNA-seq, differential gene expression);
- Validate and interpret the transcriptomic analyses (RT-PCR, WB, GSEA, GO);

AIM1.3: to characterise the potential use of the proposed CDKi in combination with chemotherapeutic drugs to reduce toxicity burden on patients and evaluation of its efficacy in chemo-resistant settings.

Tasks:

- Determine the synergistic potential of combination treatments with CDKi and clinically relevant chemotherapeutic drugs (vincristine and cisplatin);
- Generate and characterise chemo-resistant MB cell lines;
- Evaluate CDKi effects on chemo-resistant MB cell lines;

PROJECT2: MYC amplification is the strongest adverse prognostic factor, predominantly associated with group 3 MB patients. However, MYC-dependent biology remains poorly understood in MB. The interaction of MYC with MIZ1 has been recently reported as a defining hallmark for group 3 MB development (Vo et al., 2016). Considering the failure of MYC-targeted therapeutic strategies and the role of miRNAs in medulloblastoma, understanding the link between MYC/MIZ1 regulatory axis and microRNA network in group 3 biology could unveil mechanisms of gene regulation that would help to identify therapeutic vulnerabilities for this subgroup. In this scenario, we will explore a new possible strategy to target MIZ1 using microRNAs, with the aim to disrupt its interaction with MYC and ability to sustain G3 MB cells. The main aims of this project are:

AIM2.1: to identify MIZ1 targeting miRNAs that could serve as a new targeted therapeutic tool to implement the current standard of care for group 3 MB patients.

Tasks:

- Characterise the phenotype of group 3 MB cells overexpressing MIZ1-targeting miRNA;
- Define the transcriptomic profiles of group 3 MB cells overexpressing MIZ1-targeting miRNA (RNA-seq, GO);
- Evaluate the potential use of MIZ1-targeting miRNA to implement chemotherapy;

AIM2.2: to determine the regulatory role of MYC/MIZ1 complex and its influence over microRNAs expression in medulloblastoma cell lines.

Tasks:

- Characterise the phenotype of G3 vs SHH MB cell lines after MIZ1 knockdown;
- Identify the miRNA signature of G3 MB cell line after MIZ1 knockdown;
- Validate the miRNA signature by RT-qPCR;
- Characterise the phenotype of CRISPR/CAS9 model of MYC and MIZ1 knockout cells.

Chapter 4:

Targeting CDKs for MB treatment

4.1 Background

Medulloblastoma standard of care does not account for intra- and inter-heterogeneity of the tumours, and prognosis for high-risk patients is still poor. Treatment-associated morbidities and resistance to unspecific therapies are crucial challenges in handling patients. Currently, there is an unmet need in the clinic for molecularly tailored therapies for MB, that would allow drug dosage reduction and patients quality of life improvement.

CDKs are critical players in the control of the cell cycle progression, transcription and several other cellular processes. These proteins are frequently found up-regulated in many types of cancer, including MB (M. Li et al., 2012; Mendrzyk et al., 2005). Hence, there has been a growing effort in developing small inhibitors targeting CDKs for cancer treatment. So far, first generation CDKis have shown great preclinical potential, but their effects have been frequently associated with unacceptable toxicities. Besides, treatments with these compounds showed effects that were not strictly associated with targeted CDKs, pointing at other non-targeted effects.

In the past few years, drug design approaches mainly focused on the development of more selective CDKis, and specifically CDKis targeting CDK4/CDK6/cyclin D complexes to control highly proliferating cells by blocking only G1/S phase, in an attempt to limit the generalised side-effects of broad CDK inhibition. Palbociclib is the first CDK4/6 inhibitor approved for advanced breast cancer treatment and also effective against many other solid tumours. After showing promising inhibitory effects against group 3 and SHH MB tumours, palbociclib is the only CDKi selected for MB treatment in clinical trials (Cook Sangar et al., 2017). Nonetheless, this specific CDK4/6 inhibitor has, for the most part, been associated with different mechanisms of resistance in patients (McCartney et al., 2019).

CDKs are dispensable, and they can compensate for each other's function (Santamaría et al., 2007). Therefore, we speculated that truly specific CDK inhibition, particularly as with specific CDK4/6 inhibitors, might not have been the best option considering the high adaptability of cancer cells and the quick onset of compensatory mechanisms after treatment.

Hence, we aimed at exploring the effects of currently available CDKis on MB cells and defining the mechanisms of actions in this context.

Ultimately, more potent CDKis than CDK4/6 inhibitors might already be available, and a successful therapeutic application might be dependent on a better administration schedule and sequence with currently used drugs.

4.2 Results

4.2.1 Cell cycle-related vulnerabilities in medulloblastoma

To start our project 1, we first generated a map of the most significant cell cycle related genes that are deregulated in medulloblastoma. Using the R2 algorithm, we analysed the Cavalli et al. dataset containing the expression and survival data from 612 patient samples, from the four different MB subgroups (Cavalli et al., 2017). Out of the 124 cell cycle related genes, only 16 genes were significantly modulated (FDR<0.05) across the different subgroups of MB and associated with patients survival.

MYC overexpression is confirmed to be the most crucial negative prognostic marker across MB subgroups. No CDK gene was directly identified. However, direct modulators of CDK2 (e.g. CDKN1 and CCNE1) and CDK1 (e.g. CCNA2, CDC25A and PLK1) activities were associated to survival. Moreover, gene ontology (GO) analysis of these 16 genes confirmed that not only G1/S but also G2/M checkpoint and mitotic processes are commonly altered in medulloblastoma patients (Figure 13).

The most common altered cell cycle genes resulted to be proteins with direct or indirect catalytic activity (CDKN1B, HDAC2, PLK1, TTK, CDC7, CCNA2 and CDC25A), and particularly kinases (CDKN1B, PLK1, TTK and CCNA2). Inhibitors for PLK1 and HDAC2 have been already pre-therapeutically tested for MB (Coni et al., 2017; Timme et al., 2020), whilst the other kinases are not pharmacologically druggable. This prompted us to investigate if targeting CDKs different from CDK4/6 is a good strategy for MB treatment (Table 10).

Gene	p-value
MYC	1.1E-10
ORC1	2.0E-04
MAD2L1	3.7E-0.4
PLK1	5.4E-0.4
HDAC2	5.0E-03
CDC25A	5.5E-03
YWHAE	0.010
CCNE1	0.011
TGFB1	0.011
TTK	0.014
CCNA2	0.016
FZR1	0.030
MCM3	0.030
CDKN1B	0.031
CDC45	0.031
CDC7	0.041

Figure 13 | In silico analysis of the most significant cell cycle genes altered in medulloblastoma.

Transcriptional data from 612 patients across the 4 MB subgroups have been employed to perform GO analysis against the cell cycle gene set (Cavalli et al. dataset). Results were corrected for multiple gene testing by FDR. 16 genes were significant with *p-value* FDR<0.05 (list on the left). GO analysis for the biological function term was performed on the 16 most altered cell cycle genes in MB. Results are shown on the left for 80%<fold enrichment scores>100% and FDR<0.05. Data are presented using GraphPad Prism software.

Table 10 | Gene ontology for molecular functions of most common altered cell cycle genes in MB.

GO analysis for the molecular function term was performed on the 16 most altered cell cycle genes in MB presented in Figure 13. Significant results are shown below p-value <0.05.

Gene	Molecular function	p-value
CDKN1B,HDAC2,PLK1,TTK,CDC7,CCNA2,CDC25A	catalytic activity, acting on a protein	7.00E-04
CDKN1B,PLK1,TTK,CDC7,CCNA2,CCNE1	kinase activity	2.70E-08
MCM3,ORC1,PLK1,TTK,CDC7	nucleotide binding	0.04
CDKN1B,PLK1,TTK,CDC7,CCNA2,CCNE1	transferase activity	0.01
CDKN1B,PLK1,TTK,CDC7,CCNA2,CCNE1	transferase activity, transferring phosphorus-containing groups	4.90E-07
CDKN1B,PLK1,TTK,CDC7,CCNA2	phosphotransferase activity, alcohol group as acceptor	3.30E-06
MCM3,ORC1,PLK1,TTK,CDC7	purine nucleotide binding	0.02
MCM3,ORC1,PLK1,TTK,CDC7	nucleoside phosphate binding	0.04
CDKN1B,HDAC2,PLK1,TGFB1,YWHAE, CCNA2,CCNE1,CDC25A	enzyme binding	2.30E-05
CDKN1B,PLK1,CCNA2,CCNE1,CDC25A	kinase binding	3.60E-07
CDKN1B,PLK1,CCNA2,CCNE1,CDC25A	protein kinase binding	3.40E-08
MCM3,ORC1,PLK1,TTK,CDC7	adenyl nucleotide binding	5.30E-03
MCM3,ORC1,PLK1,TTK,CDC7	ribonucleotide binding	0.02
MCM3,ORC1,PLK1,TTK,CDC7	purine ribonucleotide binding	0.02
MCM3,ORC1,PLK1,TTK,CDC7	adenyl ribonucleotide binding	5.10E-03
MCM3,ORC1,PLK1,TTK,CDC7	purine ribonucleoside triphosphate binding	0.02
MAD2L1,PLK1,TGFB1,TTK,YWHAE	identical protein binding	7.60E-03
CDKN1B,PLK1,TTK,CDC7,CCNA2	protein kinase activity	1.70E-07
MAD2L1,MYC,TGFB1,TTK,YWHAE	protein dimerization activity	8.60E-04
CDKN1B,HDAC2,MAD2L1,MCM3,MYC,ORC1,FZR1,PLK1, TGFB1,TTK,YWHAE,CDC7,CDC45,CCNA2,CCNE1, CDC25A	protein binding	4.00E-03
MCM3,ORC1,PLK1,TTK,CDC7	ATP binding	3.90E-03
MCM3,ORC1,PLK1,TTK,CDC7	drug binding	0.01
MCM3,ORC1,PLK1,TTK,CDC7	carbohydrate derivative binding	0.05

4.2.2 Screening of CDKis effects on MB cell lines proliferation

To assess the *in vitro* anti-proliferative effects of a panel of clinically relevant pan-CDKis with different CDK specificity and selectivity (Table 4), we have performed proliferation assays on a set of 5 MB cell lines belonging to different MB molecular subgroups. Cells were treated with different doses of the drugs for 72h, and cell viability was measured by MTT assay (Figure 14). Palbociclib, a specific inhibitor of CDK4/6, has been recently reported to be selectively active against group 3 and SHH MB cells (Hanaford et al., 2016). However, although more specific for HD-MB03, ONS76 and CHLA-01-MED cells, in our experiments, palbociclib did not appear among the most effective CDK inhibitors. Palbociclib showed none or a limited inhibitory effect on two of the tested SHH MB cell lines, UW228 and DAOY; in the group 3 cell line, it reduced cell proliferation no more than 70% even at the highest dose of the drug used. In addition, another CDK 4/6 specific inhibitor, LEE011, showed low efficacy in all studied cell lines.

Overall, broad CDK inhibitors showed a better anti-proliferative effect than specific CDKis. Specifically, dinaciclib, a potent inhibitor of CDK1, CDK2, CDK5 and CDK9, stood out for being the most effective pan-CDKi across the 5 different MB cell lines. CDKs inhibition by dinaciclib decreased cell growth in a dose-dependent manner and, interestingly, group 3 HD-MB03 cells emerged as the most sensitive to the drug, as shown by the lowest IC50 value across all cell lines (Table 11).

Since group 3 MB is the most aggressive MB subtype and with poorest prognosis, we mainly considered the effects of selected CDKis on HD-MB03 cells throughout the study.

We first confirmed the effects of dinaciclib and palbociclib treatments on HD-MB03 cell line by SRB assay. 72h treatments with both drugs resulted in a 15-fold growth inhibition by dinaciclib compared to palbociclib (Figure 15A). Even at the highest dosage of palbociclib, cells were still viable compared to dinaciclib treatment (Figure 15B).

In addition, we showed that dinaciclib is able to significantly slow down HD-MB03 spheroids growth compared to palbociclib at 0.1 and 1 μM in short-term evaluations (Figure 16).

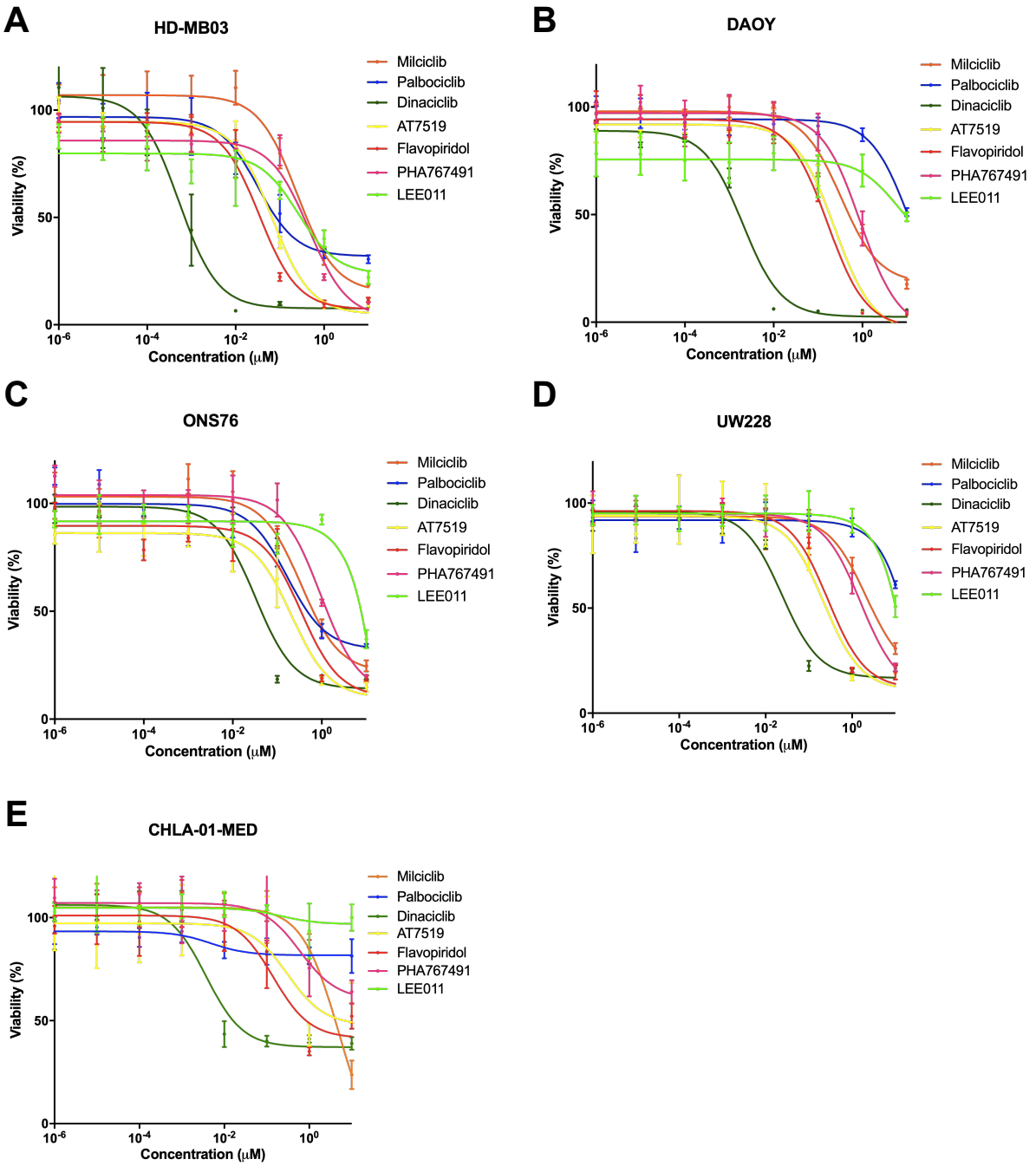

Figure 14 | Differential effects of CDK inhibitors on a panel of medulloblastoma cell lines.

Cells were treated with a 0-10 μM range of concentrations at 1:10 fold dilution with different CDKis for 72h. MB cell proliferation was examined using MTT assay for panel A-D, and with resazurin assay for panel E. Data are presented as mean ± SD (N=3, each performed in quadruplicates) using GraphPad software.
A) HD-MB03, B) DAOY, C) ONS76, D) UW228 and E) CHLA-01-MED cell line, respectively.

Table 11 | IC50 of CDKis on medulloblastoma cell lines.

IC50 values were calculated using GraphPad software after 72 h treatment of respective CDKis. N=3 independent experiments. N.D.= not determined.

IC50 (µM)	HD-MB03	DAOY	ONS76	UW228	CHLA-01-MED
Milciclib	0.16±0.17	0.57±0.21	0.24±0.16	1.92±1.35	4.1±1.12
Palbociclib	0.12±0.07	11.36±0.63	0.25±0.11	9.27±0.87	N.D.
Dinaciclib	0.001±0.001	0.004±0.003	0.04±0.02	0.02±0.002	0.02±0.01
AT7519	0.13±0.07	0.3±0.06	0.19±0.04	0.37±0.14	0.3±0.11
Flavopiridol	0.14±0.08	0.19±0.03	0.39±0.1	0.32±0.07	0.69±0.38
PHA767491	0.37±0.13	1.59±0.6	0.98±0.11	2.1±0.95	1.3±1.3
LEE011	0.27±0.02	6.3±0.61	7.3±0.3	8.7±2.6	N.D.

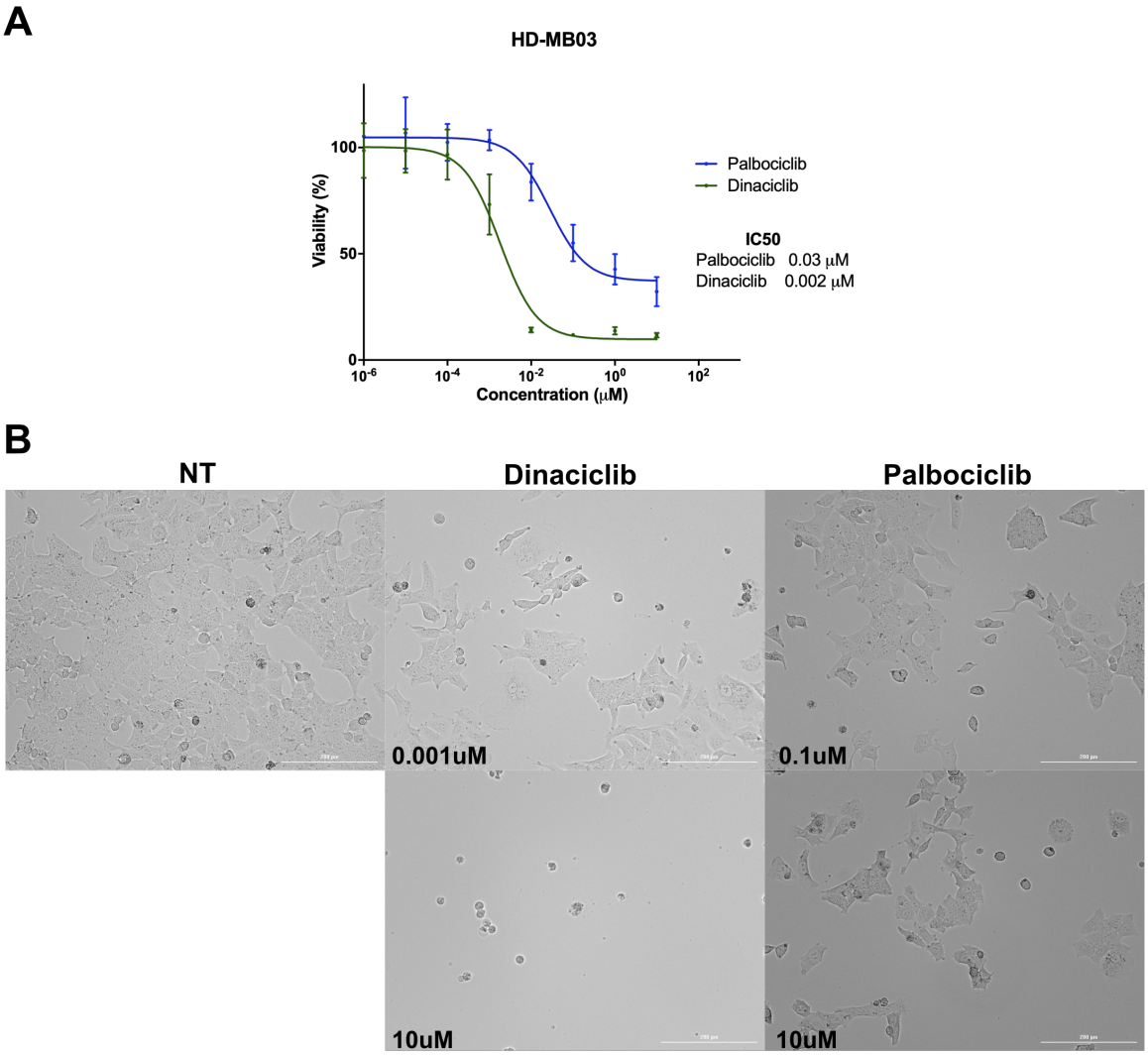

Figure 15 | Anti-proliferative effects of dinaciclib vs palbociclib on HD-MB03 cells.

A) HD-MB03 cells were treated with a 0-10 μM range of concentrations (1:10 fold dilution) for 72h. Viability was assessed using SRB assay. Data are presented as mean ± SD using GraphPad software (N=3 replicates, each performed in quadruplicates). B) Representative phase-contrast images of HD-MB03 cells treatment with dinaciclib or palbociclib at respective IC50 and highest concentration used (10μM) for 72h. Images were captured by Cytation 3 system (Biotek) at 100X total magnification.

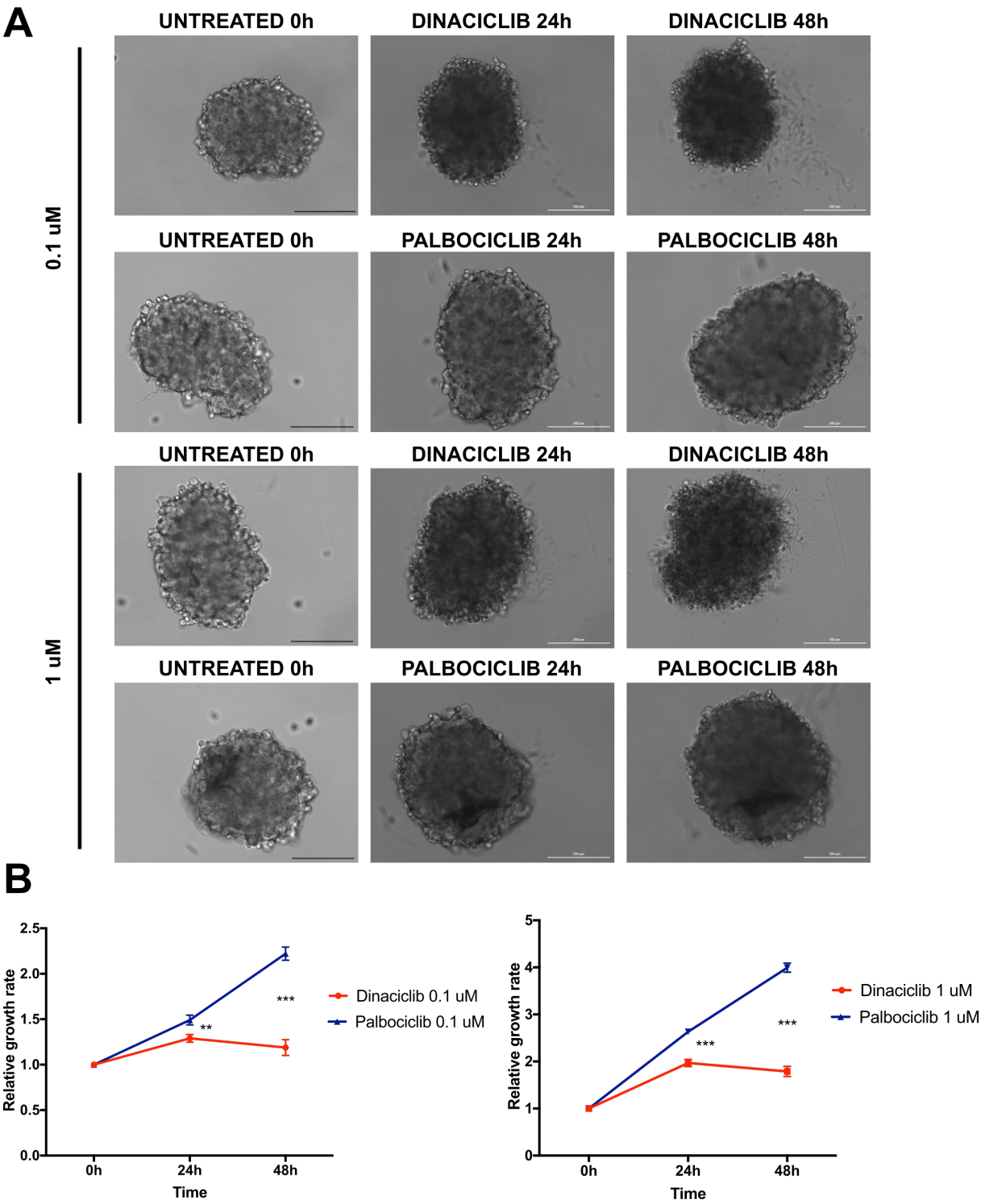

Figure 16 | Growth rates of HD-MB03 spheroids upon dinaciclib vs palbociclib treatment.

A) Formed HD-MB03 cells spheroids were treated with 0.1µM and 1µM of dinaciclib or palbociclib and imaged before treatment at time 0, at 24h after treatment and at 48h after treatment, using the Cytation 3 system (Biotek) at 100X total magnification. Scale =200µm. B) Relative growth rates are presented as mean ± SD (N=3) using GraphPad software. Time 0 values were used as reference control for respective treatment. Statistical comparisons were performed using two-tailed student's t-test where *= $p \leq 0.05$, **= $p \leq 0.01$, ***= $p \leq 0.001$.

We next challenged HD-MB03 cells to long-term effects of dinaciclib and palbociclib treatments. To this aim, the effects of the two CDKis were assessed first by long-term proliferation assay. HD-MB03 cells were treated three times with scalar concentrations of dinaciclib or palbociclib and, after 9 days, cells were stained with crystal violet solution.

Dinaciclib caused again a marked reduction in cell viability compared to palbociclib at 100-fold lower dosage of the drug (Figure 17A).

In parallel, HD-MB03 cells were treated for 24h with increasing doses of both drugs and survivor cells were left to outgrow for 2 weeks. Given the potent efficacy of dinaciclib and the more extended evaluation period, we decided to lower by 10-fold the starting concentration used for dinaciclib. Nonetheless, even at the lowest concentration of dinaciclib used (0.0001 μM), the number of outgrowing colonies was far less than with all palbociclib treatments (Figure 17B).

Altogether, these experiments demonstrated that dinaciclib is more potent than palbociclib to halt proliferation of group 3 MB HD-MB03 cells and has the ability to suppress cancer cells ability to resume growth after only 24 hours treatment at very low concentration.

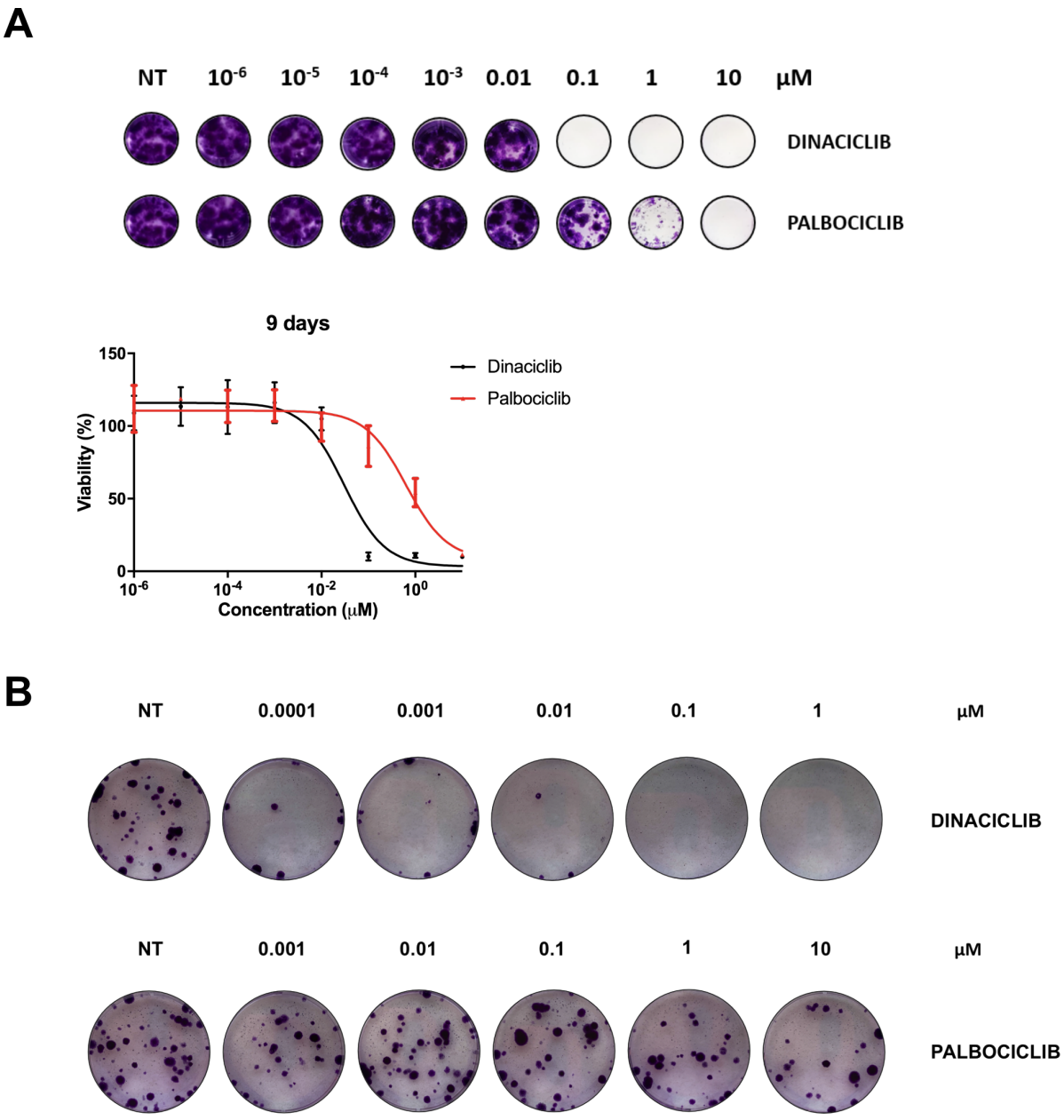

Figure 17 | Long-term proliferation and washout experiment with outgrowth formation assays of HD-MB03 cells treated with dinaciclib and palbociclib.

A) Representative images of the long-term proliferation assay (N=3). HD-MB03 cells were seeded at 200 cells/well in 96-well plate and treated with 0-10 µM at 1:10 dilution fold of dinaciclib and palbociclib for 9 days. Cells were stained with 0.5% w/v crystal violet solution. Below, the crystal violet quantification of the presented images is shown. Data are plotted using GraphPad software. B) Representative images of washout assay (N=3). Cells were treated for 24h with increasing concentrations of the drugs and seeded again at 200 cells/well in 6-well plates. Recovery from treatments was allowed over 2 weeks, after which crystal violet staining was performed.

4.2.3 Dinaciclib significantly reduces HD-MB03 cells 3D sphere formation ability

Cancer stem cells (CSC) represent a fraction of the tumour population that is responsible for the initiation, propagation, metastatic potential and resistance to treatment of the tumour (H. Liu et al., 2015).

Recently, it was shown that dinaciclib is able to repress the proliferation of cancer stem-cell-like such as Triple Negative Breast Cancer (TNBC) or T-cell acute lymphoblastic leukaemia (T-ALL) cell lines (Carey et al., 2018; Moharram et al., 2017).

Thus, we decided to evaluate the capacity of dinaciclib to target CSC properties of the aggressive group 3 MB cells and compare it with palbociclib effects. To this aim, HD-MB03 cells were treated with 0.01 µM, 0.1 µM, and 1 µM of dinaciclib and palbociclib in parallel, and 24h after, cells were seeded again in low-attachment conditions to promote the 3D-medullosphere formation. Interestingly, dinaciclib significantly inhibited medullospheres formation at all concentrations tested compared to untreated controls (NT), whilst palbociclib treatments showed a more limited inhibitory effect on tumoursphere formation, with 47% reduction being most substantial effect at 1 µM (Figure 18).

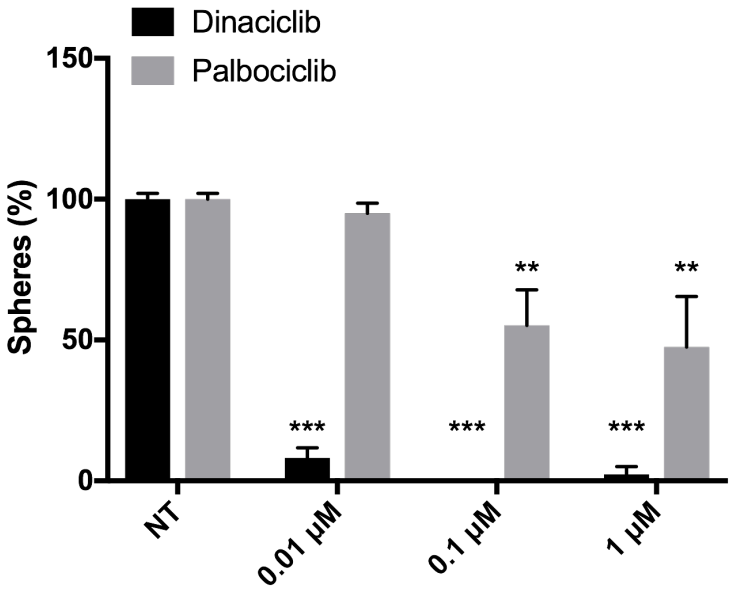

Figure 18 | Sphere formation assay after treatment with dinaciclib and palbociclib on HD-MB03 cells.

HD-MB03 cells have been treated with scalar concentrations of dinaciclib and palbociclib for 72 h, and then seeded again at 5000 cells/well in neural stem-cell media and low-attachment conditions. Spheres were counted after five days. Data are presented as mean percentage relative to untreated control ± SD (N=3, each performed in duplicates). Statistical comparisons were performed using two-tailed student's t-test where *= $p \leq 0.05$, **= $p \leq 0.01$, ***= $p \leq 0.001$.

4.2.4 Dinaciclib vs Palbociclib effects on cell cycle distribution and apoptosis

To further elucidate the inhibitory mechanisms of the two CDKis on group 3 MB cells on cell growth, we assessed cell cycle distribution and apoptosis by flow cytometry and apoptotic assays after 24h treatments with the compounds.

Treatment with dinaciclib induced a significant dose-dependent increase in the sub-G_1 cell population, starting from IC_{50} concentration (0.001 μM), compared to the untreated control. 1 μM dinaciclib generated the highest effect on sub-G1 population, reaching approximately 40% of the total cells. This observation indicated a predominant cytotoxic activity of dinaciclib (Figure 19A).

Conversely, treatment with palbociclib provoked only a significant cytostatic effect with cells arrested in G_1 phase at the IC_{50} concentration (0.1 μM) and even more so at 10 fold IC_{50} compared to untreated control (Figure 19B).

We further evaluated the cytotoxic potential of the drugs by measuring poly(ADP ribose) polymerase 1 (PARP-1) cleavage (indicated with * in Figure 19), a common marker of apoptotic induction via caspase-3 activation and caspase 3/7 activated labelling. We found that only dinaciclib induced PARP1 cleavage in HD-MB03 cells after 24h treatments, starting from 0.1 μM dose, whilst palbociclib treatments did not result in a PARP1 cleavage (Figure 20).

Caspase-mediated apoptosis was also confirmed using the CellEvent Caspase 3/7 green detection reagent, a substrate which becomes fluorescent upon cleavage by active caspases 3/7. Again, 24h treatment with 0.1 μM dinaciclib visually resulted in a robust signal detection compared to untreated cells and palbociclib effects in adherent HD-MB03 cells (Figure 21 A).

We also tested the efficacy of dinaciclib and palbociclib to induce cell death in a 3D spheroid model; HD-MB03 cell stimulation for 24h with tested drugs resulted in comparable effects with those obtained in adherent conditions (Figure 21 B and Appendix 6.1).

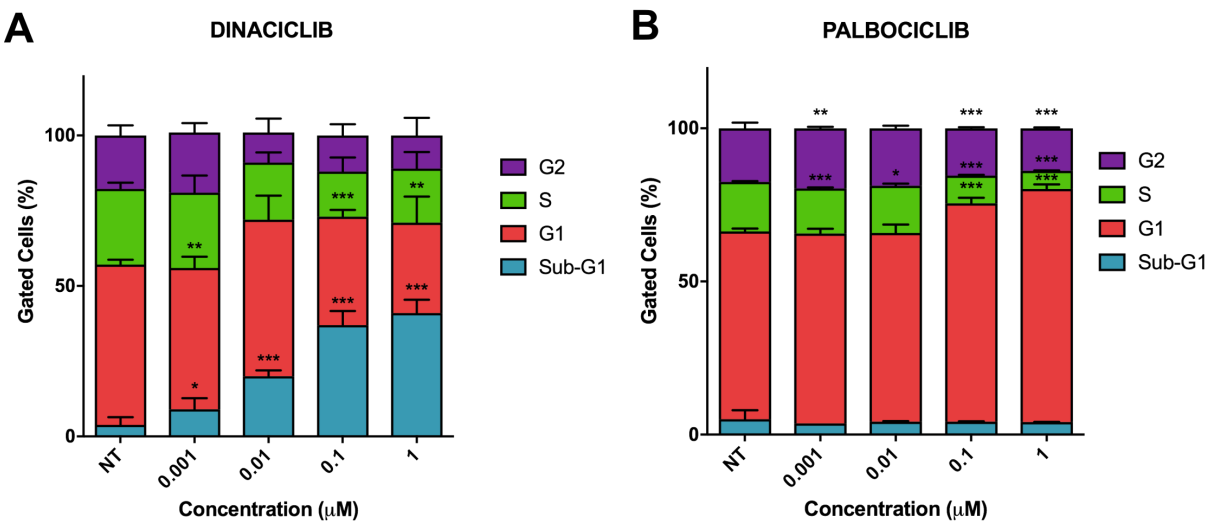

Figure 19 | Cell cycle analysis of HD-MB03 cells after treatment with dinaciclib and palbociclib.

HD-MB03 cells were treated with scalar concentrations of dinaciclib (A) and palbociclib (B) for 24 h. DNA content was measured by propidium iodide staining on flow cytometry. The percentages of cell-cycle phases are depicted in each column. Data are presented as mean ± SD of at three independent experiments and each run in triplicate. Statistical comparisons between drug treatments vs untreated control were performed using two-tailed student's t-test where *= $p \leq 0.05$, **= $p \leq 0.01$, ***= $p \leq 0.001$. NT= not treated, DMSO control.

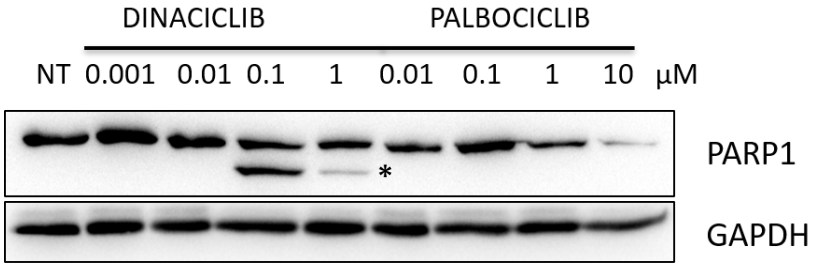

Figure 20 | PARP1 cleavage after treatment with dinaciclib and palbociclib on HD-MB03 cells.

HD-MB03 cells were treated for 24h with scalar concentrations of dinaciclib and palbociclib. 50 µg of total protein lysates were analysed by western blots. GAPDH was used as loading control. The blot shown is representative of 3 independent experiments. * shows the cleaved PARP1 fragment.

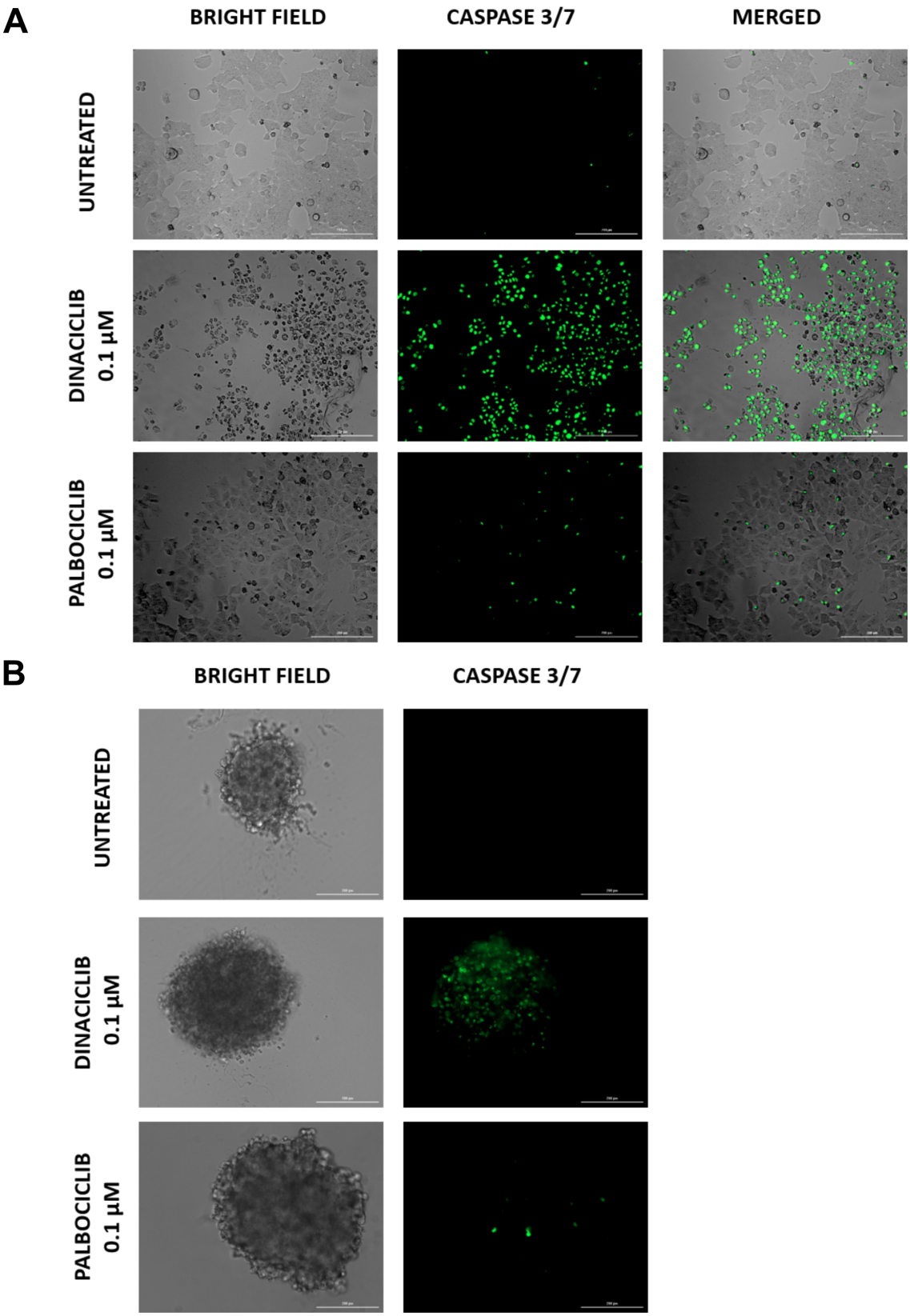

Figure 21 | Apoptotic activation after dinaciclib and palbociclib treatment in HD-MB03 cells by fluorescent microscopy.

A-B) HD-MB03 cells, 2D or cultured as 3D spheroids, were treated with 0.1µM of dinaciclib and palbociclib. After 24h treatment, CellEvent Caspase 3/7 Green detection reagent was added to each well (3µM). Fluorescent signal of apoptotic cells (green) was detected using the Cytation 3 system (Biotek) at 100X total magnification.

Finally, we wanted to gather more detailed information on how group 3 cells responded to dinaciclib by analysing individual cell fates. Understanding the patterns of cell fate choices upon treatment, gives valuable information on possible resistance mechanisms and allow us to improve treatment efficacy. Therefore, we analysed for 48h by time-lapse microscopy the morphological changes of 30 single cells upon treatment with 0.1 μM dinaciclib treatment. The majority of HD-MB03 cells died rapidly in interphase without entering mitosis (Figure 22). A small portion of cells either died in mitosis, completed division and died in the subsequent interphase or slipped. Particularly, mitotic slippage is an undesirable phenomenon for cancer treatment. Slippage entails that a cell exits mitosis without undergoing cytokinesis becoming tetraploid and potentially could re-enter cell cycle. This is a resistance modality by which cancer cells escape mitotic death unchecked and therefore calls for further study.

Nonetheless, our results showed dinaciclib as a potent inducer of apoptotic cell death in HD-MB03 cells, with mitochondria and caspases involvement, at nanomolar concentrations. Palbociclib treatments, inhibiting CDK4 and CDK6, decreased cell growth via cell cycle arrest in G1 and were less potent than dinaciclib treatments for *in vitro* MB.

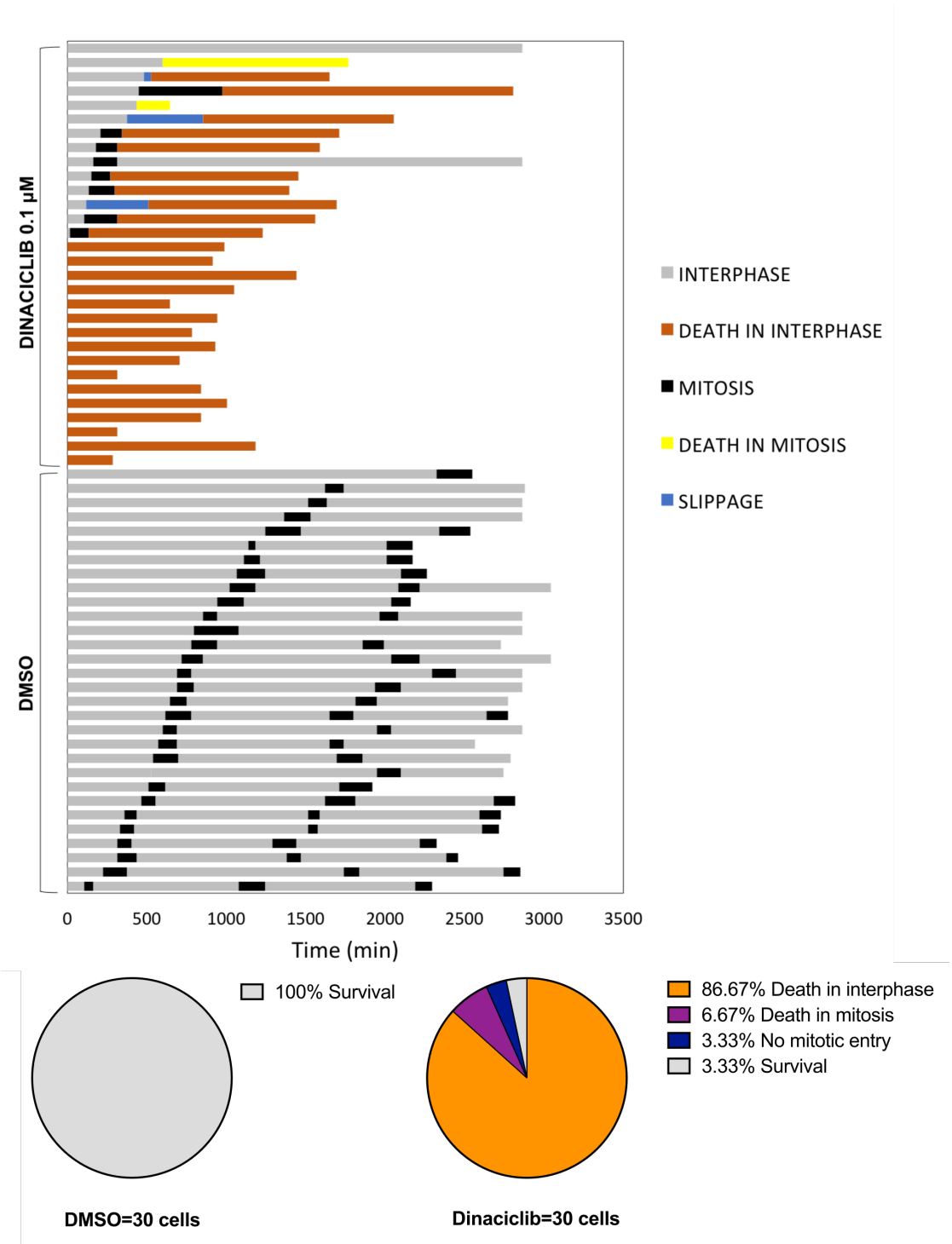

Figure 22 | Dinaciclib promotes rapid cell death in interphase in medulloblastoma.

Representative cell fate profiles of HD-MB03 cells treated with 0.1 µM dinaciclib or DMSO control (N=2). Each line depicts the fate of one single cell followed over time using time-lapse microscopy imaging. The colour of the line represents a specific cell behaviour, as indicated. A total of 30 cells per experiment from quadruplicate wells were analysed manually. Phase-contrast images were recorded every 15 minutes for 48h at 100X magnification in the Cytation 3 system (Biotek). Below, pie charts indicating the percentage of cells that either died in interphase, died in mitosis, remained in interphase or were still alive at the end of the recording (N=2).

4.2.5 Molecular mechanisms of dinaciclib sensitivity in MB

Having confirmed the better efficacy of dinaciclib than palbociclib for medulloblastoma, we further investigated the molecular mechanisms underlying the sensitivity of medulloblastoma cells to the drug.

4.2.5.1 CDK1 and CDK2 are overexpressed in MB and CDK5 and CDK9 are potential prognostic markers

Firstly, we conducted an *in silico* analysis, using the R2 software (http://r2.amc.nl), to assess the expression of the CDK1, CDK2, CDK5 and CDK9 targeted by dinaciclib and examined whether their expression was correlated to prognostic significance for MB.

We found that CDK1 and CDK2 were significantly up-regulated and CDK9 down-regulated in a cohort of 76 MB patient samples (G. Robinson, Parker, & Kranenburg, 2012) compared to 9 normal cerebellum specimens (dataset from (Roth et al., 2006) (Figure 23 A-B).

In addition, we examined whether CDKs expression was subgroup specific using the Cavalli et al. gene expression dataset (763 MB patients, (Cavalli et al., 2017)). CDK1, CDK2 and CDK5 had variable but similar levels of expression among different subgroups whilst CDK9 was consistently more expressed than the other CDKs in all MB subgroups. We also observed subgroup specific up-regulation of each CDK. Specifically, CDK1 was more expressed in WNT subgroup; CDK2 in SHH and WNT MBs; CDK5 in group 3 and CDK9 in group 4 MB (Figure 24 A and Appendix 6.2).

To extend our analysis, we generated Kaplan-Meier survival curves, again using the Cavalli et al. dataset, to evaluate the potential of CDK1, CDK2, CDK5 and CDK9 as prognostic markers. Data analysis with the R2 software showed that only the higher expression of CDK5 was significantly predictive of lower overall survival across all MB subgroups, according to the dataset used (Figure 24 B-E).

These findings suggest that CDK5 could be a potential prognostic biomarker for MB patients outcome and promising target for treatment, independently from MB subgrouping.

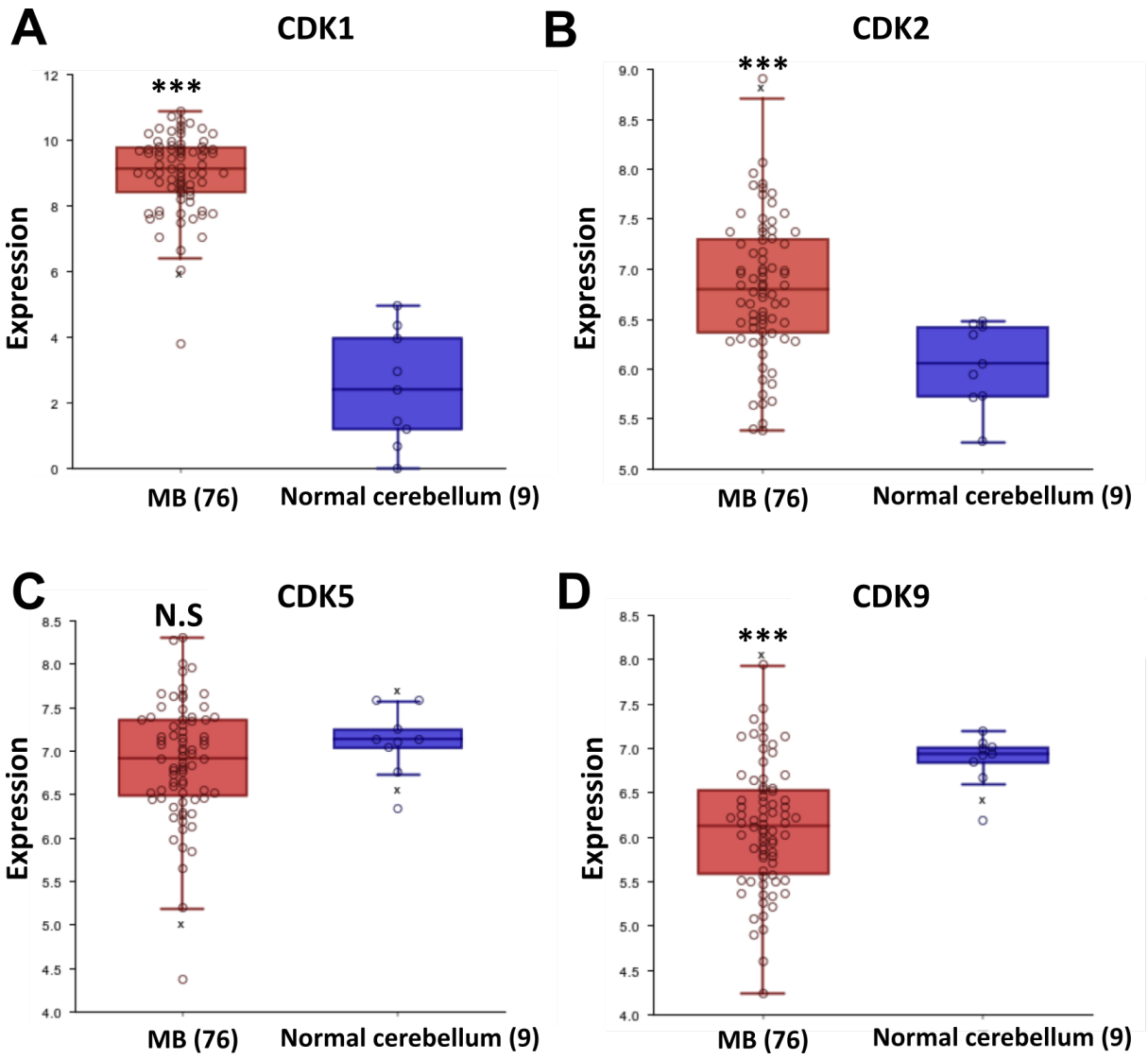

Figure 23 | CDK1, CDK2, CDK5 and CDK9 expression in MB patients vs normal cerebellum samples.

A-D) Boxplots summarising CDKs mRNA relative expression between MB patients n=76 (dataset from G. Robinson et al. 2012) and normal cerebellum samples n=9 (dataset from Roth et al. 2006). Statistical comparisons between groups were performed using one-way ANOVA where ***= $p \leq 0.001$ and N.S.= not significant. All analysis and graphs presented here were done through the R2 online software.

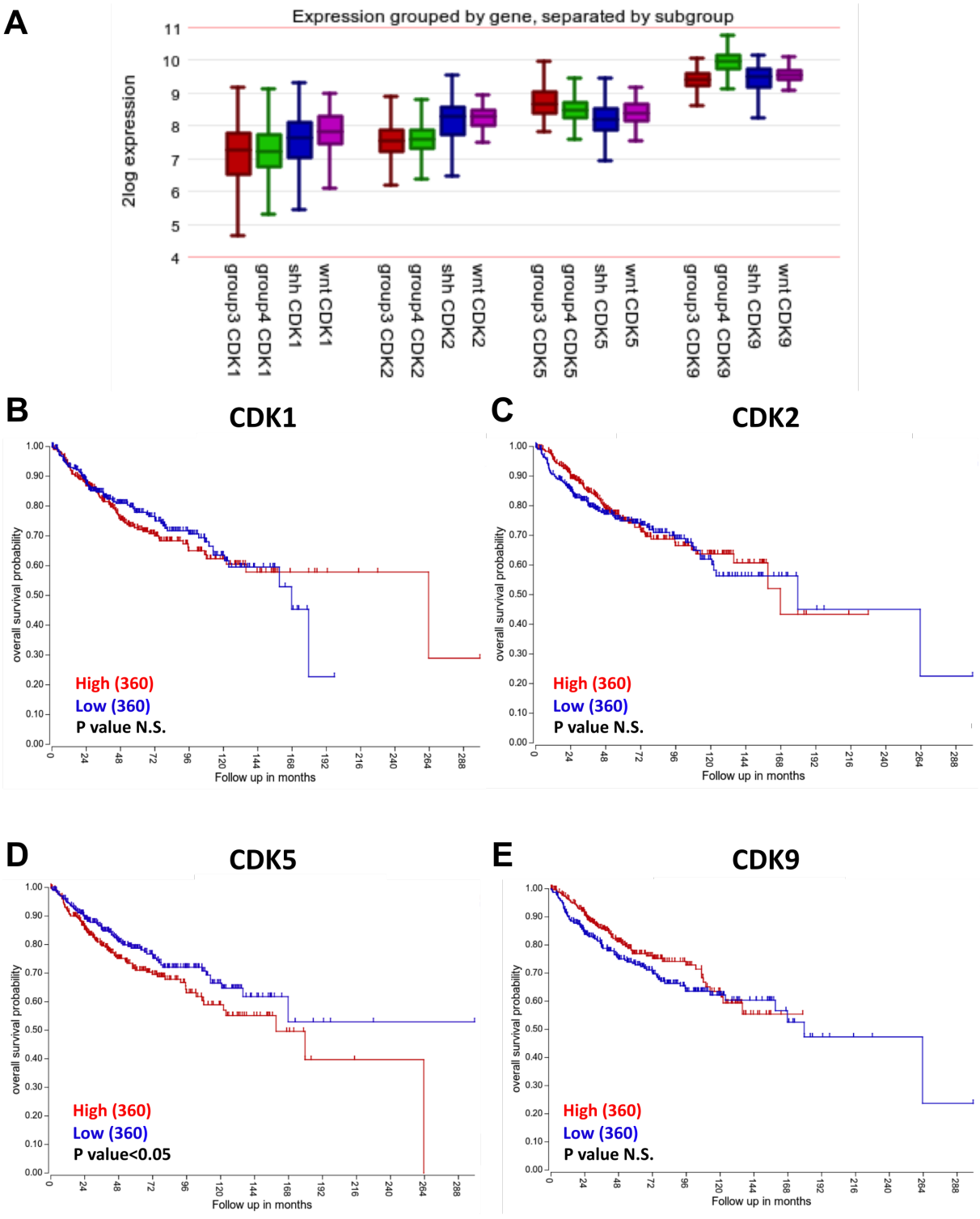

Figure 24 | CDK1, CDK2, CDK5 and CDK9 expression in MB subgroups and prognostic correlation in MB patients.

A) Dinaciclib targeted CDKs mRNA expression analysis across MB subgroups using Cavalli et al. dataset (n=763). Statistical values for each comparison were done using one-way ANOVA and can be found in the Appendix 6.2. B-E) Kaplan-Meier survival analysis based on CDK1, CDK2, CDK5 and CDK9 expression in MB patients (Cavalli et al. dataset, n=763). All analysis and graphs presented here were done through the R2 software. N.S.= not significant.

4.2.5.2 Transcriptomic effects of dinaciclib treatment in HD-MB03 cells

Due to the multiple targets of dinaciclib, we decided to employ an unbiased approach to identify key pathways involved in the cellular response to the drug. We performed an mRNA sequencing analysis comparing untreated HD-MB03 cells versus dinaciclib treated HD-MB03 cells. In order to filter out only the most critical response genes and mechanisms modulated by dinaciclib, we decided to use a relatively low dose and short incubation of the inhibitor for treatment, namely 0.001 µM (IC50 at 72h) for only 24h treatment.

As shown in the volcano plot in Figure 25 A, 627 mRNAs were significantly up-regulated (orange) and 685 down-regulated (blue) after dinaciclib treatment in HD-MB03 cells (*p-value* < 0.05), among protein-coding genes, long non-coding genes, small non-coding genes and pseudogenes.

We decided to focus on protein-coding gene alterations. The list of all significantly modulated protein-coding genes can be found in the Appendix 6.3: 92 genes were significantly upregulated and 50 down-regulated after treatment with FC>1.2 and *p-value* < 0.05.

As expected from our phenotypic results, pathway analysis by gene ontology (GO) revealed that most dinaciclib-regulated genes were involved in cell cycle and cell death, among other pathways (Figure 25 B).

To validate our sequencing results, we decided to focus on genes that were involved in cell death processes, also considering our previous results showing dinaciclib as a potent apoptotic inducer.

After only 24h treatment with dinaciclib IC50 dose, we could confirm the downregulation of BAX gene and the up-regulation of CASP9 by a single qRT-PCR in HD-MB03 cells (Figure 26). As a supplementary data to support BAX downregulation as a rapid response to dinaciclib treatments in MB, we have also observed proportional reduction of the BAX protein in ONS76 cells (Appendix 6.4).

Therefore, we hypothesised that CASP9 and BAX are involved in the early response to dinaciclib, both pointing at mitochondrial cell death mechanisms triggered by dinaciclib.

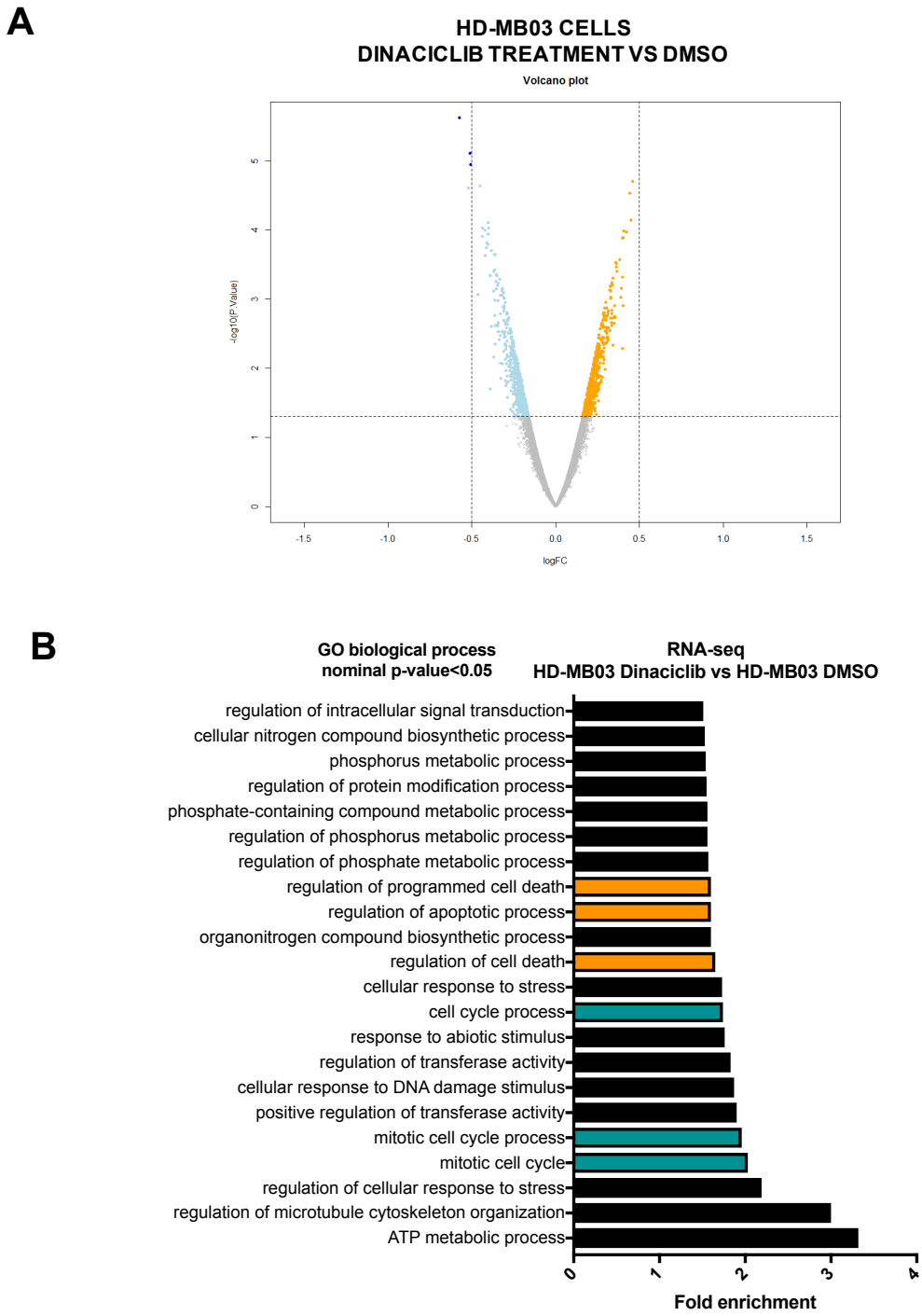

Figure 25 | RNA sequencing and pathway analysis after dinaciclib treatment in HD-MB03 cells.

A) Volcano plot of the RNA-seq data performed in HD-MB03 untreated (DMSO) cells vs HD-MB03 cells treated with 0.001 μM (IC50) dinaciclib for 24h. Blue dots represent all down-regulated genes, and orange dots represent all up-regulated genes after treatment (*p-value*<0.05). B) Gene ontology analysis of significantly up- and down-regulated genes with logFC±0.2 and *p-value*<0.05. Biological function terms with fold enrichment score≥1.5 and FDR<0.05 are presented using GraphPad Prism software. Most relevant cellular functions for the study are high-lighted with colours (orange for cell death-related functions and green for cell cycle-related functions).

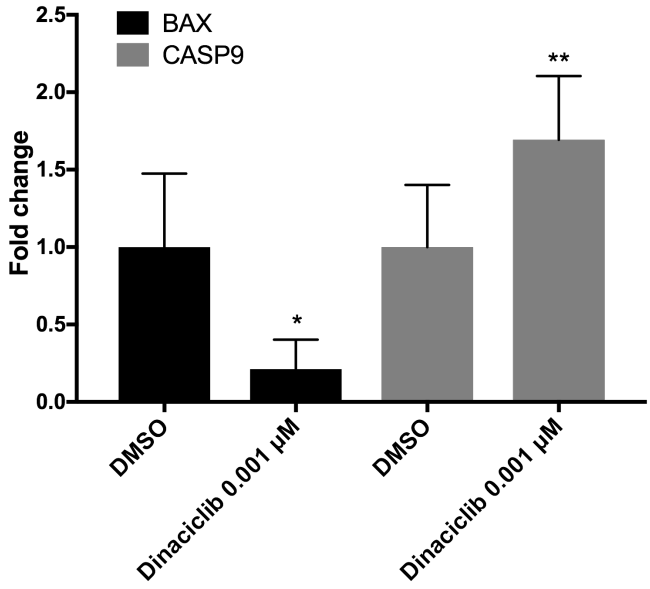

Figure 26 | RNA-seq validation by a single qRT-PCR in HD-MB03 cells.

HD-MB03 cells were treated with 0.001 µM (IC50) dinaciclib or DMSO for 24h. Total RNA was subjected to qRT-PCR analysis for BAX and CASP9 expression and normalised with actin. Plotted graphs show fold change mean ± SD (n=3). Statistical comparisons were performed using two-tailed student's t-test where: *= $p \leq 0.05$, **= $p \leq 0.01$, ***= $p \leq 0.001$.

4.2.5.3 Mechanisms of cell death mediated by dinaciclib

Next, to investigate which of the targeted CDKs was the main driver of the effects observed in cell growth inhibition and apoptosis induction, we silenced CDK1, CDK2 and CDK9 by RNAi. Specifically, we decided to study those CDKs and not CDK5, for their role in cell cycle and transcription regulation. Successively, significant effects were validated in the ONS76 cell line to investigate whether the drug acted with the same mechanism in other MB subgroups.

Upon silencing using a pool of 4 siRNAs targeting individual CDKs for 72h, we observed that CDK1 and CDK9 were responsible for the reduction of cell proliferation in both cell lines tested, with seemingly higher impact on the ONS76 cell line (Figure 27 A-B).

Apoptosis, detected through caspase 3/7 activity measurements, was significantly induced upon silencing of CDK9 in both cell lines, with a 45% induction in HD-MB03 cells and a 36% induction in ONS76 cells (Figure 27 C-D).

Overall, these findings offer possible mechanistic implications of the dinaciclib-targeted CDKs in the phenotypic effects observed after treatment. As expected, the targeting of CDK1, reduced cell proliferation mainly through cell cycle arrest, since no apoptotic effect has been observed after silencing in HD-MB03 cells. On the contrary, cell viability impairment under CDK9 silencing was a consequence of apoptotic effects in both cell lines.

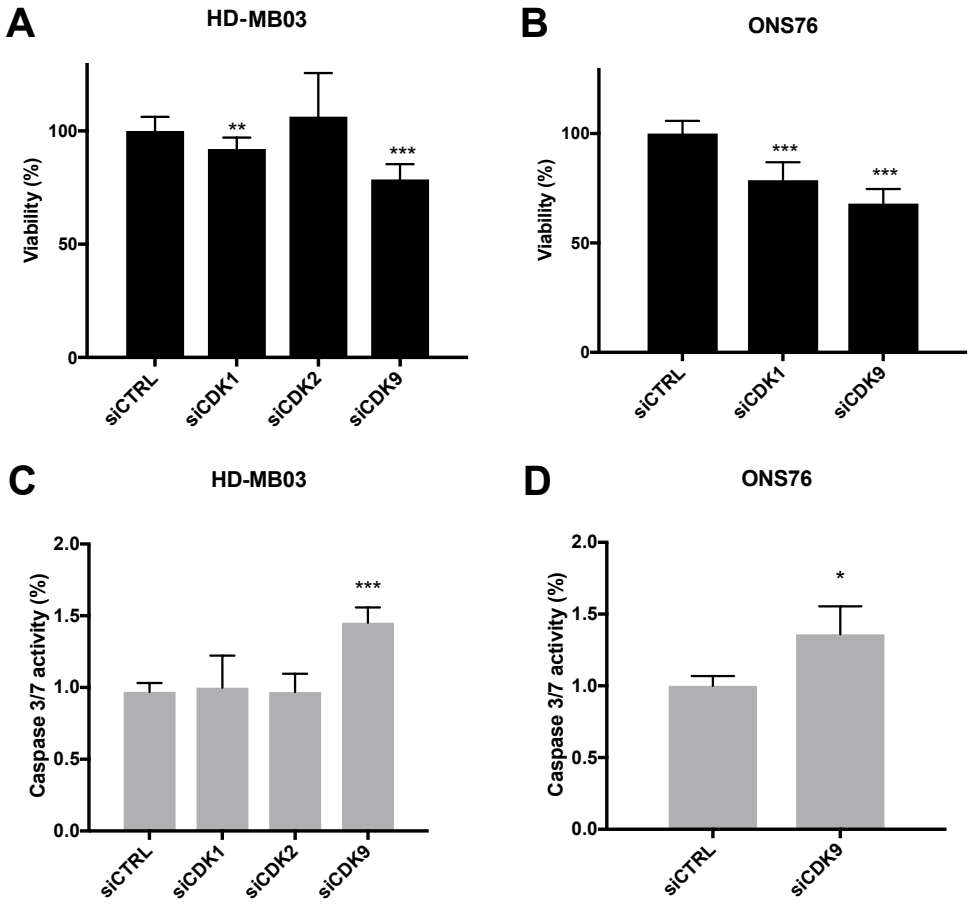

Figure 27 | CDKs silencing phenotypic effects in HD-MB03 and ONS76 cell lines via RNA interference.

HD-MB03 and ONS76 cells were transfected with siCDK1/siCDK2/siCDK9 or scramble siRNA (siCTRL) at 100nM. All siRNAs are formulated as a pool of 4 siRNAs targeting each CDKs and silencing. After 72h from transfections, viability (A-B) was assessed by MTT assay and apoptosis (C-D) was assessed by Caspase Glo assay measuring the caspase 3/7 activity. Data are presented as mean of 2 biological replicates, each performed using 4 technical replicates, ± SD. Statistical comparisons were performed using two-tailed student's t-test where: *= $p \leq 0.05$, **= $p \leq 0.01$, ***= $p \leq 0.001$.

To complete our analysis, we tested protein levels of dinaciclib targets after 24h scalar concentration treatments of the drug in HD-MB03 cells, and we assessed significant results in ONS76 cells, for biological comparison. We found that levels of CDK2 and CDK5 were mostly stable after dinaciclib treatment in HD-MB03 cells; in contrast, CDK9, and slightly CDK1, protein levels were markedly reduced at 0.1 and 1 μM of dinaciclib. CDK9 protein reductions starting from 0.1 μM was also confirmed in ONS76 cells (Figure 28 A-B).

Considering the efficacy of dinaciclib in inhibiting the transcriptional CDK9 in HD-MB03 cells, we hypothesised that its pronounced apoptotic activity could be in part due to the suppression of transcription.

In support of reduced CDK9 activity, we detected lower RNA polymerase II phosphorylation at Ser 2, a specific CDK9 phosphorylation site, along with reductions of known downstream targets of the RNA pol II, MYC and MCL-1, which are promptly influenced by RNApol II alteration due to their short half-life (Booher et al., 2014; Hashiguchi et al., 2019; Rello-Varona et al., 2019). Notably, although the down-regulation effect on MCL-1 was comparable between cell lines, MYC protein levels were markedly more affected in HD-MB03 cells than in ONS76 cells.

In addition, we considered the possibility that dinaciclib cytotoxicity might also depend on CDK1 targeting, since CDK1 protein levels reduce, albeit slightly, at apoptotic doses (0.1 and 1 μM).

Moreover, dinaciclib significantly decreased Rb phosphorylation at S807/811 in both cell lines, with a stronger effect in ONS76 cells than HD-MB03 cells.

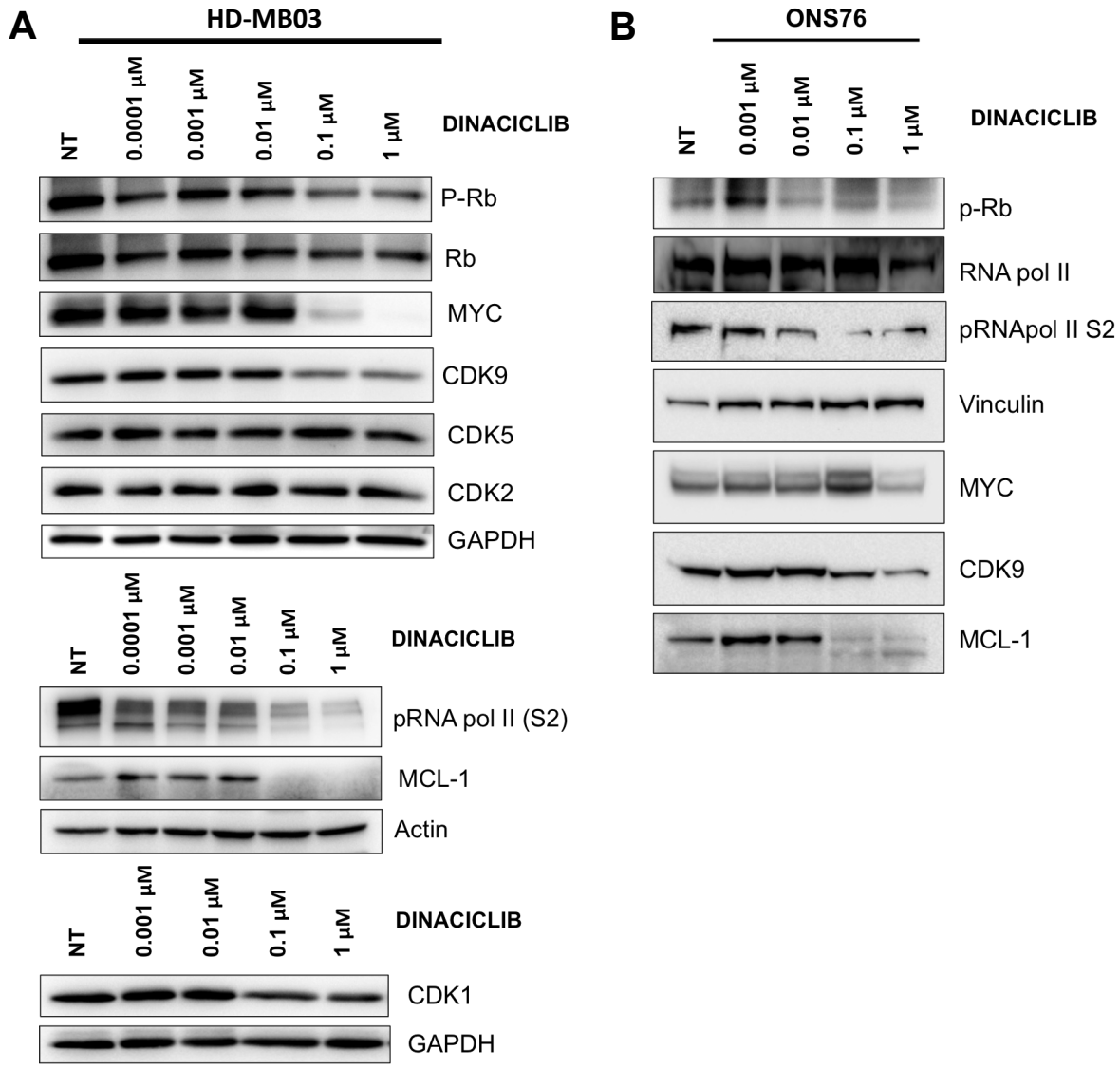

Figure 28 | Dinaciclib treatment affects key proteins involved in cell-cycle and transcription.

A-B) HD-MB03 and ONS76 cells were treated with scalar concentrations of dinaciclib for 24h. 50µg of protein lysates were subjected to immunoblotting with indicated antibodies. Vinculin, actin or GAPDH were used as loading controls. These are representative western blots from three replicates for the HD-MB03 cell line and two replicates for the ONS76 cell line.

4.2.5.4 Mechanisms of cell death mediated by dinaciclib: the BCL2 family proteins.

To further infer cell death response mechanisms triggered by dinaciclib, we first wanted to have an overview of the expression of key apoptosis-associated proteins in MB. We analysed the basal levels of PARP-1, MCL1, BCL2, BCLXL in HD-MB03, ONS76 and DAOY cell lines. We added to the panel BAX, which we observed to be rapidly regulated after dinaciclib from our RNA-seq data, and MYC because we hypothesised that MYC abundance could have a role in differential cell cycle and apoptotic responses to dinaciclib and because it has been previously shown to regulate BAX expression (Mitchell et al., 2000). Expression patterns were variable across tested cell lines, but the most characteristic differences are summarised as follows: PARP-1 expression was higher in HD-MB03 cells than other cell lines; DAOY and HD-MB03 cells had almost undetectable levels of BCLXL and BCL2, respectively; but both cell lines have high expression of MCL-1; finally, HD-MB03 cells had overall higher expression of BAX protein (Figure 29 A).

Next, since apoptosis is ultimately the result of the balance between anti-apoptotic BCL2 members (MCL1, BCLXL and BCL2), we used BCL2 homology 3 (BH3)-mimetics as a tool to differentiate apoptotic vulnerabilities across MB cell lines. HD-MB03, ONS76 and DAOY cells were subjected to 72h treatments with scalar concentrations of maritoclax (MCL-1 selective inhibitor), navitoclax (BCL-2, BCL-XL and BCL-w inhibitor) and WEHI-539 (BCL-XL selective inhibitor) (Figure 29 B-D). We observed that the specific MCL-1 inhibitor, maritoclax, was the most effective of the BH3-mimetic compounds in all the cell lines, reaching IC50 values in the nanomolar range for HD-MB03 cells (Figure 29 B).

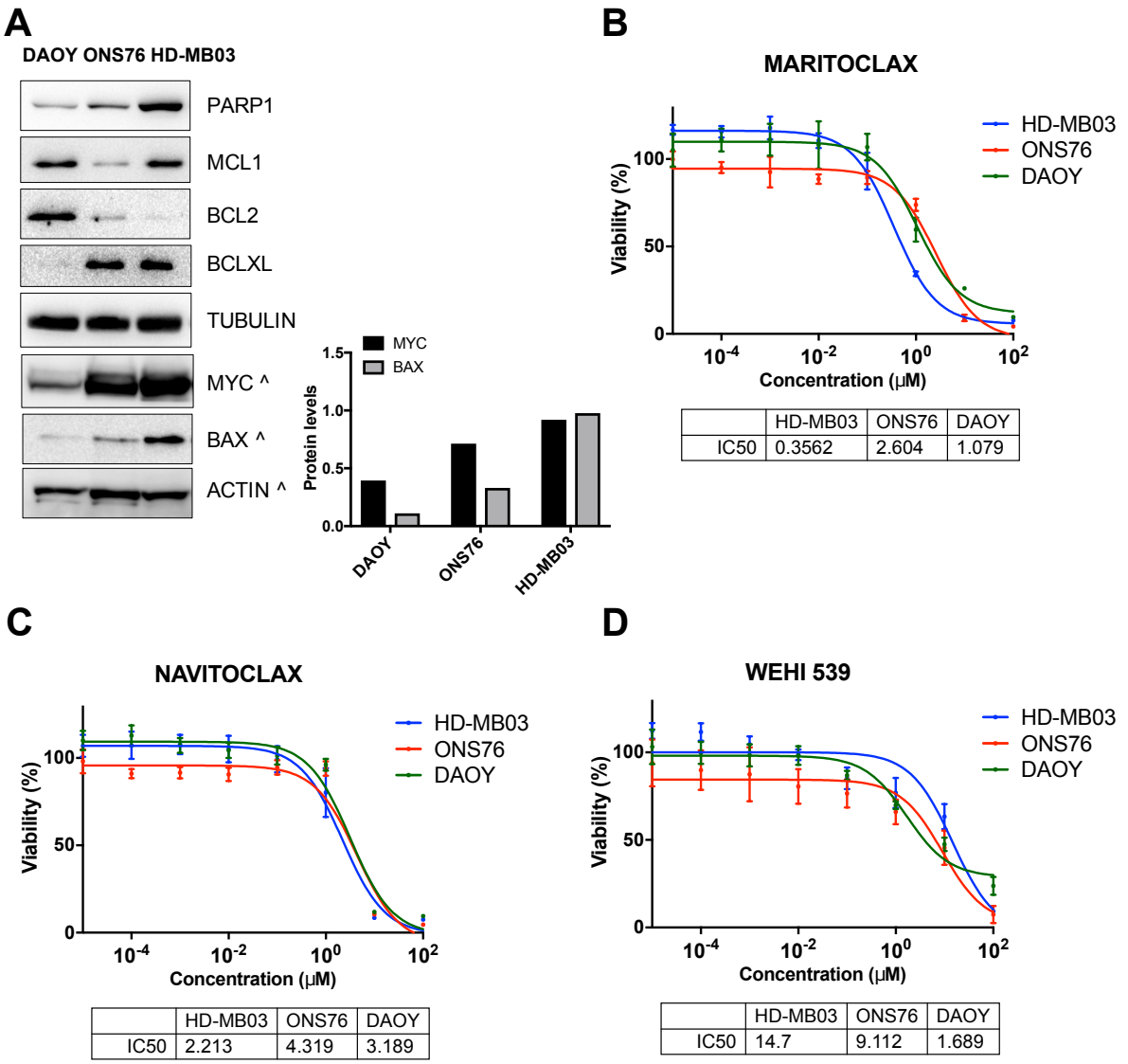

	HD-MB03	ONS76	DAOY
IC50	0.3562	2.604	1.079

	HD-MB03	ONS76	DAOY
IC50	2.213	4.319	3.189

	HD-MB03	ONS76	DAOY
IC50	14.7	9.112	1.689

Figure 29 | Regulators of mitochondrial apoptosis and functional analysis in medulloblastoma cell lines.

A) Representative western blot of two replicates showing the basal expression of key regulators of mitochondrial apoptosis pathway in DAOY, ONS76 and HD-MB03 MB cells. 50μg of protein lysates were used for immunoblotting with indicated antibodies. Tubulin and actin were used as loading controls. ^ symbol indicates proteins run on a different blot but using the same protein lysates and run at the same protein quantity. Densitometric analysis for WB ^ is provided on the right. B-D) DAOY, ONS76 and HD-MB03 cells were treated with a 0-100μM range of concentrations of maritoclax, navitoclax and WHEI 539 (1:10 fold dilution) for 72h. Viability was assessed using MTT assay. Data are presented as mean ± SD using GraphPad software (N=3 replicates, each performed in quadruplicates). IC50 values (μM) are presented below each graph.

Since we previously detected the downregulation of the anti-apoptotic MCL1 after dinaciclib treatment, we further addressed its role in dinaciclib-mediated cell death by RNAi. MCL-1 silencing using two different siRNAs resulted in viability reduction and marked apoptotic induction in both HD-MB03 and ONS76 cells (Figure 30 A-B).

As shown previously, dinaciclib induced apoptosis also in ONS76 cells, which have a weak expression of MCL-1. Moreover, the apoptotic induction via MCL-1 in ONS76 cells was confirmed by RNAi. These observations further suggest the onset of multiple mechanisms of cell death by dinaciclib, which cannot only be ascribed to MCL-1 downregulation.

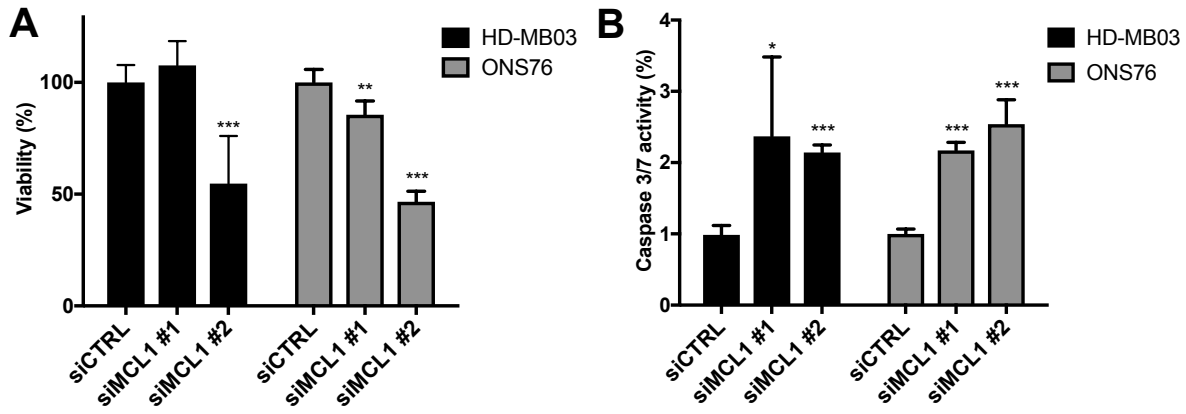

Figure 30 | MCL-1 silencing phenotypic effects in HD-MB03 and ONS76 cell lines via RNA interference.

HD-MB03 and ONS76 cells were transfected with two different siRNAs targeting MCL-1 or scramble siRNA (siCTRL) at 50nM. After 72h from transfections, viability (A) was assessed by MTT assay and apoptosis (B) was assessed by Caspase Glo assay measuring the caspase 3/7 activity. Data are presented as mean of 2 biological replicates, each performed using 4 technical replicates, ± SD. Statistical comparisons were performed using two-tailed student's t-test where: *= $p \leq 0.05$, **= $p \leq 0.01$, ***= $p \leq 0.001$.

4.2.6 Dinaciclib sensitises HD-MB03 cells to chemotherapy

In recent years, chemotherapy for cancer treatment is mostly used in combination with other agents because of its improved efficacy, such as slower development of drug resistance and lower treatment failure rate (Bozic et al., 2013). As vincristine and cisplatin are commonly used as a standard of care for MB treatment, we wanted to evaluate whether multi-CDKs targeting with dinaciclib could sensitise MB cells to these chemotherapeutic agents allowing to contain toxicity-associated side effects.

After combined treatments with dinaciclib (0.000001, 0.0001, 0.01 and 0.1 μM) and either 0-10 μM doses of vincristine at 1:10 fold dilution or 0-100 μM doses of cisplatin at 1:2.5 fold dilution, cell survival was significantly reduced compared with single chemo-drugs treatments. Leftward shifts towards lower doses of both vincristine (Figure 31 A) and cisplatin (Figure 31 B) demonstrate dose-dependent chemo-drugs fold-sensitisation by dinaciclib.

To characterise the anti-growth effects of combination treatments, combination index (CI) values were computed using CompuSyn software (Figure 31 A-B, on the right).

Both vincristine and cisplatin combinations with dinaciclib proved to have synergistic potential, with CI values < 1. Dinaciclib doses more significantly reduced cell growth of HD-MB03 cells when combined with vincristine than cisplatin. Nonetheless, dinaciclib significantly enhanced cisplatin doses efficacy at 0.16-6.4 μM range.

The results indicate that multi-CDK targeting with dinaciclib could be a promising approach to sensitise vincristine- and cisplatin-resistant HD-MB03 cells to the respective drugs.

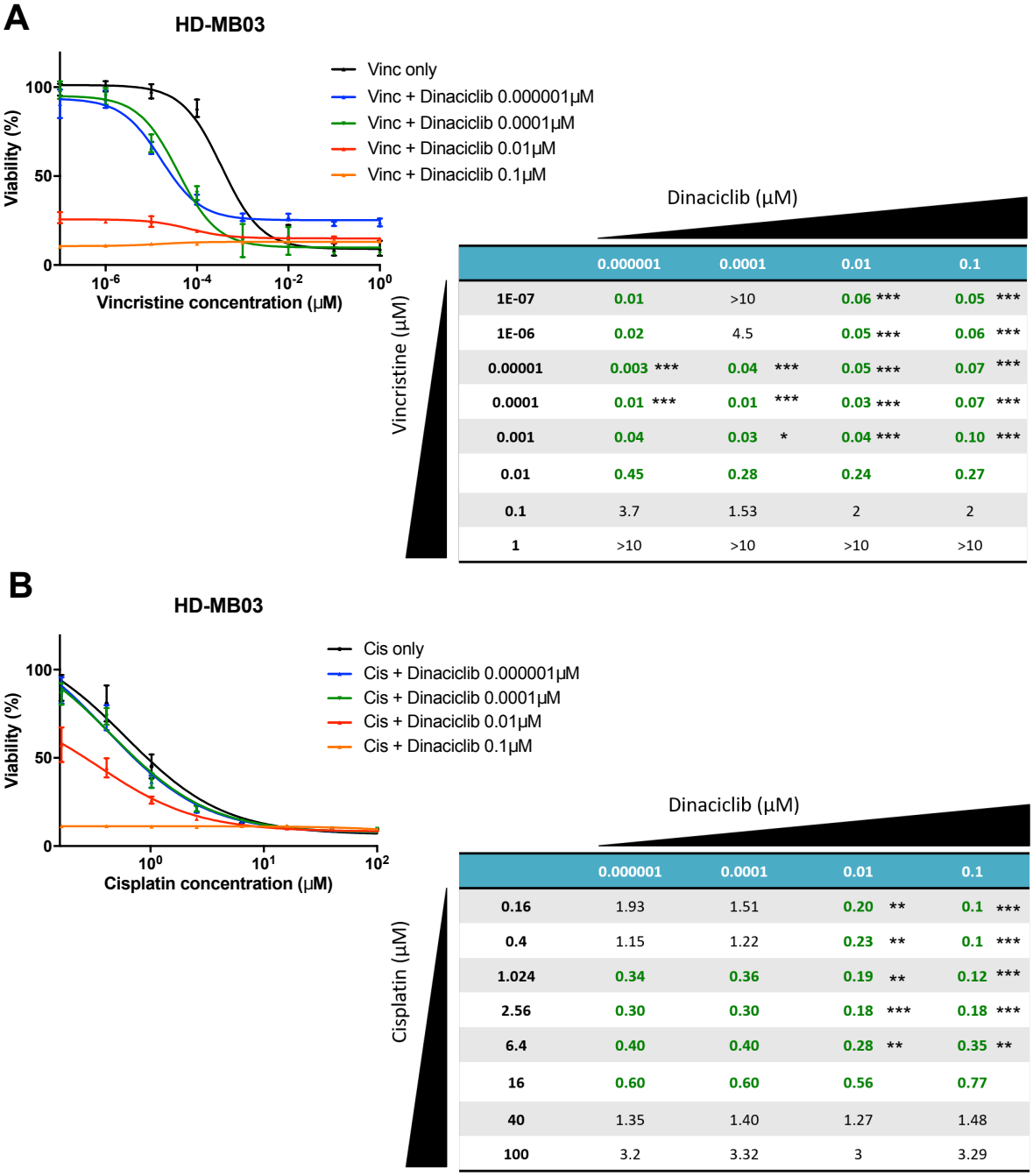

	0.000001	0.0001	0.01	0.1
1E-07	0.01	>10	0.06 ***	0.05 ***
1E-06	0.02	4.5	0.05 ***	0.06 ***
0.00001	0.003 ***	0.04 ***	0.05 ***	0.07 ***
0.0001	0.01 ***	0.01 ***	0.03 ***	0.07 ***
0.001	0.04	0.03 *	0.04 ***	0.10 ***
0.01	0.45	0.28	0.24	0.27
0.1	3.7	1.53	2	2
1	>10	>10	>10	>10

	0.000001	0.0001	0.01	0.1
0.16	1.93	1.51	0.20 **	0.1 ***
0.4	1.15	1.22	0.23 **	0.1 ***
1.024	0.34	0.36	0.19 **	0.12 ***
2.56	0.30	0.30	0.18 ***	0.18 ***
6.4	0.40	0.40	0.28 **	0.35 **
16	0.60	0.60	0.56	0.77
40	1.35	1.40	1.27	1.48
100	3.2	3.32	3	3.29

Figure 31 | Combination drug dose-response assay with chemotherapy and dinaciclib treatments in HD-MB03 cells.

HD-MB03 cells were dosed with vincristine (A) or cisplatin (B) as single-agent and in combination with dinaciclib. After 72h cell viability was determined using MTT assay. Data are presented as mean ± SD (N=3) using GraphPad software. Combination index (CI) values are presented. CI lower than 1 indicates synergistic interactions (in green), while values greater or equal than 1 indicate antagonistic or additive interactions, respectively. CI values were calculated with CompuSyn Software and are shown for distinct dose combinations. Statistical comparisons were performed between the inhibitory effect of combination treatment vs individual chemo-treatments using two-tailed student's t-test where: *= $p \leq 0.05$, **= $p \leq 0.01$, ***= $p \leq 0.001$.

4.2.7 BH3-mimetics enhance dinaciclib effects in medulloblastoma

Since we showed that dinaciclib treatments down-regulate the anti-apoptotic proteins MCL-1 and since chemo-resistance has been frequently ascribed to overexpression of BCL-2 family members (van Delft et al., 2006; Vogler et al., 2009), we asked if combination therapy with BH3-mimetics could enhance cell death by dinaciclib in medulloblastoma. For this purpose, we selected for treatment the specific MCL-1 inhibitor, maritoclax, and the broad BCL-2 inhibitor, navitoclax, targeting BCL-2, BCL-XL and BCL-w.

We treated HD-MB03 and ONS76 cells with scalar drug combinations of dinaciclib alone or dinaciclib with either maritoclax or navitoclax for 72h. MTT assay results showed that doses of maritoclax and navitoclax significantly enhanced dinaciclib growth inhibitory effects in both HD-MB03 and ONS76 cell lines (Figure 32 A-D). Overall, both BH3-mimetics were more efficient in HD-MB03 than ONS76 cells, since they synergised with lower doses of dinaciclib (Figure 32 E-H).

These suggest that co-treatments of maritoclax and navitoclax with dinaciclib have the potential to intensify treatment-response rate and to reduce the concentration of each drug needed to elicit a satisfactory inhibitory effect.

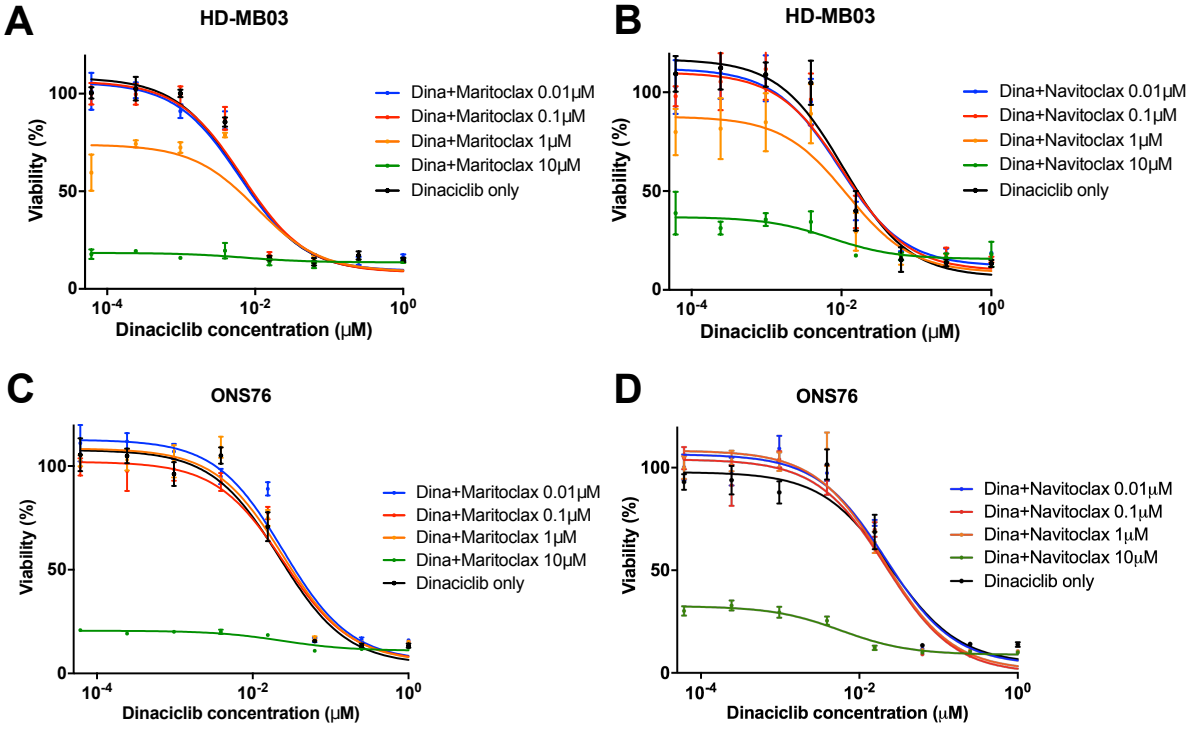

E

Maritoclax (μM)

Dinaciclib (μM)

	0.01	0.1	1	10
6.10E-5	2.53E16	>10	0.02 ***	0.001 ***
2.44E-4	2.53E16	>10	0.17 ***	0.003 ***
9.77E-4	0.09 **	>10	0.14 ***	0.006 ***
0.004	0.09	0.29	0.42 ***	0.03 ***
0.016	0.10	0.10	0.09	0.09
0.062	0.38	0.39 *	0.37	0.34
0.25	1.46	1.45	1.47	1.48
1	6.1	5.83	5.7	5.84

F

Navitoclax (μM)

Dinaciclib (μM)

	0.01	0.1	1	10
6.10E-5	>10	>10	0.003 **	0.01 ***
2.44E-4	1.13	>10	0.01 *	0.01 ***
9.77E-4	6.6	>10	0.02 *	0.01 ***
0.004	0.07	0.09	0.06	0.03 ***
0.016	0.11	0.11	0.10	0.08 **
0.062	0.31	0.31	0.30	0.32
0.25	1.30	1.27	1.20	1.24
1	5	5	5	5

G

Maritoclax (μM)

Dinaciclib (μM)

	0.01	0.1	1	10
6.10E-5	>10	>10	>10	2.43E-4 ***
2.44E-4	>10	0.15	>10	8.80E-4 ***
9.77E-4	>10	0.85	>10	0.004 ***
0.004	0.8 **	0.53 **	>10	0.01 ***
0.016	1.47	0.66	0.58	0.05 ***
0.062	0.18	0.18	0.19 *	0.12 ***
0.25	0.74	0.67 *	0.69 *	0.52 *
1	2.9	2.79	2.80	2.24

H

Navitoclax (μM)

Dinaciclib (μM)

	0.01	0.1	1	10
6.10E-5	>10	>10	>10	0.002 ***
2.44E-4	>10	>10	>10	0.003 ***
9.77E-4	>10	>10	>10	0.01 ***
0.004	>10	6.32	0.06	0.01 ***
0.016	1.47	1.14	0.7	0.01 ***
0.062	0.04	0.03 **	0.04 ***	0.03 ***
0.25	0.22	0.09 ***	0.15 ***	0.14 ***
1	0.92	0.51	0.57 ***	0.51 ***

Figure 32 | BH3-mimetics synergise with dinaciclib to inhibit medulloblastoma cell growth.

HD-MB03 and ONS76 cells were dosed with dinaciclib as single-agent and in combination with maritoclax (A-C) or navitoclax (B-D). After 72h cell viability was determined using MTT assay. Data are presented as mean ± SD (N=3) using GraphPad software. Combination index (CI) values are presented. CI lower than 1 indicates synergistic interactions (in green), while values greater or equal than 1 indicate antagonistic or additive interactions, respectively. CI values were calculated with CompuSyn Software and are shown for distinct dose combinations in HD-MB03 cells (E-F) and ONS76 cells (G-H). Statistical

comparisons were performed between the inhibitory effect of combination treatment vs dinaciclib treatment alone using two-tailed student's t-test where: *= $p \leq 0.05$, **= $p \leq 0.01$, ***= $p \leq 0.001$.

4.2.8 Generation of chemo-resistant HD-MB03 cells and dinaciclib effects

To date, the major drawback of chemotherapeutic treatments is the emergence of drug-resistant cells. One of the mechanisms of resistance is apoptotic failure, which can be due to alterations in the cell cycle- and/or apoptosis-regulating proteins (Luqmani, 2005). Since we observed that dinaciclib is a potent apoptotic inducer in medulloblastoma, we wanted to assess its efficacy in resistance settings.

To mimic the context of acquired resistance to chemotherapeutic drugs in vitro, we employed cell lines with acquired resistance to vincristine and cisplatin. Specifically, HD-MB03 cells were kept in culture for three months in the presence of progressively higher doses of chemotherapeutic drugs, until cells were able to grow with concentrations close to the respective IC50.

Resistant cells were established at final concentrations of 0.002 µM vincristine and 0.5 µM cisplatin. To confirm that each cell line acquired resistance, we assessed IC50 values of resistant cells compared to parental cells with short-term viability assays (72h). Each chemo-resistant subline showed significantly increased IC50 values than sensitive cells, with approximately a 10-fold and 2-fold increase for vincristine and cisplatin cells, respectively (Figure 33 A-B).

Acquired resistance was further validated testing the drug inhibition-response in a more extended treatment timescale (9 days) after which viability was measured by crystal violet staining. Both chemo-resistant HD-MB03 cell lines were still less affected than parental cells after long-term exposure with either vincristine or cisplatin (Figure 33 C-D). Notably, cisplatin-resistant HD-MB03 manifested overall stronger resistance to the primary inhibitor than vincristine-resistant cells in long-term treatments, with a 3-fold increase in cell viability than parental cells.

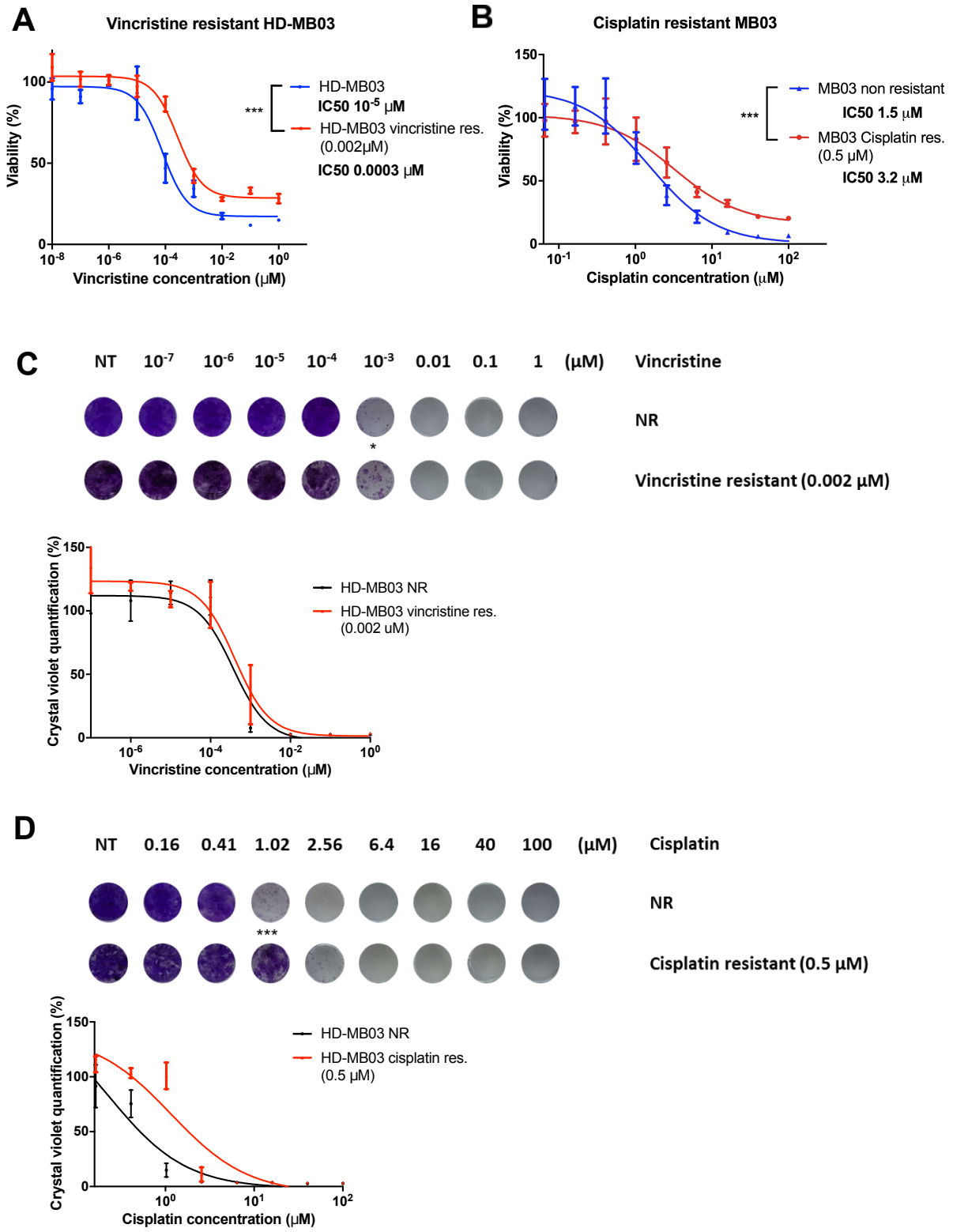

Figure 33 | Generation of vincristine and cisplatin-resistant HD-MB03 cells.

A-B) Parental and chemo-resistant HD-MB03 cells were treated with either 0-1 μM doses (1:10 fold dilution) of vincristine or 0-100 μM doses (1:2.5 fold dilution) of cisplatin for 72h. Cell viability was examined using MTT assay. Data are presented as mean ± SD (N=3) using GraphPad software. C-D) Representative images of long-term viability assay (N=3) of parental and chemo-resistant HD-MB03 cells. HD-MB03 cells were seeded at 200 cells/well and treated for 9 days with the respective chemotherapeutic drugs (3 treatments). Viability of non-resistant (NR) and resistant HD-MB03 cells was

compared using 0.5% w/v crystal violet staining. Measurements of the staining are presented below each image using GraphPad software. Statistical comparisons were performed using two-tailed student's t-test where: *= $p \leq 0.05$, **= $p \leq 0.01$, ***= $p \leq 0.001$.

4.2.9 Dinaciclib efficacy on chemo-resistant HD-MB03 cells

Following the generation of group 3 cell lines resistant to currently used chemotherapeutic drugs, we asked if dinaciclib could overcome acquired resistance.

Dinaciclib treatment of sensitive and chemo-resistant cell lines resulted in a comparable inhibition of proliferation, resulting in identical IC_{50} concentrations in short-term treatment assays (72 h) (Figure 34 A-B).

Next, we wanted to evaluate if longer exposures with dinaciclib could be more effective in chemo-resistance settings. Therefore, we evaluated dinaciclib treatment in long-term proliferation assay (9 days), with drug replacement every other day.

Vincristine-resistant HD-MB03 cells exhibited higher sensitivity than parental cells when treated at 0.01 µM dinaciclib (Figure 34 C). In contrast, cisplatin-resistant cells did not show vulnerability for dinaciclib treatment when compared with parental cells even at longer exposure with the inhibitor (Figure 34 D).

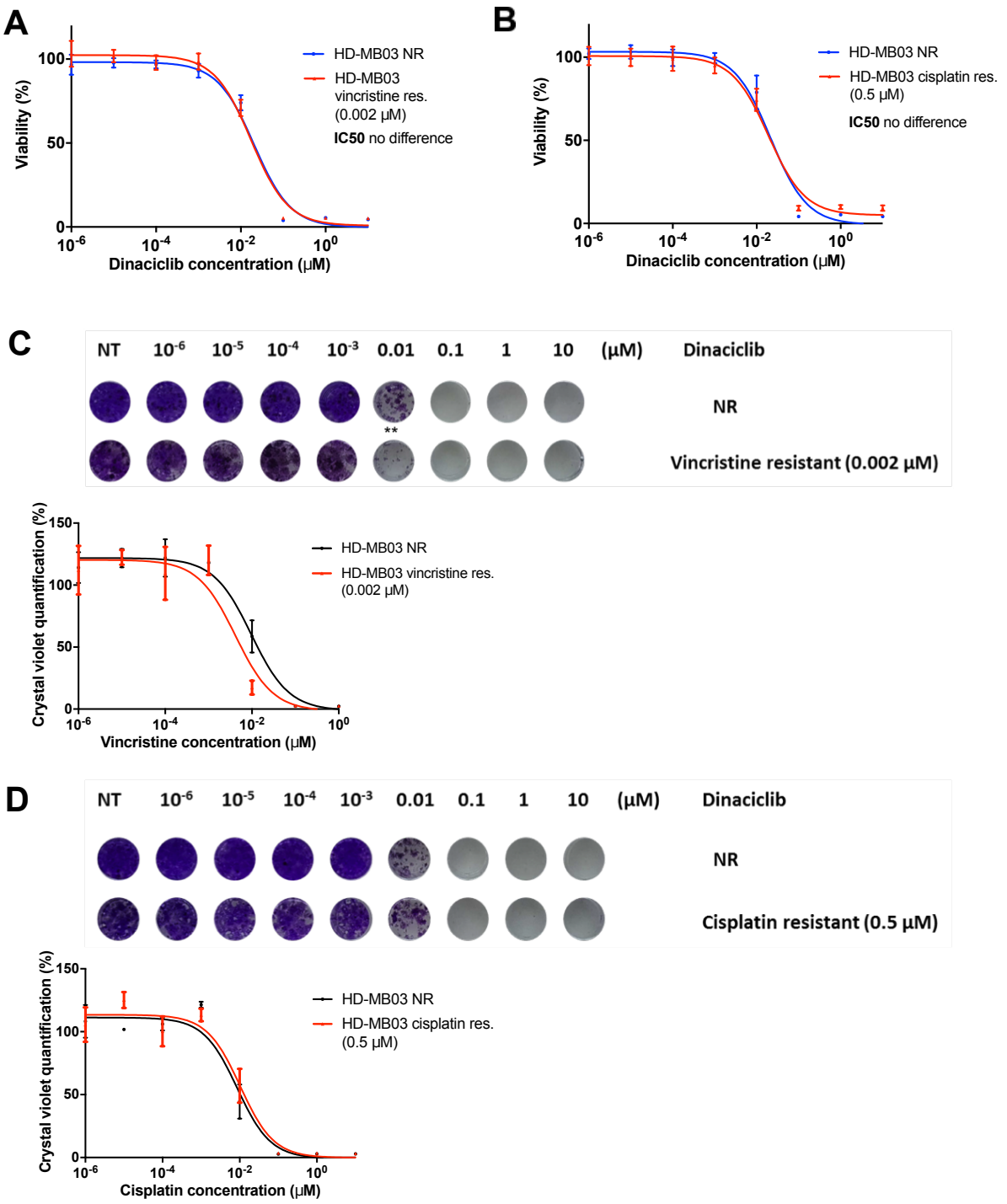

Figure 34 | Dinaciclib effects on cell viability in parental vs chemo-resistant HD-MB03 cells.

A-B) Non-resistant (NR) and chemo-resistant HD-MB03 cells were treated with a 0-10 µM range of concentrations (1:10 fold dilution) with dinaciclib for 72h. MB cell proliferation was assessed using MTT assay. Data are presented as mean ± SD (N+3) using GraphPad software. C-D) Parental and chemo-resistant HD-MB03 cells were seeded at 200 cells/well and treated for 9 days with dinaciclib 0-10 µM (1:10 fold dilution). Long-term viability is here compared using 0.5% w/v crystal violet staining. Measurements of the staining are presented below each image using GraphPad software. Statistical comparisons were performed using two-tailed student's t-test where: *= $p \leq 0.05$, **= $p \leq 0.01$, ***= $p \leq 0.001$.

4.3 Discussion

One of the hallmarks of cancer is represented by the dysregulation of the cell cycle machinery (Hanahan & Weinberg, 2011). Genomic studies have outlined how amplification of CDKs, overexpression of cyclins, inactivation of CDK inhibitors and loss of Rb expression occur frequently in different human malignancies (Malumbres & Barbacid, 2009; Shah & Schwartz, 2001).

Given the crucial role of CDKs in regulating cell cycle and transcription, targeting CDKs by small molecule inhibitors has been frequently pursued as a potential therapy option for human malignancies.

Palbociclib, a specific CDK 4/6 inhibitor, was the first CDKi approved by the FDA for the treatment of advanced breast cancer (Finn et al., 2016). The beneficial effects of palbociclib treatments have been also reported on both PDX models of SHH and MYC-amplified G3 medulloblastomas (Cook Sangar et al., 2017). The Cook Sangar et al. study led to its testing in ongoing clinical trials for recurrent medulloblastoma patients (NCT02255461 and NCT03709680). However, the initial enthusiasm for palbociclib has been tempered by recurrence and resistance episodes in almost all treated solid tumours when palbociclib is withdrawn (Cook Sangar et al., 2017).

Thus, with this research we aimed at identifying a more potent CDKi candidate to be used as targeted therapy for MB. With the ultimate goal to mimicking a possible application in the clinic, we tried to clarify, as far as possible, drug mechanism of action in MB context.

In this study, we showed that MB development and progression rely on druggable vulnerabilities that are not only limited to the G1/S checkpoint failure but are spread throughout all cell cycle stages (Figure 13). We singled out dinaciclib, a CDK1, CDK2, CDK5 and CDK9 inhibitor (Parry et al., 2010), as the most effective pan-CDKi across all cell lines and, specifically, most effective on the group 3 MB cell line (HD-MB03) (Figure 14).

In fact, the ideal drugs to advance to clinical trials are usually those with relevance to multiple cancer subtypes and, preferentially, those that show activity in poor prognosis subgroups. G3 medulloblastoma patients, as already mentioned, bear MYC amplification and are associated with the worst prognosis over all MB subgroups (Roussel & Robinson, 2013) Therefore, HD-MB03 cells were our primary *in vitro* model throughout the study.

We have showed that dinaciclib has better efficacy in short- and long-term proliferation assays than palbociclib, our reference specific-CDKi for MB treatment (Figure 15, Figure 16 and Figure 17).

Notably, long-term studies proved that dinaciclib inhibitory effects induced a prolonged cell death (2 weeks after drug withdrawal). On the contrary, with palbociclib, we observed the undesirable presence of surviving cells after treatment, even at the highest dose of the drug used. In addition to this, we showed that dinaciclib has a marked ability of blocking medulloblastoma cancer stem cells (CSCs) propagation compared to palbociclib (Figure 18). CSCs are a minority in the tumour population that is characterised by marked self-renewal and have the ability to differentiate into non-stem cancer cells (Al-Hajj & Clarke, 2004). The ability of CDKis to impair CSCs proliferation has important implications for the good outcome of the therapy in the clinic (Donnenberg & Donnenberg, 2005), since CSCs population in the tumour is also responsible for resistance to more conventional therapy, such as chemotherapy and radiotherapy, leading to relapse.

Furthermore, cell cycle arrest by palbociclib can be reversible or irreversible, with quiescent and senescent cells respectively (Campisi & D'Adda Di Fagagna, 2007). Specifically, palbociclib has already been associated with senescence induction in other tumours but not yet in MB (Leite de Oliveira & Bernards, 2018). After palbociclib treatments, we did not observe the enlarged flat cell morphology typical of senescent cells, pointing at still viable and potentially resistant cells after drug withdrawal. Nonetheless, this is just a speculation and further studies aimed at better characterising senescence induction after palbociclib in MB are required to confirm this.

Altogether these results put forward a concern for the onset of resistance when using palbociclib in MB.

We characterised dinaciclib mode of action, where dinaciclib induced strong cytotoxic effects (Figure 19 and Figure 20). These results are in line with previous publications demonstrating that dinaciclib is able to trigger the apoptotic cascade in multiple tumours (Fu et al., 2011; Gojo et al., 2013; Nguyen & Grant, 2014). Our 3D HD-MB03 culture with caspase 3/7 activation detection was crucial to prove that dinaciclib is able to infiltrate and elicit cell death in solid tumours, comparably to 2D culture (Figure 21). These data further highlighted that dinaciclib is a promising candidate to be employed in MB *in vivo* studies.

In conjunction with caspase 3/7 activity, single cell fate analysis revealed that dinaciclib elicits a predominant death in interphase in HD-MB03 cells (Figure 22). Dinaciclib's effect on cell cycle has been frequently associated to mitotic failure in many tumours, as a consequence of CDK1 inhibition (Jane et al., 2016; Lin et al., 2017; Rajput et al., 2016). In our settings, CASP9 dephosphorylation by CDK1 inhibition could explain the partial effects that we observed in mitosis (Allan & Clarke, 2007). Overall, the G2/M phase is not a major dinaciclib-target in MB, suggesting that CDK1 inhibition plays only a limited role on drug cytotoxic effects.

We speculated that dinaciclib employs different cytotoxic mechanisms depending on the tumour settings and we decided to unravel specific molecular mediators in MB.

Trying to predict MB vulnerability to dinaciclib, our preliminary *in silico* analysis showed that CDK1 and CDK2 are overexpressed in MB patients compared to normal cerebellum, while CDK5 expression was comparable and CDK9 was even lower than controls (Figure 23). Nonetheless, the low number of control samples used for the comparison might limit our ability to draw solid conclusions. In fact, the overexpression of CDK9 in MB tumours compared normal adjacent tissue has been recently described in a recent study (Song et al., 2019). Further analysis revealed that only the high expression level of CDK5 is associated with poor patients prognosis independently from MB subgrouping (Cavalli et al. dataset) (Figure 24). Nonetheless, in the same study from *Song et al.*, high expression of CDK9 has been correlated with MB high-risk patients survival and therefore proposed as prognostic marker and potential vulnerability for these patients (Song et al., 2019).

Next, we pursued identifying the immediate transcriptional alterations under dinaciclib targeting. RNAseq data indicated that cell cycle- and cell death-associated genes were among the most affected molecular players upon mild dinaciclib treatment (Figure 25). We acknowledge that 1nM dinaciclib is a rather low dose to be used, however, due to the high efficacy of the drug, we reasoned that using a milder dose would have filtered out only relevant dinaciclib response mediators.

Indeed, we found a significative downregulation of BAX and up-regulation of CASP9 mRNAs upon dinaciclib treatment in HD-MB03 cells (Figure 26). Other studies already demonstrated that dinaciclib cell death is achieved through the mitochondrial apoptotic pathway in different cancers, but a clear cell death characterisation in MB was not yet available (Alsayegh et al., 2017; Gregory et al., 2015; Varadarajan et al., 2015).

Additionally, we asked which of the targeted CDKs was responsible for the transcriptional and phenotypic effects and to what extent. We showed that dinaciclib treatment mostly reduced CDK9 and, marginally, CDK1 protein levels in MB cells. CDK9 targeting by RNAi revealed that CDK9 is the only mediator of cell growth inhibition via apoptotic induction in both HD-MB03 cells and ONS76 cells; conversely, RNAi-targeting of CDK1 elicited cell growth reductions but could not explain the strong apoptotic effects in MB cells (Figure 27), corroborating even more our cell fate results.

Further, CDK9 targeting by dinaciclib dephosphorylated the downstream target RNA pol II at Ser 2 and, in turn, reduced short-lived proteins such as MYC and the anti-apoptotic MCL-1 (Figure 28). The inhibitory effect of CDK9-activity reduction on mRNA elongation by the RNA polymerase II is corroborated by previous studies in different tumour settings, and so is the mediated degradation of MYC and of the anti-apoptotic BCL-2 family proteins (Booher et al., 2014; Hashiguchi et al., 2019). Specifically, the recent study of *Song et al.* further demonstrated that specific CDK9 inhibition in HD-MB03 cells provokes MYC and BCL2 proteins mRNA downregulation (Song et al., 2019).

Notably, we observed a stronger reduction in MYC protein in the group 3 cell line than in the SHH cell line (Figure 28). Group 3 MB depends on MYC to exhibit characteristic subgroup properties and CDK9 has been previously reported as a druggable vulnerability specific for MYC-relying tumours (C. H. Huang et al., 2014; Rowland et al., 2016). Therefore, a stronger transcriptional impact on MYC in HD-MB03 cells might partially explain the higher sensitivity of this subgroup to the drug.

In order to complete our characterisation of dinaciclib apoptotic induction in MB, we need to consider that mitochondrial apoptosis is the result of anti- or pro- apoptotic BCL2 proteins, such as MCL-1 or BAX, inhibition or activation, which ultimately relies on the interaction with pro-apoptotic BH3-only members (Youle & Strasser, 2008).

We showed that basal expression of BCL2 family proteins is variable in MB *in vitro* models (Figure 29). Nonetheless, there was no strong association between the anti-apoptotic MCL-1 protein abundance in HD-MB03 and ONS76 cells and apoptotic induction. In fact, very different basal levels of MCL-1 resulted in comparable apoptotic induction under MCL-1 inhibition with maritoclax or RNAi in the two MB cell lines (Figure 30). Similarly, we showed that the pro-apoptotic BAX protein is much more expressed in HD-MB03 cells than in ONS76 cells but again this does not seem to impact on a differential *in vitro* response to dinaciclib.

Furthermore, we observed reductions of the pro-apoptotic BAX in both cell lines, which would suggest that BAX is not directly involved the MCL-1-mediated apoptosis triggered by dinaciclib in MB (Figure 26 and Appendix 6.4).

A recent publication from *Xiaoou Xu et al.* demonstrated how dinaciclib actually can induce apoptosis in a BAX-independent manner through BAK (Xu et al., 2020). In addition, MCL-1 is able to bind alternatively to either BAX or BAK (Czabotar et al., 2014). These data suggest that, BAK might have a crucial role in mitochondrial apoptosis induction.

While the reduction of CDK9-dependent anti-apoptotic proteins alone is sometimes enough to trigger apoptosis, such reduction has also been proposed to sensitise tumour cells to other apoptotic stimuli like microtubule instability, as with vincristine, or DNA damage, as with cisplatin (Lam et al., 2001; Shapiro, 2006). In medulloblastoma, synergistic effects have been observed when CDKis were administered sequentially with conventional chemotherapeutic drugs (Song et al., 2019).

Therefore, we addressed the possibility of using dinaciclib to sensitise clinically used chemotherapy. Cisplatin and vincristine are currently the first-line chemotherapeutic drugs for medulloblastoma treatment in the clinic. To date, combination treatments are the main mode of cancer therapy, aiming at blocking development of resistance and lowering drug toxicities (Bozic et al., 2013).

Here, we showed that dinaciclib synergises with both cisplatin and vincristine at specific drug doses (Figure 31).

Additionally, BH3-mimetics have been recently proposed for combination therapies for their role of boosting cytotoxic effects of various agents, including CDK9 inhibitors (Inoue-Yamauchi et al., 2017). Since dinaciclib mechanism of action is mainly interfering with MCL-1 mediated apoptotic pathway, we asked if a complete inhibition of MCL-1 with maritoclax or a reduction in compensatory BCL2 members with navitoclax could have boosted dinaciclib inhibitory effects. We demonstrated that combinatorial strategies with BH3-mimetics synergise with dinaciclib and could be an additional option to improve therapeutic protocols for MB (Figure 32).

Finally, since chemoresistance is one of the major causes of relapse in patients, we addressed the use of dinaciclib chemo-resistant settings. We acknowledge that the short time (6 months) used for the generation of these *in vitro* resistant models might be a limitation in our study and that the onset of solid mechanisms of resistance should be further validated. Nonetheless,

our preliminary data in long-term assays showed that dinaciclib could re-sensitise vincristine-resistant MB cells to treatment (Figure 34).

In addition, the overexpression of BCL2 members is frequently associated to chemotherapy resistance (Konopleva et al., 2002). We have shown that dinaciclib is able to reduce MCL-1 expression, and other studies indicate that dinaciclib downregulates also other BCL2 proteins (Rello-Varona et al., 2019). This potentially might explain the benefit of using dinaciclib in chemoresistance contexts, although further studies are required to confirm this.

Altogether, we have demonstrated that the broad targeting of MB cells with dinaciclib would be a better option than specific CDK4/6 inhibition, prompting for more advanced pre-clinical and clinical studies in MB.

We showed that dinaciclib extensive cytotoxic effects are mainly mediated by CDK9 inhibition and the consequent transcriptional effect on apoptotic proteins, particularly MCL-1, and more limitedly to CDK1 inhibition and G2/M failure. We have not explored the role CDK5 targeting in MB, nonetheless it has already been shown as critical for anti-tumour immune response *in vivo* and further hinting at the benefit of using this broad-CDKi for treatment (Dorand et al., 2016).

Dinaciclib has reached clinical trials III for many malignancies, showing encouraging anti-cancer activity, however monotherapy with dinaciclib is still under consideration due to unwanted toxicities (Parry et al., 2010). Nevertheless, we have demonstrated the potential of using dinaciclib in different combination therapies. These new preclinical data lay the foundation for more tailored drug strategies, where combinations with dinaciclib may provide a safer and more effective solution for MB patients.

4.4 Future directions

Further studies are required to complete our overview on the dinaciclib-cell death characterisation in MB. Particularly, the critical involvement of BH3-only proteins in the MCL-1 mediated apoptosis needs to be identified.

BCL2 proteins levels have been shown to be predictive of dinaciclib-induced apoptosis in solid tumours (Booher et al., 2014). Even though MCL-1 is often referred to as the main mediator of dinaciclib effects and it is mediator of apoptosis in our MB *in vitro* models, the contribution of other anti-apoptotic BCL2 members should be explored.

Moreover, localisation studies on BAX and BAK proteins might be useful to confirm our hypothesis that dinaciclib induces a BAX-independent mitochondrial apoptosis.

Finally, since we showed that MB *in vitro* models bear different basal levels of both pro-apoptotic and anti-apoptotic BCL2 family members, further studies should aim at exploring how and at which extent this influences drug response in MB subgroups. These findings are paramount in order to employ dinaciclib in combination therapies as it would anticipate the emergence of resistance mechanisms and, overall, it would generate safer treatment protocols with reduced toxicities.

Chapter 5:

Targeting MYC/MIZ1 for G3 MB treatment

5.1 Background

MYC overexpression and amplification are mainly associated with group 3 MB, with the presence of metastasis at diagnosis and with poorest outcomes among MB subgroups (Roussel & Robinson, 2013). Nevertheless, the role of MYC in medulloblastoma tumourigenesis is still poorly characterised.

MYC plays a central role in many mechanisms such as proliferation, apoptosis and cell cycle (Frenzel et al., 2010). It carries out its function regulating transcription in both positive and negative fashions. Traditionally, MYC activates transcription of Enhancer Box sites (E-boxes) on regulated genes when bound to MAX (Conacci-Sorrell et al., 2014). Instead, MYC can heterodimerise with MIZ1 to induce transcriptional repression, suppressing, for example, negative cell-cycle regulators, such as CDKN1A and CDKN1B, and driving proliferation (Bretones et al., 2015; Hönnemann et al., 2012).

To further complicate the picture of MYC regulation networks, microRNAs have been shown to be both MYC-regulated and MYC-regulators (Psathas & Thomas-Tikhonenko, 2014).

MYC family members, mainly MYC and MYCN, represent interesting driver genes to study in medulloblastoma, since they are often over-expressed or amplified in a subgroup-specific manner. MYC over-expression is usually associated with WNT and group 3 MBs, whereas MYCN is usually expressed in SHH and group 4 MBs. Only a few years ago, *Vo et al.* showed that MIZ1 interacts more strongly with MYC than MYCN and that this discrepancy in binding affinity provokes gene expression alterations underpinning group 3 and SHH MBs diversity (Vo et al., 2016).

Altogether, these observations suggest subgroup-specific roles of MYC family members and interacting partners to shape medulloblastoma in different subgroups. Understanding these associations might be crucial to tackle medulloblastoma heterogeneity.

Significant improvements have been made in medulloblastoma diagnosis and treatment mainly due to a better understanding of the molecular underpinnings of the tumour. A consensus has been reached over the concept that medulloblastoma is not a single disease but a complex collection of heterogeneous variants. Nonetheless, treatment-related morbidity and mortality are still a significant burden. Specifically, outcomes are sub-optimal when it comes to high risk, metastatic and relapsed patients.

Here, we aim to fill this gap, giving insights on MYC transcriptional networks, specifically looking at the importance of the interaction with MIZ1 to trigger group 3 development.

Furthermore, given the failure of all the attempts to target MYC, we put forward a novel strategy to hit MYC-driven group 3 medulloblastoma, impairing its balance in binding with MIZ1 through microRNAs.

5.2 Results

5.2.1 Expression levels of MYC and MIZ1 in MB cell lines and patient samples

To identify suitable cellular models to employ in our experiments, we first measured by real-time qPCR and western blot analysis endogenous mRNA and protein levels of MIZ1 and MYC in different MB cell lines.

mRNA expression analysis indicated higher levels of the MIZ1 gene in DAOY and HD-MB03 cell lines and overall the highest MYC expression in HD-MB03 cells (Figure 35 A-B), confirming that group 3 cell line (HD-MB03) is characterised by MYC over-expression/amplification.

It should be noted that, at this point, we decided to adopt the DAOY cell line as the only representative model of SHH MB, considering that MIZ1 mRNA expression levels were more comparable to those of the group 3 cell line than the other SHH MB cell lines (ONS76 and UW228).

For protein quantification, we have also included the CHLA-01-R-MED cell line, which is the metastatic match for the CHLA-01-MED cell-line, to the panel of cells to evaluate MYC abundance in more aggressive MB variants. MYC protein expression was significantly higher in the more aggressive G4 variant compared to the primary tumour-derived cell line, highlighting MYC key role in aggressive MB (Figure 35 C).

Further, we evaluated MIZ1 protein level across the cell lines. We found that MIZ1 is particularly abundant in HD-MB03 and CHLA-01-R-MED cells (Figure 35 C), supporting the hypothesis that MIZ1 activity might be essential alongside MYC to shape aggressive MB phenotypes.

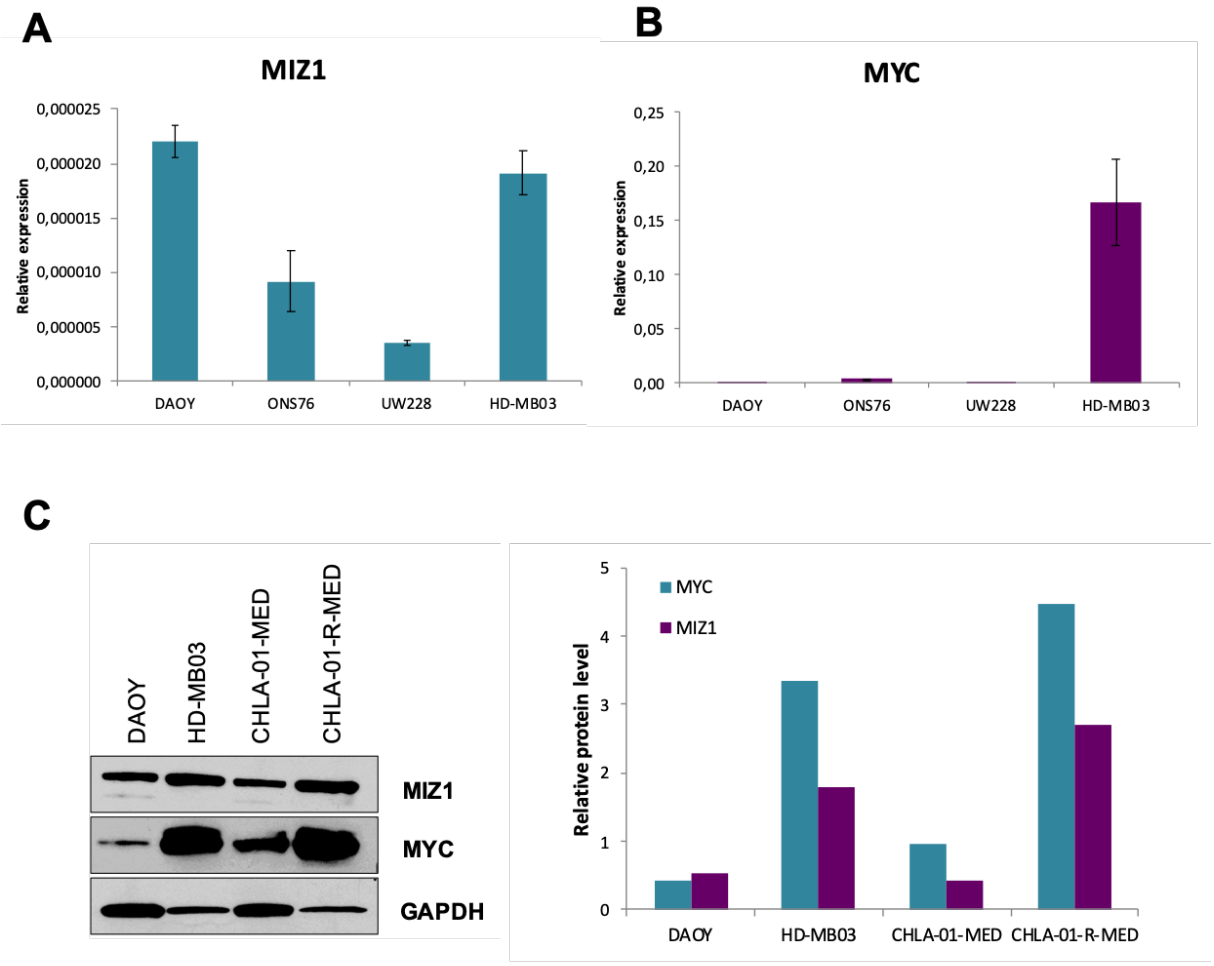

Figure 35 | MYC and MIZ1 mRNA and protein expression in medulloblastoma cell lines.

A-B) Analysis of the endogenous mRNA expression of MIZ1 and MYC in MB cell lines. Plotted graphs indicate relative expression of the genes of interest, normalised to beta-actin housekeeping gene. Results are presented as mean ± SD (N=3). C) MIZ1 and MYC protein expression was analysed by western blot. 50 µg of proteins were used for all samples. On the right, densitometric analysis was obtained by comparing the levels of each protein to GAPDH as loading control. WB shown is one representative of N=3 experiments.

Next, to further confirm the significance of these findings, we evaluated the gene expression levels of MYC and MIZ1 in a set of 763 primary MB specimens by using the R2 genomic and visualization platform (R2: Genomics Analysis and Visualization Platform http://r2.amc.nl (Cavalli et al., 2017).

As also previously reported, MYC expression is specifically high in WNT and G3 subgroups (Figure 36), whereas SHH and G4 subgroups characteristically express MYCN and not MYC (Roussel & Robinson, 2013). Conversely, MIZ1 is well expressed across all subtypes of MB without showing a specific enrichment pattern for specific subgroups (Figure 37).

This confirms that group 3 MB molecular identity does not depend only on MIZ1 expression, but it is entrenched by the exclusive interaction with MYC (Vo et al., 2016).

Based on these preliminary evaluations, we decided to use the HD-MB03 cell line for group 3 MB and the DAOY cell line for SHH MB as our cellular models for comparative studies. We propose that these two *in vitro* models can better highlight MYC/MIZ1 and MYCN/MIZ1 alternative regulations in group 3 and SHH MBs and therefore unravel clues behind very different prognostic fates.

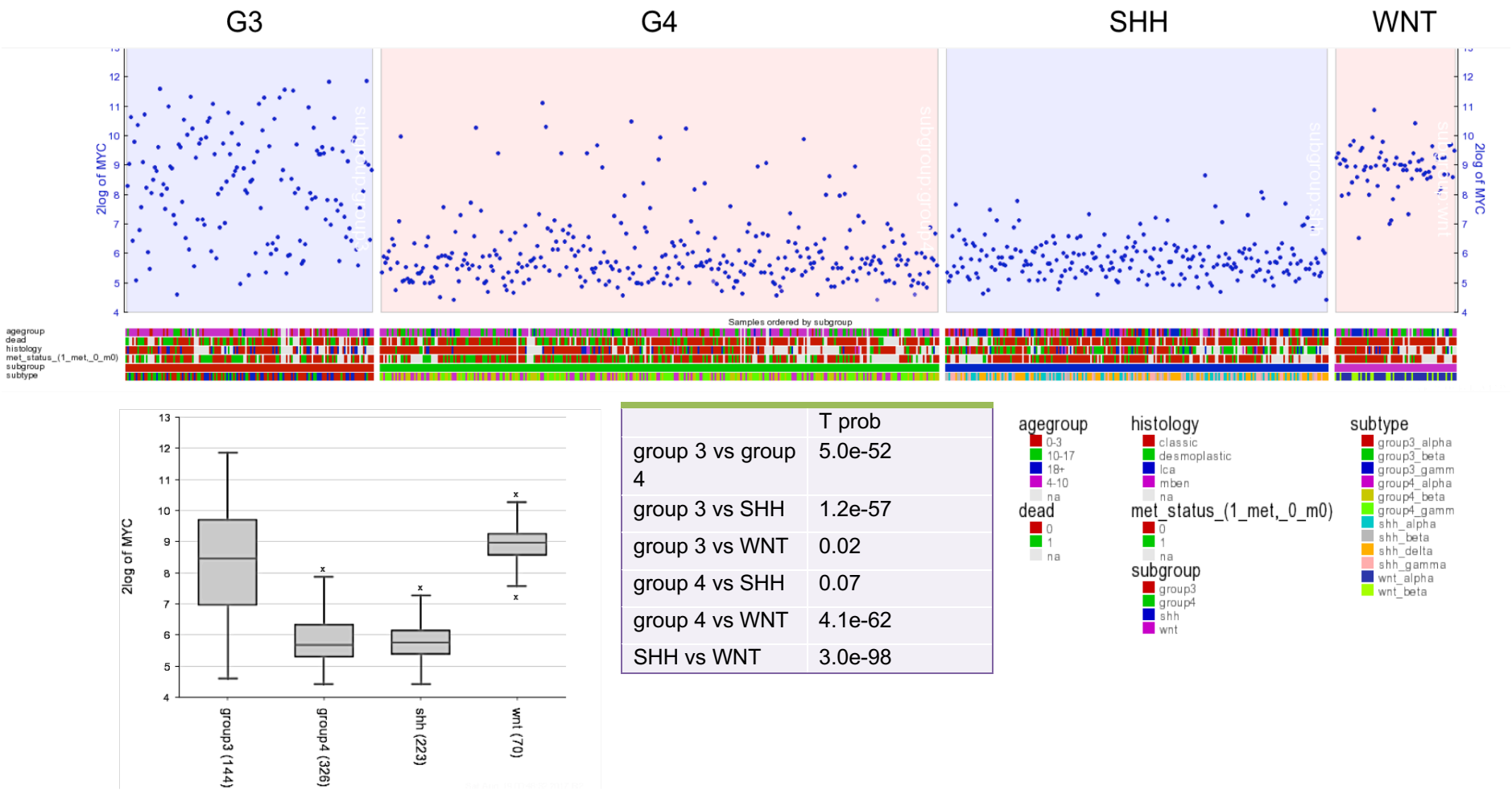

	T prob
group 3 vs group 4	5.0e-52
group 3 vs SHH	1.2e-57
group 3 vs WNT	0.02
group 4 vs SHH	0.07
group 4 vs WNT	4.1e-62
SHH vs WNT	3.0e-98

Figure 36 | Expression level of MYC in 763 medulloblastoma patients.

YY graph generated using R2 online tool, showing expression levels of MYC in all patients analysed in Cavalli et al. study. A total of 763 samples is used in the analysis divided in the four main molecular subgroups: WNT (70), SHH (223), G3 (144), G4 (326). Statistical significance of data shown is presented as p-value. Clinical and molecular information of the patients used for the clustering analysis are reported in the right side of the figure.

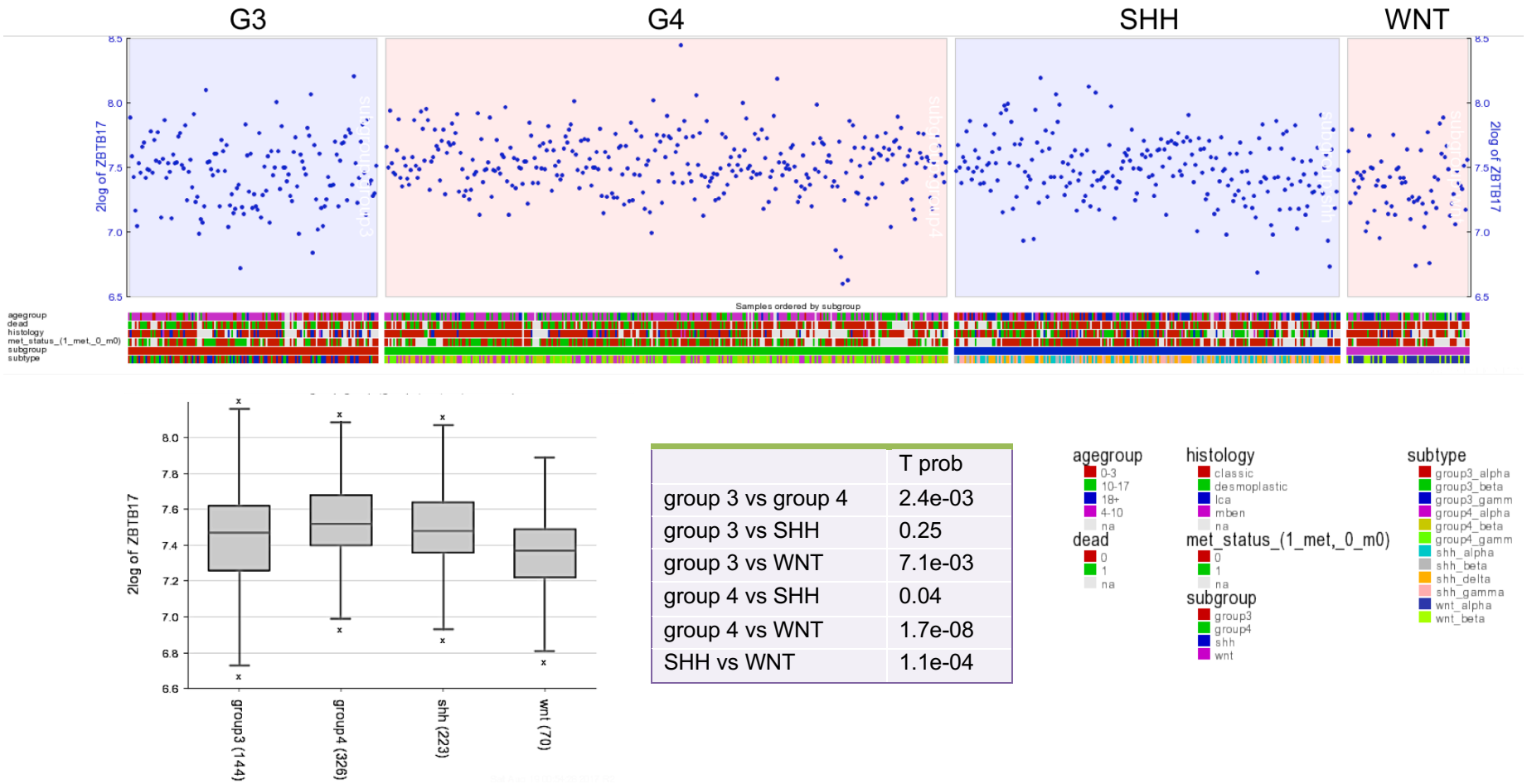

	T prob
group 3 vs group 4	2.4e-03
group 3 vs SHH	0.25
group 3 vs WNT	7.1e-03
group 4 vs SHH	0.04
group 4 vs WNT	1.7e-08
SHH vs WNT	1.1e-04

Figure 37 | Expression level of MIZ1 in 763 medulloblastoma patients.

YY graph generated using R2 online tool, showing expression levels of MIZ1 in all patients analysed in Cavalli et al. study. A total of 763 samples is used in the analysis divided in the four main molecular subgroups: WNT (70), SHH (223), G3 (144), G4 (326). Statistical significance of data shown is presented as p-value. Clinical and molecular patient information used for the clustering analysis is reported in the right side of the figure.

5.2.2 miR-124-3p targets MIZ1

With the final aim of targeting MIZ1 for MB treatment, we decided to use microRNAs for their ability to post-transcriptionally downregulate gene expression.

In order to investigate which microRNA represses MIZ1 expression, we carried out an *in silico* analysis for the prediction of miRNA/MIZ1 binding sites using the TargetScan program (www.targetscan.org) (Figure 38 A). 4 microRNAs were predicted to have highly conserved binding sites on the 3'-UTR of the MIZ1 gene, namely miR-124-3p.1, miR-6766-3p, miR-219a-5p and hsa-miR-4782-3p. We decided to evaluate miR-124-3p.1 because of its overall higher pairing scores and because miR-124-3p is known to be poorly expressed in medulloblastoma, acting as a tumour suppressor microRNA in this context (Mollashahi et al., 2019).

To identify whether miR-124-3p directly targeted MIZ1, dual-luciferase reporter assay was performed. As shown in Figure 38 B, we cloned the 3'UTR of MIZ1 downstream of the coding sequence of the luciferase gene in the pGL3 reporter plasmid.

HEK293T cells were co-transfected with two different "wild-type" or two "reverse" plasmids, containing one or 3 copies of the MIZ1-3'UTR, and with the miR-124-3p precursor (pre-124-3p) or precursor scramble miRNA (pre-CTRL). Compared to the pre-CTRL, miR-124-3p significantly decreased the firefly luciferase activity in both wild-type reporters, with a stronger reduction in the cells with the reporter having 3 copies of MIZ1 binding site. Furthermore, miR-124-3p did not alter the activity of both reverse plasmids (Figure 39). These observations indicated that miR-124-3p directly targeted MIZ1 by interacting with the predicted binding site.

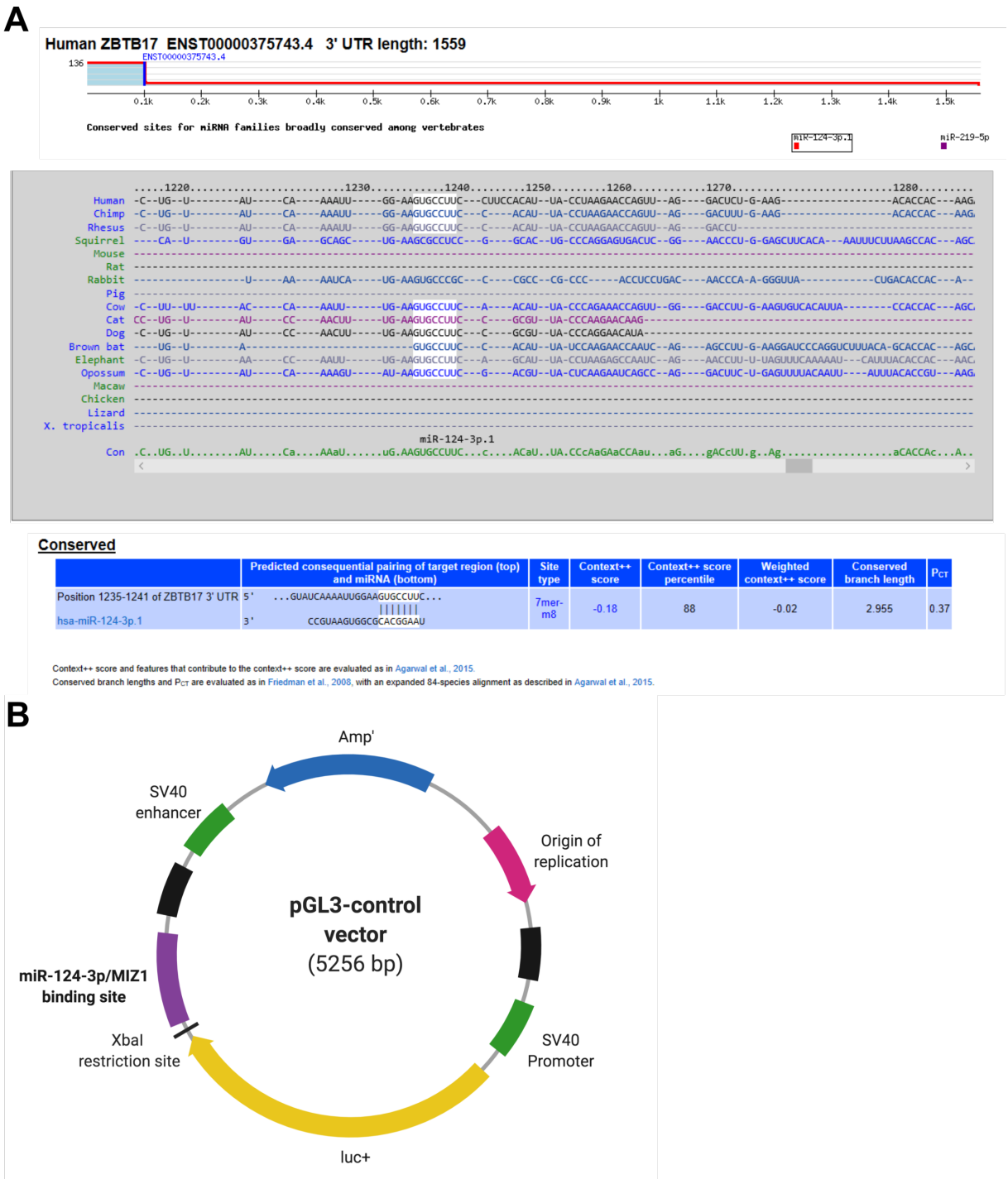

Figure 38 | Selection of miR-124-3p targeting MIZ1 gene.

Here it's presented the TargetScan page for the prediction of MIZ1 3'UTR binding sites. A) At the top is the 3'UTR profile. Below the profile are predicted conserved sites for miRNAs broadly conserved among vertebrates. In the blue box, is shown the predicted binding site sequence for miR-124-3p. B) Scheme of the luciferase plasmid used to assess miR124-3p direct targeting on MIZ1 3'UTR by dual luciferase assay.

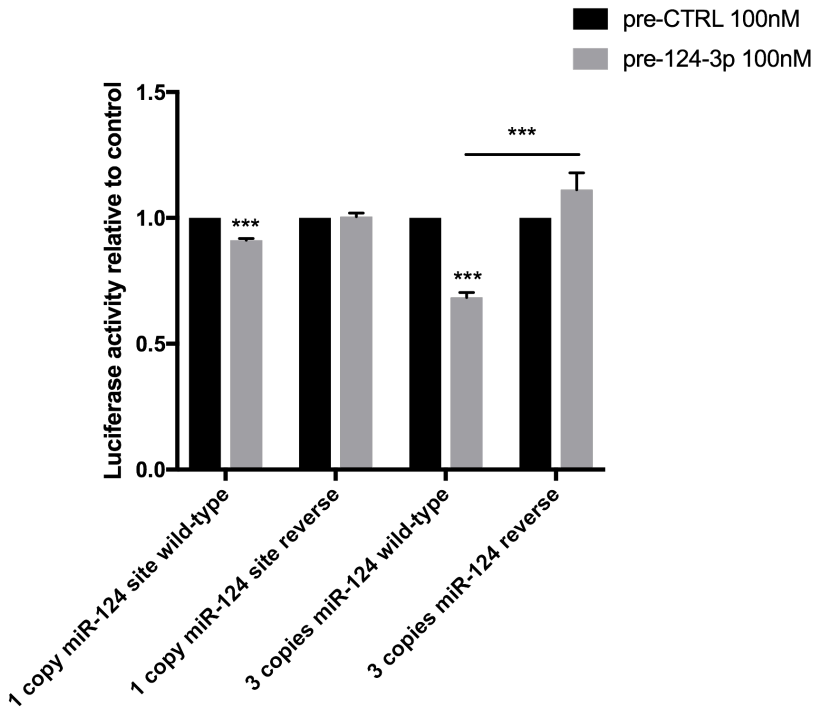

Figure 39 | Dual-luciferase assay results: MIZ1 is a target of mir-124-3p.

Dual-luciferase assay results confirming the binding site of miR-124-3p on MIZ1 3'UTR. Briefly, HEK293T cells were co-transfected with renilla plasmid and wild-type or reverse constructs together with the precursor of miR-124-3p (pre-124-3p) or the precursor scramble microRNA (pre-CTRL). Renilla and Luciferase activity were measured after 24h from transfection.
The relative luciferase activity ratio (firefly Luciferase/Renilla luciferase) ± SEM was calculated from quadruplicate technical replicates and for N=3.
Data are presented using GraphPad software. Statistical comparisons were performed using two-tailed student's t-test where *= $p \leq 0.05$, **= $p \leq 0.01$, ***= $p \leq 0.001$.

In addition, the endogenous mRNA and protein levels of MIZ1 were significantly reduced in HD-MB03 cells overexpressing miR-124-3p compared to precursor scramble miRNA control (Figure 40). Specifically, MIZ1 mRNA levels were significantly reduced by 20% after 72h from transfection compared to control (Figure 40 B). Densitometric analysis of MIZ1 protein expression levels revealed that the strongest effect in protein down-regulation is reached at 72h from transfection, with 60% of protein reduction. Interestingly, MYC protein levels were also down-regulated after miR-124-3p overexpression but the mRNA expression was induced (Figure 40 C).

Altogether, these results confirm that MIZ1 mRNA is a functional target of miR-124-3p and that the suppression of MIZ1 alters MYC levels.

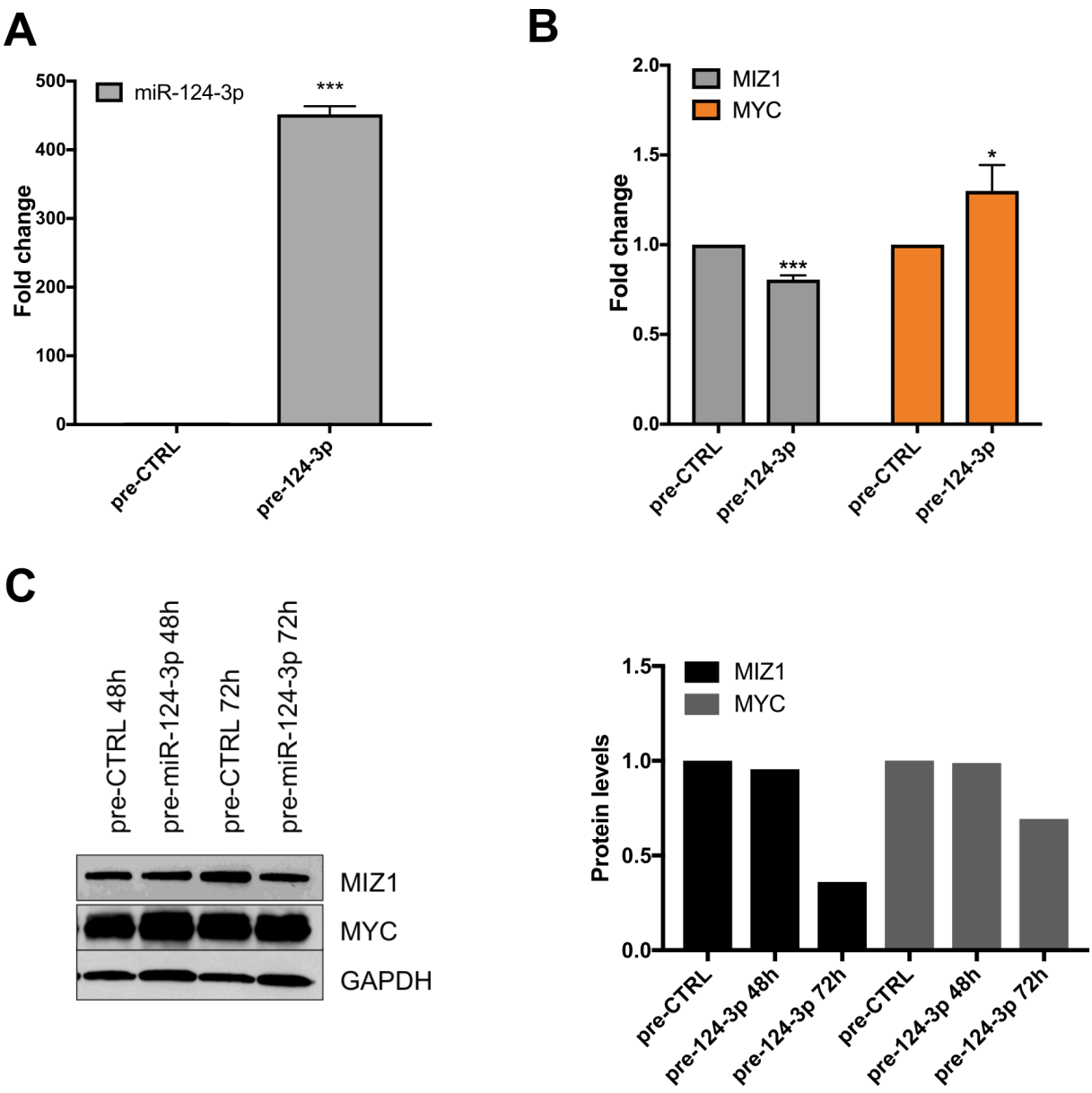

Figure 40 | MIZ1 and MYC mRNA and protein levels following miR-124-3p over-expression in HD-MB03 cells.

A) miR-124-3p expression in HD-MB03 cells transfected for 72h with miR-124-3p precursor (pre-124-3p) or negative miRNA control (pre-CTRL). B) MIZ1 and MYC mRNA expression levels in HD-MB03 cells transfected with pre-124-3p or pre-CTRL after 72h. Plotted graphs indicate expression fold change of the genes of interest expressed as mean ± SD (N=3). C) Western blot analysis of MIZ1 and MYC proteins in HD-MB03 cells after 72h transfection with pre-124-3p or pre-CTRL in HD-MB03 cells. 50 µg of proteins were used for all samples. Densitometric quantifications are provided on the right: protein levels are expressed as fold change relative to the control (pre-CTRL), arbitrarily set to 1. WB shown is one representative of N=3 replicates.
Statistical comparisons were performed using two-tailed student's t-test where *= $p \leq 0.05$, **= $p \leq 0.01$, ***= $p \leq 0.001$.

5.2.3 miR-124-3p overexpression inhibits proliferation of group 3 MB cells

We next examined the phenotypic effects of miR-124-3p overexpression in group 3 and SHH cells. HD-MB03 and DAOY cells were transfected with scalar concentrations of miR-124-3p precursor or scramble miRNA precursor for 72h. Cell viability was significantly compromised in group 3 cells (20% reduction) but not in SHH cells, suggesting that MYC/MIZ1 balance and interaction is somehow crucial for group 3 MB progression, where also MYC is overexpressed, but not for SHH MB. This result further prompted us to pursue MIZ1 as potential target for group 3 treatment (Figure 41).

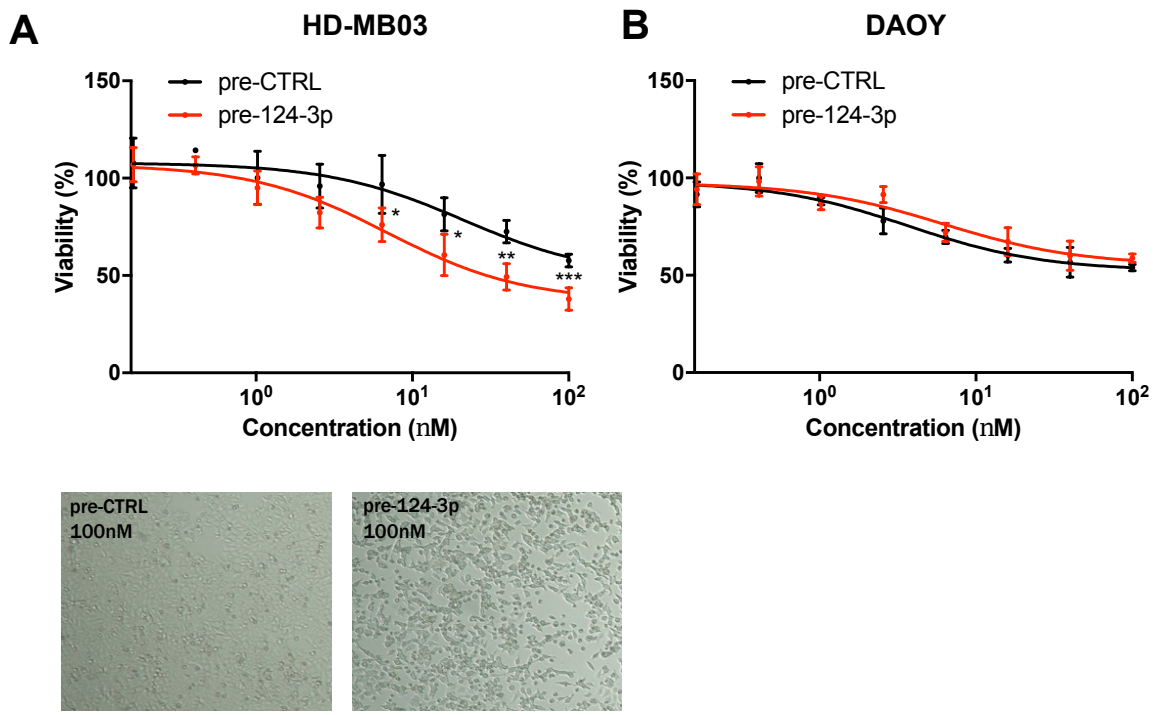

Figure 41 | miR-124-3p overexpression effect on HD-MB03 vs DAOY cell proliferation.

A-B) MTT assay was performed after 72h from transfection of scramble miRNA precursor (pre-CTRL) vs miR-124-3p precursor (pre-124-3p) in HD-MB03 cells (A) and DAOY cells (B).
Precursor microRNAs were transfected at 0-100nM concentration range at 1:2.5 fold dilution. Phase-contrast images are presented for transfections of pre-CTRL and pre-124-3p in HD-MB03 cells at the highest concentration used to assess cell viability (100nM). Cells were observed using inverted Vert.A1 AXIO (Zeiss) microscope (x40 magnification).
Data are presented as mean ± SD (N=3) using GraphPad software. Statistical comparisons were performed using two-tailed student's t-test where *= $p \leq 0.05$, **= $p \leq 0.01$, ***= $p \leq 0.001$.

5.2.4 Functional role of miR-124-3p in group 3 medulloblastoma

To gain a better understanding of miR-124-3p role in group 3 MB, we performed an RNA sequencing analysis of HD-MB03 cells overexpressing miR-124-3p. By analysing the transcriptomic data, 5992 genes among protein-coding, long non-coding, small non-coding and pseudogenes were found significatively modulated with a *p-value* < 0.05 (Figure 42 A). Specifically, we found 152 upregulated protein-coding genes with fold change (FC) >2 and 142 down-regulated protein-coding genes with FC < 0.5. Although statistically significant, MIZ1 downregulation (FC<0.8) did not pass our analysis cut off (Appendix 6.5).

A subsequent gene ontology (GO) analysis of biological process and molecular function terms was conducted in order to investigate the biological significance of modulated genes. The analysis revealed a significant enrichment of altered genes for biological processes involved in cell-cycle progression and cell division (Figure 42 B). The molecular functions that miR-124-3p overexpression affected were predominantly microtubule binding and CDKs regulator activity (Figure 42 C).

Among modulated genes, we were more interested in looking at the downregulated genes as in potential targets of miR-124-3p that could shed light on the miRNA regulatory functions and tumour suppressive properties in MB. miR-124-3p targets could in fact be exploited as druggable vulnerabilities of group 3 MB.

In order to scale down the pool of genes and focus on the putatively most relevant and functional miR-124-3p targets, we cross-referenced the list of repressed genes from our transcriptomic data with the miR-124-3p target predictions from TargetScan and miRDB algorithms (www.mirdb.org). In doing so, we obtained a list of strong candidates target genes, presented in Figure 43 A with respective fold change values.

To verify the reliability of the sequencing, we picked the top downregulated gene on the list, namely vimentin (VIM), for validation with single assay qRT-PCR. Results showed a 75% reduction in VIM gene expression after miR-124-3p overexpression in HD-MB03 cells, validating sequencing data (Figure 43 B).

Finally, time-lapse microscopy showed that miR-124-3p overexpression shifted HD-MB03 cells fate towards an increased death in interphase (approximately 20%) and in mitosis (16%) compared to control cells (Figure 44).

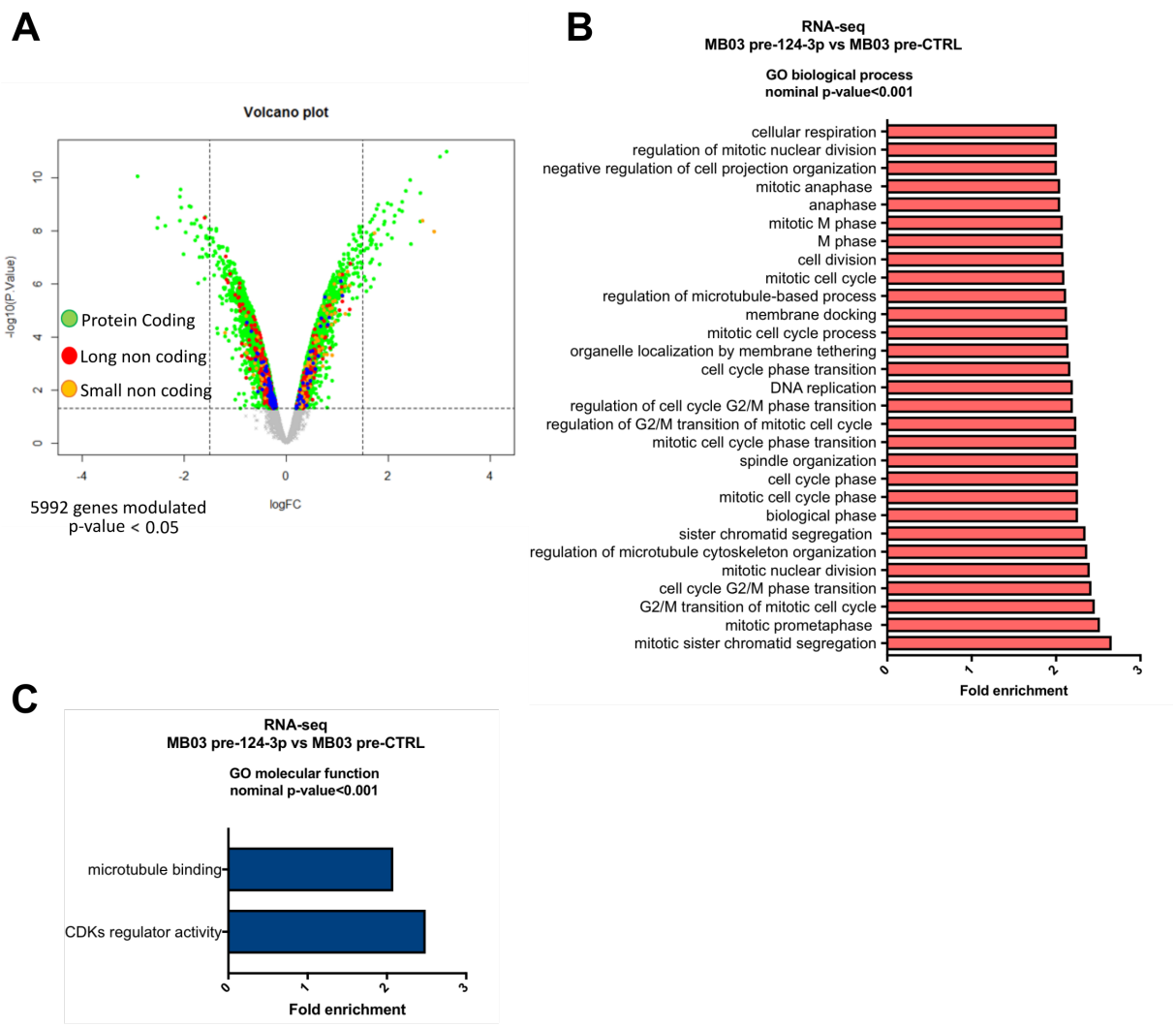

Figure 42 | Transcriptomic analysis following miR-124-3p overexpression in HD-MB03 cells.

A) Volcano plot of the distribution of genes differentially expressed in HD-MB03 cells transfected with miR-124-3p precursor (pre-124-3p) vs negative miRNA control (pre-CTRL), assessed by RNA-seq. B-C) Gene ontology analysis of significantly up- and down-regulated genes (FC>1.2 and p-value<0.001) after miR-124-3p overexpression in HD-MB03 cells. Biological function and molecular function terms with fold enrichment score≥2 are presented using GraphPad Prism software.

A

Potential miR-124-3p targets in group 3 MB

Gene name	Fold change
PRKAA2	0,51
LAMC1	0,50
CHST14	0,50
NME4	0,50
QKI	0,49
CCND2	0,49
DNAJC1	0,49
AMOT	0,48
CPT1A	0,48
SGPL1	0,48
CTDSP2	0,46
TRIB3	0,45
SEMA5A	0,45
NEURL1B	0,45
SNAI2	0,44
DNASE2	0,44
CTDSP1	0,44
PLP2	0,43
CAV1	0,43
SERINC2	0,42
TP53INP1	0,41
MAN2A1	0,40
GPT2	0,35
IQGAP1	0,34
B4GALT1	0,33
VIM	0,25

B

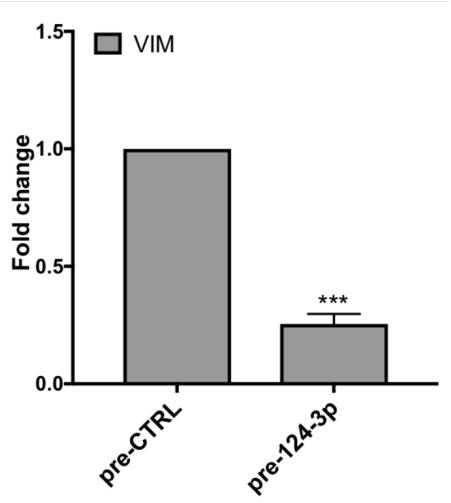

Figure 43 | Potential targets of miR-124-3p in group 3 medulloblastoma.

A) List of down-regulated genes from sequencing transcriptomic analysis after miR-124-3p over-expression in HD-MB03 cells cross-referenced with miR-124-3p target predictions from TargetScan and miRDB algorithms.

B) Vimentin (VIM) mRNA expression levels by qRT-PCR in HD-MB03 cells transfected with pre-124-3p or pre-CTRL after 72h. Plotted graphs indicate expression fold change of the gene of interest expressed as mean ± SD (N=3) using GraphPad Prism software. Statistical comparisons were performed using two-tailed student's t-test where *= $p \leq 0.05$, **= $p \leq 0.01$, ***= $p \leq 0.001$.

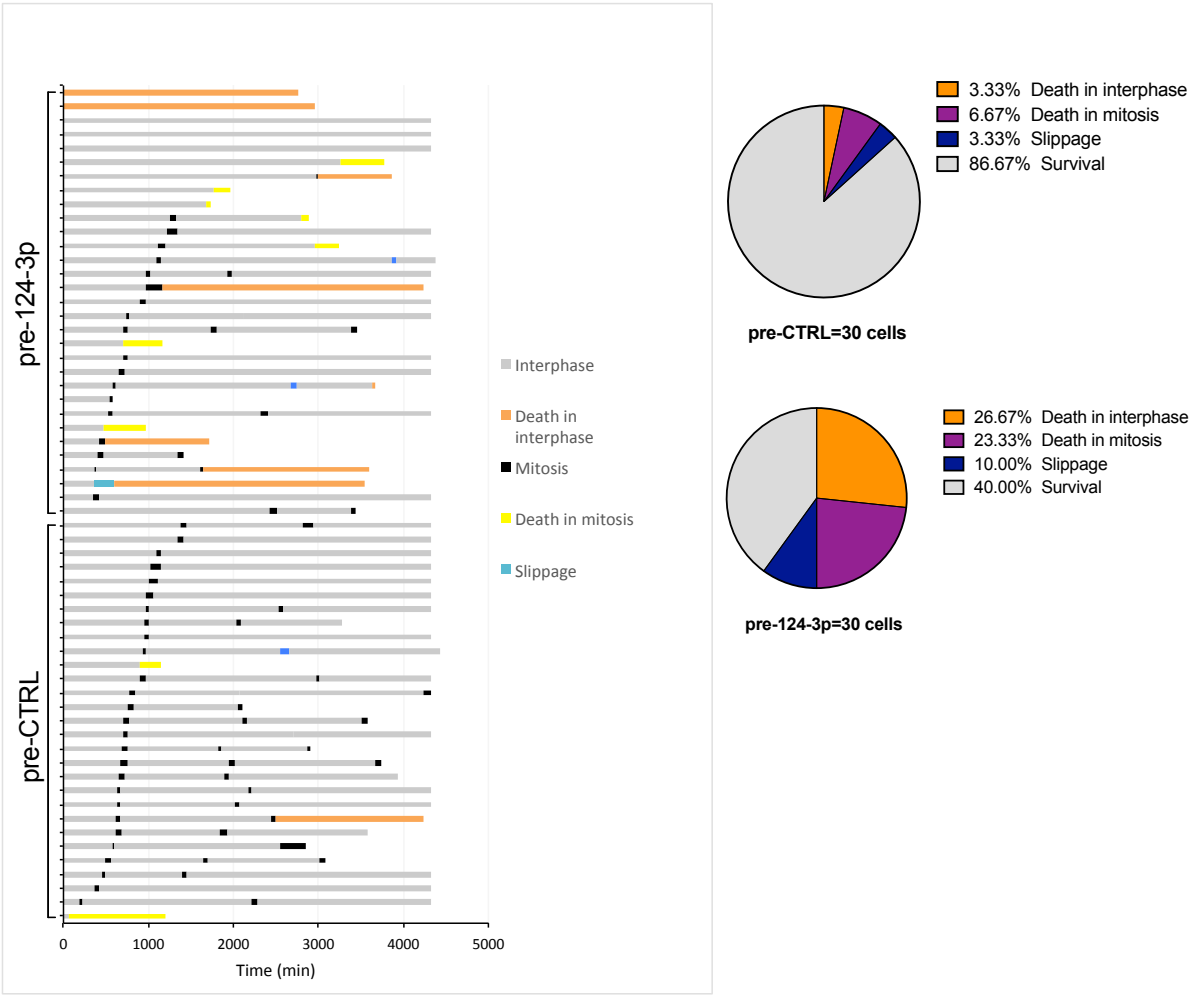

Figure 44 | Cell fate profiles of HD-MB03 cells overexpressing miR-124-3p.

Representative cell fate profiles of HD-MB03 cells transfected with 100 nM pre-CTRL or pre-124-3p (N=2). Each line depicts the fate of one single cell followed over time using time-lapse microscopy imaging. The colour of the line represents a specific cell behaviour, as indicated. A total of 30 cells per experiment from quadruplicate wells were analysed manually. Phase-contrast images were recorded every 15 minutes for 72h at 100X magnification in the Cytation 3 system (Biotek). On the right, pie charts indicating the percentage of cells that either died in interphase, died in mitosis or were still alive at the end of the recording (N=2).

5.2.5 miR-124-3p enhances HD-MB03 cells sensitivity to chemotherapeutic drugs

After identifying miR-124-3p as new possible therapeutic tool for group 3 MB, we evaluated potential synergistic effects with cytotoxic drugs used in the clinic. Firstly, HD-MB03 cells were transfected with 80 nM of the miR-124-3p precursor (pre-124-3p) or the negative control (pre-CTRL) and, after 48h from transfection, cells were treated with scalar concentrations of the drugs for another 72h hours. We found that miR-124-3p overexpression significantly enhanced vincristine and cisplatin effects over HD-MB03 cell proliferation (Figure 45).

These observations suggest that miR-124-3p could be used to enhance cellular sensitivity to conventional chemotherapy, allowing the reduction of cytotoxic doses and treatment associated side effects.

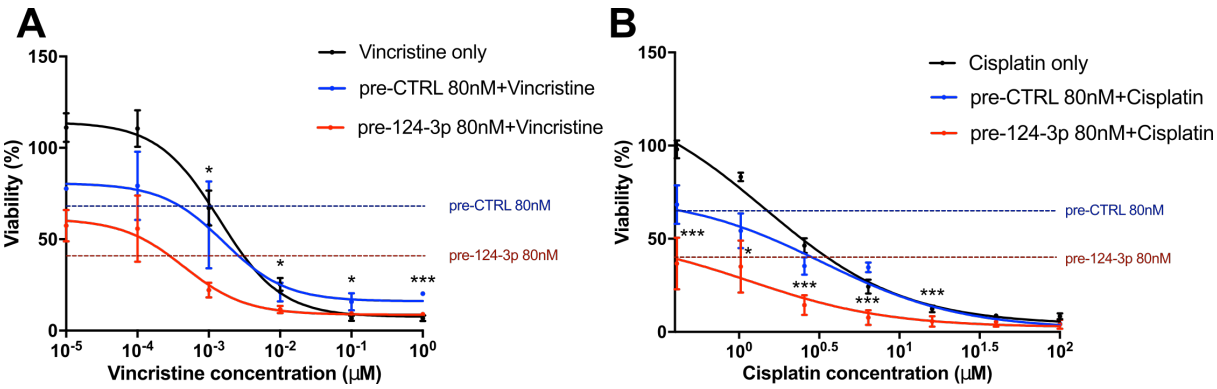

Figure 45 | miR-124-3p in combination treatment with chemotherapeutic drugs.

HD-MB03 cells were transfected with 80 nM of the miR-124-3p precursor (pre-124-3p) or the negative miRNA precursor (pre-CTRL). After 48h from transfections, cells were treated with vincristine at 0-10 μM concentration range and 1:10 fold dilution (A), and cisplatin at 0-100 μM concentration range at 1:2.5 fold dilution (B). Cell proliferation was then evaluated by MTT assay. Data are presented as mean ± SD (N=3) using GraphPad software. Dotted lines represent reference cell viability after single transfections with pre-CTRL or pre-124-3p (80nM).

Statistical comparisons were performed between the two combinations chemodrug+pre-CTRL vs chemodrug+pre-124-3p using two-tailed student's t-test where *= $p \leq 0.05$, **= $p \leq 0.01$, ***= $p \leq 0.001$.

5.2.6 MIZ1 knockdown

In order to further investigate the role of MIZ1 in group 3 development and compare our previous results with miR-124-3p overexpression, we performed RNAi-mediated knockdown of MIZ1 in the HD-MB03 cell line. After 72h from transfection, we confirmed that silencing of MIZ1 was effective by using qRT-PCR and by western blot analysis. Specifically, we measured a significative reduction in MIZ1 mRNA expression (50%) (Figure 46 A) and a more substantial downregulation at protein level (90%) compared to cells transfected with the non-targeting siRNA (Figure 46 B).

To evaluate how changes in MIZ1 and MYC levels could impact each other, we also evaluated mRNA expression of MIZ1 and MYC in both siMIZ1 and siMYC conditions in HD-MB03 cells. Interestingly, downregulating MIZ1 or MYC (siMIZ1 or siMYC), seemed to induce the mRNA expression of the respective interacting partner (Figure 46 A/C).

Nonetheless, despite the significant rise in MYC mRNA expression upon MIZ1 silencing, we reported a 30% reduction in MYC protein level, similar to what we observed with the over-expression of miR-124-3p (Figure 46 B).

Next, following the approach used with miR-124-3p over-expression, we evaluated the phenotypical consequences of reducing MIZ1 endogenous levels in group 3 versus SHH settings.

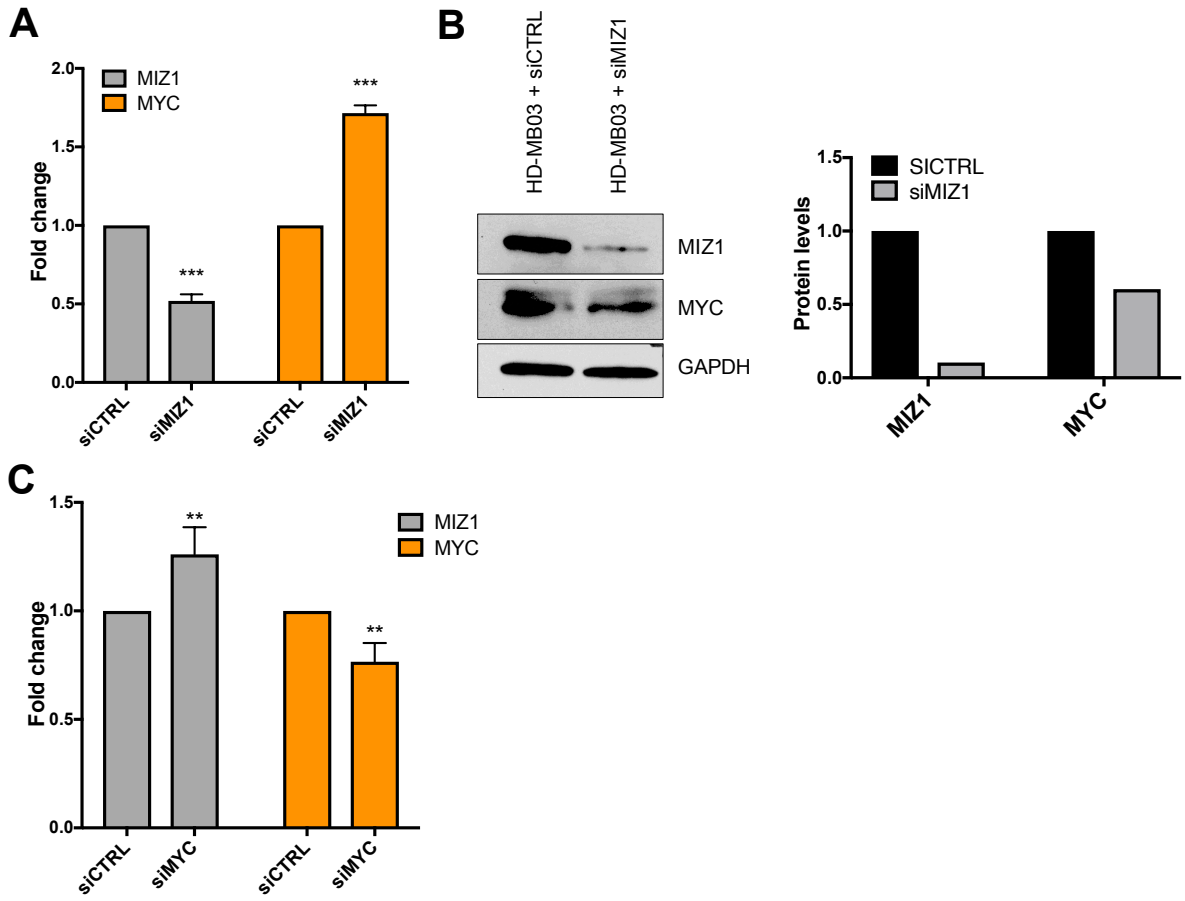

Figure 46 | MIZ1 and MYC mRNA and protein levels after MIZ1 silencing in HD-MB03.

A and C) Miz1 and MYC mRNA expression levels in HD-MB03 cells transfected with non-targeting siRNA (siCTRL) and MIZ1 siRNA (siMIZ1) or MYC siRNA (siMYC) after 72h. Plotted graphs indicate expression fold change of the genes of interest expressed as mean ± SD (N=3). B) Western blot analysis of MIZ1 and MYC proteins in HD-MB03 cells after 72h transfection with control siRNA (siCTRL) or Miz1 siRNA (siMIZ1). 50 µg of proteins were used for all samples. Densitometric quantifications are provided on the right: protein levels are expressed as fold change relative to the control (siCTRL), arbitrarily set to 1. WB shown is one representative of N=3 replicates.
Statistical comparisons were performed using two-tailed student's t-test where *= $p \leq 0.05$, **= $p \leq 0.01$, ***= $p \leq 0.001$.

5.2.7 Silencing of endogenous MIZ1 inhibits proliferation of group 3 MB cells

To investigate the unique MYC/MIZ1 contribution to group 3 MB development, we measured cell proliferation upon MIZ1 silencing in HD-MB03 cells vs DAOY cells. After 72h from transfection, scalar concentrations of siMIZ1 were able to significantly impair proliferation in a concentration dependent manner in HD-MB03 (20% reduction) but not in DAOY cells, comparing to control siRNA (siCTRL) (Figure 47 A-B). These results further suggest the importance of MIZ1 role in group 3 MB.

Furthermore, in order to study which phenotypic effects were directly induced by miR-124-3p targeting via MIZ1 in HD-MB03 cells, we performed time-lapse microscopy imaging on HD-MB03 cells upon MIZ1 downregulation by RNAi. We observed a 11% cell fate increase towards death in mitosis (Figure 48).

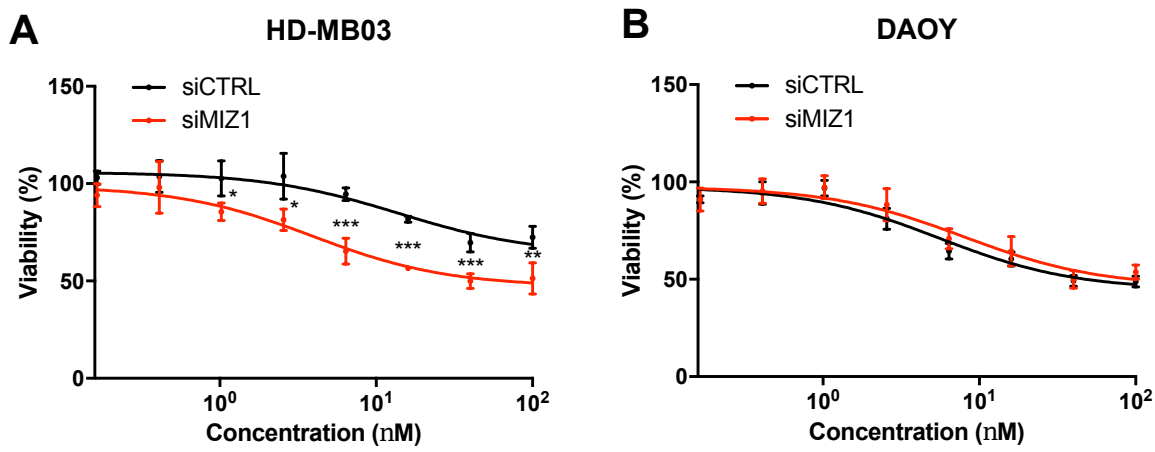

Figure 47 | MIZ1 knockdown effects on HD-MB03 vs DAOY cells proliferation.

A-B) MTT assay was performed after 72h from transfection of non-targeting siRNA (siCTRL) vs MIZ1 siRNA (siMIZ1) in HD-MB03 cells (A) and DAOY cells (B).
siRNAs were transfected at 0-100nM concentration range at 1:2.5 fold dilution.
Data are presented as mean ± SD (N=3) using GraphPad software. Statistical comparisons were performed using two-tailed student's t-test where *= $p \leq 0.05$, **= $p \leq 0.01$, ***= $p \leq 0.001$.

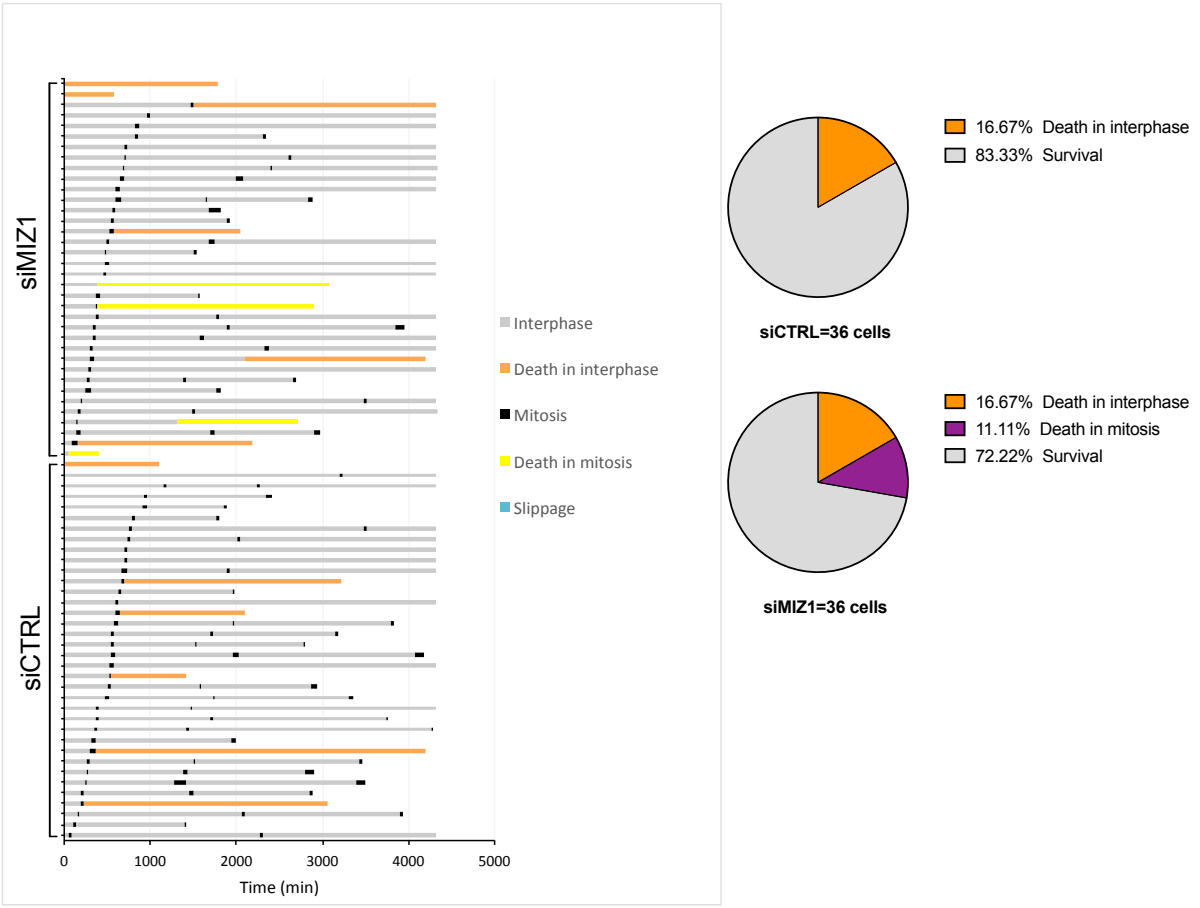

Figure 48 | Cell fate profiles of HD-MB03 cells upon MIZ1 downregulation by RNAi.

Representative cell fate profiles of HD-MB03 cells transfected with 100 nM siCTRL or siMIZ1 (N=2). Each line depicts the fate of one single cell followed over time using time-lapse microscopy imaging. The colour of the line represents a specific cell behaviour, as indicated. A total of 36 cells per experiment from quadruplicate wells were analysed manually. Phase-contrast images were recorded every 15 minutes for 72h at 100X magnification in the Cytation 3 system (Biotek). On the right, pie charts indicating the percentage of cells that either died in interphase, died in mitosis or were still alive at the end of the recording (N=2).

5.2.8 Screening of MYC/MIZ1-regulated microRNA network

After confirming the effective MIZ1 knockdown upon siRNA silencing (Figure 49), we next performed an expression profile analysis of a panel of 800 human miRNAs on HD-MB03 cells with the MIZ1 knock-down versus HD-MB03 cells transfected with the siRNA control by using the NanoString platform (NanoString Technologies).

A total of 43 miRNAs resulted in being potentially deregulated after MIZ1 knockdown (set cut off: $p \leq 0.055$). As shown in Figure 49, 13 miRNAs were identified significantly up-regulated and 30 down-regulated in studied conditions.

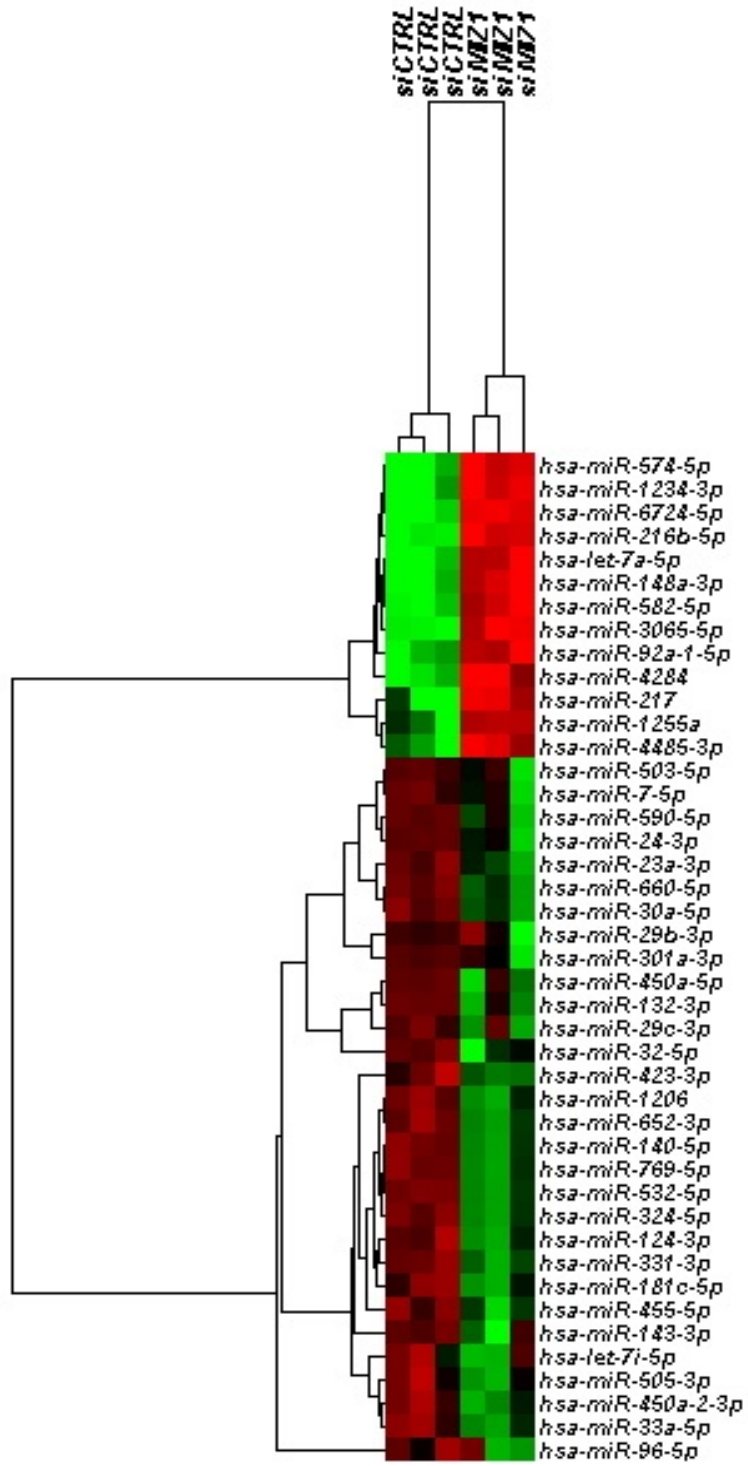

Figure 49 | Heatmap of differentially expressed miRNAs upon Miz1 silencing in HD-MB03 cells.

HD-MB03 cells have been transfected either with control siRNA (siCTRL) or Miz1 siRNA (siMIZ1) for 72h and, after validation of MIZ1 silencing, they have been processed for miRNA profiling by NanoString. Red: upregulated miRNA in siMIZ1 condition; Green: downregulated miRNA in siMIZ1 condition. P values ≤ 0,055 were considered to generate the heatmap. Comparison of expression between samples was made using a linear scale.

5.2.9 miRNA profile validation

We next validated the modulation of some differentially expressed microRNAs by using single assay qRT-PCR. Specifically, let-7i, miR-30a, miR-32, miR-331 and miR-324 were confirmed to be down-regulated after MIZ1 silencing (Figure 50 A**)**.

We also tested the expression of other miRNAs, which did not emerge from the high-throughput screening, but which have been associated with medulloblastoma and more importantly group 3 MB (X. S. Liu et al., 2013a). Specifically, we assessed the expression of miR-30b, which is correlated to MYC-triggered MBs, being downregulated after MIZ1 silencing; then, we evaluated the expression of few members of the oncogenic miR-17-92 cluster (O'Donnell et al., 2005), which were identified as down-regulated in MIZ1 knockdown settings (Figure 50 B**)**.

We concluded that MIZ1 knockdown altered miRNA expression profile of HD-MB03 cell line but further analyses are required to accurately identify and confirm the miRNAs directly regulated by MIZ1/MYC repressive complex.

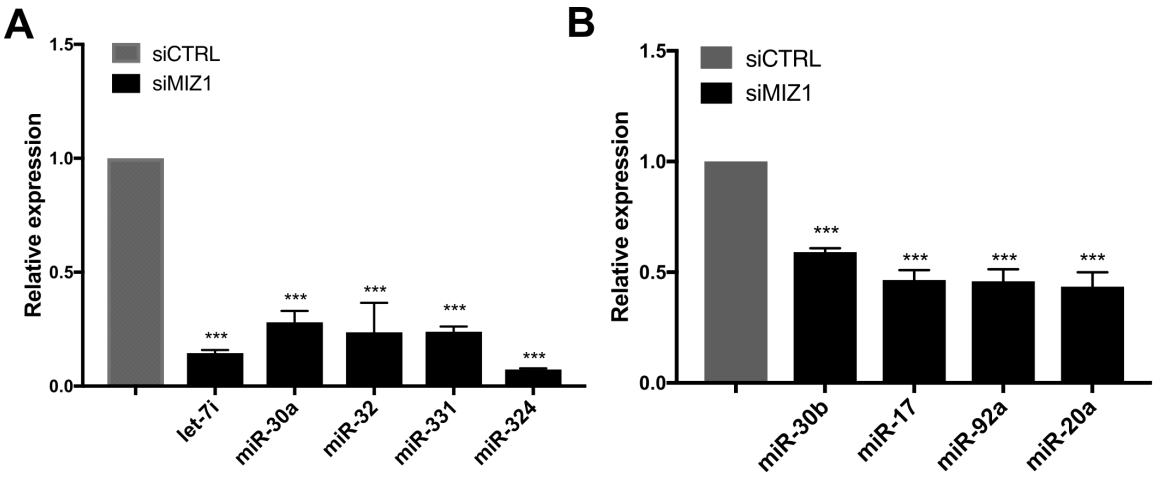

Figure 50 | Validation of NanoString microRNA profile by qRT-PCR.

A) Validation of microRNA from the siCTRL vs siMIZ1 screening on HD-MB03. B) Expression analysis of microRNAs associated with MB and MYC status.
The expression of each microRNA was analysed by qRT-PCR and results were normalised to the expression values of the RNU44 housekeeping microRNA.
Data are presented as mean ± SD (N=3) using GraphPad software. Statistical comparisons were performed using two-tailed student's t-test where *= $p \leq 0.05$, **= $p \leq 0.01$, ***= $p \leq 0.001$.

5.2.10 MYC and MIZ1 knockout in vitro models

To corroborate the results obtained with the previous approaches, the MIZ1 silencing and miR-124-3p over-expression, we decided to generate CRISPR/Cas9 mediated MIZ1 and MYC knockout cellular models for group 3 MB.

To this aim, crRNAs were designed in the gene body of MIZ1 and MYC spanning exons coding for the protein domains of MIZ1 and MYC that coordinate the formation of the MYC/MIZ1 complex. After transfection of the CAS9 complex, cells were puromycin-selected and subjected to indel analysis to verify the presence of mutant cells.

Successful recombination in our MYC and MIZ1 targeted samples was confirmed by T7EI digestion, which recognised heteroduplexes of mutant PCR amplicons in both crMYC and crMIZ1 cell populations indicated as red stars in Figure 51. Then, we clonally expanded our cells and finally we were able to generate four crMYC and five crMIZ1 clones that were subjected to Sanger sequencing of the targeted regions and western blot analysis to confirm MYC and MIZ1 knockouts.

No positive cell clones were isolated for crMYC. This did not come as a surprise since, during the process of single-cell selection, it was challenging and mostly impossible to grow MYC-knockout clones. Almost all crMYC lines seemed to have reached a senescent state and did not proliferate after few passages (Figure 52). Therefore, we hypothesised that genetic deletion of MYC is deleterious for group 3 MB cells survival. Ultimately, that would explain why we were not able to isolate mutated cells.

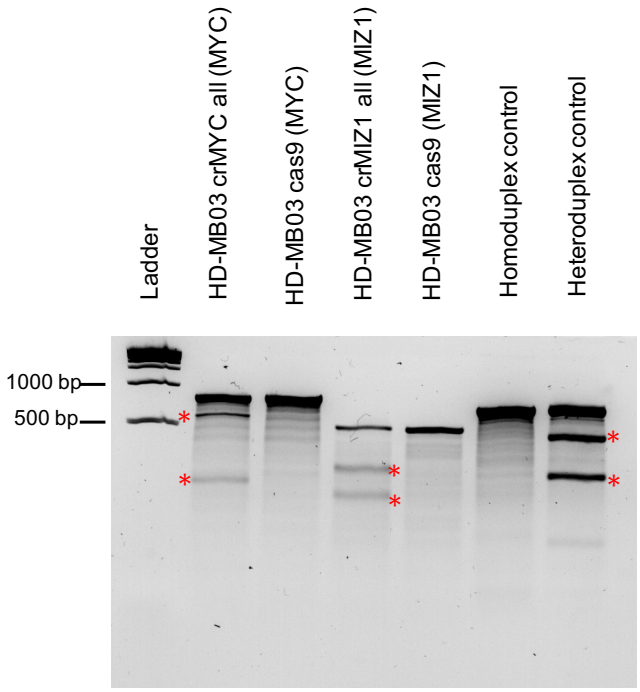

Figure 51 | T7EI digestion of crMYC and crMIZ1 cellular pools.

Red stars show the cleavage products of the samples indicated above each lane by T7EI. The DNA fragments were amplified around the CRISPR/Cas9 target sites by PCR using gene-specific primers from extracted genomic DNA. The presence of mismatches was detected by T7EI digestion resulting in the generation of products with different molecular sizes. This observation indicates that, after CRISPR/Cas9 editing, insertions/deletions (INDELS) mutations have happened and crMYC and crMIZ1 targeting were successful. HD-MB03 transfected with only Cas9 expressing plasmid was used as a negative control.
Quick-Load 1 kb DNA Ladder (NEB) was used in the first lane as reference.

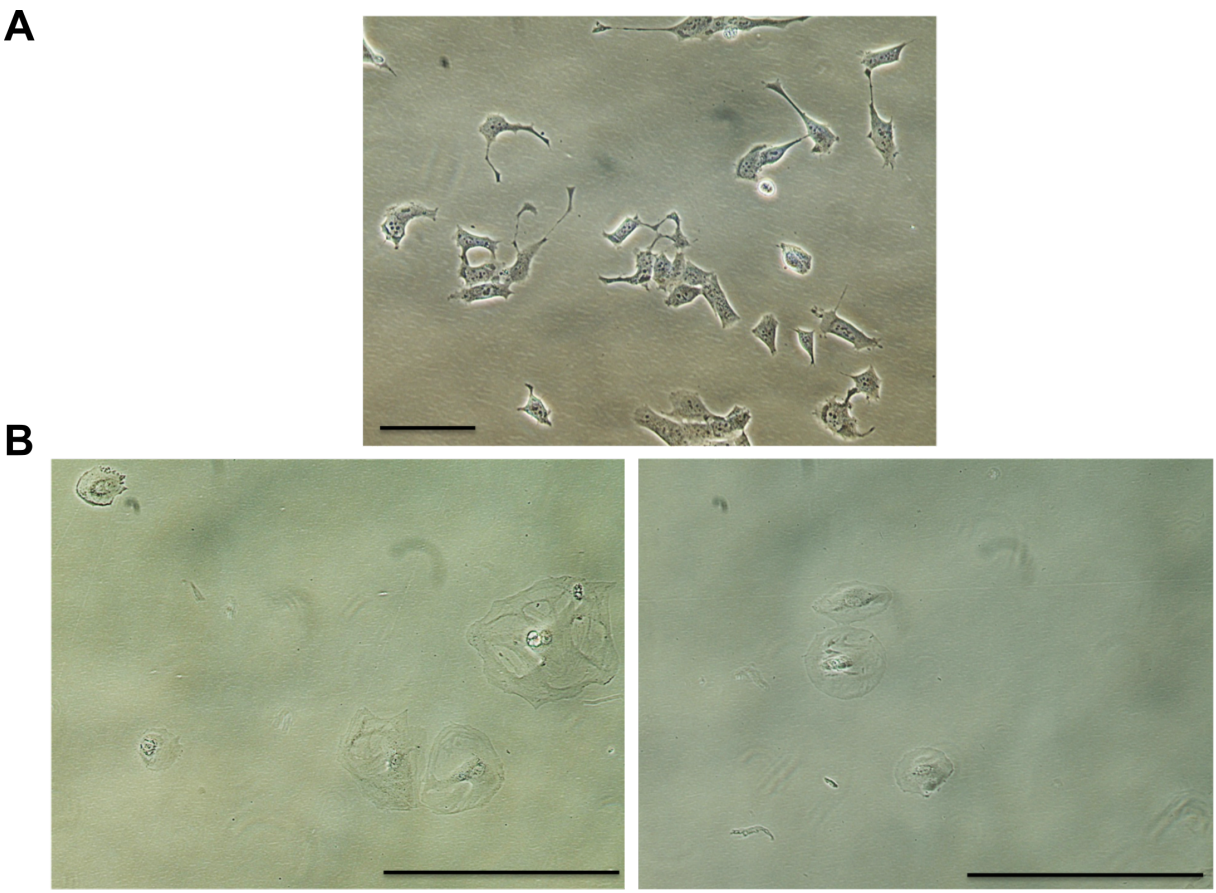

Figure 52 | Phase-contrast images of HD-MB03 wild-type cells vs crMYC HD-MB03 clones.

A) HD-MB03 wild-type cells B) two representative clones from the crMYC HD-MB03 pool of cells. Images were taken during the clonal expansion step from single cells transfected with CRISPR/CAS9 system targeting MYC. Cells were observed using the inverted Vert.A1 AXIO (Zeiss) microscope at A) x40 and B) x100 magnification. Scale bar: A-B) 100 µm.

We carried on evaluations on few crMIZ1 clones that we were able to grow sufficiently for further testing. From the sequencing results, we could only observe heterozygous deletions of MIZ1 in our clones (Figure 53). This was also confirmed by western blot analysis, where only reductions and not complete knockouts of the MIZ1 protein were observed. Overall, crMIZ1 n.21 clone showed the highest level of MIZ1 knockdown among all collected CRISPR cell lines and crMIZ1 n.8 and 21 showed the lowest MYC protein levels (Figure 54).

During CRISPR clones culturing, we observed different phenotypes and cell behaviours (Figure 55). Briefly, crMIZ1 n.3 cells did not proliferate showing an enlarged and senescent morphology, and for these reasons, we could not test them for MIZ1 deletion or evaluate them further. crMIZ1 n.21 cells assumed a round-shape morphology and become quite slow to grow.

crMIZ1 n.8 and 24 and crMIZ1 n.26 and 28 manifested an intermediate phenotype between wildtype and crMIZ1 n.21 cells, with the presence of some round shaped cells.

Although we were not able to generate clean homozygous deletions for MIZ1, we decided to use the obtained crMIZ1 cell lines with different degrees of MIZ1 reduction to confirm results obtained with MIZ1 silencing mediated by RNA-interference.

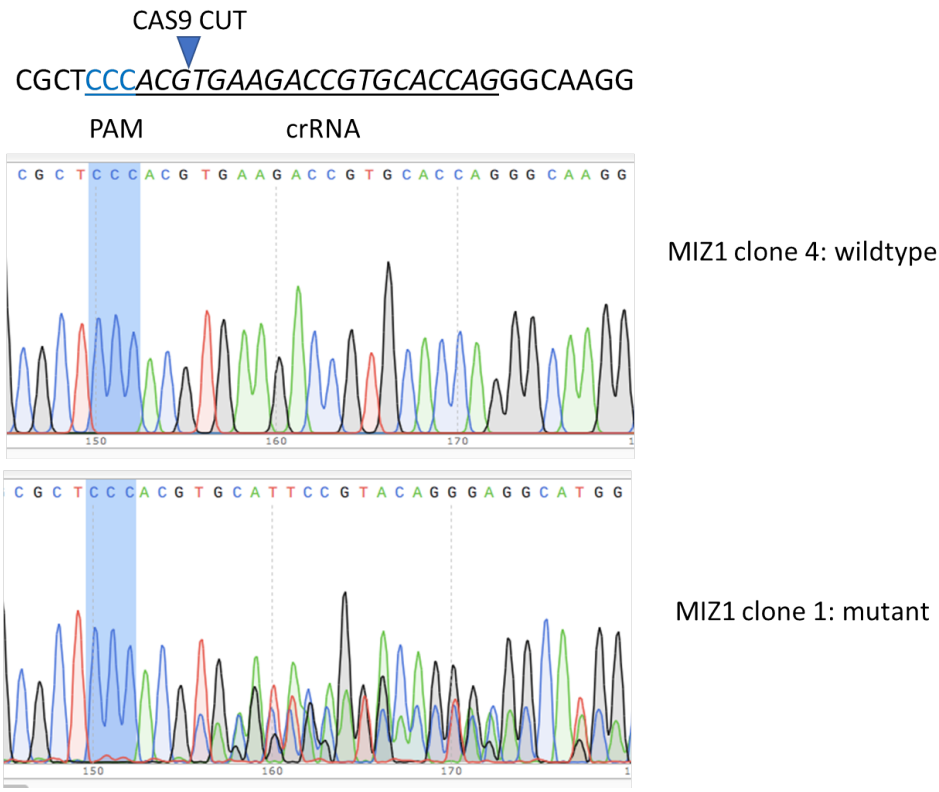

Figure 53 | Sanger sequencing data from wild-type and mutated crMIZ1 clones.

The image represents a schematic illustration of MIZ1 gene sequence around target locus to detect mutations at the targeted site. The crMIZ1 target sequence and PAM domain are indicated. Below, waveform data from DNA sequencer displaying the sequence obtained from PCR fragments of genomic DNA from 2 representative MIZ1 clones.

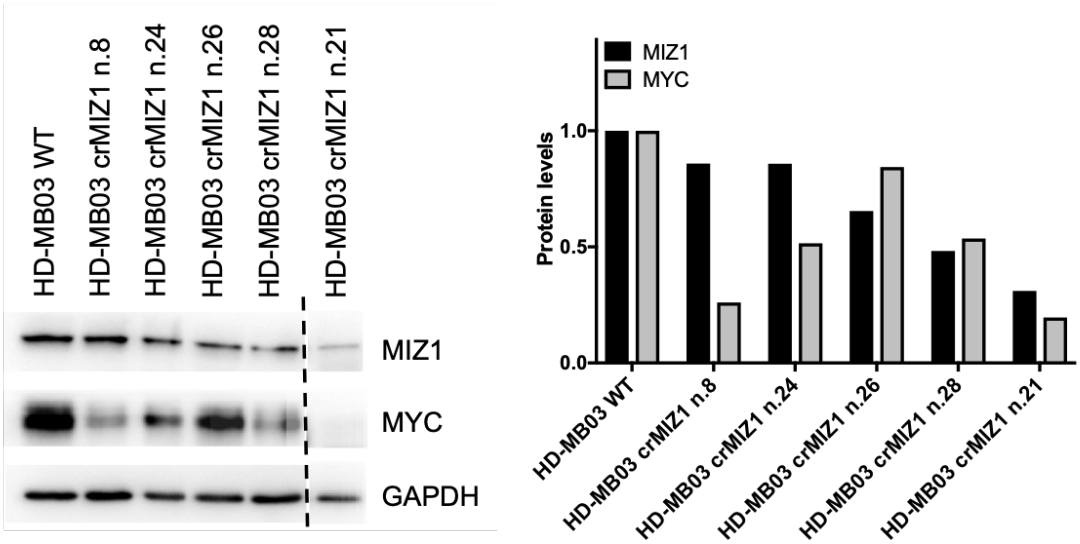

Figure 54 | Western blot analysis of MIZ1 protein levels in HD-MB03 crMIZ1 clones.

Representative western blot images for crMIZ1 HD-MB03 clones vs HD-MB03 wild-type (WT) (N=2). 50 µg of proteins were used for all samples. GAPDH was used as loading control. Dotted line indicates where WB image was cut, due to removal of a not discussed crMIZ1 clone; uncropped WB image is shown in the Appendix 6.6. Densitometric quantifications are provided on the right: protein levels are expressed as fold change relative to the control (HD-MB03 WT), arbitrarily set to 1.

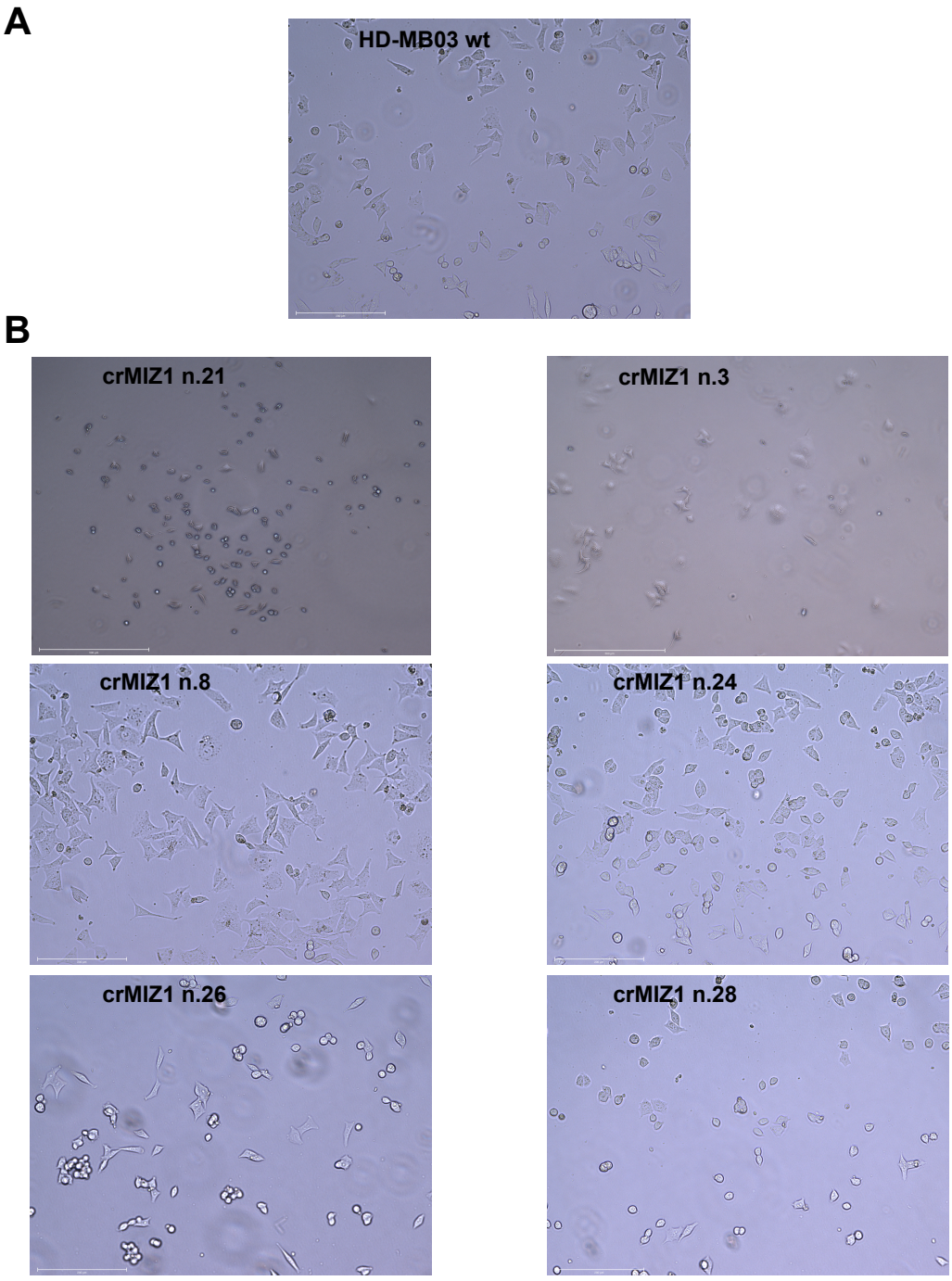

Figure 55 | Phase-contrast images of HD-MB03 wild-type cells vs crMIZ1 clones.

A) HD-MB03 wild-type cells B) 6 clones derived from HD-MB03 cells transfected with CRISPR/CAS9 system targeting MIZ1. Cells were observed at EVOS FL Auto Imaging System (ThermoFisher) at x100 magnification.

5.2.11 Validation of MIZ1-silencing phenotypic effects

To further confirm the effects of MIZ1 loss on cell proliferation, we measured cell growth rates of HD-MB03 wild-type cells versus crMIZ1 clones at 24h, 48h and 72h (Figure 56).

Overall, various degrees of MIZ1 reduction in crMIZ1 clones were able to significantly slow down cell proliferation rates compared to parental HD-MB03 cells. Particularly, crMIZ1 n.26 and 28 clones showed considerably slower growth rates when compared to other cell lines. This observation is consistent with the lower levels of MIZ1 protein in these clones than any other clone.

It should be noted that, in this study, we were not able to perform proliferation assays on the crMIZ1 n.21 line. In fact, culture of these cells was very challenging, and the growth rate was too slow to be compared with the other clones in the same assay. Nonetheless, we kept expanding this line and we observed the emergence of two sub-lines: an adherent line and a suspension line (Figure 57).

Furthermore, crMIZ1 n.21 clone showed the highest degree of MIZ1 knock-down in the western blot result, further consolidating the hypothesis that MIZ1 is directly controlling cell proliferation among other possible pathways.

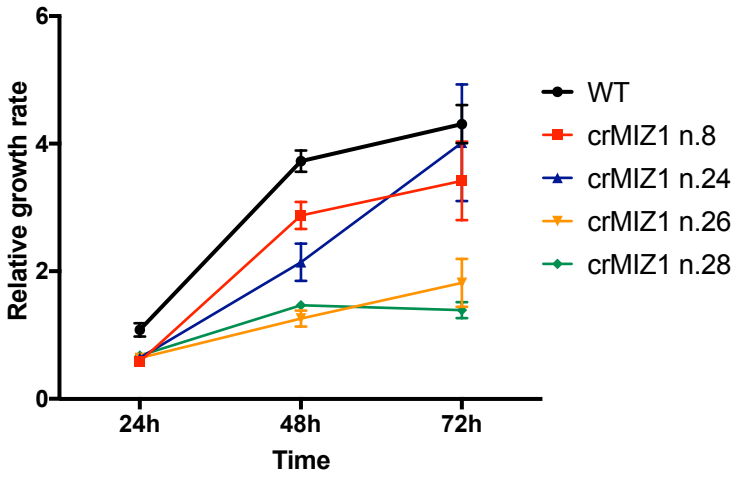

	24h	48h	72h
WT vs crMIZ1 n.8	**	*	ns
WT vs crMIZ1 n.24	**	**	ns
WT vs crMIZ1 n.26	**	***	**
WT vs crMIZ1 n.28	**	***	***

Figure 56 | crMIZ1 HD-MB03 clones vs parental HD-MB03 cells growth rates.

All HD-MB03 cell lines were seeded at 2000 cells/well in a 96-well plate. Cell viability was measured at 0h, 24h, 48h and 72h by MTT assay. Data are presented as mean ± SEM (N=2) using GraphPad software. HD-MB03 wild-type values were used as reference control. Statistical comparisons, presented below the graph, were performed using two-tailed student's t-test where *= $p \leq 0.05$, **= $p \leq 0.01$, ***= $p \leq 0.001$ and ns= not significant.

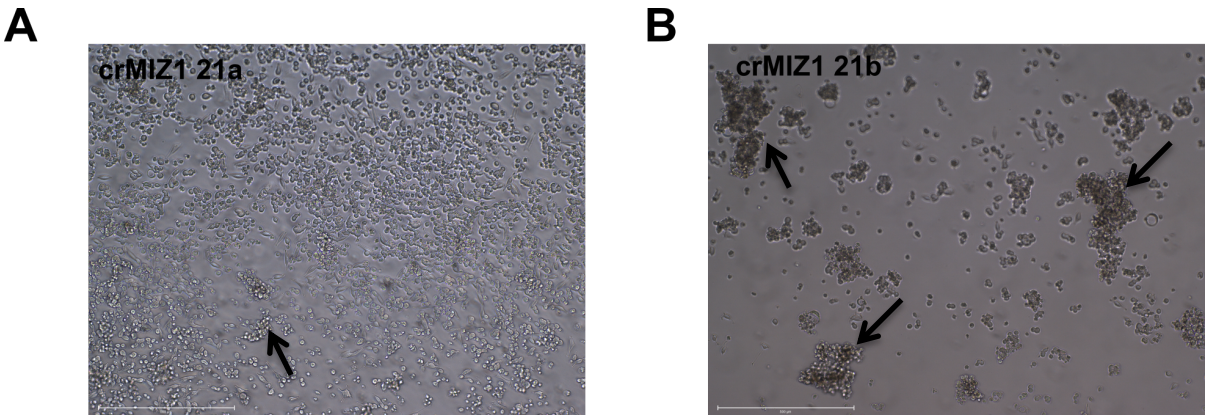

Figure 57 | Phase-contrast images of HD-MB03 crMIZ1 n.21 sub-cell lines.

crMIZ1 n.21 cells were observed at EVOS FL Auto Imaging System (ThermoFisher) at x100 magnification. Since suspension cells were firstly observed as in Figure 55 B, cells were kept in culture for subsequent 3 weeks were suspension cells and adherent cells were expanded in separate flasks: crMIZ1 n.21a being cells grown from the original adherent population and crMIZ1 n.21b being cells obtained from suspension cells.

5.3 Discussion

Group 3 is known in the clinic to have the worst overall survival rate (less than 50%) and it is molecularly characterised by the amplification and overexpression of MYC gene (Eilers & Eisenman, 2008; Taylor et al., 2012).

Members of the MYC family are differentially expressed in medulloblastoma. Group 3 and WNT MB patients are characterised by a higher expression of MYC, whereas MYCN over-expression is generally associated with SHH and G4 medulloblastomas (Kawauchi et al., 2012; Oliver et al., 2005). Recently *Vo et al.*, demonstrated that MYC interaction with MIZ1 is crucial for the definition of the group 3 biology. Furthermore, the Roussel group revealed that MYC has the highest affinity to MIZ1 among MYC family members, whereas MYCN exhibits a much lower binding affinity for MIZ1, resulting in a reduced transcriptional repression activity (Vo et al., 2016).

Since MIZ1 is expressed consistently across different MB patient samples (Figure 37) and since MYC overexpression is also found in milder tumours such as WNT MBs, we hypothesised that a key to decode outcome differences between less aggressive MB variants and more aggressive ones could hide behind the characteristic MYC/MIZ1 transcriptional context in G3 MB.

On the same note, it has been recently shown that the disruption of MYC/MIZ1 interaction shifts MB development towards a less proliferative state and contributes to the differences G3 and SHH tumours (Mathsyaraja & Eisenman, 2016). Furthermore, we reported *in vitro* that the G3 cell line (HD-MB03) and the G4 secondary cell line (CHLA-01-MED) showed higher protein expression of both MYC and MIZ1 compared to SHH and primary G4 cell lines, further supporting our hypothesis that MYC/MIZ1 interplay is crucial for aggressive phenotypes (Figure 35 C).

Notably, MYC is often referred to as an undruggable target, due to the lack of binding sites for drug development and its pleiotropic nature. Much work has been done to target the expression and its binding with partner proteins; however, more traditional strategies using small inhibitors have failed to reach satisfactory requirements for *in vivo* trials (Zinzalla, 2016; Zirath et al., 2013).

In the present study, we attempted a novel approach of targeting MYC transcriptional partner, MIZ1, through microRNAs, as a new strategy for disrupting MYC/MIZ1 regulation networks in aggressive MB.

Starting from computational studies, we identified and confirmed miR-124-3p as potential tool to target MIZ1 (Figure 38 and Figure 39). miR-124-3p is a crucial player in the developed cerebellum and it is a known tumour suppressor microRNA in medulloblastoma (Hohjoh & Fukushima, 2007; Mollashahi et al., 2019).

We have assessed that overexpression of miR-124-3p causes tumour growth inhibition in a G3 but not in a SHH *in vitro* model (Figure 41). Other recent studies showed that ectopic re-expression of miR-124 leads to proliferation reduction *in vivo* in MB and drives neuronal differentiation (Sabelström et al., 2019; Silber et al., 2013).

Silencing MIZ1 by RNAi corroborated our findings and was in line with previous studies, confirming the importance of MIZ1 specifically for group 3 MB development and progression (Figure 47) (Vo et al., 2016).

We find ourselves in discordance with other studies showing that either overexpression of miR-124 or MIZ1 down-regulation resulted in the growth reduction also in SHH models (Jiuyi Lu et al., 2013; Pierson et al., 2008). As previously discussed by Vo. et al, it is the loss in the MYC/MIZ1 interaction to achieve different transcriptional landscapes and give rise to different MB fates during cerebellar development (Vo et al., 2016). Here, overexpressing miR-124-3p, we obtained a 60% downregulation of MIZ1 protein (Figure 40 C), while by using RNAi we obtained up to 90% MIZ1 reduction (Figure 46 B). In our settings, we were not disrupting the actual interaction between MYC and MIZ1, and the residual MIZ1 protein might still interact with MYC or MYCN and mitigate the effect shown in our settings. Further to this, the interaction between MYCN and MIZ1 is weaker than with MYC and it is considered dispensable for the SHH tumourigenesis (Peukert et al., 1997). Altogether, this could potentially explain why we did not observe any effect in the DAOY cell line, while in HD-MB03 cells, were MYC/MIZ1 interaction is stronger, the shifts in MIZ1 abundance have a stronger impact.

In addition, the growth reduction effects generated with exogenous miR-124-3p expression might be due to indirect effects via inhibition of other miR-124-3p targets, independently from MIZ1. Cell fate profiles results also seem to validate this possibility, since downregulation of MIZ1 by RNAi mainly caused an increased mitotic cell death while miR-124-3p overexpression induced an extra inhibitory effect in interphase (Figure 44 and Figure 48). Furthermore, it has already been shown that miR-124 mediates its inhibitory effects on cell proliferation in MB via targeting CDK6, which might explain the increased interphase death that we observed in our settings (Pierson et al., 2008).

To our knowledge, for the first time, our RNAseq data provided information on the transcriptional output of miR-124-3p over-expression in G3 MB, which pointed to predominant alterations of cell cycle functions, particularly the G2/M stage (Figure 42), and which is also in alignment with cell fate results. In view of using miRNAs as therapeutic tools, functional analyses are crucial to predict side-effects and to use miRNAs in combination therapies to enhance treatment outcome. We put forward the idea that miR-124-3p could potentially be used as monotherapy in group 3 MB, considering its tumour suppressive roles in MB and its predominant impact on cell cycle.

Moreover, we showed that it would be beneficial to restore miR-124-3p expression in parallel with conventional chemotherapy (vincristine and cisplatin), to improve treatment of G3 MB as it would allow to lower doses of non-targeted cytotoxic agents (Figure 45). miR-124-3p has been already proposed to sensitise glioblastoma to other alkylating agents and, for the first time we demonstrated its booster capacity in medulloblastoma (Qiao et al., 2017).

As mentioned, the relevance of tipping MYC/MIZ1 equilibrium is found in the study of complex underpinning transcriptional regulations. MYC transcriptional regulation is very complex as it can both activate and inhibit transcription upon binding with different cofactors, MAX and MIZ1 being the most studied. At the same time, MIZ1 mainly activates transcription of its target genes but MIZ1 recruitment is shown as necessary for gene expression inhibition, and specifically MYC/MIZ1 transcription has been shown to have impact on neuronal differentiation in MB (Vo et al., 2016). Furthermore, MYC/MIZ1 interaction facilitates MYC stabilisation and protection from proteasomal degradation (Wiese et al., 2013).

Interestingly, we showed that downregulating MIZ1 through miR-124-3p overexpression or RNAi provoked MYC protein downregulation but MYC mRNA transcriptional upregulation (Figure 40 and 46). In a group 3 context, where MYC overexpression is an hallmark for tumour progression, this new balance with different MYC and MIZ1 protein abundance might have a greater impact than in a SHH model. For example, this new system might shift transcriptional networks to mimic MB settings without MYC overexpression.

Taken together, these results might reflect a different MYC transcriptional activity, possibly due to MYC protein downregulation after MIZ1 silencing.

Here, we showed that MIZ1 reduction triggers a widespread downregulation of microRNA expression (Figure 49). Overall, we validated 5 miRNAs being significantly downregulated in siMIZ1 conditions from high-throughput data (Figure 50): miR-30a, miR-324, miR-331, let-7i

and miR-32. Each miRNA was previously shown to be down-regulated in tumour conditions and, more importantly, associated to MYC-driven tumours.

The expression of members of the miR-30 family as well as let-7 family is known to be under the transcriptional regulation of MYC (Chang et al., 2008).

In addition, the observation that members of the miR-17/92 oncogenic cluster are repressed after MIZ1 reduction is positive evidence of the beneficial effect of MIZ1 reduction in MB and support that MYC protein levels are diminished upon MIZ1 silencing, since MYC is usually synergistic with the cluster expression (X. S. Liu et al., 2013; Mestdagh et al., 2010).

Altogether, the expression level of all validated miRNAs in our study are indication of tumourigenic settings. Therefore, is it possible to consider that the MIZ1 reduction actually shifts G3 cells towards milder MB phenotypes.

In this scenario, the MIZ1-mediated stabilisation of MYC is required for broad miRNA modulation and, conversely, repression of a subset of miRNAs, and that these regulations are crucial to shape G3 identity.

Finally, we have generated MIZ1 mutant models in G3 MB cells. We could not obtain complete knockouts for MIZ1 gene and this could be due to gene amplification within G3 MB or to the fact that complete MIZ1 loss might be lethal, since MIZ1 impacts on cell proliferation and since MYC/MIZ1 interaction is key for this subgroup. Nonetheless, we have confirmed our findings showing that MIZ1 reductions lead to cell proliferation impairment compared to wild-type cells using CRISPR/CAS9 model (Figure 56). Furthermore, from preliminary observations, we assessed that loss of MIZ1 provokes dramatic changes in cells phenotype, particularly by loss of cell adhesion (Figure 57).

In conclusion, MIZ1 represents an attractive target for group 3 MB. We have demonstrated that MIZ1 down-regulation impact on cell proliferation and potentially tips MYC/MIZ1 balance towards milder MB phenotypes.

miRNAs negatively regulate genes at a post-transcriptional level and have potential as tools for cancer treatment. We put forward the idea of using miR-124-3p as treatment for G3 MB as it would be suitable in combination therapies with conventional drugs.

5.4 Future directions

Future tasks should aim at dissecting transcriptional network shifts upon MYC/MIZ1 knockdowns and MYC/MIZ1 binding-deficient settings through ChIP-seq analyses. A better overview of the transcriptional impact of MYC alone, MIZ1 alone or MYC/MIZ1 impaired systems would validate our findings and clarify the actual influence of MIZ1 on the tumorigenic activity of MYC in group 3 MB.

A lot still needs to be done to find key connections between MYC/MIZ1 regulated miRNAs and targeted networks. A first step could be testing other up-regulated miRNAs from our Nanostring screening, which interestingly are excluded from the generalised repressive control of MYC.

According to preliminary results, we were able to generate at least one MIZ1-mutant cell line with a stable MIZ1 knockdown through CRISPR-Cas9 system. This model will be useful to corroborate previous results obtained with miR-124-3p and siMIZ1 systems.

Finally, we have identified miR-124-3p as potential targeted therapy against MIZ1 in G3 MB. Further studies will need to address the problems of using small RNAs as therapy such as the efficacy of targeting cancer cells, miRNA stability in bodily fluids, penetration of cellular membranes and delivery method.

Nonetheless, good efficiency has been recently shown towards the delivery of siRNAs to the CNS and miR-124 administration *in vivo* was already attempted with inhibitory effects on glioma growth, pointing at a promising future for the use of microRNAs as therapeutic tools (Wei et al., 2013).

Chapter 6:

Appendix

6.1 HD-MB03 spheroids

Below, time 0 images of the spheroids presented in Figure 21. These images were taken before treatment with respective inhibitors or DMSO, proving that the difference in size with the untreated control spheroid depended on a difference in plating (scale=200µm).

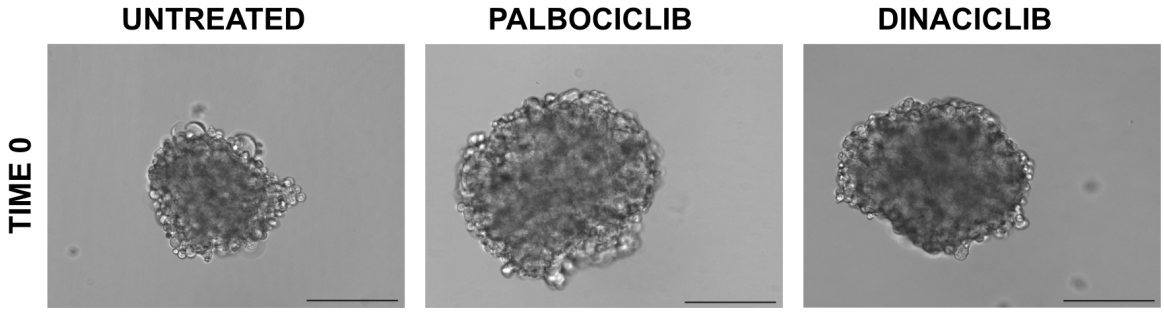

6.2 Relative expression of CDK1, CDK2, CDK5 and CDK9 mRNA in MB subgroups

Below, student's two tailed t-test results for the mRNA expression levels comparisons of dinaciclib-targeted CDKs in MB subgroups. Significant differences are shown in bold (p-value<0.05).

CDK1: Combination	t-test
group3 vs group4	0.36
group3 vs shh	**1.2e-04**
group3 vs wnt	**2.9e-06**
group4 vs shh	**3.1e-05**
group4 vs wnt	**4.0e-08**
shh vs wnt	**0.02**

CDK2: Combination	t-test
group3 vs group4	0.17
group3 vs shh	**2.7e-21**
group3 vs wnt	**1.7e-20**
group4 vs shh	**3.5e-29**
group4 vs wnt	**1.3e-23**
shh vs wnt	0.2

CDK5: Combination	t-test
group3 vs group4	**1.8e-07**
group3 vs shh	**3.3e-23**
group3 vs wnt	**3.0e-07**
group4 vs shh	**1.1e-16**
group4 vs wnt	**0.03**
shh vs wnt	**1.4e-03**

CDK9: Combination	t-test
group3 vs group4	**2.4e-53**
group3 vs shh	0.29
group3 vs wnt	**8.3e-05**
group4 vs shh	**1.3e-49**
group4 vs wnt	**1.6e-20**
shh vs wnt	**0.02**

6.3 Protein-coding genes differentially expressed in HD-MB03 cells treated with IC50 dinaciclib vs DMSO.

92 protein-coding genes were found up-regulated and 50 down-regulated after HD-MB03 cells treatment with DMSO or IC50 dinaciclib for 24h (0.8<FC>1.2, *p-value*<0.05) Genes that have been validated by single qRT-PCR are indicated in bold, namely CASP9 and BAX.

Gene Name	chr	chr_start	chr_stop	strand	logFC	P.Value	adj.P.Val	FC
TLN2	chr12	57768471	57772793	-	0,45	0,00007	0,092	1,366
ZFAT	chr3	49020459	49023495	+	0,44	0,00003	0,053	1,358
XIRP2	chr1	227730425	227735411	-	0,42	0,00011	0,092	1,340
MLLT11	chr6	30743199	30744554	-	0,41	0,00010	0,092	1,326
ANXA2	chr16	19716456	19858467	+	0,40	0,00124	0,226	1,323
CCDC15	chr19	48954815	48961798	+	0,40	0,00013	0,092	1,321
HTRA1	chr20	50794894	50882676	+	0,40	0,00013	0,092	1,320
AANAT	chr15	64165517	64356259	-	0,40	0,00048	0,165	1,318
CYP2W1	chr17	28724348	28727935	-	0,40	0,00512	0,313	1,317
ATF7IP2	chr17	4937130	4940251	-	0,39	0,00070	0,181	1,311
ALDH7A1	chr1	155610205	155614967	+	0,39	0,00094	0,197	1,308
RBM14	chr9	136791355	136793257	+	0,38	0,00027	0,132	1,303
RTP1	chr19	45815410	45863290	-	0,36	0,00030	0,139	1,282
TUBB2B	chr16	87830023	87869488	-	0,35	0,00186	0,241	1,278
MICALCL	chr12	119178642	119221131	+	0,35	0,00124	0,226	1,277
RASSF2	chr1	53087179	53142632	-	0,35	0,00178	0,240	1,277
SFI1	chrX	48590042	48608867	+	0,34	0,00188	0,241	1,268
SLC9A7	chr7	99616946	99632407	+	0,34	0,00050	0,166	1,267
KCNF1	chr14	73490964	73493392	+	0,34	0,00062	0,181	1,266
BOC	chr4	173331695	173335125	-	0,34	0,00145	0,240	1,262
ATM	chr21	25734570	25772460	+	0,33	0,00162	0,240	1,261
BAALC	chr8	143603913	143609773	-	0,33	0,00058	0,178	1,261
EXD3	chr19	45606994	45645629	-	0,33	0,00217	0,253	1,259
VARS	chr19	57363511	57365353	+	0,33	0,00066	0,181	1,257
PRELID2	chr20	49982999	49988886	+	0,33	0,00189	0,241	1,255

LPCAT3	chr10	125823546	125853695	+	0,33	0,00097	0,197	1,255
MAP3K7CL	chr1	32885994	32898441	+	0,33	0,00065	0,181	1,253
EHD3	chr19	50797704	50804929	-	0,32	0,00285	0,265	1,252
SHC1	chr22	23894004	23895227	+	0,32	0,00074	0,181	1,250
MFAP3L	chr1	150265399	150269580	-	0,32	0,00390	0,288	1,245
ATP5D	chr5	177301198	177303744	-	0,32	0,00257	0,259	1,244
GNB3	chr11	3087116	3166739	-	0,31	0,00147	0,240	1,243
ATP1B1	chr14	20455191	20457772	+	0,31	0,00155	0,240	1,241
MSRB2	chr1	169394870	169460669	-	0,31	0,00159	0,240	1,241
LGALS3	chr21	25585656	25607517	-	0,31	0,00174	0,240	1,240
ALG10B	chr1	161505430	161524013	+	0,31	0,00350	0,281	1,239
USB1	chr11	6680782	6683401	-	0,31	0,00368	0,281	1,238
DGAT1	chr19	49642125	49658642	+	0,31	0,00419	0,298	1,237
RAB26	chr22	29554808	29581337	-	0,31	0,00272	0,264	1,237
ZDHHC15	chr16	3065297	3082192	+	0,31	0,00297	0,265	1,237
RMI2	chr1	156591762	156594299	+	0,31	0,00176	0,240	1,236
PDE6H	chr19	1086579	1095380	-	0,30	0,00313	0,268	1,235
KRBOX1	chr20	17941597	17968980	-	0,30	0,00135	0,236	1,235
TUBB2A	chr10	122990806	123008817	-	0,30	0,00199	0,242	1,232
MARK4	chr3	53224707	53256052	-	0,30	0,00441	0,301	1,232
COMMD3	chr4	4290251	4321786	+	0,30	0,00110	0,213	1,231
PRKCH	chr12	55817919	55821879	+	0,30	0,00290	0,265	1,230
CYLD	chr3	122412332	122416051	-	0,30	0,00255	0,259	1,229
VARS2	chr7	128455849	128458418	+	0,30	0,00201	0,242	1,229
TAC4	chr17	19337554	19378182	-	0,30	0,01034	0,349	1,227
ARHGAP26	chr14	30622112	30735812	+	0,29	0,00292	0,265	1,226
BAD	chr6	31834608	31839766	+	0,29	0,00170	0,240	1,226
RTKN	chr11	62787415	62790405	+	0,29	0,00135	0,236	1,225
ZFYVE26	chr2	201071433	201085750	+	0,29	0,00189	0,241	1,223
WDR76	chr3	24117160	24495282	-	0,29	0,00507	0,313	1,222
RGS7BP	chr7	44999475	45076469	+	0,29	0,00178	0,240	1,222
TMEM120A	chr3	49357176	49358600	-	0,29	0,00157	0,240	1,222
PHKB	chr9	110243811	110256640	-	0,29	0,00360	0,281	1,221
STAG3	chr1	85580761	85583962	+	0,29	0,00749	0,329	1,221

PDK1	chr19	17405722	17433724	+	0,29	0,00372	0,281	1,220
ZNF695	chr11	73974667	73983307	-	0,29	0,00450	0,301	1,219
RHBDD2	chr12	39293228	39443390	-	0,29	0,00169	0,240	1,219
GUCA1C	chr1	67685061	67688338	+	0,29	0,00681	0,322	1,219
HIST1H2BN	chr6	33289302	33298401	+	0,29	0,00841	0,338	1,219
RRAGC	chr11	61391687	61398863	+	0,28	0,00156	0,240	1,218
CLDN11	chrX	23983720	24027186	-	0,28	0,00423	0,298	1,218
TNC	chr5	71032670	71067689	-	0,28	0,00577	0,313	1,218
HPS3	chr6	30600400	30618612	-	0,28	0,00257	0,259	1,216
C3orf67	chr17	19383442	19387240	-	0,28	0,00237	0,258	1,216
LNP1	chr12	57472255	57488814	-	0,28	0,00357	0,281	1,216
ERAP2	chr3	170864875	170870483	-	0,28	0,00250	0,259	1,215
KRT80	chr7	135092363	135170795	-	0,28	0,01336	0,366	1,213
ACSL1	chr22	20441519	20495883	-	0,28	0,00413	0,296	1,213
RBFA	chr2	96143166	96145440	-	0,28	0,00420	0,298	1,212
PLPPR4	chr12	57452323	57459280	+	0,28	0,00553	0,313	1,211
DPYSL2	chr6	31661229	31666283	-	0,27	0,00246	0,259	1,209
ATXN10	chr7	97852118	97872542	-	0,27	0,00224	0,254	1,209
CREM	chr11	8682411	8714759	+	0,27	0,00605	0,314	1,208
TCEA2	chr16	29995294	30005793	+	0,27	0,00370	0,281	1,208
TEAD2	chr3	53088483	53130462	-	0,27	0,00240	0,258	1,207
ACCS	chr3	118900557	119146068	-	0,27	0,00389	0,288	1,207
MYC	chr17	7402975	7404137	-	0,27	0,01606	0,387	1,207
C1S	chrM	14149	14673	-	0,27	0,01482	0,379	1,207
DTX3L	chr16	15949577	16143074	+	0,27	0,00657	0,320	1,206
CASP9	chr5	80626228	80654983	-	0,27	0,00576	0,313	1,205
ZNF341	chr3	51395867	51500002	-	0,27	0,01290	0,360	1,205
NEIL2	chr2	216632828	216664436	+	0,27	0,00699	0,324	1,204
MLF1	chr17	29560547	29567137	-	0,27	0,00378	0,284	1,204
COX16	chr19	55654146	55674715	+	0,27	0,00626	0,317	1,203
IKZF2	chr10	91906589	91909483	-	0,27	0,00268	0,264	1,202
STS	chr6	31530219	31542448	-	0,26	0,00844	0,338	1,202
GPR137B	chr1	241590102	241677376	-	0,26	0,00473	0,306	1,200
B9D1	chr17	49838309	49848017	-	-0,31	0,00097	0,197	0,809

HILPDA	chr6	30908242	30926459	+	-0,31	0,00138	0,236	0,808
WDR5B	chr16	50742050	50801935	+	-0,31	0,00316	0,268	0,808
ORMDL2	chr14	61187559	61550976	+	-0,31	0,00124	0,226	0,808
ZBTB49	chr10	22315974	22320308	+	-0,31	0,00201	0,242	0,807
TKT	chr19	45079288	45305283	+	-0,31	0,00149	0,240	0,807
IKZF5	chr6	3153669	3157526	-	-0,31	0,00303	0,265	0,806
SNX5	chr3	42809483	42942792	+	-0,31	0,00080	0,185	0,806
POLR2E	chr12	14973022	14981865	+	-0,31	0,00131	0,234	0,804
APOA1BP	chr16	11249619	11351762	+	-0,32	0,00070	0,181	0,804
IL32	chrX	75368427	75523502	-	-0,32	0,00861	0,338	0,803
NIPSNAP1	chr16	2140803	2154165	+	-0,32	0,00076	0,181	0,801
SCAF1	chr8	144314584	144326910	-	-0,32	0,00294	0,265	0,801
MRPL17	chr16	57999546	58021618	+	-0,32	0,00071	0,181	0,801
FCGR2A	chr12	38316578	38329728	+	-0,32	0,00088	0,193	0,801
MRPL39	chr14	55124110	55145413	+	-0,33	0,01388	0,366	0,797
CCDC181	chr10	23095506	23122013	+	-0,33	0,00842	0,338	0,796
APEX1	chr1	169105697	169132722	+	-0,33	0,00336	0,281	0,795
OSBPL5	chr12	6839954	6847393	+	-0,33	0,00088	0,193	0,795
RAB24	chr19	1241746	1244826	+	-0,34	0,00296	0,265	0,791
APH1A	chr4	169986597	170033031	-	-0,34	0,00059	0,178	0,789
MIF	chr1	154962298	154974395	-	-0,34	0,00220	0,254	0,789
C19orf48	chr2	31234337	31269447	+	-0,34	0,00105	0,204	0,788
HPCA	chr21	29077471	29175889	+	-0,34	0,00227	0,255	0,788
BCCIP	chr12	6976186	7018510	-	-0,35	0,00246	0,259	0,787
SNAI1	chr5	145471799	145835369	-	-0,35	0,00064	0,181	0,787
TRAPPC2P1	chr6	31777518	31795953	-	-0,35	0,00046	0,162	0,784
EML2	chr9	137306896	137423262	-	-0,35	0,00044	0,162	0,782
PYCRL	chr8	103140710	103230305	+	-0,35	0,00071	0,181	0,782
GABPA	chr11	108222484	108369102	+	-0,36	0,00022	0,119	0,779
HMGB2	chr3	113211003	113287459	+	-0,36	0,00448	0,301	0,778
C14orf169	chr2	10911937	10914225	+	-0,36	0,00104	0,204	0,778
ZSCAN25	chrX	46599252	46759172	-	-0,36	0,00172	0,240	0,777
WDR13	chr22	31488688	31618586	+	-0,37	0,00023	0,119	0,776
SLC1A7	chr20	4780023	4823645	-	-0,38	0,00020	0,114	0,767

HSPB8	chr11	12276080	12359144	+	-0,39	0,01986	0,397	0,763
SLC7A5	chr6	3224261	3231730	-	-0,39	0,00046	0,162	0,763
SYMPK	chr3	187197486	187201465	+	-0,40	0,00009	0,092	0,758
TMEM141	chr11	66616582	66627347	+	-0,40	0,00008	0,092	0,757
MSTO1	chr5	126541841	126595418	-	-0,41	0,00016	0,103	0,755
SLC25A11	chr16	10326434	10483638	+	-0,41	0,00015	0,103	0,752
TLCD1	chr7	983199	989640	+	-0,41	0,00018	0,110	0,751
CSNK1G1	chr17	76453351	76470117	+	-0,42	0,00023	0,119	0,747
BCAS4	chr10	122461525	122514908	+	-0,42	0,00010	0,092	0,747
BAX	chr11	124954121	125041489	+	-0,44	0,00012	0,092	0,738
IQCK	chr15	60347134	60402883	-	-0,45	0,00002	0,052	0,731
IER3	chr1	151057758	151068497	+	-0,46	0,00086	0,193	0,725
JMJD4	chr2	166888487	167259753	+	-0,51	0,00001	0,048	0,704
NDUFAF3	chr8	134477788	134713049	-	-0,51	0,00001	0,048	0,701
METTL1	chr15	62390526	62844631	+	-0,52	0,00002	0,052	0,697

6.4 BAX is downregulated after dinaciclib treatments in ONS76 cells.

Western blot analysis of BAX protein in ONS76 cells after 24h treatment with scalar doses of dinaciclib. 50 µg of proteins were used for all samples. Densitometric quantifications are provided on the right: protein levels are expressed as fold change relative to the control (NT), arbitrarily set to 1. WB shown is one representative of N=2 replicates.

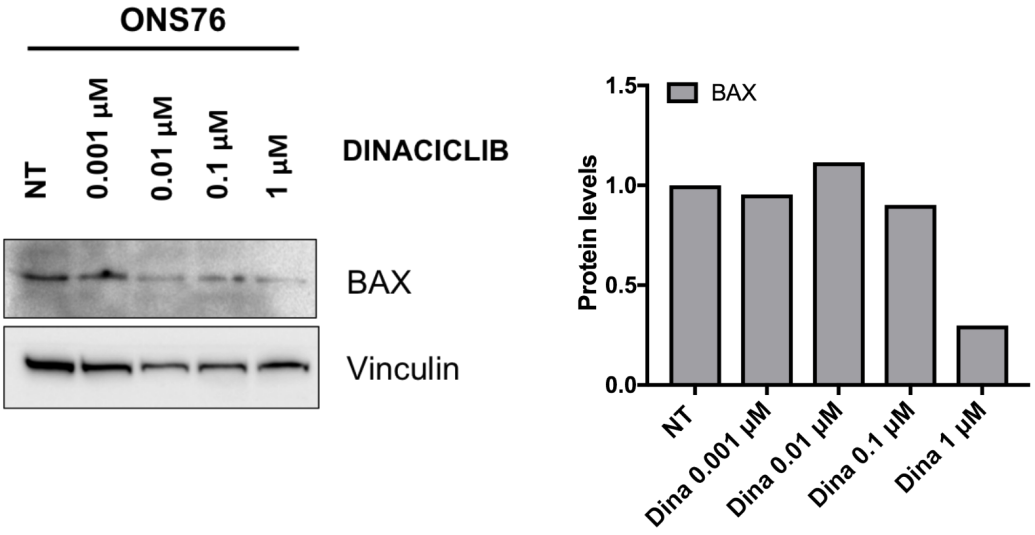

6.5 Protein-coding genes differentially expressed in HD-MB03 cells over-expressing pre-miR-124-3p vs pre-miR-CTRL.

152 protein-coding genes resulted up-regulated and 142 down-regulated in HD-MB03 cells transfected with pre-miR-124-3p compared to HD-MB03 cells transfected with pre-miR-CTRL for 72h (0.5<FC>2, *p-value* <0.05). Genes that have been validated by single qRT-PCR are indicated in bold, namely VIM. We also reported a significant ZBTB17 (MIZ1) down-regulation after miR-124-3p over-expression in HD-MB03 cells, as shown at the very end of this table.

Gene Name	chr	chr_start	chr_stop	strand	logFC	P.Value	adj.P.Val	FC
CAMKV	chr3	49857988	49870222	-	3,14	0,000000 00001	0,000000 10339	8,82
CPLX1	chr4	784957	826198	-	3,01	0,000000 00002	0,000000 10339	8,04
CCDC181	chr1	16939487 0	16946066 9	-	2,63	0,000000 00036	0,000000 67963	6,19
CHGA	chr14	92923080	92935293	+	2,63	0,000000 00427	0,000001 90500	6,17
TTR	chr18	31591726	31599021	+	2,44	0,000000 03122	0,000005 21594	5,44
PHF21B	chr22	44881162	45009999	-	2,43	0,000000 00012	0,000000 39054	5,40
SCG3	chr15	51681353	51721031	+	2,34	0,000000 00031	0,000000 67963	5,07
PDC	chr1	18644356 6	18646112 2	-	2,28	0,000000 00080	0,000001 11443	4,84
MMP24	chr20	35226654	35277000	+	2,27	0,000000 00178	0,000001 22612	4,84
SCAMP5	chr15	74957219	75021496	+	2,22	0,000000 00158	0,000001 22171	4,65
CDK5R2	chr2	21895965 5	21896216 2	+	2,12	0,000000 00267	0,000001 66541	4,35
BEX1	chrX	10306265 1	10306424 0	-	2,07	0,000000 01822	0,000003 69128	4,19

FAM57B	chr16	30024427	30052978	-	2,05	0,000000 00102	0,000001 11443	4,16
IER3	chr6	30743199	30744554	-	1,99	0,000000 01318	0,000003 03474	3,97
CELF3	chr1	15170240 4	15171681 4	-	1,99	0,000000 00091	0,000001 11443	3,97
CHRNB2	chr1	15456778 1	15458002 6	+	1,93	0,000000 00443	0,000001 90500	3,82
TRNP1	chr1	26993707	27000898	+	1,92	0,000000 00546	0,000002 04595	3,77
KCNB1	chr20	49363877	49484297	-	1,91	0,000000 00175	0,000001 22612	3,75
BCO1	chr16	81238448	81291142	+	1,86	0,000000 03252	0,000005 21594	3,62
PDE6H	chr12	14973022	14981865	+	1,83	0,000000 17468	0,000016 27634	3,56
ABCC5	chr3	18391993 4	18401801 5	-	1,80	0,000000 00859	0,000002 45278	3,48
RUNDC3A	chr17	44308413	44318671	+	1,80	0,000000 00099	0,000001 11443	3,48
EPHA8	chr1	22563564	22603594	+	1,77	0,000000 04447	0,000006 38677	3,41
GABBR1	chr6	29555629	29633976	-	1,76	0,000000 00144	0,000001 17887	3,39
SCRT1	chr8	14433056 5	14433628 1	-	1,76	0,000000 03163	0,000005 21594	3,39
SV2C	chr5	76083172	76353939	+	1,72	0,000000 00262	0,000001 66541	3,30
TAC4	chr17	49838309	49848017	-	1,72	0,000000 64838	0,000039 57246	3,28
DDN	chr12	48995149	48999309	-	1,70	0,000000 01282	0,000003 00402	3,26
SRRM3	chr7	76201900	76287288	+	1,69	0,000000 11529	0,000012 60733	3,22

PRR7	chr5	177446445	177456286	+	1,69	0,00000002206	0,00000402085	3,22
GABRA5	chr15	26866363	26949207	+	1,68	0,00000000357	0,00000187358	3,21
NRCAM	chr7	108147623	108456717	-	1,67	0,00000002879	0,00000497110	3,18
KCNH6	chr17	63523334	63548977	+	1,66	0,00000001922	0,00000370951	3,16
RAB3A	chr19	18196784	18204074	-	1,65	0,00000130218	0,00005975766	3,15
NMNAT2	chr1	183248237	183418602	-	1,65	0,00000003299	0,00000521594	3,14
GGACT	chr13	100530164	100589528	-	1,65	0,00000014610	0,00001497733	3,14
MAST1	chr19	12833951	12874951	+	1,65	0,00000001465	0,00000325934	3,14
SYT4	chr18	43267878	43277650	-	1,64	0,00000015805	0,00001553958	3,12
PCBP3	chr21	45643694	45942454	+	1,64	0,00000002297	0,00000412973	3,11
PAX5	chr9	36833275	37034185	-	1,63	0,00000000458	0,00000190500	3,10
CNGB3	chr8	86553977	86743675	-	1,59	0,00000004403	0,00000638677	3,01
HAGHL	chr16	726936	735525	+	1,57	0,00000004527	0,00000638677	2,98
FAM124A	chr13	51222334	51284241	+	1,57	0,00000001134	0,00000278345	2,97
SPINK4	chr9	33218365	33248567	+	1,57	0,00000189199	0,00007410945	2,97
SLC13A2	chr17	28473293	28497781	+	1,55	0,00000072638	0,00004205126	2,93
DCX	chrX	111293780	111412375	-	1,53	0,00000005396	0,00000721770	2,89

SPOCK1	chr5	136975298	137598379	-	1,53	0,00000053515	0,00003459243	2,89
PITPNC1	chr17	67377281	67697261	+	1,51	0,00000005490	0,00000721770	2,85
ARSI	chr5	150296343	150339307	-	1,49	0,00000000654	0,00000221304	2,81
ENO2	chr12	6913745	6923698	+	1,48	0,00000017276	0,00001627634	2,78
CHGB	chr20	5911430	5925361	+	1,48	0,00000001666	0,00000352602	2,78
SNAP25	chr20	10218830	10307418	+	1,47	0,00000003264	0,00000521594	2,78
ADAMTSL1	chr9	18473894	18910950	+	1,47	0,00000001087	0,00000278345	2,78
PDE6C	chr10	93612588	93666010	+	1,46	0,00000023998	0,00002067186	2,76
NAPB	chr20	23374519	23421519	-	1,46	0,00000006733	0,00000849481	2,75
TMEM198	chr2	219543663	219550595	+	1,45	0,00000005678	0,00000737739	2,73
NOG	chr17	56593699	56595590	+	1,45	0,00000003655	0,00000559141	2,73
SVOP	chr12	108907741	109021240	-	1,45	0,00000103988	0,00005110588	2,73
NEGR1	chr1	71395940	72282734	-	1,45	0,00000015223	0,00001536555	2,73
HBQ1	chr16	180453	181181	+	1,44	0,00000001083	0,00000278345	2,72
CCDC80	chr3	112596794	112649530	-	1,44	0,00000000886	0,00000247442	2,71
SLC43A2	chr17	1569267	1628886	-	1,42	0,00000119738	0,00005672198	2,68
CHPF	chr2	219538947	219543787	-	1,42	0,00000001119	0,00000278345	2,68

SEMA3A	chr7	83955777	84492724	-	1,42	0,000000 00658	0,000002 21304	2,68
STMN3	chr20	63639705	63657682	-	1,41	0,000000 03443	0,000005 37895	2,66
SAG	chr2	23330781 6	23334705 5	+	1,41	0,000000 52815	0,000034 30915	2,66
RASL10B	chr17	35731649	35743521	+	1,40	0,000000 15618	0,000015 52538	2,64
MBP	chr18	76978827	77133683	-	1,39	0,000000 38573	0,000028 75883	2,62
TMC6	chr17	78110458	78132407	-	1,39	0,000000 08810	0,000010 32243	2,62
ARR3	chrX	70268305	70281840	+	1,39	0,000000 23444	0,000020 50896	2,62
POU4F2	chr4	14663889 3	14664247 4	+	1,39	0,000003 22104	0,000102 81189	2,62
DUSP2	chr2	96143166	96145440	-	1,38	0,000000 37838	0,000028 53505	2,59
AP3B2	chr15	82659281	82709914	-	1,37	0,000000 04786	0,000006 61113	2,58
CPNE7	chr16	89575768	89597246	+	1,36	0,000000 02428	0,000004 30463	2,57
TMEM158	chr3	45224466	45226278	-	1,36	0,000000 05166	0,000006 98795	2,56
SLC7A8	chr14	23125295	23183674	-	1,35	0,000000 24103	0,000020 67186	2,54
LGALS3BP	chr17	78971238	78980109	-	1,34	0,000000 39559	0,000028 83879	2,54
ECE2	chr3	18424965 0	18429303 1	+	1,32	0,000000 02012	0,000003 79132	2,49
LHFPL4	chr3	9498361	9553802	-	1,32	0,000000 41840	0,000029 79226	2,49
MFSD12	chr19	3538261	3574290	-	1,31	0,000000 01385	0,000003 13433	2,49

A2M	chr12	9067664	9116229	-	1,31	0,000000 11768	0,000012 76151	2,48
ASPHD1	chr16	29900375	29919864	+	1,31	0,000000 97019	0,000049 15387	2,47
BSN	chr3	49554489	49671545	+	1,30	0,000003 55342	0,000109 71296	2,47
SPRYD3	chr12	53064316	53079420	-	1,30	0,000000 17947	0,000016 53813	2,46
KCNIP2	chr10	10182597 4	10184392 0	-	1,30	0,000000 12035	0,000012 94501	2,46
NEUROD4	chr12	55019945	55030014	+	1,29	0,000000 04848	0,000006 62651	2,45
FBXO41	chr2	73254682	73284431	-	1,28	0,000000 91345	0,000047 89616	2,43
UNC119	chr17	28546707	28552668	-	1,25	0,000000 18023	0,000016 53813	2,37
SLC4A8	chr12	51391317	51515763	+	1,23	0,000000 03260	0,000005 21594	2,35
NAT8L	chr4	2059512	2069089	+	1,23	0,000000 10636	0,000011 82803	2,34
ZNF385A	chr12	54369133	54391298	-	1,22	0,000000 46986	0,000031 61803	2,34
UNC13A	chr19	17601328	17688365	-	1,22	0,000001 82885	0,000073 38889	2,33
LAMP5	chr20	9514358	9530524	+	1,22	0,000014 00846	0,000279 35421	2,33
PSD	chr10	10240261 7	10242153 9	-	1,21	0,000000 15441	0,000015 46657	2,32
GPC2	chr7	10016960 6	10017737 2	-	1,21	0,000000 07826	0,000009 42094	2,32
INA	chr10	10327716 3	10329035 1	+	1,21	0,000001 32086	0,000059 75766	2,31
NPDC1	chr9	13703947 0	13704620 3	-	1,21	0,000000 06970	0,000008 71070	2,31

NSMF	chr9	137447570	137459334	-	1,20	0,00000037502	0,00002853505	2,29
CHRM3	chr1	239386565	239915452	+	1,18	0,00000023612	0,00002051890	2,26
PCP4	chr21	39867317	39929397	+	1,17	0,00000132078	0,00005975766	2,24
VASH1	chr14	76762189	76783015	+	1,16	0,00000058198	0,00003653914	2,24
RELL2	chr5	141636950	141641077	+	1,16	0,00000130671	0,00005975766	2,23
UNC80	chr2	209771993	209999300	+	1,16	0,00000071022	0,00004160493	2,23
C12orf73	chr12	103950202	103965708	-	1,15	0,00000043365	0,00003009092	2,23
SEMA3C	chr7	80742538	80922359	-	1,15	0,00000097804	0,00004935222	2,22
TMEM145	chr19	42313325	42325062	+	1,14	0,00000188363	0,00007404204	2,20
ATP6V0A1	chr17	42458844	42522611	+	1,13	0,00000119684	0,00005672198	2,19
GRIA1	chr5	153489615	153813869	+	1,13	0,00000007529	0,00000923372	2,19
DOCK4	chr7	111726110	112206411	-	1,13	0,00000029419	0,00002397760	2,18
SNRPC	chr6	34757406	34773794	+	1,12	0,00000011482	0,00001260733	2,18
C19orf24	chr19	1275438	1279249	+	1,12	0,00000144737	0,00006351949	2,17
SYN1	chrX	47571898	47619853	-	1,12	0,00000107652	0,00005193414	2,17
NPTX1	chr17	80467148	80477843	-	1,11	0,00000101046	0,00005022429	2,17
MRM1	chr17	36601572	36608971	+	1,11	0,00000018354	0,00001672465	2,16

NEFM	chr8	24913012	24919098	+	1,11	0,000000 57325	0,000036 33899	2,16
DEAF1	chr11	644233	706715	-	1,11	0,000000 31368	0,000025 25193	2,16
SLC5A6	chr2	27199587	27212958	-	1,10	0,000000 96090	0,000048 87178	2,15
SEZ6	chr17	28954901	29006440	-	1,09	0,000001 54352	0,000066 19062	2,13
OGDHL	chr10	49734643	49762379	-	1,09	0,000000 50945	0,000033 59279	2,13
LNP1	chr3	10040119 3	10045631 9	+	1,09	0,000002 93587	0,000097 87699	2,13
MPP4	chr2	20164487 0	20169869 4	-	1,09	0,000000 93597	0,000048 35339	2,12
CTXN1	chr19	7924485	7926166	-	1,08	0,000001 07547	0,000051 93414	2,12
MAK	chr6	10762723	10838555	-	1,08	0,000000 27130	0,000022 67486	2,12
PTPRZ1	chr7	12187308 9	12206203 6	+	1,08	0,000001 33215	0,000059 86075	2,11
AMPD2	chr1	10961610 4	10963205 1	+	1,07	0,000000 59632	0,000036 91012	2,10
KCNK12	chr2	47516581	47570939	-	1,07	0,000000 85198	0,000046 19717	2,10
TMEM51	chr1	15152532	15220480	+	1,07	0,000000 37718	0,000028 53505	2,09
SLCO4A1	chr20	62642445	62685785	+	1,06	0,000000 70136	0,000041 45679	2,09
SLC19A3	chr2	22768521 0	22771801 2	-	1,05	0,000001 79979	0,000072 82899	2,08
FREM2	chr13	38687129	38887131	+	1,05	0,000013 83176	0,000277 94838	2,07
PLD6	chr17	17200995	17206315	-	1,05	0,000000 17384	0,000016 27634	2,07

XKR7	chr20	31968002	32003387	+	1,05	0,000002 57626	0,000090 45045	2,07
PIK3R3	chr1	46040140	46133036	-	1,05	0,000000 67521	0,000040 94625	2,07
ASIC1	chr12	50057548	50083611	+	1,05	0,000000 21068	0,000018 67916	2,07
BAALC	chr8	103140710	103230305	+	1,05	0,000002 63217	0,000090 71545	2,07
SRGAP1	chr12	63844293	64162221	+	1,05	0,000001 95563	0,000075 92244	2,07
MAPK8IP3	chr16	1706183	1770317	+	1,04	0,000014 17595	0,000281 41731	2,06
PAQR5	chr15	69298947	69407780	+	1,04	0,000001 66359	0,000069 76033	2,05
UBAP1L	chr15	65092770	65115197	-	1,04	0,000014 83793	0,000291 90908	2,05
MAPK8IP2	chr22	50600685	50613981	+	1,04	0,000000 14953	0,000015 21011	2,05
FBXL16	chr16	692498	705829	-	1,03	0,000003 41154	0,000106 74964	2,04
ARHGEF3	chr3	56727418	57079329	-	1,02	0,000002 65468	0,000090 71545	2,03
XPR1	chr1	180632004	180890251	+	1,02	0,000000 51529	0,000033 63976	2,03
TMCC2	chr1	205228176	205273343	+	1,02	0,000000 34467	0,000027 24524	2,03
HIST1H3E	chr6	26224199	26227473	+	1,02	0,000001 88462	0,000074 04204	2,03
TTC12	chr11	113314529	113383544	+	1,02	0,000000 88752	0,000047 34142	2,02
LIMK2	chr22	31212239	31280080	+	1,01	0,000000 40933	0,000029 67557	2,02
NTMT1	chr9	129608884	129636131	+	1,01	0,000000 38107	0,000028 57343	2,02

CLCN4	chrX	10156945	10237660	+	1,01	0,000002 14836	0,000081 94987	2,01
DPP7	chr9	13711054 2	13711517 7	-	1,01	0,000000 39513	0,000028 83879	2,01
C3orf14	chr3	62318973	62336213	+	1,01	0,000015 62064	0,000304 11569	2,01
KIF21B	chr1	20096939 0	20102370 0	-	1,01	0,000023 76793	0,000406 62677	2,01
PLXNA2	chr1	20802224 2	20824432 0	-	-1,00	0,000022 17107	0,000384 31802	0,50
COL6A1	chr21	45981737	46005050	+	-1,00	0,000004 63722	0,000130 57844	0,50
NME4	chr16	396725	410367	+	-1,00	0,000000 58010	0,000036 53914	0,50
HERPUD1	chr16	56932048	56944863	+	-1,00	0,000051 19073	0,000691 78657	0,50
LOXL4	chr10	98247690	98268250	-	-1,00	0,000000 58677	0,000036 66486	0,50
MTHFD2	chr2	74198562	74217565	+	-1,00	0,000000 95378	0,000048 87178	0,50
AQP3	chr9	33441154	33447611	-	-1,00	0,022742 14767	0,060250 85034	0,50
PDE3B	chr11	14643723	14872044	+	-1,01	0,000000 17489	0,000016 27634	0,50
QKI	chr6	16341400 0	16357859 6	+	-1,02	0,000000 28673	0,000023 51540	0,49
VASH2	chr1	21295052 0	21299203 7	+	-1,02	0,000002 98253	0,000098 83018	0,49
NHLH1	chr1	16036706 7	16037284 8	+	-1,02	0,000000 28534	0,000023 51540	0,49
SLC44A3	chr1	94820342	94895246	+	-1,02	0,000039 71518	0,000578 40464	0,49
CCND2	chr12	4273772	4305350	+	-1,03	0,000000 62748	0,000038 50810	0,49

TNNT1	chr19	55132794	55149354	-	-1,03	0,000000 35097	0,000027 41302	0,49
DNAJC1	chr10	21756537	22003769	-	-1,03	0,000000 90840	0,000047 87164	0,49
NANOS1	chr10	11902971 6	11903373 2	+	-1,03	0,000000 36791	0,000028 39859	0,49
ATP1A2	chr1	16011575 9	16014359 1	+	-1,04	0,000000 68169	0,000040 94625	0,49
TP73	chr1	3652520	3736201	+	-1,04	0,000001 38955	0,000061 39298	0,49
PTGFR	chr1	78303884	78539749	+	-1,04	0,000001 99547	0,000077 04801	0,49
LAMB1	chr7	10792379 9	10800325 5	-	-1,04	0,000000 15869	0,000015 53958	0,49
NPC2	chr14	74476192	74494177	-	-1,05	0,000004 21481	0,000121 96525	0,48
FADS1	chr11	61799625	61829318	-	-1,05	0,000003 04145	0,000099 77492	0,48
TNC	chr9	11501957 8	11511825 7	-	-1,05	0,000068 26921	0,000841 94418	0,48
ADD3	chr10	10999636 8	11013556 5	+	-1,05	0,000002 83018	0,000095 46939	0,48
SNTB1	chr8	12053574 5	12081327 3	-	-1,05	0,000619 90592	0,004044 95551	0,48
MORC4	chrX	10681387 1	10700024 4	-	-1,06	0,000001 54644	0,000066 19062	0,48
AMOT	chrX	11277450 3	11284081 5	-	-1,06	0,000001 57878	0,000066 93900	0,48
IL21R	chr16	27402162	27452042	+	-1,06	0,000000 37659	0,000028 53505	0,48
TRIM55	chr8	66126896	66175487	+	-1,06	0,000000 34802	0,000027 34541	0,48
SNAP23	chr15	42491233	42545356	+	-1,06	0,000001 21034	0,000057 13000	0,48

CPT1A	chr11	68754620	68844410	-	-1,06	0,000001 84071	0,000073 44880	0,48
SGPL1	chr10	70815961	70881173	+	-1,07	0,000001 71000	0,000070 12076	0,48
ATF4	chr22	39519695	39522685	+	-1,07	0,000000 91982	0,000047 89616	0,48
CCDC28A	chr6	13877350 9	13879331 9	+	-1,07	0,000000 98163	0,000049 35222	0,48
TAPBP	chr6	33299694	33314387	-	-1,07	0,000000 39544	0,000028 83879	0,47
CDC25C	chr5	13828526 5	13833835 5	-	-1,08	0,000002 39827	0,000087 90523	0,47
TPP1	chr11	6612763	6619461	-	-1,08	0,000009 43101	0,000215 22387	0,47
CSNK1G1	chr15	64165517	64356259	-	-1,08	0,000001 84154	0,000073 44880	0,47
CLDN15	chr7	10123209 2	10123882 0	-	-1,08	0,000004 26229	0,000122 38471	0,47
CEP170B	chr14	10486528 0	10489677 0	+	-1,09	0,000000 50388	0,000033 39326	0,47
SKP2	chr5	36151989	36184319	+	-1,09	0,000002 55522	0,000090 45045	0,47
CHRNB1	chr17	7445061	7457707	+	-1,09	0,000003 30789	0,000104 59319	0,47
CDT1	chr16	88803213	88809258	+	-1,10	0,000003 57524	0,000110 12741	0,47
EMP2	chr16	10528422	10580698	-	-1,10	0,000000 16405	0,000015 94549	0,47
ITGA9	chr3	37452115	37823514	+	-1,10	0,000001 85317	0,000073 68865	0,47
SLC1A4	chr2	64988477	65023865	+	-1,10	0,000000 13885	0,000014 46070	0,47
DHTKD1	chr10	12068972	12123225	+	-1,10	0,000002 35898	0,000086 70725	0,47

NCAPG	chr4	17810902	17844862	+	-1,11	0,000001 91949	0,000074 74041	0,46
FXYD3	chr19	35115879	35124324	+	-1,11	0,000000 46882	0,000031 61803	0,46
KCNJ4	chr22	38426327	38455199	-	-1,11	0,000001 78880	0,000072 82899	0,46
RAB26	chr16	2140803	2154165	+	-1,11	0,000000 46345	0,000031 51012	0,46
ATP2B4	chr1	203626561	203744081	+	-1,12	0,000000 30984	0,000025 09668	0,46
TMEM97	chr17	28319095	28328685	+	-1,12	0,000000 19408	0,000017 44364	0,46
KIAA0101	chr15	64364311	64387687	-	-1,13	0,000000 22365	0,000019 69592	0,46
CTDSP2	chr12	57819927	57846739	-	-1,13	0,000138 83434	0,001378 05156	0,46
FBN2	chr5	128257909	128659185	-	-1,14	0,000002 43718	0,000088 62467	0,46
SOX2	chr3	181711924	181714436	+	-1,14	0,000002 50051	0,000089 40518	0,46
NR2E3	chr15	71792638	71818259	+	-1,14	0,000000 72396	0,000042 05126	0,45
PBXIP1	chr1	154944076	154956123	-	-1,14	0,000000 13589	0,000014 26530	0,45
TRIB3	chr20	362835	397559	+	-1,15	0,000000 04523	0,000006 38677	0,45
SEMA5A	chr5	9035026	9546075	-	-1,15	0,000000 05500	0,000007 21770	0,45
MARCO	chr2	118942166	118994660	+	-1,16	0,000000 20638	0,000018 42241	0,45
NEURL1B	chr5	172641266	172691540	+	-1,16	0,000000 42927	0,000029 96185	0,45
SLC2A3	chr12	7919230	7936275	-	-1,17	0,000002 57785	0,000090 45045	0,45

LMNA	chr1	156082573	156140089	+	-1,17	0,00000416269	0,00012138404	0,44
NMU	chr4	55595229	55636698	-	-1,18	0,00000267615	0,00009121138	0,44
SNAI2	chr8	48917690	48921740	-	-1,18	0,00005011199	0,00068623214	0,44
SEPT9	chr17	77280569	77500596	+	-1,19	0,00000047320	0,00003167999	0,44
DNASE2	chr19	12875211	12881468	-	-1,19	0,00000026075	0,00002193347	0,44
MRLN	chr10	59736692	59756041	-	-1,20	0,00009555807	0,00106522525	0,44
ADM2	chr22	50481556	50486440	+	-1,20	0,00000041939	0,00002979226	0,44
CTDSP1	chr2	218398256	218405941	+	-1,20	0,00000135031	0,00005986075	0,44
CACNG6	chr19	53992288	54012669	+	-1,20	0,00000144369	0,00006351949	0,43
PLP2	chrX	49171926	49175239	+	-1,20	0,00000041987	0,00002979226	0,43
GCH1	chr14	54842008	54902852	-	-1,21	0,00000024886	0,00002120471	0,43
SLC28A3	chr9	84275457	84340683	-	-1,21	0,00000036773	0,00002839859	0,43
RAB13	chr1	153981617	153986358	-	-1,21	0,00000027713	0,00002301619	0,43
CAV1	chr7	116524785	116561184	+	-1,21	0,00000158140	0,00006693900	0,43
LGALS1	chr22	37675608	37679806	+	-1,22	0,00000056878	0,00003623051	0,43
AXL	chr19	41219203	41261766	+	-1,23	0,00000134706	0,00005986075	0,43
DDB2	chr11	47214465	47239240	+	-1,23	0,00000017262	0,00001627634	0,43

CARS	chr11	3000922	3057613	-	-1,25	0,000000 13169	0,000013 93584	0,42
AHNAK	chr11	62433542	62556235	-	-1,25	0,000000 03856	0,000005 79095	0,42
GADD45G	chr9	89605013	89606555	+	-1,26	0,000005 58639	0,000149 31117	0,42
SERINC2	chr1	31409565	31434680	+	-1,26	0,000003 52828	0,000109 19376	0,42
SUSD2	chr22	24181259	24189110	+	-1,26	0,000000 48918	0,000032 58394	0,42
SLC1A5	chr19	46774883	46788594	-	-1,26	0,000000 12692	0,000013 53988	0,42
PARP14	chr3	122680618	122730840	+	-1,28	0,000000 03884	0,000005 79095	0,41
PRR11	chr17	59155499	59204705	+	-1,30	0,000002 87927	0,000096 78767	0,41
TP53INP1	chr8	94925972	94949411	-	-1,30	0,000000 09480	0,000010 72439	0,41
PSME1	chr14	24136158	24138967	+	-1,32	0,000000 04349	0,000006 38677	0,40
SPARC	chr5	151661096	151687165	-	-1,32	0,000000 26060	0,000021 93347	0,40
MAN2A1	chr5	109689366	109869625	+	-1,33	0,000000 03665	0,000005 59141	0,40
CDCA7L	chr7	21900900	21946084	-	-1,34	0,000000 14552	0,000014 97733	0,40
MFAP4	chr17	19383442	19387240	-	-1,35	0,000072 09354	0,000874 31735	0,39
HIST1H4C	chr6	26103876	26104310	+	-1,36	0,000046 36542	0,000645 86739	0,39
CTH	chr1	70411218	70439851	+	-1,36	0,000000 19193	0,000017 36874	0,39
CDON	chr11	125955796	126063335	-	-1,37	0,000000 00958	0,000002 61987	0,39

PKP1	chr1	201283452	201332993	+	-1,38	0,00000000821	0,00000245278	0,38
DAAM2	chr6	39792298	39904877	+	-1,38	0,00000006625	0,00000844014	0,38
SSTR2	chr17	73165012	73176633	+	-1,40	0,00000005784	0,00000744101	0,38
CAMK2B	chr7	44217150	44334577	-	-1,42	0,00000046146	0,00003151012	0,37
KCNK6	chr19	38319844	38332076	+	-1,43	0,00000008253	0,00000975598	0,37
TNNC2	chr20	45823214	45833745	-	-1,44	0,00000002548	0,00000445756	0,37
SLC44A2	chr19	10602457	10644559	+	-1,45	0,00000001902	0,00000370951	0,37
TSC22D3	chrX	107713221	107777342	-	-1,47	0,00000000855	0,00000245278	0,36
PSAT1	chr9	78297143	78330093	+	-1,49	0,00000000860	0,00000245278	0,36
DDIT4	chr10	72273920	72276036	+	-1,50	0,00000001724	0,00000359182	0,35
PHGDH	chr1	119659798	119744215	+	-1,51	0,00000003239	0,00000521594	0,35
GPT2	chr16	46884378	46931297	+	-1,52	0,00000001828	0,00000369128	0,35
INSIG1	chr7	155297776	155310235	+	-1,52	0,00000000796	0,00000245278	0,35
IQGAP1	chr15	90388218	90502243	+	-1,54	0,00000002022	0,00000379132	0,34
CDKN1A	chr6	36676460	36687339	+	-1,54	0,00000008250	0,00000975598	0,34
ERBB3	chr12	56079857	56103505	+	-1,54	0,00000008918	0,00001035643	0,34
FBLN1	chr22	45502238	45601135	+	-1,57	0,00000007493	0,00000923372	0,34

MXRA5	chrX	3308565	3346641	-	-1,57	0,000000 01499	0,000003 27933	0,34
C2orf71	chr2	29060976	29074261	-	-1,57	0,000000 01862	0,000003 70172	0,34
B4GALT1	chr9	33104082	33167356	-	-1,59	0,000000 00293	0,000001 74515	0,33
LMO2	chr11	33858576	33892289	-	-1,60	0,000000 62801	0,000038 50810	0,33
APOBEC2	chr6	41053304	41064511	+	-1,65	0,000000 04632	0,000006 46584	0,32
PTRF	chr17	42402452	42423517	-	-1,65	0,000000 09323	0,000010 63782	0,32
RP11-766F14.2	chr4	99636529	99654648	-	-1,68	0,000000 00695	0,000002 27904	0,31
SMOC1	chr14	69854131	70032366	+	-1,68	0,000000 00626	0,000002 21304	0,31
NES	chr1	156668763	156677397	-	-1,71	0,000000 09716	0,000010 89697	0,31
H1F0	chr22	37805093	37807436	+	-1,73	0,000000 92404	0,000047 92613	0,30
HSPB1	chr7	76302544	76304295	+	-1,75	0,000000 01631	0,000003 50885	0,30
SMYD1	chr2	88067780	88113387	+	-1,76	0,000000 00379	0,000001 90500	0,30
ACOT11	chr1	54542257	54639192	+	-1,78	0,000000 02174	0,000004 01873	0,29
ASNS	chr7	97852118	97872542	-	-1,81	0,000000 00538	0,000002 04595	0,29
MYOD1	chr11	17719568	17722131	+	-1,86	0,000000 00530	0,000002 04595	0,28
PCK2	chr14	24094053	24110598	+	-1,87	0,000000 00121	0,000001 12808	0,27
SLC7A11	chr4	138164097	138242349	-	-1,90	0,000000 00112	0,000001 12808	0,27

LITAF	chr16	11547722	11636381	-	-1,97	0,000000 01145	0,000002 78345	0,26
VIM	chr10	17228259	17237593	+	-2,01	0,000000 07644	0,000009 28706	0,25
TUBB2B	chr6	3224261	3231730	-	-2,06	0,000000 00129	0,000001 12808	0,24
ARHGAP9	chr12	57472255	57488814	-	-2,07	0,000000 00027	0,000000 67963	0,24
GDF15	chr19	18374731	18389176	+	-2,09	0,000000 00404	0,000001 90500	0,23
INHBE	chr12	57452323	57459280	+	-2,09	0,000000 00049	0,000000 81155	0,23
CHAC1	chr15	40952962	40956519	+	-2,38	0,000000 00632	0,000002 21304	0,19
KIF19	chr17	74326210	74355820	+	-2,51	0,000000 00319	0,000001 74649	0,18
NUPR1	chr16	28532708	28539174	-	-2,53	0,000000 00759	0,000002 42952	0,17
MGP	chr12	14881181	14885926	-	-2,92	0,000000 00008	0,000000 36881	0,13

Gene Name	chr	chr_start	chr_stop	strand	logFC	P.Value	adj.P.Val	FC
ZBTB17 (MIZ1)	chr1	15941869	15976132	-	-0,27	0,033	0,079	0,83

6.6 Western blot analysis of HD-MB03 crMIZ1 clones

Following preliminary MIZ1 and MYC protein quantifications in crMIZ1 clones by WB analysis, we had difficulties in culturing crMIZ1 n.20 cells, presented here in the original WB. Therefore, we decided to disregard this clone from further functional analysis. Raw WB images (below) have been cropped where dotted lines are placed to make Figure 54.

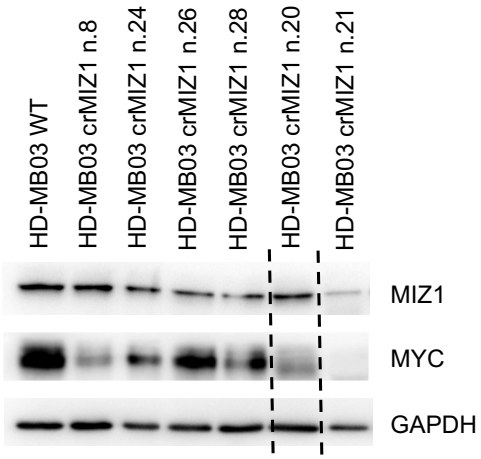

Research experience, Publications and Conferences

During the first year, I had the opportunity to join for six months an internationally recognised team of experts in microRNA biology (Carlo Croce's team) at the Ohio State University (USA). This experience allowed me to perform the microRNA profiling and validation presented in this thesis, set a new experimental technique, namely the High-throughput sequencing of RNA isolated by crosslinking immunoprecipitation (HITS-CLIP, data not shown), and to acquire skills to work with animals in research (i.e. animal handling, subcutaneous injection of tumour cells, animal autopsy etc.).

In my last year, I joined for seven months Michela Garofalo's lab (Transcriptional Networks in Lung Cancer) at the Cancer Research Institute (CRUK), Manchester, UK. During this time, I conducted few experiments presented in this work, such as the silencing of CDKs and assessment of the effects on apoptosis/proliferation. Furthermore, I collaborated with the team to complete the revisions for the recently submitted paper "Vulnerability of drug-resistant EML4-ALK rearranged lung cancer to transcriptional inhibition".

Publications:

- **Marta Buzzetti**, Sonia Morlando, Dimitris Solomos, Ammara Mehmood, Caroline Topham and Gianpiero Di Leva (2020): Pre-clinical efficacy of the CDK inhibitor dinaciclib in medulloblastoma, *Biochemistry and cell biology.* (Under submission)

- **Marta Buzzetti**, Elisabet Fernandez Potente, Aishwarya Damodaran Nambiar, Caroline Topham and Gianpiero Di Leva (2020): Targeting MIZ1 via miR-124 as a new therapeutic tool for medulloblastoma, *Non-coding RNA.* (Under submission)

- Athanasios R. Paliouras[‡], **Marta Buzzetti**[‡], Lei Shi[‡], Ian J. Donaldson, Peter Magee, Sudhakar Sahoo, Hui-Sun Leong, Matteo Fassan, Matthew Carter, Gianpiero Di Leva, Matthew Krebs, Fiona Blackhall, Christine M. Lovly and Michela Garofalo (2020): Vulnerability of drug-resistant EML4-ALK rearranged lung cancer to transcriptional inhibition, *EMBO Molecular Medicine*.

- Yuri D'Alessandra, Mattia Chiesa, Maria Cristina Carena, Antonio P. Beltrami, Paola Rizzo, **Marta Buzzetti**, Veronica Ricci, Roberto Ferrari, Alessandro Fucili, Ugolino Livi, Aneta Aleksova, Giulio Pompilio, Gualtiero I. Colombo (2020): Differential role of

circulating microRNA to track progression and ore-symptomatic stage of chronic heart failure, *European Journal of Heart Failure*. (Under review)

- Sonia Gioffré, Veronica Ricci, Chiara Vavassori, Clarissa Ruggeri, Mattia Chiesa, Ivana Alfieri, Silvia Zorzan, **Marta Buzzetti**, Giuseppina Milano, Alessandro Scopece, Laura Castiglioni, Luigi Sironi, Giulio Pompilio, Gualtiero I. Colombo, Yuri D'Alessandra (2019): Plasmatic and chamber-specific modulation of cardiac microRNAs in an acute model of DOX-induced cardiotoxicity, *Biomedicine & Pharmacotherapy*.

- Clarissa Ruggeri, Sonia Gioffré, Mattia Chiesa, **Marta Buzzetti**, Giuseppina Milano, Alessandro Scopece, Laura Castiglioni, Marta Pontremoli, Luigi Sironi, Giulio Pompilio, Gualtiero I. Colombo, Yuri D'Alessandra (2018): A Specific Circulating MicroRNA Cluster Is Associated to Late Differential Cardiac Response to Doxorubicin-Induced Cardiotoxicity In Vivo, *Hindawi*.

- Douglas G. Cheung, **Marta Buzzetti** & Gianpiero Di Leva (2017): miRNAs in bone metastasis, *Expert Review of Endocrinology & Metabolism*.

Conferences:

- ESMO/EACR Symposium on Signalling Pathways in Cancer 2018: Cyclin-dependent kinases (CDKs); Vall d'Hebron Institute of Oncology, Barcelona, Spain. EACR Travel Bursary Prize winner.

- Childhood Cancer 2017: Precision Treatment for Childhood and Young Person Cancer - Hype or Hope?; Newcastle, UK. Poster presentation.

- Manchester RNA Salon by RNA Society for the academic year 2018/2019.

- RNA Salon activities by RNA Society for the academic year 2017/2018. Sponsorship winner to host "Manchester RNA Salon" (three meetings) to foster engaging relations among local/regional RNA researchers with diverse scientific backgrounds, experiences and/or interests.

Bibliography

Aklilu, M., Kindler, H. L., Donehower, R. C., Mani, S., & Vokes, E. E. (2003). Phase II study of flavopiridol in patients with advanced colorectal cancer. *Annals of Oncology*. https://doi.org/10.1093/annonc/mdg343

Al-Hajj, M., & Clarke, M. F. (2004). Self-renewal and solid tumor stem cells. In *Oncogene*. https://doi.org/10.1038/sj.onc.1207947

Allan, L. A., & Clarke, P. R. (2007). Phosphorylation of Caspase-9 by CDK1/Cyclin B1 Protects Mitotic Cells against Apoptosis. *Molecular Cell*. https://doi.org/10.1016/j.molcel.2007.03.019

Alsayegh, K., Matsuura, K., Sekine, H., & Shimizu, T. (2017). Dinaciclib potently suppresses MCL-1 and selectively induces the cell death in human iPS cells without affecting the viability of cardiac tissue. *Scientific Reports*. https://doi.org/10.1038/srep45577

Amati, B., Alevizopoulos, K., & Vlach, J. (1998). Myc and the cell cycle. In *Frontiers in bioscience : a journal and virtual library*. https://doi.org/10.2741/A239

Ambros, V., Bartel, B., Bartel, D. P., Burge, C. B., Carrington, J. C., Chen, X., Dreyfuss, G., Eddy, S. R., Griffiths-Jones, S., Marshall, M., Matzke, M., Ruvkun, G., & Tuschl, T. (2003). A uniform system for microRNA annotation. *RNA (New York, N.Y.)*, *9*(3), 277–279. https://doi.org/10.1261/rna.2183803

Archer, T. C., Mahoney, E. L., & Pomeroy, S. L. (2017). Medulloblastoma: Molecular Classification-Based Personal Therapeutics. In *Neurotherapeutics*. https://doi.org/10.1007/s13311-017-0526-y

Arif, A. (2012). Extraneuronal activities and regulatory mechanisms of the atypical cyclin-dependent kinase Cdk5. *Biochemical Pharmacology*, *84*(8), 985–993. https://doi.org/10.1016/J.BCP.2012.06.027

Bailey, P., & Cushing, H. (1925). *Medulloblastoma Cerebelli: A Common Type of Midcerebellar Glioma of Childhood*. American Medical Association.

Bandopadhayay, P., Bergthold, G., Nguyen, B., Schubert, S., Gholamin, S., Tang, Y., Bolin, S., Schumacher, S. E., Zeid, R., Masoud, S., Yu, F., Vue, N., Gibson, W. J., Paolella, B. R., Mitra, S., Cheshier, S., Qi, J., Liu, K.-W., Wechsler-Reya, R., … Cho, Y.-J. (2014). BET-bromodomain inhibition of MYC-amplified medulloblastoma. *Clinical Cancer Research : An Official Journal of the American Association for Cancer Research*, *20*(4), 912–925. https://doi.org/10.1158/1078-0432.CCR-13-2281

Bansal, L. R., Belair, J., Cummings, D., & Zuccoli, G. (2015). Late-Onset Radiation-Induced Vasculopathy and Stroke in a Child With Medulloblastoma. *Journal of Child Neurology*. https://doi.org/10.1177/0883073814538501

Baroukh, N. N., & Van Obberghen, E. (2009). Function of microRNA-375 and microRNA-124a in pancreas and brain. In *FEBS Journal*. https://doi.org/10.1111/j.1742-4658.2009.07353.x

Bartel, D. P. (2009). MicroRNAs: Target Recognition and Regulatory Functions. In *Cell* (Vol. 136, Issue 2, pp. 215–233). https://doi.org/10.1016/j.cell.2009.01.002

Bernstein, E., Caudy, a a, Hammond, S. M., & Hannon, G. J. (2001). Role for a bidentate ribonuclease in the initiation step of RNA interference. *Nature*, *409*(6818), 363–366.

https://doi.org/10.1038/35053110

Boissonneault, V., Plante, I., Rivest, S., & Provost, P. (2008). MicroRNA-298 and microRNA-328 regulate expression of mouse beta -amyloid precursor protein converting enzyme 1. *The Journal of Biological Chemistry*. https://doi.org/10.1074/jbc.M807530200

Bolin, S., Borgenvik, A., Persson, C. U., Sundström, A., Qi, J., Bradner, J. E., Weiss, W. A., Cho, Y. J., Weishaupt, H., & Swartling, F. J. (2018). Combined BET bromodomain and CDK2 inhibition in MYC-driven medulloblastoma. *Oncogene*. https://doi.org/10.1038/s41388-018-0135-1

Booher, R. N., Hatch, H., Dolinski, B. M., Nguyen, T., Harmonay, L., Al-Assaad, A.-S., Ayers, M., Nebozhyn, M., Loboda, A., Hirsch, H. A., Zhang, T., Shi, B., Merkel, C. E., Angagaw, M. H., Wang, Y., Long, B. J., Lennon, X. Q., Miselis, N., Pucci, V., … Strack, P. (2014). MCL1 and BCL-xL Levels in Solid Tumors Are Predictive of Dinaciclib-Induced Apoptosis. *PLoS ONE*, *9*(10), e108371. https://doi.org/10.1371/journal.pone.0108371

Bornstein, G., Bloom, J., Sitry-Shevah, D., Nakayama, K., Pagano, M., & Hershko, A. (2003). Role of the SCFSkp2 Ubiquitin Ligase in the Degradation of p21Cip1 in S Phase. *Journal of Biological Chemistry*, *278*(28), 25752–25757. https://doi.org/10.1074/jbc.M301774200

Bozic, I., Reiter, J. G., Allen, B., Antal, T., Chatterjee, K., Shah, P., Moon, Y. S., Yaqubie, A., Kelly, N., Le, D. T., Lipson, E. J., Chapman, P. B., Diaz, L. A., Vogelstein, B., & Nowak, M. A. (2013). Evolutionary dynamics of cancer in response to targeted combination therapy. *ELife*. https://doi.org/10.7554/eLife.00747

Bretones, G., Delgado, M. D., & León, J. (2015). Myc and cell cycle control. In *Biochimica et Biophysica Acta - Gene Regulatory Mechanisms*. https://doi.org/10.1016/j.bbagrm.2014.03.013

Buonamici, S., Williams, J., Morrissey, M., Wang, A., Guo, R., Vattay, A., Hsiao, K., Yuan, J., Green, J., Ospina, B., Yu, Q., Ostrom, L., Fordjour, P., Anderson, D. L., Monahan, J. E., Kelleher, J. F., Peukert, S., Pan, S., Wu, X., … Dorsch, M. (2010). Interfering with Resistance to Smoothened Antagonists by Inhibition of the PI3K Pathway in Medulloblastoma. *Science Translational Medicine*, *2*(51), 51ra70-51ra70. https://doi.org/10.1126/scitranslmed.3001599

Burdette-Radoux, S., Tozer, R. G., Lohmann, R. C., Quirt, I., Ernst, D. S., Walsh, W., Wainman, N., Colevas, A. D., & Eisenhauer, E. A. (2004). Phase II trial of flavopiridol, a cyclin dependent kinase inhibitor, in untreated metastatic malignant melanoma. *Investigational New Drugs*. https://doi.org/10.1023/B:DRUG.0000026258.02846.1c

Bushati, N., & Cohen, S. M. (2007). microRNA functions. *Annu Rev Cell Dev Biol*, *23*, 175–205. https://doi.org/10.1146/annurev.cellbio.23.090506.123406

Campaner, S., Doni, M., Hydbring, P., Verrecchia, A., Bianchi, L., Sardella, D., Schleker, T., Perna, D., Tronnersjö, S., Murga, M., Fernandez-Capetillo, O., Barbacid, M., Larsson, L. G., & Amati, B. (2010). Cdk2 suppresses cellular senescence induced by the c-myc oncogene. *Nature Cell Biology*. https://doi.org/10.1038/ncb2004

Campisi, J., & D'Adda Di Fagagna, F. (2007). Cellular senescence: When bad things happen to good cells. In *Nature Reviews Molecular Cell Biology*. https://doi.org/10.1038/nrm2233

Carey, J. P. W., Karakas, C., Bui, T., Chen, X., Vijayaraghavan, S., Zhao, Y., Wang, J., Mikule, K.,

Litton, J. K., Hunt, K. K., & Keyomarsi, K. (2018). Synthetic lethality of PARP inhibitors in combination with MYC blockade is independent of BRCA status in triple-negative breast cancer. *Cancer Research*. https://doi.org/10.1158/0008-5472.CAN-17-1494

Cavalli, F. M. G., Remke, M., Rampasek, L., Peacock, J., Shih, D. J. H., Luu, B., Garzia, L., Torchia, J., Nor, C., Morrissy, A. S., Agnihotri, S., Thompson, Y. Y., Kuzan-Fischer, C. M., Farooq, H., Isaev, K., Daniels, C., Cho, B.-K., Kim, S.-K., Wang, K.-C., … Taylor, M. D. (2017). Intertumoral Heterogeneity within Medulloblastoma Subgroups. *Cancer Cell*, *31*(6), 737-754.e6. https://doi.org/10.1016/j.ccell.2017.05.005

Chang, T.-C., Yu, D., Lee, Y.-S., Wentzel, E. A., Arking, D. E., West, K. M., Dang, C. V, Thomas-Tikhonenko, A., & Mendell, J. T. (2008). Widespread microRNA repression by Myc contributes to tumorigenesis. *Nature Genetics*, *40*(1), 43–50. https://doi.org/10.1038/ng.2007.30

Chen, C.-Z., Li, L., Lodish, H. F., & Bartel, D. P. (2004). MicroRNAs modulate hematopoietic lineage differentiation. *Science (New York, N.Y.)*, *303*(5654), 83–86. https://doi.org/10.1126/science.1091903

Chen, X. X., Xie, F. F., Zhu, X. J., Lin, F., Pan, S. S., Gong, L. H., Qiu, J. G., Zhang, W. J., Jiang, Q. W., Mei, X. L., Xue, Y. Q., Qin, W. M., Shi, Z., & Yan, X. J. (2015). Cyclin-dependent kinase inhibitor dinaciclib potently synergizes with cisplatin in preclinical models of ovarian cancer. *Oncotarget*. https://doi.org/10.18632/oncotarget.3717

Cheung, Zelda H Ip, N. Y. (2012). Cdk5: a multifaceted kinase in neurodegenerative diseases. *Trends in Cell Biology*, *22*(3), 169–175. https://doi.org/10.1016/j.tcb.2011.11.003

Chiang, H. R., Schoenfeld, L. W., Ruby, J. G., Auyeung, V. C., Spies, N., Baek, D., Johnston, W. K., Russ, C., Luo, S., Babiarz, J. E., Blelloch, R., Schroth, G. P., Nusbaum, C., & Bartel, D. P. (2010). Mammalian microRNAs: Experimental evaluation of novel and previously annotated genes. *Genes and Development*, *24*(10), 992–1009. https://doi.org/10.1101/gad.1884710

Chiesa, M., Colombo, G. I., & Piacentini, L. (2017). DaMiRseq—an R/Bioconductor package for data mining of RNA-Seq data: normalization, feature selection and classification. *Bioinformatics*, *34*(8), 1416–1418. https://doi.org/10.1093/bioinformatics/btx795

Cimmino, A., Calin, G. A., Fabbri, M., Iorio, M. V., Ferracin, M., Shimizu, M., Wojcik, S. E., Aqeilan, R. I., Zupo, S., Dono, M., Rassenti, L., Alder, H., Volinia, S., Liu, C. G., Kipps, T. J., Negrini, M., & Croce, C. M. (2005). miR-15 and miR-16 induce apoptosis by targeting BCL2. *Proceedings of the National Academy of Sciences of the United States of America*. https://doi.org/10.1073/pnas.0506654102

Clifford, S. C., Lusher, M. E., Lindsey, J. C., Langdon, J. A., Gilbertson, R. J., Straughton, D., & Ellison, D. W. (2006). Wnt/Wingless Pathway Activation and Chromosome 6 Loss Characterise a Distinct Molecular Sub-Group of Medulloblastomas Associated with a Favourable Prognosis. *Cell Cycle*, *5*(22), 2666–2670. https://doi.org/10.4161/cc.5.22.3446

Conacci-Sorrell, M., McFerrin, L., & Eisenman, R. N. (2014). An overview of MYC and its interactome. *Cold Spring Harbor Perspectives in Medicine*. https://doi.org/10.1101/cshperspect.a014357

Conaco, C., Otto, S., Han, J. J., & Mandel, G. (2006). Reciprocal actions of REST and a

microRNA promote neuronal identity. *Proceedings of the National Academy of Sciences of the United States of America*. https://doi.org/10.1073/pnas.0511041103

Coni, S., Mancuso, A. B., Di Magno, L., Sdruscia, G., Manni, S., Serrao, S. M., Rotili, D., Spiombi, E., Bufalieri, F., Petroni, M., Kusio-Kobialka, M., De Smaele, E., Ferretti, E., Capalbo, C., Mai, A., Niewiadomski, P., Screpanti, I., Di Marcotullio, L., & Canettieri, G. (2017). Selective targeting of HDAC1/2 elicits anticancer effects through Gli1 acetylation in preclinical models of SHH Medulloblastoma. *Scientific Reports*. https://doi.org/10.1038/srep44079

Cook Sangar, M. L., Genovesi, L. A., Nakamoto, M. W., Davis, M. J., Knobluagh, S. E., Ji, P., Millar, A., Wainwright, B. J., & Olson, J. M. (2017). Inhibition of CDK4/6 by Palbociclib Significantly Extends Survival in Medulloblastoma Patient-Derived Xenograft Mouse Models. *Clinical Cancer Research*, *23*(19), 5802 LP – 5813.

Crawford, J. R., MacDonald, T. J., & Packer, R. J. (2007). Medulloblastoma in childhood: new biological advances. *Lancet Neurology*, *6*(12), 1073–1085. https://doi.org/10.1016/S1474-4422(07)70289-2

Czabotar, P. E., Lessene, G., Strasser, A., & Adams, J. M. (2014). Control of apoptosis by the BCL-2 protein family: Implications for physiology and therapy. In *Nature Reviews Molecular Cell Biology*. https://doi.org/10.1038/nrm3722

Dang, C. V. (2012). MYC on the Path to Cancer. *Cell*, *149*(1), 22–35. https://doi.org/10.1016/j.cell.2012.03.003

Davis, A. C., Wims, M., Spotts, G. D., Hann, S. R., & Bradley, A. (1993). A null c-myc mutation causes lethality before 10.5 days of gestation in homozygotes and reduced fertility in heterozygous female mice. *Genes and Development*, *7*(4), 671–682. https://doi.org/10.1101/gad.7.4.671

Delmore, J. E., Issa, G. C., Lemieux, M. E., Rahl, P. B., Shi, J., Jacobs, H. M., Kastritis, E., Gilpatrick, T., Paranal, R. M., Qi, J., Chesi, M., Schinzel, A., McKeown, M. R., Heffernan, T. P., Vakoc, C. R., Bergsagel, P. L., Ghobrial, I. M., Richardson, P. G., Young, R. A., … Mitsiades, C. S. (2011). BET bromodomain inhibition as a therapeutic strategy to target c-Myc. *Cell*, *146*(6), 904–917. https://doi.org/10.1016/j.cell.2011.08.017

Denli, A. M., Tops, B. B. J., Plasterk, R. H. a, Ketting, R. F., & Hannon, G. J. (2004). Processing of primary microRNAs by the Microprocessor complex. *Nature*, *432*(7014), 231–235. https://doi.org/10.1038/nature03049

Dhall, G. (2009). Medulloblastoma. *Journal of Child Neurology*, *24*(11), 1418–1430. https://doi.org/10.1177/0883073809341668

Di Leva, G., Garofalo, M., & Croce, C. M. (2014). microRNAs in cancer. *Annual Review of Pathology*, *9*, 287–314. https://doi.org/10.1146/annurev-pathol-012513-104715

Diaz-Padilla, I., Siu, L. L., & Duran, I. (2009). Cyclin-dependent kinase inhibitors as potential targeted anticancer agents. In *Investigational New Drugs*. https://doi.org/10.1007/s10637-009-9236-6

Dimova, D. K., & Dyson, N. J. (2005). The E2F transcriptional network: old acquaintances with new faces. *Oncogene*, *24*, 2810.

Doench, J. G., & Sharp, P. A. (2004). Specificity of microRNA target selection in translational repression. *Genes & Development*, *18*(5), 504–511.

https://doi.org/10.1101/gad.1184404

Donley, N., & Thayer, M. J. (2013). DNA replication timing, genome stability and cancer. Late and/or delayed DNA replication timing is associated with increased genomic instability. In *Seminars in Cancer Biology*.

Donnenberg, V. S., & Donnenberg, A. D. (2005). Multiple drug resistance in cancer revisited: The cancer stem cell hypothesis. In *Journal of Clinical Pharmacology*. https://doi.org/10.1177/0091270005276905

Dorand, R. D., Nthale, J., Myers, J. T., Barkauskas, D. S., Avril, S., Chirieleison, S. M., Pareek, T. K., Abbott, D. W., Stearns, D. S., Letterio, J. J., Huang, A. Y., & Petrosiute, A. (2016). Cdk5 disruption attenuates tumor PD-L1 expression and promotes antitumor immunity. *Science*. https://doi.org/10.1126/science.aae0477

Duffner, P. K. (2004). Long-term effects of radiation therapy on cognitive and endocrine function in children with leukemia and brain tumors. *Neurologist*, *10*. https://doi.org/10.1097/01.nrl.0000144287.35993.96

Eberhart, C. G., Kepner, J. L., Goldthwaite, P. T., Kun, L. E., Duffner, P. K., Friedman, H. S., Strother, D. R., & Burger, P. C. (2002). Histopathologic grading of medulloblastomas. *Cancer*, *94*(2), 552–560. https://doi.org/10.1002/cncr.10189

Eilers, M., & Eisenman, R. N. (2008). Myc ' s broad reach. *Genes & Development*, 2755–2766. https://doi.org/10.1101/gad.1712408.Freely

Eischen, C. M., Packham, G., Nip, J., Fee, B. E., Hiebert, S. W., Zambetti, G. P., & Cleveland, J. L. (2001). Bcl-2 is an apoptotic target suppressed by both c-Myc and E2F-1. *Oncogene*. https://doi.org/10.1038/sj.onc.1204892

El-Deiry, W. S., Tokino, T., Velculescu, V. E., Levy, D. B., Parsons, R., Trent, J. M., Lin, D., Mercer, W. E., Kinzler, K. W., & Vogelstein, B. (1993). WAF1, a potential mediator of p53 tumor suppression. *Cell*, *75*(4), 817–825. https://doi.org/10.1016/0092-8674(93)90500-P

Ellison, D. (2002). Classifying the medulloblastoma: Insights from morphology and molecular genetics. In *Neuropathology and Applied Neurobiology*. https://doi.org/10.1046/j.1365-2990.2002.00419.x

Ellison, D. W. (2010). Childhood medulloblastoma: Novel approaches to the classification of a heterogeneous disease. *Acta Neuropathologica*, *120*(3), 305–316.

Ellison, D. W., Dalton, J., Kocak, M., Nicholson, S. L., Fraga, C., Neale, G., Kenney, A. M., Brat, D. J., Perry, A., Yong, W. H., Taylor, R. E., Bailey, S., Clifford, S. C., & Gilbertson, R. J. (2011). Medulloblastoma: clinicopathological correlates of SHH, WNT, and non-SHH/WNT molecular subgroups. *Acta Neuropathologica*, *121*(3), 381–396. https://doi.org/10.1007/s00401-011-0800-8

Esau, C., Davis, S., Murray, S. F., Yu, X. X., Pandey, S. K., Pear, M., Watts, L., Booten, S. L., Graham, M., McKay, R., Subramaniam, A., Propp, S., Lollo, B. A., Freier, S., Bennett, C. F., Bhanot, S., & Monia, B. P. (2006). miR-122 regulation of lipid metabolism revealed by in vivo antisense targeting. *Cell Metabolism*, *3*(2), 87–98. https://doi.org/10.1016/j.cmet.2006.01.005

Faria, C. C., Agnihotri, S., Mack, S. C., Golbourn, B. J., Diaz, R. J., Olsen, S., Bryant, M., Bebenek, M., Wang, X., Bertrand, K. C., Kushida, M., Head, R., Clark, I., Dirks, P., Smith,

C. A., Taylor, M. D., & Rutka, J. T. (2015). Identification of alsterpaullone as a novel small molecule inhibitor to target group 3 medulloblastoma. *Oncotarget*, *6*(25), 21718–21729. http://www.ncbi.nlm.nih.gov/pmc/articles/PMC4673298/

Ferretti, E., De Smaele, E., Po, A., Di Marcotullio, L., Tosi, E., Espinola, M. S. B., Di Rocco, C., Riccardi, R., Giangaspero, F., Farcomeni, A., Nofroni, I., Laneve, P., Gioia, U., Caffarelli, E., Bozzoni, I., Screpanti, I., & Gulino, A. (2009). MicroRNA profiling in human medulloblastoma. *International Journal of Cancer*, *124*(3), 568–577. https://doi.org/10.1002/ijc.23948

Filipowicz, W., Bhattacharyya, S. N., & Sonenberg, N. (2008). Mechanisms of post-transcriptional regulation by microRNAs: are the answers in sight? *Nature Reviews. Genetics*, *9*(2), 102–114. https://doi.org/10.1038/nrg2290

Finn, R. S., Crown, J. P., Ettl, J., Schmidt, M., Bondarenko, I. M., Lang, I., Pinter, T., Boer, K., Patel, R., Randolph, S., Kim, S. T., Huang, X., Schnell, P., Nadanaciva, S., Bartlett, C. H., & Slamon, D. J. (2016). Efficacy and safety of palbociclib in combination with letrozole as first-line treatment of ER-positive, HER2-negative, advanced breast cancer: Expanded analyses of subgroups from the randomized pivotal trial PALOMA-1/TRIO-18. *Breast Cancer Research*. https://doi.org/10.1186/s13058-016-0721-5

Fischer, P. M. (2001). Recent advances and new directions in the discovery and development of cyclin-dependent kinase inhibitors. In *Current Opinion in Drug Discovery and Development*.

Flynn, J., Jones, J., Johnson, A. J., Andritsos, L., Maddocks, K., Jaglowski, S., Hessler, J., Grever, M. R., Im, E., Zhou, H., Zhu, Y., Zhang, D., Small, K., Bannerji, R., & Byrd, J. C. (2015). Dinaciclib is a novel cyclin-dependent kinase inhibitor with significant clinical activity in relapsed and refractory chronic lymphocytic leukemia. *Leukemia*. https://doi.org/10.1038/leu.2015.31

Fouad, Y. A., & Aanei, C. (2017). Revisiting the hallmarks of cancer. In *American Journal of Cancer Research*.

Fouladi, M., Chintagumpala, M., Ashley, D., Kellie, S., Gururangan, S., Hassall, T., Gronewold, L., Stewart, C. F., Wallace, D., Broniscer, A., Hale, G. A., Kasow, K. A., Merchant, T. E., Morris, B., Krasin, M., Kun, L. E., Boyett, J. M., & Gajjar, A. (2008). Amifostine Protects Against Cisplatin-Induced Ototoxicity in Children with Average-Risk Medulloblastoma. *Journal of Clinical Oncology : Official Journal of the American Society of Clinical Oncology*, *26*(22), 3749–3755. https://doi.org/10.1200/JCO.2007.14.3974

Frenzel, A., Loven, J., & Henriksson, M. A. (2010). Targeting MYC-Regulated miRNAs to Combat Cancer. *Genes & Cancer*. https://doi.org/10.1177/1947601910377488

Fu, W., Le, M., Chu, B., Wang, X., Bui, M. M., Gemmer, J., Altiok, S., & Pledger, W. J. (2011). The cyclin-dependent kinase inhibitor SCH 727965 (dinacliclib) induces the apoptosis of osteosarcoma cells. *Molecular Cancer Therapeutics*. https://doi.org/10.1158/1535-7163.MCT-11-0167

Gangaraju, V. K., & Lin, H. (2009). MicroRNAs: key regulators of stem cells. *Nature Reviews. Molecular Cell Biology*, *10*(2), 116–125. https://doi.org/10.1038/nrm2621

Garg, N., Vijayakumar, T., Bakhshinyan, D., Venugopal, C., & Singh, S. K. (2015). MicroRNA Regulation of Brain Tumour Initiating Cells in Central Nervous System Tumours. *Stem*

Cells Int, *2015*, 141793. https://doi.org/10.1155/2015/141793

Garriga, J., & Graña, X. (2004). Cellular control of gene expression by T-type cyclin/CDK9 complexes. In *Gene*. https://doi.org/10.1016/j.gene.2004.05.007

Geiss, G. K., Bumgarner, R. E., Birditt, B., Dahl, T., Dowidar, N., Dunaway, D. L., Fell, H. P., Ferree, S., George, R. D., Grogan, T., James, J. J., Maysuria, M., Mitton, J. D., Oliveri, P., Osborn, J. L., Peng, T., Ratcliffe, A. L., Webster, P. J., Davidson, E. H., & Hood, L. (2008). Direct multiplexed measurement of gene expression with color-coded probe pairs. *Nature Biotechnology*. https://doi.org/10.1038/nbt1385

Ghia, P., Scarfò, L., Perez, S., Pathiraja, K., Derosier, M., Small, K., McCrary Sisk, C., & Patton, N. (2017). Efficacy and safety of dinaciclib vs ofatumumab in patients with relapsed/refractory chronic lymphocytic leukemia. *Blood*, *129*(13), 1876–1878. https://doi.org/10.1182/blood-2016-10-748210

Giangaspero, F., Rigobello, L., Badiali, M., Loda, M., Andreini, L., Basso, G., Zorzi, F., & Montaldi, A. (1992). Large-cell medulloblastomas: A distinct variant with highly aggressive behavior. *American Journal of Surgical Pathology*. https://doi.org/10.1097/00000478-199207000-00007

Giantsoudi, D., Sethi, R. V., Yeap, B. Y., Eaton, B. R., Ebb, D. H., Caruso, P. A., Rapalino, O., Chen, Y. L. E., Adams, J. A., Yock, T. I., Tarbell, N. J., Paganetti, H., & MacDonald, S. M. (2016). Incidence of CNS Injury for a Cohort of 111 Patients Treated with Proton Therapy for Medulloblastoma: LET and RBE Associations for Areas of Injury. *International Journal of Radiation Oncology Biology Physics*. https://doi.org/10.1016/j.ijrobp.2015.09.015

Gibson, P., Tong, Y., Robinson, G., Thompson, M. C., Currle, D. S., Eden, C., Kranenburg, T. A., Hogg, T., Poppleton, H., Martin, J., Finkelstein, D., Pounds, S., Weiss, A., Patay, Z., Scoggins, M., Ogg, R., Pei, Y., Yang, Z.-J., Brun, S., … Gilbertson, R. J. (2010). Subtypes of medulloblastoma have distinct developmental origins. *Nature*, *468*(7327), 1095–1099. https://doi.org/10.1038/nature09587

Gilbertson, R. J., & Ellison, D. W. (2008). The Origins of Medulloblastoma Subtypes. *Annual Review of Pathology: Mechanisms of Disease*, *3*(1), 341–365. https://doi.org/10.1146/annurev.pathmechdis.3.121806.151518

Gillam, M. P., Nimbalkar, D., Sun, L., Christov, K., Ray, D., Kaldis, P., Liu, X., & Kiyokawa, H. (2015). MEN1 tumorigenesis in the pituitary and pancreatic islet requires CDK4 but not Cdk2. *Oncogene*. https://doi.org/10.1038/onc.2014.3

Gojo, I., Sadowska, M., Walker, A., Feldman, E. J., Iyer, S. P., Baer, M. R., Sausville, E. A., Lapidus, R. G., Zhang, D., Zhu, Y., Jou, Y. M., Poon, J., Small, K., & Bannerji, R. (2013). Clinical and laboratory studies of the novel cyclin-dependent kinase inhibitor dinaciclib (SCH 727965) in acute leukemias. *Cancer Chemotherapy and Pharmacology*. https://doi.org/10.1007/s00280-013-2249-z

Goodrich, L. V, Milenković, L., Higgins, K. M., & Scott, M. P. (1997). Altered Neural Cell Fates and Medulloblastoma in Mouse patched Mutants. *Science*, *277*(5329), 1109 LP – 1113. http://science.sciencemag.org/content/277/5329/1109.abstract

Gopalakrishnan, V., Tao, R. H., Dobson, T., Brugmann, W., & Khatua, S. (2015).

Medulloblastoma development: tumor biology informs treatment decisions. In *CNS oncology*. https://doi.org/10.2217/cns.14.58

Gregory, G. P., Hogg, S. J., Kats, L. M., Vidacs, E., Baker, A. J., Gilan, O., Lefebure, M., Martin, B. P., Dawson, M. A., Johnstone, R. W., & Shortt, J. (2015). CDK9 inhibition by dinaciclib potently suppresses Mcl-1 to induce durable apoptotic responses in aggressive MYC-driven B-cell lymphoma in vivo. In *Leukemia*. https://doi.org/10.1038/leu.2015.10

Gulino, A., Arcella, A., & Giangaspero, F. (2008). Pathological and molecular heterogeneity of medulloblastoma. *Current Opinion in Oncology*, *20*(6).

Gurney, J. G., Kadan-Lottick, N. S., Packer, R. J., Neglia, J. P., Sklar, C. A., Punyko, J. A., Stovall, M., Yasui, Y., Stacy Nicholson, H., Wolden, S., McNeil, D. E., Mertens, A. C., & Robison, L. L. (2003). Endocrine and cardiovascular late effects among adult survivors of childhood brain tumors: Childhood cancer survivor study. *Cancer*. https://doi.org/10.1002/cncr.11095

Hammond, S. M., Boettcher, S., Caudy, A. A., Kobayashi, R., & Hannon, G. J. (2001). Argonaute2, a link between genetic and biochemical analyses of RNAi. *Science (New York, N.Y.)*, *293*(5532), 1146–1150. https://doi.org/10.1126/science.1064023

Han, J., Lee, Y., Yeom, K. H., Nam, J. W., Heo, I., Rhee, J. K., Sohn, S. Y., Cho, Y., Zhang, B. T., & Kim, V. N. (2006). Molecular Basis for the Recognition of Primary microRNAs by the Drosha-DGCR8 Complex. *Cell*, *125*(5), 887–901. https://doi.org/10.1016/j.cell.2006.03.043

Hanaford, A. R., Archer, T. C., Price, A., Kahlert, U. D., Maciaczyk, J., Nikkhah, G., Kim, J. W., Ehrenberger, T., Clemons, P. A., Dančík, V., Seashore-Ludlow, B., Viswanathan, V., Stewart, M. L., Rees, M. G., Shamji, A., Schreiber, S., Fraenkel, E., Pomeroy, S. L., Mesirov, J. P., … Raabe, E. H. (2016). DiSCoVERing Innovative Therapies for Rare Tumors: Combining Genetically Accurate Disease Models with In Silico Analysis to Identify Novel Therapeutic Targets. *Clinical Cancer Research*.

Hanahan, D., & Weinberg, R. A. (2000). The hallmarks of cancer. In *Cell*. https://doi.org/10.1016/S0092-8674(00)81683-9

Hanahan, D., & Weinberg, R. A. (2011). Hallmarks of cancer: The next generation. In *Cell*. https://doi.org/10.1016/j.cell.2011.02.013

Harbour, J. W., Luo, R. X., Dei Santi, A., Postigo, A. A., & Dean, D. C. (1999). Cdk phosphorylation triggers sequential intramolecular interactions that progressively block Rb functions as cells move through G1. *Cell*, *98*(6), 859–869. https://doi.org/10.1016/S0092-8674(00)81519-6

Hashiguchi, T., Bruss, N., Best, S., Lam, V., Danilova, O., Paiva, C. J., Wolf, J., Gilbert, E. W., Okada, C. Y., Kaur, P., Drew, L., Cidado, J., Hurlin, P., & Danilov, A. V. (2019). Cyclin-dependent kinase-9 is a therapeutic target in MYC-expressing diffuse large B-cell lymphoma. *Molecular Cancer Therapeutics*. https://doi.org/10.1158/1535-7163.MCT-18-1023

Hershko, A. (1997). Roles of ubiquitin-mediated proteolysis in cell cycle control. *Current Opinion in Cell Biology*, *9*(6), 788–799. https://doi.org/10.1016/S0955-0674(97)80079-8

Hohjoh, H., & Fukushima, T. (2007). Marked change in microRNA expression during neuronal differentiation of human teratocarcinoma NTera2D1 and mouse embryonal carcinoma

P19 cells. *Biochemical and Biophysical Research Communications*. https://doi.org/10.1016/j.bbrc.2007.07.189

Hönnemann, J., Sanz-Moreno, A., Wolf, E., Eilers, M., & Elsässer, H. P. (2012). Miz1 is a critical repressor of cdkn1a during skin tumorigenesis. *PLoS ONE*. https://doi.org/10.1371/journal.pone.0034885

Horiuchi, D., Kusdra, L., Huskey, N. E., Chandriani, S., Lenburg, M. E., Gonzalez-Angulo, A. M., Creasman, K. J., Bazarov, A. V., Smyth, J. W., Davis, S. E., Yaswen, P., Mills, G. B., Esserman, L. J., & Goga, A. (2012). MYC pathway activation in triple-negative breast cancer is synthetic lethal with CDK inhibition. *Journal of Experimental Medicine*. https://doi.org/10.1084/jem.20111512

Hortobagyi, G. N., Stemmer, S. M., Burris, H. A., Yap, Y. S., Sonke, G. S., Paluch-Shimon, S., Campone, M., Blackwell, K. L., Andre, F., Winer, E. P., Janni, W., Verma, S., Conte, P., Arteaga, C. L., Cameron, D. A., Petrakova, K., Hart, L. L., Villanueva, C., Chan, A., … O'Shaughnessy, J. (2016). Ribociclib as first-line therapy for HR-positive, advanced breast cancer. *New England Journal of Medicine*. https://doi.org/10.1056/NEJMoa1609709

Huang, C. H., Lujambio, A., Zuber, J., Tschaharganeh, D. F., Doran, M. G., Evans, M. J., Kitzing, T., Zhu, N., de Stanchina, E., Sawyers, C. L., Armstrong, S. A., Lewis, J. S., Sherr, C. J., & Lowe, S. W. (2014). CDK9-mediated transcription elongation is required for MYC addiction in hepatocellular carcinoma. *Genes and Development*. https://doi.org/10.1101/gad.244368.114

Huang, G. H., Xu, Q. F., Cui, Y. H., Li, N., Bian, X. W., & Lv, S. Q. (2016). Medulloblastoma stem cells: Promising targets in medulloblastoma therapy. In *Cancer Science*. https://doi.org/10.1111/cas.12925

Hummel, T. R., Wagner, L., Ahern, C., Fouladi, M., Reid, J. M., Mcgovern, R. M., Ames, M. M., Gilbertson, R. J., Horton, T., Ingle, A. M., Weigel, B., & Blaney, S. M. (2013). A pediatric phase 1 trial of vorinostat and temozolomide in relapsed or refractory primary brain or spinal cord tumors: A children's oncology group phase 1 consortium study. *Pediatric Blood and Cancer*. https://doi.org/10.1002/pbc.24541

Hydbring, P., & Larsson, L. G. (2010). Tipping the balance: Cdk2 enables Myc to suppress senescence. In *Cancer Research*. https://doi.org/10.1158/0008-5472.CAN-10-1383

Ianes, C., Xu, P., Werz, N., Meng, Z., Henne-Bruns, D., Bischof, J., & Knippschild, U. (2016). CK1δ activity is modulated by CDK2/E-and CDK5/p35-mediated phosphorylation. *Amino Acids*. https://doi.org/10.1007/s00726-015-2114-y

Inoue-Yamauchi, A., Jeng, P. S., Kim, K., Chen, H. C., Han, S., Ganesan, Y. T., Ishizawa, K., Jebiwott, S., Dong, Y., Pietanza, M. C., Hellmann, M. D., Kris, M. G., Hsieh, J. J., & Cheng, E. H. (2017). Targeting the differential addiction to anti-apoptotic BCL-2 family for cancer therapy. *Nature Communications*. https://doi.org/10.1038/ncomms16078

Jane, E. P., Premkumar, D. R., Cavaleri, J. M., Sutera, P. A., Rajasekar, T., & Pollack, I. F. (2016). Dinaciclib, a cyclin-dependent kinase inhibitor promotes proteasomal degradation of Mcl-1 and enhances ABT-737-mediated cell death in malignant human glioma cell liness. *Journal of Pharmacology and Experimental Therapeutics*. https://doi.org/10.1124/jpet.115.230052

Jansen-Durr, P., Meichle, A., Steiner, P., Pagano, M., Finke, K., Botz, J., Wessbecher, J., Draetta, G., & Eilers, M. (1993). Differential modulation of cyclin gene expression by MYC. *Proceedings of the National Academy of Sciences of the United States of America*. https://doi.org/10.1073/pnas.90.8.3685

Jensen, M. M., Jørgensen, J. T., Binderup, T., & Kjær, A. (2008). Tumor volume in subcutaneous mouse xenografts measured by microCT is more accurate and reproducible than determined by 18F-FDG-microPET or external caliper. *BMC Medical Imaging*. https://doi.org/10.1186/1471-2342-8-16

Jones, D. T. W., Jager, N., Kool, M., Zichner, T., Hutter, B., Sultan, M., Cho, Y.-J., Pugh, T. J., Hovestadt, V., Stutz, A. M., Rausch, T., Warnatz, H.-J., Ryzhova, M., Bender, S., Sturm, D., Pleier, S., Cin, H., Pfaff, E., Sieber, L., … Lichter, P. (2012). Dissecting the genomic complexity underlying medulloblastoma. *Nature*, *488*(7409), 100–105. http://dx.doi.org/10.1038/nature11284

Jones, D. T. W., Jäger, N., Kool, M., Zichner, T., Hutter, B., Sultan, M., Cho, Y. J., Pugh, T. J., Hovestadt, V., Stütz, A. M., Rausch, T., Warnatz, H. J., Ryzhova, M., Bender, S., Sturm, D., Pleier, S., Cin, H., Pfaff, E., Sieber, L., … Lichter, P. (2012). Dissecting the genomic complexity underlying medulloblastoma. *Nature*. https://doi.org/10.1038/nature11284

Juraschka, K., & Taylor, M. D. (2019). Medulloblastoma in the age of molecular subgroups: a review. *Journal of Neurosurgery: Pediatrics*. https://doi.org/10.3171/2019.5.peds18381

Kawauchi, D., Robinson, G., Uziel, T., Gibson, P., Rehg, J., Gao, C., Finkelstein, D., Qu, C., Pounds, S., Ellison, D. W., Gilbertson, R. J., & Roussel, M. F. (2012). A mouse model of the most aggressive subgroup of human medulloblastoma. *Cancer Cell*, *21*(2), 168–180. https://doi.org/10.1016/j.ccr.2011.12.023

Kelleher, F. C., Fennelly, D., & Rafferty, M. (2006). Common critical pathways in embryogenesis and cancer. *Acta Oncologica*, *45*(4), 375–388. https://doi.org/10.1080/02841860600602946

Kessler, J. D., Hasegawa, H., Brun, S. N., Yang, Z.-J., Dutton, J. W., Wang, F., & Wechsler-Reya, R. J. (2009). N-myc alters the fate of preneoplastic cells in a mouse model of medulloblastoma. *Genes & Development*, *23*(2), 157–170. https://doi.org/10.1101/gad.1759909

Kloosterman, W. P., & Plasterk, R. H. A. (2006). The diverse functions of microRNAs in animal development and disease. *Developmental Cell*, *11*(4), 441–450. https://doi.org/10.1016/j.devcel.2006.09.009

Knockaert, M., Greengard, P., & Meijer, L. (2002). Pharmacological inhibitors of cyclin-dependent kinases. In *Trends in Pharmacological Sciences*. https://doi.org/10.1016/S0165-6147(02)02071-0

Konopleva, M., Zhao, S., Hu, W., Jiang, S., Snell, V., Weidner, D., Jackson, C. E., Zhang, X., Champlin, R., Estey, E., Reed, J. C., & Andreeff, M. (2002). The anti-apoptotic genes Bcl-XL and Bcl-2 are over-expressed and contribute to chemoresistance of non-proliferating leukaemic CD34+ cells. *British Journal of Haematology*. https://doi.org/10.1046/j.1365-2141.2002.03637.x

Kool, M., Jones, D. T. W., Jäger, N., Northcott, P. A., Pugh, T. J., Hovestadt, V., Piro, R. M., Esparza, L. A., Markant, S. L., Remke, M., Milde, T., Bourdeaut, F., Ryzhova, M., Sturm,

D., Pfaff, E., Stark, S., Hutter, S., Şeker-Cin, H., Johann, P., … Pfister, S. M. (2014). Genome Sequencing of SHH Medulloblastoma Predicts Genotype-Related Response to Smoothened Inhibition. *Cancer Cell*, *25*(3), 393–405. https://doi.org/10.1016/j.ccr.2014.02.004

Kool, M., Koster, J., Bunt, J., Hasselt, N. E., Lakeman, A., van Sluis, P., Troost, D., Meeteren, N. S., Caron, H. N., Cloos, J., Mršić, A., Ylstra, B., Grajkowska, W., Hartmann, W., Pietsch, T., Ellison, D., Clifford, S. C., & Versteeg, R. (2008). Integrated Genomics Identifies Five Medulloblastoma Subtypes with Distinct Genetic Profiles, Pathway Signatures and Clinicopathological Features. *PLoS ONE*, *3*(8), e3088. https://doi.org/10.1371/journal.pone.0003088

Krichevsky, A. M. (2003). A microRNA array reveals extensive regulation of microRNAs during brain development. *RNA*, *9*(10), 1274–1281. https://doi.org/10.1261/rna.5980303

Kumar, S. K., LaPlant, B., Chng, W. J., Zonder, J., Callander, N., Fonseca, R., Fruth, B., Roy, V., Erlichman, C., & Stewart, A. K. (2015). Dinaciclib, a novel CDK inhibitor, demonstrates encouraging single-agent activity in patients with relapsed multiple myeloma. *Blood*. https://doi.org/10.1182/blood-2014-05-573741

Lagos-Quintana, M., Rauhut, R., Lendeckel, W., & Tuschl, T. (2001). Identification of novel genes coding for small expressed RNAs. *Science*. https://doi.org/10.1126/science.1064921

Lagos-Quintana, Mariana, Rauhut, R., Yalcin, A., Meyer, J., Lendeckel, W., & Tuschl, T. (2002). Identification of tissue-specific MicroRNAs from mouse. *Current Biology*, *12*(9), 735–739. https://doi.org/10.1016/S0960-9822(02)00809-6

Lam, L. T., Pickeral, O. K., Peng, A. C., Rosenwald, A., Hurt, E. M., Giltnane, J. M., Averett, L. M., Zhao, H., Davis, R. E., Sathyamoorthy, M., Wahl, L. M., Harris, E. D., Mikovits, J. A., Monks, A. P., Hollingshead, M. G., Sausville, E. A., & Staudt, L. M. (2001). Genomic-scale measurement of mRNA turnover and the mechanisms of action of the anti-cancer drug flavopiridol. *Genome Biology*. https://doi.org/10.1186/gb-2001-2-10-research0041

Lau, N. C., Lim, L. P., Weinstein, E. G., & Bartel, D. P. (2001). An abundant class of tiny RNAs with probable regulatory roles in Caenorhabditis elegans. *Science (New York, N.Y.)*, *294*(5543), 858–862. https://doi.org/10.1126/science.1065062

Laurent, J. P., Chang, C. H., & Cohen, M. E. (1985). A classification system for primitive neuroectodermal tumors (medulloblastoma) of the posterior fossa. *Cancer*. https://doi.org/10.1002/1097-0142(19851001)56:7+<1807::AID-CNCR2820561317>3.0.CO;2-U

Lee, R. C., Feinbaum, R. L., & Ambros, V. (1993). The C. elegans heterochronic gene lin-4 encodes small RNAs with antisense complementarity to lin-14. *Cell*, *75*(5), 843–854. https://doi.org/10.1016/0092-8674(93)90529-Y

Lee, Y., Ahn, C., Han, J., Choi, H., Kim, J., Yim, J., Lee, J., Provost, P., Rådmark, O., Kim, S., & Kim, V. N. (2003). The nuclear RNase III Drosha initiates microRNA processing. *Nature*, *425*(6956), 415–419. https://doi.org/10.1038/nature01957

Lee, Y., Kim, M., Han, J., Yeom, K.-H., Lee, S., Baek, S. H., & Kim, V. N. (2004). MicroRNA genes are transcribed by RNA polymerase II. *The EMBO Journal*, *23*(20), 4051–4060. https://doi.org/10.1038/sj.emboj.7600385

Leite de Oliveira, R., & Bernards, R. (2018). Anti‐cancer therapy: senescence is the new black. *The EMBO Journal*. https://doi.org/10.15252/embj.201899386

Lewis, B. P., Burge, C. B., & Bartel, D. P. (2005). Conserved seed pairing, often flanked by adenosines, indicates that thousands of human genes are microRNA targets. *Cell*, *120*(1), 15–20. https://doi.org/10.1016/j.cell.2004.12.035

Lewis, B. P., Shih, I. H., Jones-Rhoades, M. W., Bartel, D. P., & Burge, C. B. (2003). Prediction of Mammalian MicroRNA Targets. *Cell*, *115*(7), 787–798. https://doi.org/10.1016/S0092-8674(03)01018-3

Li, K. K. W., Pang, J. C. sean, Ching, A. K. keung, Wong, C. K., Kong, X., Wang, Y., Zhou, L., Chen, Z., & Ng, H. keung. (2009). miR-124 is frequently down-regulated in medulloblastoma and is a negative regulator of SLC16A1. *Human Pathology*. https://doi.org/10.1016/j.humpath.2009.02.003

Li, M., Lockwood, W., Zielenska, M., Northcott, P., Ra, Y. S., Bouffet, E., Yoshimoto, M., Rutka, J. T., Yan, H., Taylor, M. D., Eberhart, C., Hawkins, C. E., Lam, W., Squire, J. A., & Huang, A. (2012). Multiple CDK/CYCLIND genes are amplified in medulloblastoma and supratentorial primitive neuroectodermal brain tumor. *Cancer Genetics*. https://doi.org/10.1016/j.cancergen.2012.03.002

Lim, L. P., Glasner, M. E., Yekta, S., Burge, C. B., & Bartel, D. P. (2003). Vertebrate microRNA genes. *Science (New York, N.Y.)*, *299*(5612), 1540. https://doi.org/10.1126/science.1080372

Lim, L. P., Lau, N. C., Garrett-Engele, P., Grimson, A., Schelter, J. M., Castle, J., Bartel, D. P., Linsley, P. S., & Johnson, J. M. (2005). Microarray analysis shows that some microRNAs downregulate large numbers of target mRNAs. *Nature*, *433*(7027), 769–773. https://doi.org/10.1038/nature03315

Lin, S. F., Lin, J. Der, Hsueh, C., Chou, T. C., & Wong, R. J. (2017). A cyclin-dependent kinase inhibitor, dinaciclib in preclinical treatment models of thyroid cancer. *PLoS ONE*. https://doi.org/10.1371/journal.pone.0172315

Liu, G., Gandara, D. R., Lara, P. N., Raghavan, D., Doroshow, J. H., Twardowski, P., Kantoff, P., Oh, W., Kim, K. M., & Wilding, G. (2004). A Phase II Trial of Flavopiridol (NSC #649890) in Patients with Previously Untreated Metastatic Androgen-Independent Prostate Cancer. *Clinical Cancer Research*. https://doi.org/10.1158/1078-0432.CCR-03-0050

Liu, H., Lv, L., & Yang, K. (2015). Chemotherapy targeting cancer stem cells. *American Journal of Cancer Research*, *5*(3), 880–893.

Liu, X. S., Chopp, M., Wang, X. L., Zhang, L., Hozeska-Solgot, A., Tang, T., Kassis, H., Zhang, R. L., Chen, C., Xu, J., & Zhang, Z. G. (2013a). MicroRNA-17-92 cluster mediates the proliferation and survival of neural progenitor cells after stroke. *Journal of Biological Chemistry*, *288*(18), 12478–12488. https://doi.org/10.1074/jbc.M112.449025

Liu, X. S., Chopp, M., Wang, X. L., Zhang, L., Hozeska-Solgot, A., Tang, T., Kassis, H., Zhang, R. L., Chen, C., Xu, J., & Zhang, Z. G. (2013b). MicroRNA-17-92 Cluster Mediates the Proliferation and Survival of Neural Progenitor Cells after Stroke. *The Journal of Biological Chemistry*, *288*(18), 12478–12488. https://doi.org/10.1074/jbc.M112.449025

Louis, D. N., Ohgaki, H., Wiestler, O. D., Cavenee, W. K., Burger, P. C., Jouvet, A., Scheithauer, B. W., & Kleihues, P. (2007). The 2007 WHO classification of tumours of the central

nervous system. *Acta Neuropathologica*, *114*(2), 97–109. https://doi.org/10.1007/s00401-007-0243-4

Louis, D. N., Perry, A., Reifenberger, G., von Deimling, A., Figarella-Branger, D., Cavenee, W. K., Ohgaki, H., Wiestler, O. D., Kleihues, P., & Ellison, D. W. (2016). The 2016 World Health Organization Classification of Tumors of the Central Nervous System: a summary. *Acta Neuropathologica*, *131*(6), 803–820. https://doi.org/10.1007/s00401-016-1545-1

Lu, Jiuyi, Chen, M., Ren, X. R., Wang, J., Lyerly, H. K., Barak, L., & Chen, W. (2013). Regulation of Hedgehog Signaling by Myc-Interacting Zinc Finger Protein 1, Miz1. *PLoS ONE*. https://doi.org/10.1371/journal.pone.0063353

Lu, Jun, Getz, G., Miska, E. a, Alvarez-Saavedra, E., Lamb, J., Peck, D., Sweet-Cordero, A., Ebert, B. L., Mak, R. H., Ferrando, A. a, Downing, J. R., Jacks, T., Horvitz, H. R., & Golub, T. R. (2005). MicroRNA expression profiles classify human cancers. *Nature*, *435*(7043), 834–838. https://doi.org/10.1038/nature03702

Lu, Y., Labak, C. M., Jain, N., Purvis, I. J., Guda, M. R., Bach, S. E., Tsung, A. J., Asuthkar, S., & Velpula, K. K. (2017). OTX2 expression contributes to proliferation and progression in Myc-amplified medulloblastoma. *American Journal of Cancer Research*, *7*(3), 647–656. http://www.ncbi.nlm.nih.gov/pmc/articles/PMC5385649/

Lujambio, A., & Lowe, S. W. (2012). The microcosmos of cancer. In *Nature*. https://doi.org/10.1038/nature10888

Lundberg, A. S., & Weinberg, R. A. (1998). Functional Inactivation of the Retinoblastoma Protein Requires Sequential Modification by at Least Two Distinct Cyclin-cdk Complexes. *Molecular and Cellular Biology*, *18*(2), 753–761.

Luqmani, Y. A. (2005). Mechanisms of Drug Resistance in Cancer Chemotherapy. *Medical Principles and Practice*, *14(suppl 1*(Suppl. 1), 35–48. https://doi.org/10.1159/000086183

Macias, E., Kim, Y., De Marval, P. L. M., Klein-Szanto, A., & Rodriguez-Puebla, M. L. (2007). Cdk2 deficiency decreases ras/CDK4-dependent malignant progression, but not myc-induced tumorigenesis. *Cancer Research*. https://doi.org/10.1158/0008-5472.CAN-07-2119

Malumbres, M. (2014). Cyclin-dependent kinases. *Genome Biology*, *15*(6), 122. https://doi.org/10.1186/gb4184

Malumbres, M., & Barbacid, M. (2001). To cycle or not to cycle: a critical decision in cancer. *Nature Reviews Cancer*, *1*, 222.

Malumbres, M., & Barbacid, M. (2009). Cell cycle, CDKs and cancer: A changing paradigm. In *Nature Reviews Cancer*. https://doi.org/10.1038/nrc2602

Malumbres, M., Pevarello, P., Barbacid, M., & Bischoff, J. R. (2008). CDK inhibitors in cancer therapy: what is next? *Trends in Pharmacological Sciences*. https://doi.org/10.1016/j.tips.2007.10.012

Marino, S, Vooijs, M., van Der Gulden, H., Jonkers, J., & Berns, A. (2000). No Title. *Genes Dev*, *14*(8), 994.

Marino, Silvia. (2005a). Medulloblastoma: developmental mechanisms out of control. *Trends in Molecular Medicine*, *11*(1), 17–22. https://doi.org/10.1016/j.molmed.2004.11.008

Marino, Silvia. (2005b). Medulloblastoma: developmental mechanisms out of control. *Trends in Molecular Medicine*, *11*(1), 17–22. https://doi.org/10.1016/j.molmed.2004.11.008

Martín, A., Odajima, J., Hunt, S. L., Dubus, P., Ortega, S., Malumbres, M., & Barbacid, M. (2005). Cdk2 is dispensable for cell cycle inhibition and tumor suppression mediated by p27Kip1 and p21Cip1. *Cancer Cell*. https://doi.org/10.1016/j.ccr.2005.05.006

Mathsyaraja, H., & Eisenman, R. N. (2016a). Parsing Myc Paralogs in Oncogenesis. *Cancer Cell*, *29*(1), 1–2. https://doi.org/10.1016/j.ccell.2015.12.009

Mathsyaraja, H., & Eisenman, R. N. (2016b). Parsing Myc Paralogs in Oncogenesis. *Cancer Cell*, *29*(1), 1–2. https://doi.org/10.1016/j.ccell.2015.12.009

McCartney, A., Migliaccio, I., Bonechi, M., Biagioni, C., Romagnoli, D., De Luca, F., Galardi, F., Risi, E., De Santo, I., Benelli, M., Malorni, L., & Di Leo, A. (2019). Mechanisms of Resistance to CDK4/6 Inhibitors: Potential Implications and Biomarkers for Clinical Practice. In *Frontiers in Oncology*. https://doi.org/10.3389/fonc.2019.00666

McClendon, A. K., Dean, J. L., Rivadeneira, D. B., Yu, J. E., Reed, C. A., Gao, E., Farber, J. L., Force, T., Koch, W. J., & Knudsen, E. S. (2012). CDK4/6 inhibition antagonizes the cytotoxic response to anthracycline therapy. *Cell Cycle*. https://doi.org/10.4161/cc.21127

McManamy, C. S., Pears, J., Weston, C. L., Hanzely, Z., Ironside, J. W., Taylor, R. E., Grundy, R. G., Clifford, S. C., & Ellison, D. W. (2007). Nodule formation and desmoplasia in medulloblastomas - Defining the nodular/desmoplastic variant and its biological behavior. *Brain Pathology*. https://doi.org/10.1111/j.1750-3639.2007.00058.x

Mendell, J. T. (2008). miRiad Roles for the miR-17-92 Cluster in Development and Disease. In *Cell*. https://doi.org/10.1016/j.cell.2008.04.001

Mendrzyk, F., Radlwimmer, B., Joos, S., Kokocinski, F., Benner, A., Stange, D. E., Neben, K., Fiegler, H., Carter, N. P., Reifenberger, G., Korshunov, A., & Lichter, P. (2005). Genomic and protein expression profiling identifies CDK6 as novel independent prognostic marker in medulloblastoma. *Journal of Clinical Oncology*. https://doi.org/10.1200/JCO.2005.02.8589

Merchant, T. E., Kun, L. E., Krasin, M. J., Wallace, D., Chintagumpala, M. M., Woo, S. Y., Ashley, D. M., Sexton, M., Kellie, S. J., Ahern, V., & Gajjar, A. (2008). A Multi-Institution Prospective Trial of Reduced-Dose Craniospinal Irradiation (23.4 Gy) Followed by Conformal Posterior Fossa (36 Gy) and Primary Site Irradiation (55.8 Gy) and Dose-Intensive Chemotherapy for Average-Risk Medulloblastoma. *International Journal of Radiation Oncology, Biology, Physics*, *70*(3), 782–787. https://doi.org/10.1016/j.ijrobp.2007.07.2342

Mestdagh, P., Fredlund, E., Pattyn, F., Schulte, J. H., Muth, D., Vermeulen, J., Kumps, C., Schlierf, S., De Preter, K., Van Roy, N., Noguera, R., Laureys, G., Schramm, A., Eggert, A., Westermann, F., Speleman, F., & Vandesompele, J. (2010). MYCN/c-MYC-induced microRNAs repress coding gene networks associated with poor outcome in MYCN/c-MYC-activated tumors. *Oncogene*, *29*(9), 1394–1404. http://dx.doi.org/10.1038/onc.2009.429

Mita, M. M., Joy, A. A., Mita, A., Sankhala, K., Jou, Y. M., Zhang, D., Statkevich, P., Zhu, Y., Yao, S. L., Small, K., Bannerji, R., & Shapiro, C. L. (2014). Randomized phase II trial of the

cyclin-dependent kinase inhibitor Dinaciclib (MK-7965) versus capecitabine in patients with advanced breast cancer. *Clinical Breast Cancer*. https://doi.org/10.1016/j.clbc.2013.10.016

Mitchell, K. O., Ricci, M. S., Miyashita, T., Dicker, D. T., Jin, Z., Reed, J. C., & El-Deiry, W. S. (2000). Bax is a transcriptional target and mediator of c-Myc-induced apoptosis. *Cancer Research*.

Moharram, S. A., Shah, K., Khanum, F., Marhäll, A., Gazi, M., & Kazi, J. U. (2017). Efficacy of the CDK inhibitor dinaciclib in vitro and in vivo in T-cell acute lymphoblastic leukemia. *Cancer Letters*, *405*, 73–78. https://doi.org/10.1016/J.CANLET.2017.07.019

Mollashahi, B., Aghamaleki, F. S., & Movafagh, A. (2019). The Roles of miRNAs in Medulloblastoma: A Systematic Review. *Journal of Cancer Prevention*. https://doi.org/10.15430/jcp.2019.24.2.79

Montagnoli, A., Fiore, F., Eytan, E., Carrano, A. C., Draetta, G. F., Hershko, A., & Pagano, M. (1999). Ubiquitination of p27 is regulated by Cdk-dependent phosphorylation and trimeric complex formation. *Genes & Development*, *13*(9), 1181–1189.

Morfouace, M., Shelat, A., Jacus, M., Freeman, B. B., Turner, D., Robinson, S., Zindy, F., Wang, Y.-D., Finkelstein, D., Ayrault, O., Bihannic, L., Li, X.-N., Olson, J. M., Robinson, G. W., Guy, R. K., Stewart, C. F., Gajjar, A., & Roussel, M. F. (2014). Pemetrexed and gemcitabine as combination therapy for the treatment of Group3 medulloblastoma. *Cancer Cell*, *25*(4), 516–529. https://doi.org/10.1016/j.ccr.2014.02.009

Moxon-Emre, I., Bouffet, E., Taylor, M. D., Laperriere, N., Scantlebury, N., Law, N., Spiegler, B. J., Malkin, D., Janzen, L., & Mabbott, D. (2014). Impact of craniospinal dose, boost volume, and neurologic complications on intellectual outcome in patients with medulloblastoma. *Journal of Clinical Oncology*. https://doi.org/10.1200/JCO.2013.52.3290

Mulhern, R. K., Merchant, T. E., Gajjar, A., Reddick, W. E., & Kun, L. E. (2017). Late neurocognitive sequelae in survivors of brain tumours in childhood. *The Lancet Oncology*, *5*(7), 399–408. https://doi.org/10.1016/S1470-2045(04)01507-4

Murphy, B. L., Obad, S., Bihannic, L., Ayrault, O., Zindy, F., Kauppinen, S., & Roussel, M. F. (2013). Silencing of the miR-17~92 cluster family inhibits medulloblastoma progression. *Cancer Research*, *73*(23), 10.1158/0008-5472.CAN-13–0927. https://doi.org/10.1158/0008-5472.CAN-13-0927

Muscal, J. A., Scorsone, K. A., Zhang, L., Ecsedy, J. A., & Berg, S. L. (2013). Additive effects of vorinostat and MLN8237 in pediatric leukemia, medulloblastoma, and neuroblastoma cell lines. *Investigational New Drugs*. https://doi.org/10.1007/s10637-012-9831-9

Muthalagu, N., Junttila, M. R., Wiese, K. E., Wolf, E., Morton, J., Bauer, B., Evan, G. I., Eilers, M., & Murphy, D. J. (2014). BIM Is the Primary Mediator of MYC-Induced Apoptosis in Multiple Solid Tissues. *Cell Reports*. https://doi.org/10.1016/j.celrep.2014.07.057

Nasi, S., Ciarapica, R., Jucker, R., Rosati, J., & Soucek, L. (2001). Making decisions through Myc. In *FEBS Letters*. https://doi.org/10.1016/S0014-5793(01)02118-4

Nguyen, T. K., & Grant, S. (2014). Dinaciclib (SCH727965) inhibits the unfolded protein response through a CDK1- And 5-dependent mechanism. *Molecular Cancer Therapeutics*. https://doi.org/10.1158/1535-7163.MCT-13-0714

Northcott, P. A., Buchhalter, I., Morrissy, A. S., Hovestadt, V., Weischenfeldt, J., Ehrenberger, T., Gröbner, S., Segura-Wang, M., Zichner, T., Rudneva, V. A., Warnatz, H. J., Sidiropoulos, N., Phillips, A. H., Schumacher, S., Kleinheinz, K., Waszak, S. M., Erkek, S., Jones, D. T. W., Worst, B. C., … Lichter, P. (2017). The whole-genome landscape of medulloblastoma subtypes. *Nature*. https://doi.org/10.1038/nature22973

Northcott, P. A., Fernandez-L, A., Hagan, J. P., Ellison, D. W., Grajkowska, W., Gillespie, Y., Grundy, R., Van Meter, T., Rutka, J. T., Croce, C. M., Kenney, A. M., & Taylor, M. D. (2009). The miR-17/92 polycistron is up-regulated in Sonic hedgehog-driven medulloblastomas and induced by N-myc in Sonic hedgehog-treated cerebellar neural precursors. *Cancer Research*, *69*(8), 3249–3255. https://doi.org/10.1158/0008-5472.CAN-08-4710

Northcott, P. A., Jones, D. T. W., Kool, M., Robinson, G. W., Gilbertson, R. J., Cho, Y.-J., Pomeroy, S. L., Korshunov, A., Lichter, P., Taylor, M. D., & Pfister, S. M. (2012). Medulloblastomics: The End of the Beginning. *Nature Reviews. Cancer*, *12*(12), 818–834. https://doi.org/10.1038/nrc3410

Northcott, P. A., Korshunov, A., Witt, H., Hielscher, T., Eberhart, C. G., Mack, S., Bouffet, E., Clifford, S. C., Hawkins, C. E., French, P., Rutka, J. T., Pfister, S., & Taylor, M. D. (2011). Medulloblastoma Comprises Four Distinct Molecular Variants. *Journal of Clinical Oncology*, *29*(11), 1408–1414. https://doi.org/10.1200/JCO.2009.27.4324

Northcott, P. A., Lee, C., Zichner, T., Stütz, A. M., Erkek, S., Kawauchi, D., Shih, D. J. H., Hovestadt, V., Zapatka, M., Sturm, D., Jones, D. T. W., Kool, M., Remke, M., Cavalli, F., Zuyderduyn, S., Bader, G., VandenBerg, S., Esparza, L. A., Ryzhova, M., … Pfister, S. M. (2014). Enhancer hijacking activates GFI1 family oncogenes in medulloblastoma. *Nature*, *511*(7510), 428–434. https://doi.org/10.1038/nature13379

Northcott, P. A., Nakahara, Y., Wu, X., Feuk, L., Ellison, D. W., Croul, S., Mack, S., Kongkham, P. N., Peacock, J., Dubuc, A., Ra, Y.-S., Zilberberg, K., Mcleod, J., Scherer, S. W., Rao, J. S., Eberhart, C. G., Grajkowska, W., Gillespie, Y., Lach, B., … Taylor, M. D. (2009). Multiple recurrent genetic events converge on control of histone lysine methylation in medulloblastoma. *Nature Genetics*, *41*(4), 465–472. https://doi.org/10.1038/ng.336

Northcott, P. A., Shih, D. J. H., Peacock, J., Garzia, L., Sorana Morrissy, A., Zichner, T., Stutz, A. M., Korshunov, A., Reimand, J., Schumacher, S. E., Beroukhim, R., Ellison, D. W., Marshall, C. R., Lionel, A. C., Mack, S., Dubuc, A., Yao, Y., Ramaswamy, V., Luu, B., … Taylor, M. D. (2012). Subgroup-specific structural variation across 1,000 medulloblastoma genomes. *Nature*, *488*(7409), 49–56. http://dx.doi.org/10.1038/nature11327

O'Connell, M. J., Raleigh, J. M., Verkade, H. M., & Nurse, P. (1997). Chk1 is a wee1 kinase in the G2 DNA damage checkpoint inhibiting cdc2 by Y15 phosphorylation. *EMBO Journal*. https://doi.org/10.1093/emboj/16.3.545

O'Donnell, K. A., Wentzel, E. A., Zeller, K. I., Dang, C. V, & Mendell, J. T. (2005). c-Myc-regulated microRNAs modulate E2F1 expression. *Nature*, *435*(7043), 839–843. http://dx.doi.org/10.1038/nature03677

Oliver, T. G., Read, T. A., Kessler, J. D., Mehmeti, A., Wells, J. F., Huynh, T. T., Lin, S. M., & Wechsler-Reya, R. J. (2005). Loss of patched and disruption of granule cell development

in a pre-neoplastic stage of medulloblastoma. *Development*, *132*(10), 2425–2439. https://doi.org/10.1242/dev.01793

Ostrom, Q. T., Gittleman, H., Truitt, G., Boscia, A., Kruchko, C., & Barnholtz-Sloan, J. S. (2018). CBTRUS statistical report: Primary brain and other central nervous system tumors diagnosed in the United States in 2011-2015. In *Neuro-Oncology*.

Otto, T., & Sicinski, P. (2017). Cell cycle proteins as promising targets in cancer therapy. *Nature Reviews. Cancer*, *17*(2), 93–115. https://doi.org/10.1038/nrc.2016.138

Packer, R. J. (2008). Childhood brain tumors: Accomplishments and ongoing challenges. *Journal of Child Neurology*. https://doi.org/10.1177/0883073808320758

Packer, R. J., Gajjar, A., Vezina, G., Rorke-Adams, L., Burger, P. C., Robertson, P. L., Bayer, L., LaFond, D., Donahue, B. R., Marymont, M. H., Muraszko, K., Langston, J., & Sposto, R. (2006). Phase III Study of Craniospinal Radiation Therapy Followed by Adjuvant Chemotherapy for Newly Diagnosed Average-Risk Medulloblastoma. *Journal of Clinical Oncology*, *24*(25), 4202–4208. https://doi.org/10.1200/JCO.2006.06.4980

Packer, R. J., Goldwein, J., Nicholson, H. S., Vezina, L. G., Allen, J. C., Ris, M. D., Muraszko, K., Rorke, L. B., Wara, W. M., Cohen, B. H., & Boyett, J. M. (1999). Treatment of Children With Medulloblastomas With Reduced-Dose Craniospinal Radiation Therapy and Adjuvant Chemotherapy: A Children's Cancer Group Study. *Journal of Clinical Oncology*, *17*(7), 2127. https://doi.org/10.1200/JCO.1999.17.7.2127

Padmakumar, V. C., Aleem, E., Berthet, C., Hilton, M. B., & Kaldis, P. (2009). Cdk2 and Cdk4 Activities Are Dispensable for Tumorigenesis Caused by the Loss of p53. *Molecular and Cellular Biology*. https://doi.org/10.1128/mcb.00952-08

Parry, D., Guzi, T., Shanahan, F., Davis, N., Prabhavalkar, D., Wiswell, D., Seghezzi, W., Paruch, K., Dwyer, M. P., Doll, R., Nomeir, A., Windsor, W., Fischmann, T., Wang, Y., Oft, M., Chen, T., Kirschmeier, P., & Lees, E. M. (2010). Dinaciclib (SCH 727965), a novel and potent cyclin-dependent kinase inhibitor. *Molecular Cancer Therapeutics*. https://doi.org/10.1158/1535-7163.MCT-10-0324

Pei, Y., Liu, K. W., Wang, J., Garancher, A., Tao, R., Esparza, L. A., Maier, D. L., Udaka, Y. T., Murad, N., Morrissy, S., Seker-Cin, H., Brabetz, S., Qi, L., Kogiso, M., Schubert, S., Olson, J. M., Cho, Y. J., Li, X. N., Crawford, J. R., … Wechsler-Reya, R. J. (2016). HDAC and PI3K Antagonists Cooperate to Inhibit Growth of MYC-Driven Medulloblastoma. *Cancer Cell*. https://doi.org/10.1016/j.ccell.2016.02.011

Peukert, K., Staller, P., Schneider, A., Carmichael, G., Hänel, F., & Eilers, M. (1997). An alternative pathway for gene regulation by Myc. *EMBO Journal*. https://doi.org/10.1093/emboj/16.18.5672

Pierson, J., Hostager, B., Fan, R., & Vibhakar, R. (2008). Regulation of cyclin dependent kinase 6 by microRNA 124 in medulloblastoma. *Journal of Neuro-Oncology*. https://doi.org/10.1007/s11060-008-9624-3

Pizer, B., & Clifford, S. (2008). Medulloblastoma: New insights into biology and treatment. In *Archives of Disease in Childhood: Education and Practice Edition*. https://doi.org/10.1136/adc.2007.136655

Pizer, B. L., & Clifford, S. C. (2009). The potential impact of tumour biology on improved clinical practice for medulloblastoma: progress towards biologically driven clinical trials.

British Journal of Neurosurgery, *23*(4), 364–375. https://doi.org/10.1080/02688690903121807

Pomeroy, S. L., Tamayo, P., Gaasenbeek, M., Sturla, L. M., Angelo, M., McLaughlin, M. E., Kim, J. Y. H., Goumnerova, L. C., Black, P. M., Lau, C., Allen, J. C., Zagzag, D., Olson, J. M., Curran, T., Wetmore, C., Biegel, J. A., Poggio, T., Mukherjee, S., Rifkin, R., … Golub, T. R. (2002). Prediction of central nervous system embryonal tumour outcome based on gene expression. *Nature*, *415*(6870), 436–442. http://proxy.lib.ohio-state.edu/login?url=http://search.ebscohost.com/login.aspx?direct=true&db=mnh&AN=11807556&site=ehost-live

Pomeroy, S., Sengupta, S., & Pomeranz Krummel, D. (2017). The evolution of medulloblastoma therapy to personalized medicine. In *F1000Research*. https://doi.org/10.12688/f1000research.10859.1

Pozo, K., Castro-Rivera, E., Tan, C., Plattner, F., Schwach, G., Siegl, V., Meyer, D., Guo, A., Gundara, J., Mettlach, G., Richer, E., Guevara, J. A., Ning, L., Gupta, A., Hao, G., Tsai, L. H., Sun, X., Antich, P., Sidhu, S., … Bibb, J. A. (2013). The Role of Cdk5 in Neuroendocrine Thyroid Cancer. *Cancer Cell*. https://doi.org/10.1016/j.ccr.2013.08.027

Psathas, J. N., & Thomas-Tikhonenko, A. (2014). MYC and the art of microRNA maintenance. *Cold Spring Harbor Perspectives in Medicine*. https://doi.org/10.1101/cshperspect.a014175

Qiao, W., Guo, B., Zhou, H., Xu, W., Chen, Y., Liang, Y., & Dong, B. (2017). miR-124 suppresses glioblastoma growth and potentiates chemosensitivity by inhibiting AURKA. *Biochemical and Biophysical Research Communications*. https://doi.org/10.1016/j.bbrc.2017.02.120

Rajput, S., Khera, N., Guo, Z., Hoog, J., Li, S., & Ma, C. X. (2016). Inhibition of cyclin dependent kinase 9 by dinaciclib suppresses cyclin B1 expression and tumor growth in triple negative breast cancer. *Oncotarget*. https://doi.org/10.18632/oncotarget.10870

Ramaswamy, V., Remke, M., Bouffet, E., Bailey, S., Clifford, S. C., Doz, F., Kool, M., Dufour, C., Vassal, G., Milde, T., Witt, O., von Hoff, K., Pietsch, T., Northcott, P. A., Gajjar, A., Robinson, G. W., Padovani, L., André, N., Massimino, M., … Pomeroy, S. L. (2016). Risk stratification of childhood medulloblastoma in the molecular era: The Current Consensus. *Acta Neuropathologica*, *131*(6), 821–831. https://doi.org/10.1007/s00401-016-1569-6

Ransohoff, K. J., Sarin, K. Y., & Tang, J. Y. (2015). Smoothened Inhibitors in Sonic Hedgehog Subgroup Medulloblastoma. *Journal of Clinical Oncology*, *33*(24), 2692–2694. https://doi.org/10.1200/JCO.2015.62.2225

Reinhart, B. J., Slack, F. J., Basson, M., Pasquinelll, A. E., Bettlnger, J. C., Rougvle, A. E., Horvitz, H. R., & Ruvkun, G. (2000). The 21-nucleotide let-7 RNA regulates developmental timing in Caenorhabditis elegans. *Nature*. https://doi.org/10.1038/35002607

Rello-Varona, S., Fuentes-Guirado, M., López-Alemany, R., Contreras-Pérez, A., Mulet-Margalef, N., García-Monclús, S., Tirado, O. M., & García del Muro, X. (2019). Bcl-x L inhibition enhances Dinaciclib-induced cell death in soft-tissue sarcomas. *Scientific Reports*. https://doi.org/10.1038/s41598-019-40106-7

Rickert, P., Seghezzi, W., Shanahan, F., Cho, H., & Lees, E. (1996). Cyclin C/CDK8 is a novel CTD kinase associated with RNA polymerase II. *Oncogene*, *12*(12), 2631–2640.

Robinson, G., Parker, M., & Kranenburg, T. A. (2012). Novel mutations target distinct subgroups of medulloblastoma. *Nature*. https://doi.org/10.1038/nature11213

Robinson, G., Parker, M., Kranenburg, T. A., Lu, C., Chen, X., Ding, L., Phoenix, T. N., Hedlund, E., Wei, L., Zhu, X., Chalhoub, N., Baker, S. J., Huether, R., Kriwacki, R., Curley, N., Thiruvenkatam, R., Wang, J., Wu, G., Rusch, M., … Gilbertson, R. J. (2012). Novel mutations target distinct subgroups of medulloblastoma. *Nature*, *488*(7409), 43–48. https://doi.org/10.1038/nature11213

Robinson, G. W., Orr, B. A., Wu, G., Gururangan, S., Lin, T., Qaddoumi, I., Packer, R. J., Goldman, S., Prados, M. D., Desjardins, A., Chintagumpala, M., Takebe, N., Kaste, S. C., Rusch, M., Allen, S. J., Onar-Thomas, A., Stewart, C. F., Fouladi, M., Boyett, J. M., … Gajjar, A. (2015). Vismodegib Exerts Targeted Efficacy Against Recurrent Sonic Hedgehog–Subgroup Medulloblastoma: Results From Phase II Pediatric Brain Tumor Consortium Studies PBTC-025B and PBTC-032. *Journal of Clinical Oncology*, *33*(24), 2646–2654. https://doi.org/10.1200/JCO.2014.60.1591

Roth, R. B., Hevezi, P., Lee, J., Willhite, D., Lechner, S. M., Foster, A. C., & Zlotnik, A. (2006). Gene expression analyses reveal molecular relationships among 20 regions of the human CNS. *Neurogenetics*. https://doi.org/10.1007/s10048-006-0032-6

Roussel, M. F., & Robinson, G. W. (2013). Role of MYC in Medulloblastoma. *Cold Spring Harbor Perspectives in Medicine*, *3*(11), a014308. https://doi.org/10.1101/cshperspect.a014308

Rowland, T., Paiva, C., Rowley, J., Chen, A., Drew, L., Hurlin, P., Chang, B. H., & Danilov, A. V. (2016). Selective Targeting Cyclin-Dependent Kinase-9 (CDK9) Downmodulates c-MYC and Induces Apoptosis in Diffuse Large B-Cell Lymphoma (DLBCL) Cells. *Blood*. https://doi.org/10.1182/blood.v128.22.289.289

Rutkowski, S., Bode, U., Deinlein, F., Ottensmeier, H., Warmuth-Metz, M., Soerensen, N., Graf, N., Emser, A., Pietsch, T., & Wolff, J. E. (2005). Treatment of early childhood medulloblastoma by postoperative chemotherapy alone. *N Engl J Med*, *352*. https://doi.org/10.1056/NEJMoa042176

Sabelström, H., Petri, R., Shchors, K., Jandial, R., Schmidt, C., Sacheva, R., Masic, S., Yuan, E., Fenster, T., Martinez, M., Saxena, S., Nicolaides, T. P., Ilkhanizadeh, S., Berger, M. S., Snyder, E. Y., Weiss, W. A., Jakobsson, J., & Persson, A. I. (2019). Driving Neuronal Differentiation through Reversal of an ERK1/2-miR-124-SOX9 Axis Abrogates Glioblastoma Aggressiveness. *Cell Reports*. https://doi.org/10.1016/j.celrep.2019.07.071

Sanchez, Y., Wong, C., Thoma, R. S., Richman, R., Wu, Z., Piwnica-Worms, H., & Elledge, S. J. (1997). Conservation of the Chk1 checkpoint pathway in mammals: Linkage of DNA damage to Cdk regulation through Cdc25. *Science*. https://doi.org/10.1126/science.277.5331.1497

Santamaría, D., Barrière, C., Cerqueira, A., Hunt, S., Tardy, C., Newton, K., Cáceres, J. F., Dubus, P., Malumbres, M., & Barbacid, M. (2007). Cdk1 is sufficient to drive the mammalian cell cycle. *Nature*. https://doi.org/10.1038/nature06046

Schafer, K. A. (1998). The Cell Cycle: A Review. *Veterinary Pathology*, *35*(6), 461–478. https://doi.org/10.1177/030098589803500601

Schmittgen, T. D., & Livak, K. J. (2008). Analyzing real-time PCR data by the comparative CT method. *Nature Protocols*, *3*(6), 1101–1108. https://doi.org/10.1038/nprot.2008.73

Schroeder, K., & Gururangan, S. (2014). Molecular variants and mutations in medulloblastoma. In *Pharmacogenomics and Personalized Medicine*. https://doi.org/10.2147/PGPM.S38698

Schwalbe, E. C., Lindsey, J. C., Nakjang, S., Crosier, S., Smith, A. J., Hicks, D., Rafiee, G., Hill, R. M., Iliasova, A., Stone, T., Pizer, B., Michalski, A., Joshi, A., Wharton, S. B., Jacques, T. S., Bailey, S., Williamson, D., & Clifford, S. C. (2017). Novel molecular subgroups for clinical classification and outcome prediction in childhood medulloblastoma: a cohort study. *The Lancet Oncology*. https://doi.org/10.1016/S1470-2045(17)30243-7

Schwarz, D. S., Hutvágner, G., Du, T., Xu, Z., Aronin, N., & Zamore, P. D. (2003). Asymmetry in the assembly of the RNAi enzyme complex. *Cell*, *115*(2), 199–208. https://doi.org/10.1016/S0092-8674(03)00759-1

Shah, M. A., & Schwartz, G. K. (2001). Cell cycle-mediated drug resistance: An emerging concept in cancer therapy. In *Clinical Cancer Research*.

Shapiro, G. I. (2006). Cyclin-dependent kinase pathways as targets for cancer treatment. In *Journal of Clinical Oncology*. https://doi.org/10.1200/JCO.2005.03.7689

Sherr, C. J., Beach, D., & Shapiro, G. I. (2016). Targeting CDK4 and CDK6: From discovery to therapy. In *Cancer Discovery*. https://doi.org/10.1158/2159-8290.CD-15-0894

Shih, D. J. H., Northcott, P. A., Remke, M., Korshunov, A., Ramaswamy, V., Kool, M., Luu, B., Yao, Y., Wang, X., Dubuc, A. M., Garzia, L., Peacock, J., Mack, S. C., Wu, X., Rolider, A., Morrissy, A. S., Cavalli, F. M. G., Jones, D. T. W., Zitterbart, K., … Taylor, M. D. (2014). Cytogenetic prognostication within medulloblastoma subgroups. *Journal of Clinical Oncology*. https://doi.org/10.1200/JCO.2013.50.9539

Silber, J., Hashizume, R., Felix, T., Hariono, S., Yu, M., Berger, M. S., Huse, J. T., Vandenberg, S. R., David James, C., Graeme Hodgson, J., & Gupta, N. (2013). Expression of miR-124 inhibits growth of medulloblastoma cells. *Neuro-Oncology*. https://doi.org/10.1093/neuonc/nos281

Sjostrom, S. K., Finn, G., Hahn, W. C., Rowitch, D. H., & Kenney, A. M. (2005). The Cdk1 complex plays a prime role in regulating N-myc phosphorylation and turnover in neural precursors. *Developmental Cell*. https://doi.org/10.1016/j.devcel.2005.07.014

Small, E. M., & Olson, E. N. (2011). Pervasive roles of microRNAs in cardiovascular biology. *Nature*, *469*(7330), 336–342. https://doi.org/10.1038/nature09783

Song, H., Bhakat, R., Kling, M. J., Coulter, D. W., Chaturvedi, N. K., Ray, S., & Joshi, S. S. (2019). Targeting cyclin-dependent kinase 9 sensitizes medulloblastoma cells to chemotherapy. *Biochemical and Biophysical Research Communications*. https://doi.org/10.1016/j.bbrc.2019.09.118

Soucek, T., Pusch, O., Hengstschläger-Ottnad, E., Adams, P. D., & Hengstschläger, M. (1997). Deregulated expression of E2F-1 induces cyclin A- and E-associated kinase activities independently from cell cycle position. *Oncogene*, *14*, 2251.

Stanton, B. R., Perkins, A. S., Tessarollo, L., Sassoon, D. A., & Parada, L. F. (1992). Loss of N-

myc function results in embryonic lethality and failure of the epithelial component of the embryo to develop. *Genes and Development*, *6*(12), 2235–2247. https://doi.org/10.1101/gad.6.12a.2235

Stephenson, J. J., Nemunaitis, J., Joy, A. A., Martin, J. C., Jou, Y. M., Zhang, D., Statkevich, P., Yao, S. L., Zhu, Y., Zhou, H., Small, K., Bannerji, R., & Edelman, M. J. (2014). Randomized phase 2 study of the cyclin-dependent kinase inhibitor dinaciclib (MK-7965) versus erlotinib in patients with non-small cell lung cancer. *Lung Cancer*. https://doi.org/10.1016/j.lungcan.2013.11.020

Sun, Y., Luo, Z. M., Guo, X. M., Su, D. F., & Liu, X. (2015). An updated role of microRNA-124 in central nervous system disorders: A review. *Frontiers in Cellular Neuroscience*. https://doi.org/10.3389/fncel.2015.00193

Suryo Rahmanto, A., Savov, V., Brunner, A., Bolin, S., Weishaupt, H., Malyukova, A., Rosén, G., Čančer, M., Hutter, S., Sundström, A., Kawauchi, D., Jones, D. T., Spruck, C., Taylor, M. D., Cho, Y., Pfister, S. M., Kool, M., Korshunov, A., Swartling, F. J., & Sangfelt, O. (2016). FBW7 suppression leads to SOX9 stabilization and increased malignancy in medulloblastoma. *The EMBO Journal*. https://doi.org/10.15252/embj.201693889

Swartling, F. J., Savov, V., Persson, A. I., Chen, J., Hackett, C. S., Northcott, P. A., Grimmer, M. R., Lau, J., Chesler, L., Perry, A., Phillips, J. J., Taylor, M. D., & Weiss, W. A. (2012). Distinct Neural Stem Cell Populations Give Rise to Disparate Brain Tumors in Response to N-MYC. *Cancer Cell*. https://doi.org/10.1016/j.ccr.2012.04.012

Tansey, W. P., & P., W. (2014). Mammalian MYC Proteins and Cancer. *New Journal of Science*, *2014*, 1–27. https://doi.org/10.1155/2014/757534

Taylor, M. D., Northcott, P. A., Korshunov, A., Remke, M., Cho, Y.-J., Clifford, S. C., Eberhart, C. G., Parsons, D. W., Rutkowski, S., Gajjar, A., Ellison, D. W., Lichter, P., Gilbertson, R. J., Pomeroy, S. L., Kool, M., & Pfister, S. M. (2012). Molecular subgroups of medulloblastoma: the current consensus. *Acta Neuropathologica*, *123*(4), 465–472. https://doi.org/10.1007/s00401-011-0922-z

Thompson, M. C., Fuller, C., Hogg, T. L., Dalton, J., Finkelstein, D., Lau, C. C., Chintagumpala, M., Adesina, A., Ashley, D. M., Kellie, S. J., Taylor, M. D., Curran, T., Gajjar, A., & Gilbertson, R. J. (2006). Genomics Identifies Medulloblastoma Subgroups That Are Enriched for Specific Genetic Alterations. *Journal of Clinical Oncology*, *24*(12), 1924–1931. https://doi.org/10.1200/JCO.2005.04.4974

Timme, N., Han, Y., Liu, S., Yosief, H. O., García, H. D., Bei, Y., Klironomos, F., MacArthur, I. C., Szymansky, A., von Stebut, J., Bardinet, V., Dohna, C., Künkele, A., Rolff, J., Hundsdörfer, P., Lissat, A., Seifert, G., Eggert, A., Schulte, J. H., … Henssen, A. G. (2020). Small-Molecule Dual PLK1 and BRD4 Inhibitors are Active Against Preclinical Models of Pediatric Solid Tumors. *Translational Oncology*. https://doi.org/10.1016/j.tranon.2019.09.013

Topham, C., Tighe, A., Ly, P., Bennett, A., Sloss, O., Nelson, L., Ridgway, R. A., Huels, D., Littler, S., Schandl, C., Sun, Y., Bechi, B., Procter, D. J., Sansom, O. J., Cleveland, D. W., & Taylor, S. S. (2015). MYC Is a Major Determinant of Mitotic Cell Fate. *Cancer Cell*. https://doi.org/10.1016/j.ccell.2015.06.001

Uziel, T., Karginov, F. V, Xie, S., Parker, J. S., Wang, Y.-D., Gajjar, A., He, L., Ellison, D.,

Gilbertson, R. J., Hannon, G., & Roussel, M. F. (2009). The miR-17~92 cluster collaborates with the Sonic Hedgehog pathway in medulloblastoma. *Proceedings of the National Academy of Sciences of the United States of America*, *106*(8), 2812–2817. https://doi.org/10.1073/pnas.0809579106

Uziel, T., Zindy, F., Sherr, C. J., & Roussel, M. F. (2006). The CDK inhibitor p18Ink4c is a tumor suppressor in medulloblastoma. In *Cell Cycle*. https://doi.org/10.4161/cc.5.4.2475

van Delft, M. F., Wei, A. H., Mason, K. D., Vandenberg, C. J., Chen, L., Czabotar, P. E., Willis, S. N., Scott, C. L., Day, C. L., Cory, S., Adams, J. M., Roberts, A. W., & Huang, D. C. S. (2006). The BH3 mimetic ABT-737 targets selective Bcl-2 proteins and efficiently induces apoptosis via Bak/Bax if Mcl-1 is neutralized. *Cancer Cell*. https://doi.org/10.1016/j.ccr.2006.08.027

van Rooij, E., Sutherland, L. B., Qi, X., Richardson, J. a, Hill, J., & Olson, E. N. (2007). Control of stress-dependent cardiac growth and gene expression by a microRNA. *Science (New York, N.Y.)*, *316*(5824), 575–579. https://doi.org/10.1126/science.1139089

Varadarajan, S., Poornima, P., Milani, M., Gowda, K., Amin, S., Wang, H. G., & Cohen, G. M. (2015). Maritoclax and dinaciclib inhibit MCL-1 activity and induce apoptosis in both a MCL-1-dependent and -independent manner. *Oncotarget*. https://doi.org/10.18632/oncotarget.3706

Venkataraman, S., Alimova, I., Balakrishnan, I., Harris, P., Birks, D. K., Griesinger, A., Amani, V., Cristiano, B., Remke, M., Taylor, M. D., Handler, M., Foreman, N. K., & Vibhakar, R. (2014). Inhibition of BRD4 attenuates tumor cell self-renewal and suppresses stem cell signaling in MYC driven medulloblastoma. *Oncotarget*, *5*(9), 2355–2371. http://www.ncbi.nlm.nih.gov/pmc/articles/PMC4058011/

Ventura, A., Young, A. G., Winslow, M. M., Lintault, L., Meissner, A., Erkeland, S. J., Newman, J., Bronson, R. T., Crowley, D., Stone, J. R., Jaenisch, R., Sharp, P. A., & Jacks, T. (2008). Targeted Deletion Reveals Essential and Overlapping Functions of the miR-17∼92 Family of miRNA Clusters. *Cell*. https://doi.org/10.1016/j.cell.2008.02.019

Vladoiu, M. C., El-Hamamy, I., Donovan, L. K., Farooq, H., Holgado, B. L., Sundaravadanam, Y., Ramaswamy, V., Hendrikse, L. D., Kumar, S., Mack, S. C., Lee, J. J. Y., Fong, V., Juraschka, K., Przelicki, D., Michealraj, A., Skowron, P., Luu, B., Suzuki, H., Morrissy, A. S., … Taylor, M. D. (2019). Childhood cerebellar tumours mirror conserved fetal transcriptional programs. *Nature*. https://doi.org/10.1038/s41586-019-1158-7

Vo, B. H. T., Wolf, E., Kawauchi, D., Gebhardt, A., Rehg, J. E., Finkelstein, D., Walz, S., Murphy, B. L., Youn, Y. H., Han, Y. G., Eilers, M., & Roussel, M. F. (2016). The Interaction of Myc with Miz1 Defines Medulloblastoma Subgroup Identity. *Cancer Cell*, *29*(1), 5–16. https://doi.org/10.1016/j.ccell.2015.12.003

Vogler, M., Butterworth, M., Majid, A., Walewska, R. J., Sun, X. M., Dyer, M. J. S., & Cohen, G. M. (2009). Concurrent up-regulation of BCL-XL and BCL2A1 induces approximately 1000-fold resistance to ABT-737 in chronic lymphocytic leukemia. *Blood*. https://doi.org/10.1182/blood-2008-08-173310

Wanzel, M., Herold, S., & Eilers, M. (2003). Transcriptional repression by Myc. In *Trends in Cell Biology*. https://doi.org/10.1016/S0962-8924(03)00003-5

Waszak, S. M., Northcott, P. A., Buchhalter, I., Robinson, G. W., Sutter, C., Groebner, S.,

Grund, K. B., Brugières, L., Jones, D. T. W., Pajtler, K. W., Morrissy, A. S., Kool, M., Sturm, D., Chavez, L., Ernst, A., Brabetz, S., Hain, M., Zichner, T., Segura-Wang, M., … Pfister, S. M. (2018). Spectrum and prevalence of genetic predisposition in medulloblastoma: a retrospective genetic study and prospective validation in a clinical trial cohort. *The Lancet Oncology*. https://doi.org/10.1016/S1470-2045(18)30242-0

Wei, J., Wang, F., Kong, L. Y., Xu, S., Doucette, T., Ferguson, S. D., Yang, Y., McEnery, K., Jethwa, K., Gjyshi, O., Qiao, W., Levine, N. B., Lang, F. F., Rao, G., Fuller, G. N., Calin, G. A., & Heimberger, A. B. (2013). MiR-124 inhibits STAT3 signaling to enhance T cell-mediated immune clearance of glioma. *Cancer Research*. https://doi.org/10.1158/0008-5472.CAN-12-4318

Weissman, A. M. (2001). Themes and variations on ubiquitylation. *Nature Reviews Molecular Cell Biology*, *2*, 169. http://dx.doi.org/10.1038/35056563

Whiteway, S. L., Harris, P. S., Venkataraman, S., Alimova, I., Birks, D. K., Donson, A. M., Foreman, N. K., & Vibhakar, R. (2013). Inhibition of cyclin-dependent kinase 6 suppresses cell proliferation and enhances radiation sensitivity in medulloblastoma cells. *Journal of Neuro-Oncology*. https://doi.org/10.1007/s11060-012-1000-7

Wibroe, M., Cappelen, J., Castor, C., Clausen, N., Grillner, P., Gudrunardottir, T., Gupta, R., Gustavsson, B., Heyman, M., Holm, S., Karppinen, A., Klausen, C., Lönnqvist, T., Mathiasen, R., Nilsson, P., Nysom, K., Persson, K., Rask, O., Schmiegelow, K., … Juhler, M. (2017). Cerebellar mutism syndrome in children with brain tumours of the posterior fossa. *BMC Cancer*, *17*, 439. https://doi.org/10.1186/s12885-017-3416-0

Wiese, K. E., Walz, S., von Eyss, B., Wolf, E., Athineos, D., Sansom, O., & Eilers, M. (2013). The Role of MIZ-1 in MYC-Dependent Tumorigenesis. *Cold Spring Harbor Perspectives in Medicine*, *3*(12), a014290. https://doi.org/10.1101/cshperspect.a014290

Wu, S., Huang, S., Ding, J., Zhao, Y., Liang, L., Liu, T., Zhan, R., & He, X. (2010). Multiple microRNAs modulate p21Cip1/Waf1 expression by directly targeting its 3' untranslated region. *Oncogene*, *29*(15), 2302–2308. https://doi.org/10.1038/onc.2010.34

Xu, X., Eshima, S., Kato, S., Fisher, D. E., Sakurai, H., Hayakawa, Y., & Yokoyama, S. (2020). Rational Combination Therapy for Melanoma with Dinaciclib by Targeting BAK-Dependent Cell Death. *Molecular Cancer Therapeutics*. https://doi.org/10.1158/1535-7163.MCT-19-0451

Yi, R., O'Carroll, D., Pasolli, H. A., Zhang, Z., Dietrich, F. S., Tarakhovsky, A., & Fuchs, E. (2006). Morphogenesis in skin is governed by discrete sets of differentially expressed microRNAs. *Nature Genetics*, *38*(3), 356–362. https://doi.org/10.1038/ng1744

Yi, R., Qin, Y., Macara, I. G., & Cullen, B. R. (2003). Exportin-5 mediates the nuclear export of pre-microRNAs and short hairpin RNAs. *Genes and Development*, *17*(24), 3011–3016. https://doi.org/10.1101/gad.1158803

Yock, T. I., Yeap, B. Y., Ebb, D. H., Weyman, E., Eaton, B. R., Sherry, N. A., Jones, R. M., MacDonald, S. M., Pulsifer, M. B., Lavally, B., Abrams, A. N., Huang, M. S., Marcus, K. J., & Tarbell, N. J. (2016). Long-term toxic effects of proton radiotherapy for paediatric medulloblastoma: A phase 2 single-arm study. *The Lancet Oncology*. https://doi.org/10.1016/S1470-2045(15)00167-9

Youle, R. J., & Strasser, A. (2008). The BCL-2 protein family: Opposing activities that mediate

cell death. In *Nature Reviews Molecular Cell Biology*. https://doi.org/10.1038/nrm2308

Zhukova, N., Ramaswamy, V., Remke, M., Pfaff, E., Shih, D. J. H., Martin, D. C., Castelo-Branco, P., Baskin, B., Ray, P. N., Bouffet, E., von Bueren, A. O., Jones, D. T. W., Northcott, P. A., Kool, M., Sturm, D., Pugh, T. J., Pomeroy, S. L., Cho, Y.-J., Pietsch, T., … Tabori, U. (2013). Subgroup-Specific Prognostic Implications of TP53 Mutation in Medulloblastoma. *Journal of Clinical Oncology*, *31*(23), 2927–2935. https://doi.org/10.1200/JCO.2012.48.5052

Zinzalla, G. (2016). Targeting MYC: Is it getting any easier? In *Future Medicinal Chemistry*. https://doi.org/10.4155/fmc-2016-0119

Zirath, H., Frenzel, A., Oliynyk, G., Segerström, L., Westermark, U. K., Larsson, K., Persson, M. M., Hultenby, K., Lehtiö, J., Einvik, C., Påhlman, S., Kogner, P., Jakobsson, P. J., & Henriksson, M. A. (2013). MYC inhibition induces metabolic changes leading to accumulation of lipid droplets in tumor cells. *Proceedings of the National Academy of Sciences of the United States of America*. https://doi.org/10.1073/pnas.1222404110